Interaction between cortical state, dopaminergic modulation, attention and decision making

Jochem van Kempen

A thesis submitted for the degree of Doctor of Philosophy

Institute of Neuroscience, Newcastle University

31st August 2019

Abstract

Cortical activity reveals spontaneous fluctuations that are not solely determined by external inputs, but reflect changes to the underlying excitability of neurons, referred to as cortical state. These fluctuations are partly linked to fluctuations in arousal, whereby they influence sensory processing as well as behavioural performance. During active versus inactive states, the cortex is more desynchronised and displays suppressed low-frequency and increased high-frequency activity, as well as lower correlations in population spiking activity. Selective attention facilitates the prioritisation of task-relevant sensory inputs over those which are irrelevant. When attention is directed towards the receptive field of the recorded neuronal population, firing rates increase and, interestingly, this area of the cortex desynchronises in a comparable manner to that observed during cortical state fluctuations. Because of these similarities, it has been suggested that cortical state and selective attention might rely on related underlying circuit mechanisms.

In this thesis, I investigated cortical state changes across different spatiotemporal scales and across species, using pupil diameter as an across-species proxy for neuromodulatory controlled central arousal state. In the first chapter, I describe how global, arousal-mediated state fluctuations influence specific behavioural and electro-encephalographic (EEG) signatures of perceptual decision-making in human subjects. Arousal strongly affects behaviour and task-related activity across the brain, including in visual, association, and motor cortex.

In the second chapter, I described how top down covert attention affects neuronal signatures of cortical state within sensory areas and their coordination between visual areas in Macaque monkeys. Using a Hidden Markov Model (HMM), I classified periods of vigorous (On) and faint (Off) population spiking activity. These periods were coordinated in a top-down manner across brain areas along the visual hierarchy during selective attention and this coordination was furthermore predictive of behavioural performance.

Finally, in the third study, I tested how the local effects of attention induced cortical state changes within a single area are influenced by iontophoretic administration of dopaminergic drugs. Dopamine strongly affects neural activity in parietal cortex, with specific modulations of activity related to attentional processing.

These results highlight the strong influences of cortical state and attention on neural activity and behaviour, as well as the crucial role of the interaction between these two functions. They furthermore shed light on the neural mechanisms that underlie cortical state fluctuations, top-down attention and perceptual decision making, from small scale modulations of single neuron firing rates, to the way activity within and across brain areas is coordinated and finally to the way they influence behavioural performance.

Table of Contents

Table of Figures

Table of Abbreviations

5-HT	5-hydroxytryptamine (serotonin)
ACh	Acetylcholine
ADHD	Attention deficit hyperactivity disorder
ANOVA	Analysis of variance
AR	Adrenergic receptor
AUROC	Area under the receiver operator characteristic
BF	Basal forebrain
BIC	Bayes information criterion
BOLD	Blood oxygenated level dependence
BPD	Baseline pupil diameter
CA	Catecholamine
cAMP	Cyclic adenosine monophosphate
COMT	Catechol O-methyltransferase
CPP	Centroparietal positivity
CRT	Cathode ray tube
CSD	Current source density
DA	Dopamine
DAT	Dopamine transporter
dlPFC	Dorsolateral prefrontal cortex
DNA	Deoxyribonucleic acid
DV	Decision variable
EEG	Electroencephalography
EM	Expectation maximisation
ERP	Event related potential
EW	Edinger-Westphal
FDR	False discovery rate
FEF	Frontal eye fields
FF	Fano factor
FFT	Fast Fourier transform
fMRI	Functional magnetic resonance imaging
GLM	General linear model
HCN	Hyperpolarisation-activated cyclic nucleotide-gated
HMM	Hidden Markov model
IPS	Intraparietal sulcus
IRF	Impulse response function
IT	Inferior temporal cortex
ITPC	Inter-trial phase coherence
LC	Locus coeruleus
LFP	Local field potential
LGN	Lateral geniculate nucleus
LHB	Left hemispheric β-power
LIP	Lateral intraparietal area
mACh	Muscarinic acetylcholine receptor
M-cells	Magnocellular cells
MI	Modulation index
MRI	Magnetic resonance imaging
MST	Medial superior temporal area
MT	Medial temporal area
MU	Multi-unit
MUA	Multi-unit activity
MUAe	Multi-unit activity envelope
NA	Noradrenaline
nACh	Nicotinic acetylcholine receptor
NB	Nucleus basalis
NMDA	N-Methyl-D-aspartate
P-cells	Parvocellular cells
PFC	Prefrontal cortex
PLR	Pupil light reflex
PPC	Posterior parietal cortex
PR	Pupil response

REM	Rapid eye movement
RF	Receptive field
RGB	Red green blue
ROC	Receiver operator characteristic
RT	Reaction time
RTcv	Reaction time coefficient of variation
SC	Superior colliculus
Sci	Superior colliculus (intermediate layers)
SCs	Superior colliculus (superficial layers)
SEM	Standard error of the mean
SF	Saccade field
SN	Substantia nigra
SNR	Signal-to-noise ratio
STFT	Short time Fourier transform
SU	Single-unit
TSE	Temporal spectral evolution
TTA	Transition triggered average
VIF	Variance inflation factor
Vm	Membrane potential (voltage)
VTA	Ventral tegmental area

Chapter 1 - General Introduction

This chapter contains a review of the literature relevant to this thesis. In each of the three following chapters I discuss an independent experimental project. Accordingly, each of these chapters will have their own introduction, methods, results and discussion section that is tailored to that chapter's more specific topic. Finally, I will discuss the overarching relevance of these experimental projects in the context of existing knowledge, and highlight potential areas of future research in the general discussion in chapter 5.

Here I briefly outline the contributions of my colleagues to the experimental chapters.

The influence of cortical state fluctuations on the neural signatures of perceptual decision making is discussed in Chapter 2. For this project, I did not collect the data, but obtained it through a collaboration with the lab of Professor Mark Bellgrove (Monash University). This chapter has recently been published (van Kempen et al., 2019). The published article has been adapted for this thesis.

Part of the data described in chapter 3 has been collected together with Michael Boyd, who discussed different aspects of some of these data in his PhD thesis.

Similarly, part of the data analysed and discussed in chapter 4 has been collected by Christian Brandt, a former post-doctoral researcher in the lab of Alexander Thiele.

1.1 - Rationale

Both behavioural and neural responses are variable, even under repeated measurements under identical conditions (Gescheider, 1997). Early psychophysical studies investigated human responses to external stimuli in order to measure their sensory (difference) thresholds, the strength of a presented stimulus (change) required for it to be consciously perceived. These early studies found that the sensitivity with which a stimulus could be detected fluctuated over time. Therefore, in order to accurately measure sensory thresholds, multiple measurements should be taken (Gescheider, 1997).

Similarly, neural responses vary from moment to moment (Carandini, 2004; Tomko and Crapper, 1974). Part of this variability is brought about by various stochastic physiological mechanisms such as the stochastic nature of synaptic transmission and receptor diffusion (Ribrault et al., 2011). Additionally, some response variability is brought about by functions such as brain state, attention and arousal (Arieli et al., 1996; Beaman et al., 2017; Engel et al., 2016; Fontanini and Katz, 2008; Goris et al., 2014; Harris and Thiele, 2011; McGinley et al., 2015b; Rabinowitz et al., 2015; Reimer et al., 2014; Scholvinck et al., 2015). Because of the variability in both behaviour and neural activity, a central theme in neuroscientific research has been to characterise this non-stationarity

of behavioural and neural responses and to determine their relationship (Britten et al., 1996; Shadlen et al., 1996).

Studying variability in neural activity, even in response to simple stimuli, can inform us about basic neural mechanisms that support healthy brain functioning (Ringach, 2009). In addition, as neural variability is altered in for instance autism spectrum disorder, it can potentially also elucidate abnormal brain functioning (Dinstein et al., 2015).

In this thesis, I will explore the effect of fluctuations in neural excitability that occur across different spatiotemporal scales on behavioural and neural responses during cognitive tasks. These fluctuations vary from global fluctuations that influence brain-wide activity during perceptual decision-making, to smaller scale network interactions of cortical state and attention, to the local effects of selective attention within a single area and how they are influenced by neuromodulator administration. I focus specifically on the visual system but discuss research that has investigated the effects of neural excitability fluctuations in other sensory domains.

1.2 - Vision

1.2.1 - Visual pathways: from retina to cortex

Light is focused onto the retina by the cornea and the lens where it stimulates cone and rod photoreceptors. Rod photoreceptors are more sensitive to light than cone receptors, due to their higher levels of photosensitive pigment and signal amplification, and are therefore suited for vision during low light levels. Cone receptors in primates are specifically sensitive to one of three parts of the light spectrum and selectively absorb light with short (426nm), medium (530nm) or long (555nm) wavelengths, corresponding to blue, green and red colours, respectively (Merbs and Nathans, 1992). The signals from photoreceptors are combined and processed by retinal ganglion cells. The limited region of the retina for which ganglion cells process the inputs from photoreceptors comprises the receptive field (RF) for a given cell.

Visual information that is projected onto the retina is sent to three subcortical regions: the pretectal region and the superior colliculus (SC) of the midbrain as well as the lateral geniculate nucleus (LGN) of the thalamus (Kandel et al., 2000). Whereas the pretectal region of the midbrain controls the amount of light that hits the retina by driving constrictions in pupil diameter in response to luminance increases, as well as controlling optokinetic reflexes, the projections to SC and LGN relay (indirectly) to the cerebral cortex and support visual perception and higher cognitive function. Projections from the retina terminate onto superficial layers of the SC (SCs), where a map of the contralateral visual field is constructed, and projected via the pulvinar in the thalamus to the cortex. As approximately only 10% of retinal axons project to SCs, this pathway is thought to support relatively basic visual perception. Finally, with approximately 90% of retinal projections terminating in the LGN, this geniculo-cortical pathway comprises the principal route through which visual information is sent to the cortex, and will be discussed in greater detail below.

There are multiple types of ganglion cells in the retina that each process and convey separate aspects of the visual scene (Kandel et al., 2000). The majority of ganglion cells comprise the larger magnocellular (M-cells) and the smaller parvocellular (P-cells) cells. These cells can process signals from the same photoreceptor in parallel to convey functionally distinct information (Kaplan and Shapley, 1986) and project to separate layers of the LGN (Kandel et al., 2000; Kaplan and Shapley, 1982). Within LGN, M-cells have larger RFs and respond with shorter latencies compared to P-cells. They are furthermore selective for lower spatial frequencies and have much higher contrast sensitivity (Kaplan and Shapley, 1982). P-cells, on the other hand, have smaller RFs and respond to higher spatial frequencies. Additionally, P-cells respond selectively to specific wavelengths, and thus allow colour processing (Kaplan and Shapley, 1982; Livingstone and Hubel, 1988). Because of these functional differences, M-cells are thought to mainly process features such as depth and movement, whereas P-cells process more fine features such as form and colour (Kandel et al., 2000; Livingstone and Hubel, 1988). These functionally distinct layers in LGN remain segregated and project to separate cortical layers in primary visual cortex (V1).

1.2.2 - The cortical microcircuit

Although many differences exist between areas of the neocortex and across species, similarities in the anatomical structure, input-output connectivity patterns and information flow have led to the proposal of the canonical cortical microcircuit that is repeated across the neocortex (Douglas and Martin, 2004). The cortex is made up of six layers that show organisation according to an area's afferents, the connectivity of neurons within this area and its efferents. These layers can be coarsely subdivided (from superficial to deep layers) into supragranular, granular and infragranular layers. Additionally, in higher animals such as cats and primates, the cortex is also organised into cortical microcolumns (Hubel and Wiesel, 1968; Mountcastle, 1957). Spanning the cortical layers, cells within these columns receive the same restricted input from upstream areas and therefore show similar response characteristics such as RF location and orientation tuning.

Within a column, granular layers receive and integrate input from the thalamus or upstream areas. From here, excitatory cells project towards the cortical surface (vertical along the direction of the column) and terminate in supragranular layer 2/3. This information is then sent to infragranular layer 5, which projects further to layer 6 and to subcortical structures and provides feedback to supragranular layers. Layer 6 projects back to the thalamus and provides modulatory feedback to the input layer, thereby controlling the input to the cortical column. Lateral connections between columns, and feedforward projections to other brain areas occur across cortical layers but are most common in supragranular layers 2/3 (Blasdel et al., 1985; Rockland and Lund, 1983). Feedback projections predominantly originate in infragranular layers and mainly target layer 1, which consists mostly of the apical (long range) dendrites of pyramidal cells and

axon terminals, and layer 5 (Markov et al., 2014). Feedback can, however, also target other layers.

Although this basic framework of cortical organisation is found across the cortex, variations on this central theme can indicate some important functional differences. For instance, differences in the thickness of the granular layer in V1 (~500 μm) compared to those in other (visual) cortical areas such as V4 (200 μm) highlight their anatomical and functional dissociation (Hof and Morrison, 1995; Lund and Yoshioka, 1991). Accordingly, the granular layer in V1, but not in V4, can be subdivided into layers 4A, 4B, 4Cα and 4Cβ. This particular laminar segregation supports the functional separation of the two different cortical pathways processing visual information.

1.2.3 - Visual pathways: two cortical pathways

The clear anatomical and functional segregation of M and P-cells, originating in the retina and continuing through cortex, has led to the influential theory that there are two largely distinct parallel cortical pathways: a dorsal and a ventral stream (Mishkin et al., 1983). The dorsal stream runs along V1, V2, V3, the middle temporal area (MT) and the medial superior temporal area (MST) before projecting to the parietal cortex. The ventral stream includes cortical areas V1, V2, V3, and V4 and runs further along the temporal lobe to areas TEO, TE and inferior temporal cortex (IT). Although both pathways process input from both M and P-cells and their segregation might not be as straightforward as often thought (Merigan and Maunsell, 1993), the ventral stream primarily processes input from P-cells and is specialised in object and colour vision, whereas the dorsal stream predominantly processes information originating in M-cells and is associated with spatial and motion processing. Accordingly, the ventral and dorsal pathway were named the “what” and “where” pathway (Mishkin et al., 1983).

In V1, projections from M-cells in LGN terminate in layer 4Cα and are relayed to layer 4B (Boyd et al., 2000), where cells are orientation and often movement direction selective, from where direct and indirect afferents to MT originate. The indirect afferents first project to the thick stripes in V2 before relaying to MT (and further to parietal areas). Projections from P-cells, on the other hand, terminate in layer 4Cβ and project further to layer 2/3 (Boyd et al., 2000). The projections that terminate in layer 2/3 can be further subdivided in those that project to blobs, and those that terminate in the interblob regions. Cells in blobs, which likely also receive magnocellular input (Callaway and Wiser, 1996; Livingstone and Hubel, 1988), have relatively large RFs and are selective to colour but not to orientation. Cells in the interblob do not have explicit colour-coding but have fine orientation selectivity and the capacity of discriminating high spatial frequencies. Cells in blobs and interblobs project to separate regions in V2, the thin and pale stripes, respectively.

Thus, information from the same retinal image is segregated and processed by different groups of retinal ganglion cells and projected to separate layers of the LGN. Although there is substantial mixing of the input provided by M and P-cells in V1, there is also

considerable functional segregation along areas in the dorsal and ventral pathway (Livingstone and Hubel, 1988; Mishkin et al., 1983). The dorsal pathway primarily processes movement, luminance differences and is involved in stereopsis. The ventral pathway, on the other hand, processes more fine-grained information about higher spatial frequencies and colour. This functional specialisation is highlighted by visual illusions which revealed that various visual features mediated by the dorsal "where" pathway (e.g. depth perception) depend strongly on differences in luminance (Livingstone and Hubel, 1988). With equiluminance, contextual perspective cues such as converging lines that normally bring about e.g. size illusions are greatly diminished.

1.2.4 - Corticocortical communication

Visual information from V1 is thus sent downstream along the two pathways described above. The nature of this across-area communication, and how it is influenced by task demands, is an area of active research. Although the progression of information across the visual hierarchy can be examined by investigating the timing of the response to a stimulus across visual areas (Schmolesky et al., 1998), to investigate the direct communication between areas, simultaneous recordings across these areas are required.

Signal transmission can be measured through correlations of spiking activity across areas (Munk et al., 1992; Nowak et al., 1999, 1995). In these studies, the strength of cross-correlations between cells across visual areas was shown to depend on retinotopic alignment and similarities in stimulus preferences. Stronger correlations (on a faster temporal scale) were found for cell pairs with RFs that were closer together and had similar orientation tuning curves.

In addition to stronger pairwise correlations, findings of synchronous oscillatory activity, particularly in the gamma frequency range (30-60 Hz), were thought to benefit signal transmission between cells within and across areas (Eckhorn et al., 1988; Engel et al., 1992). Although early theories that proposed a role for synchronous activity in perceptual binding (Singer, 1999) were not supported by experimental findings (Thiele and Stoner, 2003), later theories argued that "communication through coherence" is crucial for efficient signal transmission and cognition (Fries, 2005). In this framework, oscillatory synchrony allows a spike sent by one cell to arrive during a time window of excitability in the other cell, thereby serving effective communication. These oscillatory interactions are often measured in the local field potential (LFP), where electrodes inserted into brain tissue measure activity from the inhibitory and excitatory synaptic processes of large neural populations (Kajikawa and Schroeder, 2011). Feedforward and feedback components of interareal interactions have been proposed to map onto different frequency bands. Specifically, gamma frequency synchronisation has been proposed to carry feedforward signals, whereas feedback signals are mediated by frequencies in the alpha (9-12 Hz) or beta (13-20 Hz) range (Bastos et al., 2015; Bosman et al., 2012; van Kerkoerle et al., 2014). Accordingly, feedforward stimulus processing is associated with directional gamma-band coupling (Bastos et al., 2015; Bosman et al., 2012; van Kerkoerle et al., 2014), estimated using granger causal analyses, whereas task-

related feedback activity is mediated through lower frequencies in the alpha and beta range (Bastos et al., 2015; van Kerkoerle et al., 2014).

Whether oscillatory coupling between areas is indeed necessary for across areas communication remains to be determined, but within-area synchrony of activity plausibly benefits signal transmission. Within V1, spikes locked to specific phases of the gamma oscillation were more selective for stimulus orientation and showed a reduction of information-limiting correlations (see section 1.4.2 - below), suggesting that the gamma phase can modulate information coding (Womelsdorf et al., 2012). Additionally, Jia et al. (2013) found that pairwise spiking correlations between V1 and V2 were enhanced with stronger gamma oscillations in the V1 LFP. Although spikes in V1 were more often followed by a spike in V2 with enhanced gamma oscillations in V1, these spikes were more strongly locked to the V1 gamma phase compared to the V2 gamma phase. This suggested that gamma, rather than allowing bidirectional synchronous activity across V1 and V2, synchronised activity in V1 to more effectively elicit a spike in V2. This hypothesis was supported by Zandvakili and Kohn (2015), who found that V2 spikes were preceded by temporally synchronous bursts of spikes in V1. In these studies, however, recordings were performed in anaesthetised animals (Jia et al., 2013; Zandvakili and Kohn, 2015), and varying levels of gamma were induced by different visual stimuli (Jia et al., 2013). As emphasised by the authors (Jia et al., 2013), modulation of oscillatory coupling might thus still be relevant in task performing animals during cognitive tasks (see below).

Finally, another, perhaps more biologically plausible, mechanism of information transfer across areas is through selective combination of input from a subset of the upstream neural population (Semedo et al., 2019). Here, rather than sending the combined information from an entire neural population downstream, information transfer occurs through a "communication subspace" in which a lower dimensional signal (only selected information) is passed on to the next information processing stage. More specifically, the activity in downstream neurons can only be predicted from activity fluctuations in upstream areas along a specific dimension (the subspace). Activity fluctuations in the upstream areas along other dimensions are not predictive of activity changes downstream and are considered private dimensions. Fluctuations along private dimensions are thus hidden from the target neurons, allowing for selective across-area information transmission. The exact information that is sent depends on the presented stimulus, and speculatively, might depend on task-demands and could be determined in a feedback manner by selectively adjusting the synaptic weights of feedforward connections.

1.3 - **Cortical state**

Cortical activity reveals spontaneous activity fluctuations that are not solely determined by external inputs, but reflect changes to the underlying excitability of neurons, referred to as cortical state. These fluctuations in network activity are often studied using electro-encephalography (EEG), where electrodes placed on the scalp measure the activity of

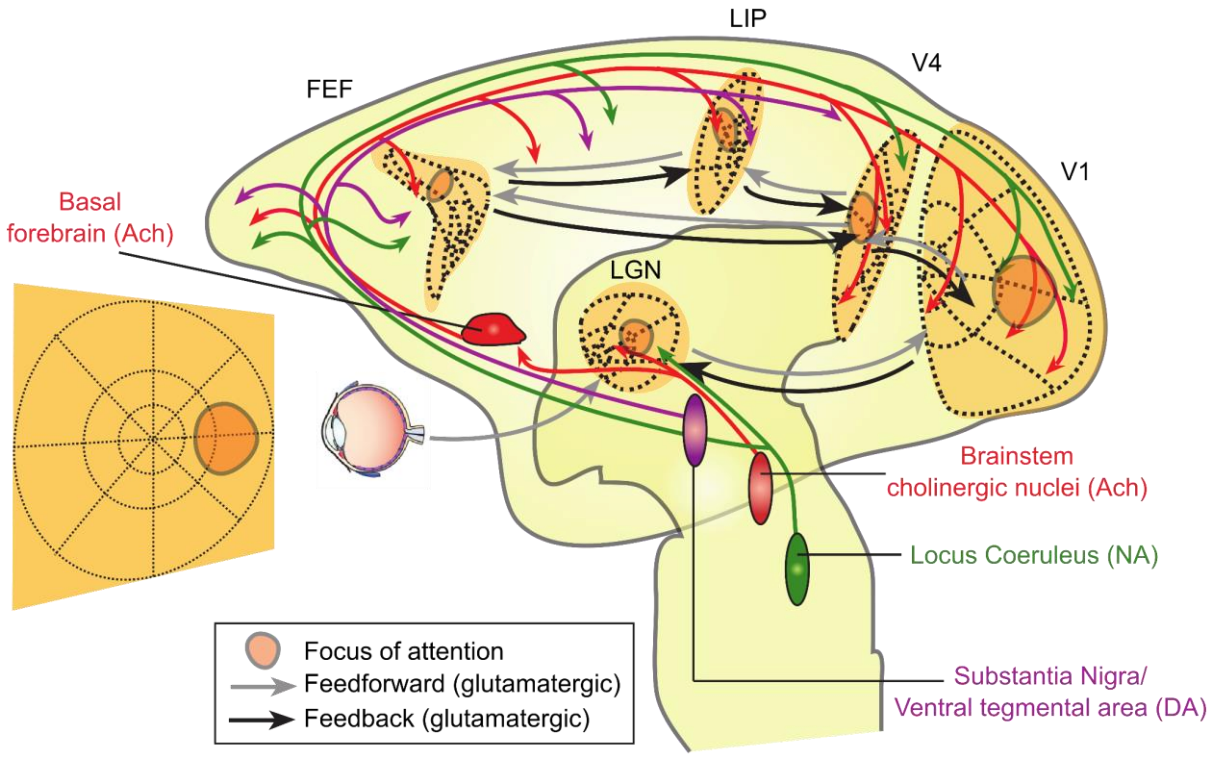

Figure 1-1. The visual attention network in the macaque brain and its proposed modulation by neuromodulatory influences. Visual information traverses from the eye through the LGN to various areas in the cortex via glutamatergic feedforward projections. Contextual information is thought to originate in higher-order areas and sent back to early visual areas via glutamatergic feedback projections. Spatially focused attention affects neural processing at specific retinotopic locations throughout the cortical hierarchy. Neuromodulatory influences can modulate activity at various information processing stages. LGN: Lateral geniculate nucleus; V1-V4: early visual areas 1-4; LIP: lateral intraparietal area; FEF: frontal eye field. Adapted with permission from Harris & Thiele (2011).

large populations of neurons (Steriade et al., 1993b), LFP, or intracellular membrane potential recordings, as there is a strong relationship between the membrane potential (Vm) of individual neurons and the activity of the surrounding population (Steriade et al., 1993c).

Cortical states were originally studied under anaesthesia and as part of the sleep-wake cycle. Under either condition dramatic changes in the EEG signal, the firing rate, and Vm were observed (Contreras and Steriade, 1995; Steriade et al., 2001). Especially during slow-wave sleep, hyperpolarised states with low firing rates and high amplitude low-frequency EEG and Vm dynamics alternate with depolarised states during which firing rates are higher and EEG and the Vm reveals reduced levels of low-frequency and increased levels of high-frequency activity (Steriade et al., 2001). During slow-wave sleep, the histogram of Vm reveals a bimodal distribution, indicative of the occurrence of depolarised and hyperpolarised states (Steriade et al., 2001), classically referred to as Up and Down states, respectively.

Although cortical states fluctuate strongly between sleep-wake states and prolonged periods of hyperpolarisation (Down states) were found to be abolished during rapid eye movement (REM) sleep and wakefulness (Steriade et al., 2001), more recent research has found that state fluctuations also occur during wakefulness (McGinley et al., 2015b;

Ringach, 2009), even if activity fluctuations are somewhat reduced. Activity fluctuations within wakefulness states, from quiet and inattentive to active and vigilant, have been associated with changes in cognitive functions, such as arousal and attention, and can influence neural responses, information coding and behaviour (Harris and Thiele, 2011; Lee and Dan, 2012). During less active/inactive states, cortical activity is highly synchronous, characterised by increased low-frequency oscillations and high spike-spike correlations. During active states, the cortex is more desynchronised and displays suppressed low-frequency and increased high-frequency activity, as well as lower correlations in population spiking activity. During synchronous states, individual neurons fire in a more correlated manner, which is thought to lead to more redundancy across the neural population and limit the amount of information that can be processed (Zohary et al., 1994). In support of this, fluctuations in cortical state can modulate sensory responses (Arieli et al., 1996; Beaman et al., 2017; McGinley et al., 2015a; Reimer et al., 2014; Scholvinck et al., 2015), and perception can be impaired from optogenetically induced low-frequency spike-spike correlations in V4 (Nandy et al., 2019).

Several neural mechanisms have been proposed to bring about fluctuations in cortical state (Harris, 2013; Harris and Thiele, 2011), including by thalamic drive (Poulet et al., 2012), neuromodulatory regulation (Lee and Dan, 2012) and/or driven by feedback projections (Zagha et al., 2013). These mechanisms show great overlap with the mechanisms thought to drive the neural activity changes associated with attention.

1.4 - **Attention**

Attention describes the ability to prioritise and preferentially process one or several stimuli out of all the currently available (sensory) information. Attention can be driven exogenously, by external events, or endogenously, according to internal goals (Posner, 1980). With exogenous (bottom-up) attention, a stimulus is automatically attended to due to the physical salience of the stimulus. Endogenous attention is voluntarily directed towards a stimulus according to internal goals (Posner, 1980) and is therefore often referred to as top-down, or selective, attention. Selective attention, by filtering irrelevant and amplifying behaviourally relevant information, is an essential intervention between perception and action and is therefore critical for many aspects of human behaviour (e.g. learning, decision making and action selection).

Within a typical visual scene, attention can be directed towards a location in visual space (spatial attention) (Posner, 1980), an object (object-based attention) (Duncan, 1984) or feature (feature-based attention, e.g. colour or orientation) (Rossi and Paradiso, 1995). A further subdivision of attention can be made according to overt or covert attention (Posner, 1980; Posner et al., 1982). With overt attention, orientation towards the object of attention is achieved via explicit eye or head movements. During covert attention, on the other hand, attention is directed towards the stimulus without any overt movement that brings the object in the centre of gaze. Behaviourally, spatial cueing of a target stimulus results in faster reaction times (RT) (Posner, 1980) and increased perceptual sensitivity (Bashinski and Bacharach, 1980). In addition to these behavioural effects of

selective visual attention, attentional modulation of neural activity has been observed in various visual areas along the visuocortical hierarchy (Figure 1-1).

1.4.1 - Attentional modulation of firing rates

1.4.1.1 - Visual cortex

In one of the early studies to show attentional effects on neural activity, monkeys attended to one of two stimuli during a match-to-sample task whilst either one or both of the stimuli were placed inside the RF of V4 neurons (Moran and Desimone, 1985). Additionally, the stimuli were chosen such that one of the stimuli elicited a large response (effective stimulus) whereas the other was ineffective at driving cellular activity. With attention directed towards the effective stimulus, the cells had higher firing rates compared to when attention was directed towards the ineffective stimulus. This attentional modulation was not seen when only a single stimulus was presented inside the RF and attention was directed in- or outside of the RF. Moreover, this effect was not specific to V4, as comparable effects were found in IT.

Similar results were found by Motter (1993), who tested the responses of V1, V2 and V4 cells in an orientation discrimination task during which attention was directed towards or away from a bar stimulus inside the RF. Here, monkeys reported whether the orientation of the bar was left or right tilted. On some trials, the target was the only stimulus on the screen, but on the majority of trials 2-7 distractor stimuli were also presented. Roughly a third of recorded cells in all areas revealed attentional modulation, but most of these cells only showed modulation in the presence of distracting stimuli. In line with the idea that attention can selectively process specific information by filtering out distracting information, these early results thus suggested that attention mainly affected neuronal activity in visual cortex when there is competition between stimuli in the visual field. Qualitatively similar results, with larger attentional effects when multiple stimuli were presented, were found for area V2 and V4 (Luck et al., 1997) and area MT and MST (Treue and Maunsell, 1996). These findings (amongst others) led to the proposal of the biased competition model of attention (Desimone, 1998; Desimone and Duncan, 1995). In this framework, limited processing capacity leads to stimuli competing for resources through mutual inhibition. Attention can prioritise the processing of one (or several) of these stimuli (or their features) by introducing a bias in the representation of these stimuli, thereby selectively biasing the competition and preferentially processing the object of attention.

In the following years, investigations into the mechanism by which attention biases stimulus representations led to mixed results. Attentional modulation was found to differentially affect the response to different orientations, usually with larger effects for the preferred orientation in absolute terms, but not in relative terms. Specifically, relative to the non-attended condition, proportional changes were identical for all orientations (McAdams and Maunsell, 1999; Motter, 1993). This led to the hypothesis that attention multiplicatively scales the response of sensory neurons (with a constant

factor) by changing its response gain (Figure 1-2a), without changing its selectivity (McAdams and Maunsell, 1999). Other studies found attention to increase the response sensitivity by altering the contrast response function, i.e. increasing the contrast gain (Figure 1-2b) (Reynolds et al., 2000). Here, neurons specifically showed stronger responses to stimuli of lower salience, without affecting its response to highly salient stimuli. This type of attentional modulation leads to a leftward shift, rather than a multiplicative increase, in the contrast-response function. Additionally, feature-based attention has been found to multiplicatively increase the response gain as well as to simultaneously decrease activity to non-preferred stimuli, adding a suppressive component to the modulatory effects of attention (Martinez-Trujillo and Treue, 2004; Treue and Trujillo, 1999). The combination of these two effects can be described as a bimodal gain change (Figure 1-2c), increasing the response to preferred and decreasing the response to non-preferred stimuli (which sharpens the neural tuning function), and led to the formulation of the feature similarity gain model (Treue and Trujillo, 1999).

These different findings, describing varying modulatory effects of attention on neural activity gain changes, have later been incorporated into one normalisation model of attention (Lee and Maunsell, 2009; Ni et al., 2012; Reynolds and Heeger, 2009; Sanayei et al., 2015). In this framework, attention is not only considered to change the response gain of excitatory cells, but also of inhibitory cells. The inhibitory influence normalises the attention-induced increased excitation, but this normalisation is dependent on the stimulus size and the neural tuning function, as well as on the size of the attentional field. Variation in these parameters can reproduce the different effects of gain change described above (Reynolds and Heeger, 2009).

1.4.1.2 - Parietal and frontal cortex

Alongside these studies in visual cortex, others investigated the effects of attention in parietal and frontal areas (Figure 1-1), in particular in the lateral intraparietal area (LIP), frontal eye fields (FEF) and the dorsolateral prefrontal cortex (dlPFC).

Although the parietal cortex is classically seen as an integration and association area, fundamental to the combination of sensory, motor and cognitive information, its role in selective attention has long been relatively controversial. Central to this debate was the distinction between attention and intention, arguing that the parietal cortex is either primarily involved in attention-related processes (Colby and Goldberg, 1999), or that its main role is action-related to control motor output (Snyder et al., 2000). Here I discuss only a subset of the studies that have revealed the role of the parietal cortex in visual attention, but an extensive review of this debate can be found elsewhere (Freedman and Ibos, 2018).

Some of the first studies to show attentional modulation of activity in parietal cortex revealed that cells in area 7 showed stronger responses to stimuli that were viewed actively (reporting a luminance change) compared to when these stimuli were viewed passively (Bushnell et al., 1981). Later studies particularly focused on LIP, a subdivision

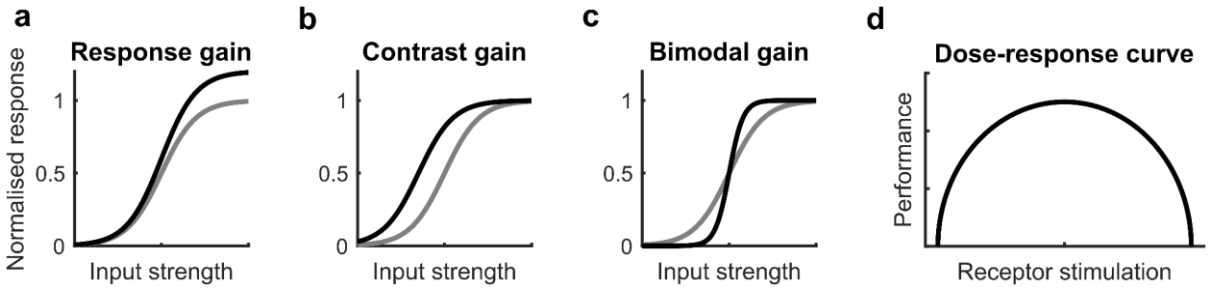

Figure 1-2. Neural gain and the neuromodulatory dose-response curve. The effects of a change in (**a**) response gain, (**b**) contrast gain or (**c**) bimodal gain on a neuron's output given a certain input. The grey and black curve represent the input-response curve before and after gain change, respectively. (**d**) Neuromodulatory dose-response curve. Optimal performance is achieved at intermediate levels of receptor stimulation.

of the posterior parietal cortex which lies in the intraparietal sulcus and receives input from thalamic nuclei and early visual areas (e.g. V4 and MT), sends projections to the superior colliculus and is reciprocally connected to frontal areas (e.g. FEF) (Blatt et al., 1990; Lewis and Van Essen, 2000; Patrick Hardy and Lynch, 1992). LIP neurons moreover have visual receptive fields (Blatt et al., 1990), and are involved in oculomotor control (Andersen et al., 1992). Their role in cognitive processes was established when neurons in LIP were found to display spatially specific delay-period activity during memory-guided saccade tasks (Gnadt and Andersen, 1988). In this task, the monkeys were briefly presented with a peripheral target stimulus during fixation. After a variable delay period, the monkey was required to make a saccade to the remembered location in order to obtain a reward. LIP neurons revealed working-memory related activity, showing spatially selective activity which persists throughout delay periods when all visual cues have been removed.

A further role in attention was underscored by the finding that LIP neurons respond selectively to task-relevant or salient stimuli (Gottlieb et al., 1998) and that their visual response is enhanced and sustained when task relevant features or locations are attended to (Bisley and Goldberg, 2010; Colby et al., 1996). These and other findings have led to the hypothesis that LIP acts as a priority map, where objects are represented by neural activity proportional to their behavioural relevance (Bisley and Goldberg, 2010; Thompson et al., 2005). Selective attention is thought to signal this priority by modulating the representation of visual space given by sensory input, filtering irrelevant and enhancing relevant information (Baluch and Itti, 2011; Reynolds and Heeger, 2009).

Similar to parietal areas, frontal areas such as the FEF and the dlPFC, that respectively lie posterior to or along the posterior end of the arcuate sulcus, are typically associated with the control of cognitive functions such as top-down attention and working memory (Buschman and Miller, 2007; Corbetta and Shulman, 2002). FEF and dlPFC activity reflects the relevance of task-related visual information, showing spatially selective activity which persists throughout delay periods when all visual cues have been removed (Armstrong et al., 2009; Funahashi et al., 1989).

Further support for the implication of these areas in attention and target selection comes from studies where direct activity manipulations have been performed. For instance, subthreshold microstimulation of either the FEF (Moore and Fallah, 2001) or the LIP

(Cutrell and Marrocco, 2002) influences behavioural performance on spatial attention tasks, and subthreshold microstimulation in dlPFC biases behaviour during saccadic choice tasks (Opris et al., 2005). Moreover, inactivation of the LIP (Wardak et al., 2004) or the FEF (Wardak et al., 2006) demonstrated that both areas play an important role in attentional selection at the behavioural level. These studies showed that LIP inactivation caused the largest behavioural deficits during difficult (low salience) tasks, while FEF inactivation resulted in deficits that were independent of task difficulty. These results mirror studies in humans which demonstrate that activity in parietal, but not FEF, increases with increasing attentional load (Culham et al., 2001). Similarly, inactivation of dlPFC resulted in deficits during a memory-guided, but not a visually-guided, saccade task (Sawaguchi and Iba, 2001), showing that dlPFC is particularly important for retaining information 'online' after visual stimulation has been removed. Furthermore, subthreshold microstimulation of the FEF enhances visually driven responses in lower visual areas (V4), revealing how feedback connections implement attentional enhancement of sensory signals in visual cortex (Moore and Armstrong, 2003). Importantly, subthreshold microstimulation of V4 neurons did not alter detection thresholds for luminance changes (Dagnino et al., 2015), suggesting that attentional control is regulated in higher-order areas. A specific role for the FEF in regulating visual areas during cognitive tasks is further underscored by the finding that nearly all cells that project from FEF to V4 show delay period activity during a memory-guided saccade task (Merrikhi et al., 2017). It is thus likely that feedback projections from higher areas provide the modulatory signals that alter visual stimulus representations in visual cortex.

Thus, their spatially tuned activity, causal involvement in cognitive functions such as attention, together with their strong interconnectivity (Blatt et al., 1990; Lewis and Van Essen, 2000; Selemon and Goldman-Rakic, 1988) and functional interdependence (Chafee and Goldman-Rakic, 2000), suggests that parietal and frontal areas form part of a network and jointly contribute to the attentional signals seen across visual and higher-order areas.

1.4.2 - Attentional modulation of response reliability and neuronal correlations

In addition to changes in firing rate, attention can also modulate the reliability of responses and the correlation structure of the neuronal population that represents the focus of attention. One often used measure of trial-to-trial firing rate variability is the Fano factor (FF), calculated as the ratio of the across-trial variance in the firing rates of a single neuron and its mean. Attention has been found to reduce FF (Cohen and Maunsell, 2009; Herrero et al., 2013; Mitchell et al., 2009, 2007; Rabinowitz et al., 2015), which together with neuronal gain increases can enhance a neuron's coding ability, leading to higher signal-to-noise ratios (Thiele and Bellgrove, 2018).

In addition to decreasing FF, attention also changes neuronal co-variability, termed noise correlations, that measure to what extent the trial-to-trial variability in neuronal

responses are correlated across pairs of neurons. Changes in the co-variability of a neuronal population can alter the amount of information that is encoded by this population. More specifically, neural coding is enhanced when neurons with highly similar tuning curves, i.e. high signal correlation, show a reduction in noise correlations, while neurons with low signal correlation show an increase in noise correlation (Abbott and Dayan, 1999; Averbeck et al., 2006; Panzeri et al., 1999). Here, the effect on coding can thus be investigated by determining the relationship (slope) between signal and noise correlation. Attention was indeed found to decrease noise correlations across pairs of neurons (Cohen and Maunsell, 2009; Herrero et al., 2013; Mitchell et al., 2009), which in several studies was additionally shown to depend on their signal correlation strength (Rabinowitz et al., 2015; Ruff and Cohen, 2014), revealing a decreased slope in the relationship between noise and signal correlation (Ruff and Cohen, 2014).

1.4.3 - Attentional modulation of corticocortical communication

Within a cortical area, attention can thus selectively in- and decrease firing rates and response reliability for specific neural populations, as well as modulate their neuronal co-variability. Recent studies have additionally investigated how information is transferred across areas (see section 1.2.4 - above) and how attention influences this communication.

Buschman and Miller (2007) recorded simultaneously from LIP and FEF/dlPFC in macaque monkeys during both a bottom-up and top-down attention task. Here, parietal neurons signalled the location of the target stimulus during bottom-up attention before frontal neurons, whereas this was reversed during top-down attention. Coherence between parietal and frontal areas was furthermore stronger in the gamma range during bottom-up stimulus processing, whereas it was stronger in the beta range during top-down attention. These results suggest that top-down attention is initiated in frontal cortex, after which other areas are recruited.

Attention has also been found to modulate synchronous activity between frontal and visual areas (Gregoriou et al., 2012, 2009). During simultaneous recordings in V4 and FEF in macaques, it was found that FEF firing rates distinguished between the direction of attention (towards or away from RF) before V4 (Gregoriou et al., 2009), in line with attentional signals being initiated in higher-order areas. Additionally, attention increased the between-area synchrony in the gamma frequency range (30-70 Hz), and conveyed directionally selective information from FEF to V4 as well as in the reversed direction. In line with the firing rate changes, attention specific granger causal interactions from FEF to V4 appeared earlier than those from V4 to FEF. Furthermore, attention also increased the between-area spike-field coherence, representing the alignment of spikes to the LFP phase, in both directions. Indicating that spikes in V4 were aligned to FEF LFP, and vice-versa. A follow-up study found that these effects were specific to certain cell categories in the FEF (Gregoriou et al., 2012). Cells were classified as visual, visuomovement and movement cells, of which only the visual cells showed synchronous activity with V4. Finally, lesions of frontal areas (FEF and dlPFC) both

delayed and reduced attentional modulation in V4, providing further support for a causal role of frontal areas in the control of attention (Gregoriou et al., 2014).

Bosman et al. (2012) recorded from multiple V1 and V4 locations in macaques using cortical surface electrodes during a top-down attention task. In this study, attention was directed to one of two stimuli placed inside a single V4 RF, each of which covered a separate V1 RF. The V4 location showed selective synchrony in the gamma frequency range with one of the two V1 locations, depending on which stimulus was attended, revealing retinotopically specific coherent activity between visual areas. Furthermore, gamma phase synchronisation between V1 and V4 was found to be predictive of behavioural performance (Rohenkohl et al., 2018). When attention was directed towards the RF, RTs were faster when coherence was strong. The phase relationship was, however, not predictive of RT during attend away conditions, suggesting a specific dependence of behavioural performance on attention-induced gamma synchronisation.

Finally, a more direct effect of attention on across area spiking co-variability has been described by Ruff and Cohen (2016a). In simultaneous recordings in macaque V1 and MT during a motion change detection task, attention was directed to one of two drifting gratings that each covered the RF of separate neurons in V1, but were both inside the MT RF. Although co-variability within each area was reduced with attention towards the RF, in line with previous studies (see section 1.4.2 - above), the co-variability between V1 and MT neurons was higher when attention was directed towards the RF. This effect was moreover dependent on the retinotopic location, rather than direction tuning, suggesting that attentional modulation of across area coordination is spatially determined. Lastly, it was found that microstimulation of V1 elicited more spikes in MT when attention was directed towards the RF, indicating that corticocortical communication is enhanced by attention.

1.4.4 - Attention and cortical state

As described above, switching from an inactive to an active state results in (widespread) desynchronisation of cortical activity. When attention is selectively directed towards the RF of the recorded neuronal population, this local area of the cortex desynchronises in a comparable manner to that seen during cortical state fluctuations, albeit on an overall reduced scale (i.e. less dramatically). Because of these similarities, it has been suggested that these functions rely on comparable underlying circuit mechanisms (Harris and Thiele, 2011). Indeed, both cortical state fluctuations and selective attention have been found to (partially) depend on neuromodulator availability (see below) as well as feedback from higher-level cortical areas. Both attentional engagement and cortical state fluctuations, in turn, are likely to influence perceptual decision making through their effects on sensory processing and evidence accumulation.

Although much has been learned over the last 40 years since Posner conducted his studies on visual attention in human subjects, the exact mechanisms by which attention elicits the activity changes observed throughout the network of brain areas described

above are largely unknown. Similar to cortical state fluctuations, attentional modulation has been proposed to be regulated by input from subcortical structures such as the LGN (O'Connor et al., 2002), superior colliculus (Krauzlis et al., 2013) and pulvinar (Petersen et al., 1987), feedback projections (Buschman and Miller, 2007; Desimone and Duncan, 1995; Gregoriou et al., 2014, 2012, 2009; Merrikhi et al., 2017; Moore and Armstrong, 2003; Noudoost and Moore, 2011a) and/or neuromodulatory drive (Clark and Noudoost, 2014; Herrero et al., 2008; Noudoost and Moore, 2011a, 2011b; Thiele and Bellgrove, 2018). Indeed, although neuromodulators are increasingly implicated in cognitive functioning, their influence on specific signatures of attentional processes is poorly understood.

1.5 - **Decision making**

During decision making, information from the external world, previous experience and current cognitive state is combined and evaluated in the formation of an action plan. This high-level process relies heavily on other cognitive functions such as attention and working memory, and is a crucial part of animal and human interaction with their environment. Perceptual decision making can generally be subdivided in multiple information processing stages consisting of sensory encoding (of often noisy information), decision formation, motor execution and choice evaluation (Doya, 2008; Gold and Shadlen, 2007; Kelly and O'Connell, 2015). Although there is substantial evidence for a neuromodulatory influence during reinforcement learning and reward processing (Cox and Witten, 2019; Doya, 2008; Schultz, 1998), here I mainly focus on the neural mechanisms underlying sensory encoding and in particular decision formation and how processing variability can lead to variability in behaviour.

Decision formation, during which information is collected and evaluated, acting as the translation from perception (and cognition) into action, has received much interest (Gold and Shadlen, 2007). Decision formation can be further subdivided into multiple components, including the accumulation and evaluation of evidence, setting a threshold that indicates when sufficient evidence has been collected, and the selection of the appropriate motor response. In this framework, evidence accumulation depends on the sequential sampling of momentary evidence of which the integration is represented into a single total, the decision variable (DV), that represents the evidence in favour of a certain choice (Kelly and O'Connell, 2015; Smith and Ratcliff, 2004). Evidence accumulation is terminated when the DV exceeds a threshold, which allows commitment to a categorical choice.

Whereas sensory areas represent the momentary evidence, parietal and frontal areas have been shown to represent the DV, representing the cumulative evidence in favour of a certain choice during perceptual decisions (Gold and Shadlen, 2007; Kelly and O'Connell, 2015). For example, neurons in area MT respond strongly during a motion discrimination task (Albright, 1984) and microstimulation of MT biases direction discrimination (Salzman et al., 1990), revealing their direct involvement in decision making as the source of sensory evidence.

Neural correlates of the DV have been found across oculomotor areas, such as the parietal (Platt and Glimcher, 1999; Roitman and Shadlen, 2002; Shadlen and Newsome, 2001), frontal (Ding and Gold, 2012; Kim and Shadlen, 1999) as well as subcortical areas such as the superior colliculus (Horwitz et al., 2004). Neurons in LIP, for example, reveal a gradual build-up of activity during motion discrimination that depends on stimulus strength (Platt and Glimcher, 1999; Roitman and Shadlen, 2002; Shadlen and Newsome, 2001), although this has recently been debated (Latimer et al., 2016, 2015; Shadlen et al., 2016). When aligned to the response, this activity reaches a fixed level approximately 50-100 ms prior to saccade onset (Roitman and Shadlen, 2002). Furthermore, during studies that used discrete epochs wherein stimulus shapes conferred a fixed amount of evidence, LIP neurons revealed stepwise in- or decreases directly proportional to the amount of evidence (Kira et al., 2015; Yang and Shadlen, 2007).

Additionally, both microstimulation as well as optogenetic stimulation in LIP can bias choices (Dai et al., 2014; Hanks et al., 2006), and inactivation of LIP leads to strong behavioural decrements (Zhou and Freedman, 2019), confirming LIP's causal role during perceptual decision making. In addition to firing rate changes following the presentation of sensory evidence, firing rate variability in sensory (Britten et al., 1996; Shadlen et al., 1996; Yates et al., 2017), as well as parietal areas (Shadlen and Newsome, 2001; Yates et al., 2017) influences choices and reaction times during motion discrimination. Here, when presented with the same sensory information (even without any net motion), both neural activity and behavioural performance varies. This suggests that endogenous variability in neural activity determines, in part, the behavioural response to sensory evidence.

Recent developments have made it possible to study the DV, in addition to multiple other components of decision making, using EEG in humans (Kelly and O'Connell, 2013; O'Connell et al., 2012). In these studies, the task paradigm was adjusted such that sudden transients in the visual stimulus were absent. This allowed the investigation of gradual activity changes over parietal cortex that exhibited some of the same characteristics as the DV in single cell electrophysiology, termed the centroparietal positivity (CPP) (Kelly and O'Connell, 2013; O'Connell et al., 2012). Additionally, this allowed investigation into which (and how) other information processing stages influence sensory evidence accumulation. For example, deflections over sensory cortex that reflect the selection of target stimuli can modulate the onset and build-up rate (rate of evidence accumulation) of the CPP (Loughnane et al., 2016). Moreover, endogenously fluctuating levels of attentional engagement, indexed by pre-target occipital α-band activity, correlates strongly with the build-up rate of the CPP (Kelly and O'Connell, 2013). Lastly, pre-target occipital α-band activity and RT were modulated by exposure to blue light before the experiment, thought to influence (noradrenaline-related) arousal (Newman et al., 2016). These results suggest that the speed and reliability of decision making to some degree relies on (endogenous) variability in attentional engagement, cortical state and neuromodulator availability. The full extent of their effects on separate stages of the decision making process is, however, largely unknown.

1.6 - **Neuromodulators**

Neuromodulators are assumed to affect single neuron and local network excitability in systematic ways. Rather than processing the content of (sensory) information, neuromodulators can influence neuronal functioning by modulating responsiveness to excitatory and inhibitory inputs (Berridge and Waterhouse, 2003; Winterer and Weinberger, 2004). In other words, they can 'tune' neural activity. One way through which these modulatory effects are hypothesised to occur is through neural gain regulation (Servan-Schreiber et al., 1990). Neural gain regulates a neuron's sensitivity by controlling the input-output function of a cell (Figure 1-2) and is a nonlinear, multiplicative way to combine or integrate information (Salinas and Sejnowski, 2001a; Silver, 2010). Via their effects on neural gain and excitability, neuromodulators can implement moment-by-moment changes in synaptic strength according to behavioural demands without making changes to the underlying anatomical connections (Arnsten et al., 2012; Thiele and Bellgrove, 2018). As described above, cognitive functions such as attention rely on gain modulation of neural responses to preferentially process specific sensory input (Martinez-Trujillo and Treue, 2004; Reynolds et al., 2000; Treue and Trujillo, 1999). Correspondingly, modelling studies where gain regulated neurons represent visual object locations have been able to mimic neglect, a pattern of cognitive symptoms typical after parietal lesions (Posner et al., 1984), by systematically removing nodes from the network (Salinas and Sejnowski, 2001a).

Neural manifestations of attentional gain changes are present in several areas along the visual hierarchy. Chen et al. (2008) found that neural activity in early visual cortical area V1 was strongly modulated by varying the difficulty, and thereby attentional demands, of various visual detection tasks. Similar results of modulations of neural activity by attention and task difficulty have been found for areas higher up the hierarchy, such as visual area V4 (Spitzer et al., 1988), the inferotemporal cortex (Spitzer and Richmond, 1991) and the frontal cortex (Bichot et al., 2001; Thiele et al., 2016). Whether these (multiplicative) changes in neural activity are facilitated by neuromodulators is currently unknown. There are, however, indications of changes in neural excitability elicited by the application of neuromodulators that suggest their direct involvement in neural gain changes that affect for instance signal-to-noise ratios (Oades, 1985), and that could explain (part of) their effects on cortical state (Harris and Thiele, 2011) and selective attention (Herrero et al., 2008; Thiele et al., 2012; Thiele and Bellgrove, 2018). Although little is known about neuromodulatory influences during specific stages of perceptual decision making, the reliance of decision making on cognitive functions such as attention and working memory, as well as its relationship with specific pupil diameter measures (see below) suggest a strong modulatory influence during perceptual decision making.

Here, I focus on the role of neuromodulators during attention and cortical state fluctuations, but also draw on studies that have investigated their effects during other cognitive functions such as working memory (in which specific information is kept 'online' for a short period of time), as the neural mechanisms supporting those functions are likely involved in selective attention as well. Specifically, I will discuss the

contribution of the catecholamines dopamine and noradrenaline as well as acetylcholine to the neural mechanisms that subserve selective attention and cortical state. Although other neuromodulators such as 5-hydroxytryptamine (5-HT, serotonin) are also involved in cortical state changes and selective attention (Harris and Thiele, 2011; Thiele and Bellgrove, 2018), their relationship to the measures of cortical state discussed in this thesis (e.g. pupil diameter, see below) is less well-described and will therefore not be discussed in detail.

1.6.1 - Catecholamines

Catecholamines (CA) are tyrosine amine derived hormones and neurotransmitters. Of the latter, dopamine (DA) and noradrenaline (NA) are most often associated with cognitive functions. Cortical areas receive dopaminergic projections from the ventral tegmental area (VTA) and the substantia nigra (SN), whereas noradrenergic inputs originate in the locus coeruleus (LC) (Figure 1-1) (Levitt et al., 1984; Loizou, 1969; Mark Williams and Goldman-Rakic, 1998; Porrino and Goldman-Rakic, 1982; Williams and Goldman-Rakic, 1993). Importantly, stimulation of rat LC increases both NA and DA release in parietal and frontal cortices (Devoto et al., 2005), possibly through co-transmission of DA in NA neurons (Devoto and Flore, 2006).

CA, and especially NA, were originally thought to be involved in rather general and unselective processes (e.g. arousal) due to their unselective projections in rodents. Regional and laminar specific afferents of CA projections in primates however suggested their involvement in more selective cognitive processes (Levitt et al., 1984). Both neurotransmitters act on metabotropic receptors, and influence the production of, for instance, the second messenger cyclic adenosine monophosphate (cAMP) and have widespread effects throughout the brain such as reward processing (DA) and arousal (NA). In addition, both have been implicated in more selective processes such as working memory, rule based decision making, and attentional processes (Arnsten, 1998; Noudoost and Moore, 2011a, 2011b; Ott et al., 2014; Ott and Nieder, 2019; Thiele and Bellgrove, 2018; Williams and Goldman-Rakic, 1995).

DA and NA receptor stimulation follow a non-linear dose response function (Figure 1-2d). DA stimulation follows an inverted-U dose response, whereby too little or too much stimulation produces suboptimal performance (Arnsten, 1998; Vijayraghavan et al., 2007; Zahrt et al., 1997). Likewise, NA stimulation in small doses improve, whereas higher doses decrease cognitive abilities (Arnsten, 1998; Aston-Jones et al., 1999; Aston-Jones and Cohen, 2005a). Furthermore, genetic variation in a polymorphism of the catechol O-methyltransferase (COMT) gene, an enzyme regulating central CA levels by inactivating CA neurotransmitters, correlates both with behaviour and blood oxygenated level dependence (BOLD) during a planning task (Williams-Gray et al., 2007). Specifically, significantly slower reaction times and lower BOLD activity in frontal and parietal regions were found in participants with genotypes leading to lower COMT activity, and thus higher available CA levels, compared to participants with genotypes expressing higher levels of COMT. Dependent on available baseline levels of DA and NA,

cognitive function may thus improve or decrease after administration of additional CA receptor agonists and antagonists.

Finally, a role for catecholamines during perceptual decision making comes from human studies that have investigated the P3, a parietal target detection signal that is closely related to the CPP and reflects evidence accumulation (Twomey et al., 2015) and has additionally been hypothesised to reflect the NA phasic response upon target selection (see section 1.6.1.2 - below) (Nieuwenhuis et al., 2005). Administration of methylphenidate or atomoxetine, two drugs that increase monoamine levels and thereby increase DA and NA availability, decreases RTs in a target detection task (Loughnane et al., 2019). This behavioural benefit was mediated by the build-up rate and peak latency of the P3, suggesting specific CA effects on evidence accumulation.

1.6.1.1 - Dopamine

DA acts on several subclasses of dopaminergic metabotropic receptors in the brain (D1-D5). The D1 and D5 receptors are typically classed as D1-type receptors (D1R), while D2, D3 and D4 are classed as D2-type receptors (D2R), based on similarities in their functioning (Missale et al., 1998; Seamans and Yang, 2004). The dosage of DA and the location (e.g. pre- or postsynaptic) of its receptors on the neuron determine, in part, their role and efficiency in modulating activity. Optimal stimulation of DA receptors has been hypothesised to stabilize neural activity, making it more robust to distracting stimuli, possibly through the increase and/or maintenance of GABAergic (Gamma-aminobutyric acid) receptor currents (Durstewitz et al., 2000), or by changing the synaptic strength through stimulation of N-Methyl-D-aspartate (NMDA) receptors (Arnsten et al., 2012; Flores-Hernandez, 2002). On the other hand, over stimulation could produce a situation where neural activity is overly stable and inflexible, or where activity is diminished due to excess inhibition, thereby reducing performance (Durstewitz et al., 2000).

In a cued target detection task, Clark and colleagues (1989) studied the effects of intravenously administering droperidol, a D2R antagonist, and clonidine, an α2-AR agonist (see below), on behavioural performance in humans. Overall, droperidol significantly slowed RTs, and although it had no effect on the benefit of valid cueing it decreased the relative cost of invalid cueing. This difference between valid and invalid cueing shows that DA does not unselectively increase reaction times. Instead, because it does not increase the benefit of valid but does decrease the cost of invalid cueing, D2R might be involved in attentional switching rather than engagement. A specific involvement of D1R was suggested by Müller et al. (1998). During a delayed match to sample task, oral administration of the drug pergolide, an agonist for both D1R and D2R, resulted in reduced error rates in human subjects. These effects were thought to be specific to D1R, as administration of the D2R agonist bromocriptine did not produce any changes in performance (Müller et al., 1998), suggesting that D1R is involved in working memory performance. Further evidence for dopaminergic involvement in attention comes from genetic studies. Newman et al. (2014) found that common deoxyribonucleic

acid (DNA) variations in DA transporter genes, regulating available DA levels, predicted distractibility during selective attention tasks in humans (Newman et al., 2014). In these studies, however, dopaminergic effects could not be ascribed to particular brain regions because neural activity was not measured and drug administration or genetic distinctions resulted in systemic differences in dopamine levels, rather than one localised to a specific brain region.

Several previous studies have investigated drug effects by directly applying them to a specific brain area. Sawaguchi and Goldman-Rakic (1991) applied D1R antagonists to the dlPFC while monkeys performed a memory-guided saccade task. In this task the animals had to fixate centrally while a peripheral target stimulus was presented for a short period of time. Without breaking fixation, the monkeys had to remember the target location after the stimulus was turned off, subsequently a 'go-signal' was given by removing the fixation spot and the monkeys were required to saccade towards the location where the target had previously been. Injection of these antagonists produced reversible deficits in behaviour for a few specific target locations, and because control tasks excluded visual or motor deficits these findings implicated D1R in attention/working memory processes. Furthermore, the degree of task difficulty correlated with the degree of impairment brought about by the application of the drug (Sawaguchi and Goldman-Rakic, 1994), suggesting a role in neural gain modulation. In addition to working memory, during decision making in a free choice saccade task, where the monkey is rewarded for executing a saccade towards either of two targets, administration of a D1R antagonist (SCH23390) or a D2R agonist (quinpirole) in the FEF increased the tendency of the monkey to choose to saccade towards a target in the receptive field (Noudoost and Moore, 2011a).

Other studies also investigated cellular effects of DA in awake behaving animals. Local iontophoretically administered D1R and D2R agonists altered simultaneously recorded firing rates of nearby cells in frontal cortex (Williams and Goldman-Rakic, 1995). Upon application of a D1R antagonist, cell firing in its preferred direction increased during the memory period of the task, which was reversed by the application of a D1R agonist. Unlike the specific neural and behavioural effects of D1R blockage (Sawaguchi and Goldman-Rakic, 1991; Williams and Goldman-Rakic, 1995), application of D2/3R antagonists in the frontal cortex produced general inhibitions in firing rates, seemingly unrelated to task performance (Williams and Goldman-Rakic, 1995). This could suggest that the D1R mediates attentional changes in neural gain. Indeed, the modulation by D1R antagonists followed an inverted-U dose response curve, implying the need for a delicate balance of DA for optimal performance.

Additional to the effects of D1R stimulation, Ott et al. (2014) found effects on more abstract rule-based decision making by stimulating D1R or D2R with the specific D1R agonist (SKF81297), antagonist (SCH23390) or D2R agonist (quinpirole) in the prefrontal cortex. Monkeys compared the number of dots by judging whether there were more or less in a test versus a sample stimulus. The specific rule, less or greater than, within a given trial depended on the cue presented between the sample and test stimulus. Because cues from different sensory modalities were used to indicate the same rule and

cues from the same modality were used to indicate different rules, neural activity related to specific physical properties of the cue was dissociated from the rule that it represented. Ott et al. (2014) found that the application of both the D1R and D2R agonist increased the differentiation between the neural representations for the preferred over the non-preferred rule, whereas this difference was decreased by administration of the D1R antagonist. Interestingly, D1R and D2R stimulation influenced rule coding in a different manner. Although both similarly increased the difference in the representation of preferred versus non-preferred rule coding, D1R stimulation increased the responses to the preferred rule, whereas D2R stimulation decreased the responses to the non-preferred rule. In this study, the pattern of DA stimulation thus resembled the bimodal gain change depicted in Figure 1-2c. These results show that D1R and D2R have complementary roles in enhancing the neural representation of rule-based decision making and that DA influences executive cognitive functions.

DA can have both excitatory and inhibitory effects, depending on the type of cell that is targeted. During a working memory paradigm, Jacob et al. (2013) iontophoretically released DA in the lateral prefrontal cortex whilst recording from nearby neurons. DA selectively inhibited fast-spiking and excited broad-spiking cells. Cells that were differently affected by the application of DA were moreover found to process visual stimuli on different temporal scales. Cells that were inhibited by DA showed fast visual responses and their firing rates were affected quickly after DA application. On the contrary, cells that were excited by DA responded to visual stimuli on a slower timescale and reached peak modulation by DA only after several minutes. By differently targeting distinct cell types on different time scales, DA is in the unique position to modulate the flow of information after stimulus presentation.

Finally, the administration of DA in one area can also exert effects on other areas up- or downstream along the visual pathway (Noudoost and Moore, 2011a). Indeed, administration of a D1R antagonist (SCH23390), but not a D2R agonist, in the frontal eye fields (FEF) enhanced orientation selectivity, response magnitude and response reliability in area V4, comparable with the effects of top-down attention (Noudoost and Moore, 2011a). However, as acknowledged by the authors, these studies do not exclude the possibility that these signals stimulate other areas (e.g. LIP), i.e. the effects might not be direct, but instead mediated by other structures. As mentioned above, almost all FEF neurons that provide feedback to V4 reveal delay-period activity during working memory tasks (Merrikhi et al., 2017). It therefore seems likely that D1R stimulation in FEF influences attention-related V4 activity by modulating sensory input (Noudoost and Moore, 2011a) through modulation of cells that show delay period activity. Indeed, D1R expression is higher in supragranular layers, where most feedback projections originate (Markov et al., 2014), compared to infragranular layers (Mueller et al., 2019). D2R, on the other hand, might be more involved in regulation of motor output (Soltani et al., 2013).

From the above studies it becomes clear that both D1R and D2R play a role in attentional processes. On a cellular level DA has selectively been investigated in the context of frontal/prefrontal functioning, often based on the argument that dopaminergic receptor density in other regions such as the posterior/parietal cortex is rather sparse. However,

this notion was derived from rodent data, while in primates DA innervation is comparatively strong, matching that of many primate prefrontal areas (Berger et al., 1991; Lewis et al., 1988).

As opposed to acetylcholine and noradrenaline (see below), dopamine has not been described as a main driver to influence cortical state fluctuations (Harris and Thiele, 2011; Lee and Dan, 2012). Several studies, however, suggest a modulatory role for dopamine in controlling cortical state. Bath application of dopamine increases the excitability of pyramidal cells as shown by intracellular membrane potential recordings in rodent (Yang and Seamans, 1996) and in primate (Henze et al., 2000) prefrontal cortex (PFC) slices. Excitability was specifically enhanced by lowering action potential thresholds, increasing firing to a depolarising current step, and decreasing inter-spike-intervals. This enhancement is mediated by D1R, as application of D1R-antagonist SCH23390, but not D2R-antagonist sulpiride, prevented the increased excitability (Henze et al., 2000). Furthermore, intracellular recordings in rats have revealed that stimulation of VTA, but not hippocampal or thalamic afferents, increases the duration of cortical up-states of medial or orbital PFC pyramidal cells (Lewis and O'Donnell, 2000). Again, this effect was mediated by D1R, as systemic injections of SCH23390 prevented the modulation of up-state durations.

1.6.1.2 - Noradrenaline

LC has two main modes of activity, a tonic continuously firing mode and a phasic bursting mode (Usher et al., 1999). Together these modes reveal a close relationship to arousal (Foote et al., 1980) and behavioural performance during sensory detection tasks (Aston-Jones, 1985; Aston-Jones et al., 1994; Aston-Jones and Bloom, 1981; Clayton, 2004; Rajkowski et al., 2004, 1994; Usher et al., 1999). They have been hypothesised to adaptively adjust the gain of widespread cortical circuits, thereby facilitating or disengaging from task-specific processes (Aston-Jones and Cohen, 2005a). With low tonic activity, performance is low because of drowsiness or inattentiveness, and with high tonic activity, performance is low because the subject is in a distractible (or inflexible) behavioural state. Both during low and high tonic activity, phasic responses to target stimuli are small or largely absent. On the other hand, with intermediate tonic activity phasic responses to target stimuli are prominent and behavioural performance is accurate (Aston-Jones et al., 1994). Tonic LC activity, reflecting arousal, has therefore been suggested to follow the Yerkes-Dodson law (Yerkes and Dodson, 1908), which proposed that arousal and performance follow an inverted-U relationship.

NA acts on 3 receptor families: alpha-1, alpha-2 and beta-adrenergic receptors (α1-AR, α2-AR, β-AR), of which there are several subtypes (e.g. alpha-2A, alpha-2B, etc.) (Arnsten, 1998). These subclasses of receptors, depending on their location and dosage, often have opposing effects on cellular activity and cognitive functioning (Arnsten, 1998; Thiele and Bellgrove, 2018). Whereas α1-AR stimulation generally causes excitation, stimulation of α2-AR causes inhibition and β-AR stimulation increases excitability (Berridge and Waterhouse, 2003; Devilbiss and Waterhouse, 2000; Thiele and Bellgrove,

2018). This opposing functionality of different receptor subtypes, in addition to their different affinities for NA, could explain the inverted-U shaped relationship between NA levels and performance (Arnsten, 1998; Aston-Jones and Cohen, 2005a; Thiele and Bellgrove, 2018). Lower levels of NA might engage the higher affinity α2-AR, improving working memory performance (see below), whereas higher levels of NA can additionally engage the lower affinity α1-AR, impairing task-related performance (Arnsten, 2011, 1998; Aston-Jones and Cohen, 2005a; Thiele and Bellgrove, 2018). Given the spread and abundance of NA terminals throughout the brain, NA is capable of acting on and modulating vast numbers of distributed cellular populations (Séguéla et al., 1990), and is therefore in a unique position of modulating cognitive behaviour. NA receptors most often associated with cognitive functions such as working memory are postsynaptic α-2A-adrenoceptors (α2A-AR) (Arnsten, 1998).

Cellular evidence of the association of NA in attentional processes comes from extracellular recordings of the LC (Aston-Jones and Cohen, 2005b). Aston-Jones et al. (1994) investigated LC neural activity in monkeys performing an oddball discrimination task, testing their ability to detect and respond to unpredictable and infrequent target cues embedded amongst distractor stimuli. LC neurons showed selective phasic activity after target presentation, but did not respond to distractor presentation, fixation spot onset, lever presses or juice rewards. Moreover, when switching the stimuli used for target and distractor, the target response profile reversed and neurons became selectively active for the new target stimuli (Aston-Jones et al., 1997, 1994). These results show that LC selectively responds to task-relevant stimuli, ignoring non-targets.

Alongside phasic responses, variations in tonic activity predicted variations in behavioural performance (Rajkowski et al., 1994). During periods of poor behaviour, the monkey could less reliably distinguish between targets and distractors, and the tendency to respond to any stimulus increased. This behavioural variation correlated with LC phasic response magnitude, during periods of high performance the onset of LC phasic activity correlated strongly with the timing of the behavioural response (Aston-Jones et al., 1994). Indeed, Clayton et al. (2004) found the LC activity to be more tightly coupled to the behavioural response than to the presentation of the target stimulus. Thus, an important characteristic of phasic LC activity is that its timing and widespread projections allows for fast acting effects on distributed brain regions and behaviour, influencing the stimulus-response relationship within the same trial. Thus, task-related decision processes may be facilitated by phasic LC firing whereas a lack of phasic responses, also characterised by higher tonic activity, helps to disengage from the task at hand and explore other options (Aston-Jones and Cohen, 2005b). This task (dis)engagement due to variations in tonic LC activity could be related to the variations in neural gain that lead to differences in task strategy (Eldar et al., 2013). Indeed, in a model of LC activity, phasic and tonic modes were mimicked solely by varying interaction strengths between LC neurons (Usher et al., 1999). Their output directly determined the neural gain of other nodes in the network, which reproduced all the behavioural signatures described above.

In a cued target detection task, clonidine, an α2-AR agonist, has similar effects (see section 1.6.1.1 - above) on spatial attention as droperidol (Clark et al., 1989), it did not show an effect on the benefit of valid cueing but it decreased the cost of invalid cueing. This result implicates both CA in the disengagement or the shifting of attention. Similar effects of disengagement and orienting of attention have been found in patients with parietal, but not with frontal, midbrain or temporal lesions (Posner et al., 1984). These two findings, taken together, potentially implicate CA in the parietal cortex in these attentional processes. In addition to spatial cues, Coull et al. (2001) also used temporal cueing in a visuospatial orienting task while subjects were administered with clonidine or guanfacine, both α2-AR agonists. After the administration of clonidine, but not guanfacine, impairments in the behavioural alerting effect and temporal attentional orienting were found. Moreover, clonidine speeded reaction times to invalidly cued targets in the spatial orienting task compared to placebo. Indicating that attentional focus was not just directed towards the target but also towards the distractors, facilitating attentional shifts. In addition to an effect on distractor suppression, clonidine also attenuated BOLD activity in the parietal cortex during spatially, but not during temporally cued trials, implicating α2-AR in parietal cortex in spatial distractor suppression.

Because both guanfacine and clonidine act upon α2-AR it was unexpected that guanfacine did not affect behavioural performance (Coull et al., 2001). According to the authors, this could be caused either by the use of an insufficient dose of guanfacine to alter NA activity or it could be due to differences in the affinities of the drugs for different receptor subtypes. Arnsten et al. (1988) reported a similar dissociation between different α2-AR agonists, albeit of opposite sign. They tested the effects of 3 separate α2-AR agonists (clonidine, guanfacine and B-HT920) on delayed memory performance of aged monkeys and found stronger and longer lasting effects using guanfacine compared to the other drugs. Interestingly, the in- or decrease in behavioural performance was dose-dependent for all drugs tested, but showed opposite signs across them. Whereas with little, intermediate and large amounts of drugs, performance respectively decreased, increased and decreased for clonidine and B-HT920. Guanfacine, although also acting on the α2-AR, showed the opposite relationship, possibly by acting on different α2 receptor subtypes or because of differences in its effect on pre- or postsynaptic receptors (Arnsten et al., 1988). Thus in- or decreases of α2-AR stimulation is associated with task-related changes in behaviour as well as functional magnetic resonance imaging (fMRI) activity. The effects of these drugs on the BOLD response in specific brain areas cannot, however, unquestionably be attributed to effects occurring within these areas themselves. As, for example, an effect of these drugs on the input signals to these areas may have brought about the observed changes in activity. The only way to elucidate the role of a neurotransmitter within an area is to administer the drug directly to this region.

Cellular effects of NA during cognitive tasks have focused on the effects of α2-AR during working memory (Li et al., 1999; Wang et al., 2007). Both systemic and local administration of α2-AR agonist clonidine increases dlPFC firing during a delayed response task. This effect was reversed by local iontophoretic application of α2-AR

antagonist yohimbine, confirming the local noradrenergic effect on α2-AR (Li et al., 1999). In an elegant series of experiments, Wang et al. (2007) revealed that stimulating α2A-AR promoted spatial mnemonic firing of frontal neurons in a dose-dependent manner. Interestingly, similar effects were found by blocking hyperpolarisation-activated cyclic nucleotide-gated (HCN) channels. Low doses of HCN antagonists improved direction selective firing, slightly higher levels improved selectivity but also increased overall firing rates, whereas higher levels impaired or did not affect cognitive function. Because α2A-ARs are thought to affect endogenous levels of cAMP which in turn affects the opening and closing of HCN channels, the authors next investigated the effects of both inhibition and amplification of cAMP levels and found in- and decreased delay related firing for the preferred direction of the cell, respectively. This suggested inhibitory effects of α2A-ARs on cAMP production, which blocks HCN channels. Indeed, either amplification of cAMP actions or blocking HCN channels reversed the effects of the application of α2A-AR agonists and antagonists. Altogether, these results show that NA affects working memory functioning, by altering cAMP mediated HCN channel function in frontal cortex.

In addition to the role of NA in arousal, goal-directed behaviour, and likely also selective attention (described above) NA has been found to influence specific signatures of cortical state. Direct stimulation or inhibition of LC respectively induces cortical depolarisation and desynchronisation or hyperpolarisation and synchronisation of frontal cortex in rats (Berridge and Foote, 1991; Berridge et al., 1993). Furthermore, local application of NA drugs can induce changes in neural activity associated with cortical state changes.

Constantinople et al. (2011) described the effects of anaesthesia and wakefulness on rat barrel cortex Vm. During anaesthesia, barrel cortex Vm displayed prolonged periods of synaptic quiescence alternated with short 'up-state' periods of increased activity during which Vm was more depolarised and desynchronised. Consequently, Vm displayed a bimodal distribution during anaesthesia. Similar to the activity during up-states, transitioning from the anaesthetised to the awake state eliminated the synaptic quiescence and induced a depolarised and desynchronised Vm. Local application of ACh (see section 1.6.2.1 - below) and NA markedly affected the effects of wakefulness on Vm. Infusion of various concentrations of NA α1, α2 or β antagonists (prazosin, yohimbine and propranolol, respectively) prevented cells from achieving prolonged depolarisation, under both anaesthesia and wakefulness, and resulted in bimodality of cortical Vm during wakefulness. Similarly, Polack et al. (2013) investigated the role of ACh (see section 1.6.2.1 - below) and NA in the changes elicited by locomotion on neuronal (network) activity in mouse V1. During locomotion, compared to stationary periods, the LFP and Vm were more depolarised, desynchronised, and showed less variability. Blocking NA activity through local injections of both low and high doses of α1, α2 and β noradrenergic receptor antagonists (prazosin, yohimbine and propranolol, respectively) led to Vm hyperpolarisation and it strongly decreased spontaneous variability and firing rate. Moreover, it abolished the depolarisation associated with locomotion. These

studies thus revealed a crucial role for NA in state-associated modulation of neuronal activity.

1.6.2 - Other neuromodulators

1.6.2.1 - Acetylcholine

Acetylcholine (ACh) is present both in the peripheral and central nervous system and acts on two receptor types, the ionotropic/nicotinic (nACh) and metabotropic (mACh) ACh receptor (Thiele, 2013). The cortex receives cholinergic projections from the nucleus basalis (NB), located inside the basal forebrain (BF) (Thiele, 2013). Both receptor types, but especially the mACh, have been implicated in cognitive functions such as attention and working memory (Levin and Simon, 1998a; Warburton and Rusted, 1993). There are various subtypes of the nACh receptor, composed of numerous possible arrangements consisting mainly of different α and β subunits (Dani and Bertrand, 2007). There are five subtypes of the mACh receptor (M1-M5), with M1, M2 and M4 most abundant in cortex, that subdivide into M1-type (M1, M3 and M5) and M2-type (M2 and M4) receptors, based on the family of G-proteins they interact with (Thiele, 2013).

Similar to NA and DA, ACh was originally implicated in relatively unspecific functions, such as the sleep-wake cycle and arousal, affecting brain-wide activity (Everitt and Robbins, 1997). However, lesion studies (Voytko et al., 1994) and systemic drug manipulations (Witte et al., 1997) in monkeys suggested their more specific involvement in cognitive functions such as attentional orienting. More specifically, nACh stimulation decreased the validity effect, the benefit in behavioural performance obtained from being validly cued to a spatial location, whereas mACh blockade (atropine) mainly affected alerting effects by decreasing the benefit obtained from being presented with a temporally (non-spatial) informative cue (Witte et al., 1997). Furthermore, systemic injection of mACh antagonist scopolamine affects attentional orienting in monkeys (Davidson et al., 1999). These orienting effects might be driven by parietal cortex, as the local infusion of scopolamine slowed attentional orienting, with stronger effects for the region of visual space affected by the drug administration (Davidson and Marrocco, 2000).

Cholinergic modulation of attention is furthermore bidirectional, inhibiting cholinergic functioning can decrease behavioural performance whereas stimulation can increase performance (Furey et al., 2008). Here, human subjects performed a task in which face and house stimuli were to be discriminated (matching task) in small blocks of five to seven trials. Overall, subjects displayed a bias to face stimuli, as reaction times were faster when attention was directed to faces compared to houses. Systemic injections of anticholinesterase physostigmine (reuptake inhibitor) improved task performance especially when attending to house stimuli. Scopolamine, on the other hand, reduced performance when attending to face stimuli. Because face stimuli were preferentially processed, this indicated that ACh can selectively modulate the ability to attend to houses (and suppress salient distracting information) and thus suggests that ACh

influences stimulus processing both through stimulus-driven and goal directed mechanisms. Additionally, as these effects were stronger during the later trials of the block, rather than the first trial after switching attention from face to house stimuli or vice-versa, ACh was thought to affect the maintenance of attention, rather than attentional switching (Furey et al., 2008). Furthermore, temporally precise phasic transients of ACh in prefrontal cortex aid cue detection during attention tasks in rats (Parikh et al., 2007). Deafferentation of cholinergic inputs to PFC can moreover reduce behavioural performance during attention in rats (Parikh et al., 2007) and spatial working memory in monkeys (Croxson et al., 2011). The increased ACh in frontal cortex with attention is further amplified by making the task more challenging with the introduction of distracting stimuli (St. Peters et al., 2011). Together, these results suggest a strong influence of ACh on both bottom-up salience processing, as well as top-down attentional signals.

Recent studies have also described the cellular effects that supported a role of ACh during cognitive functions such as attention. Herrero et al. (2008) revealed the attentional effects of ACh in Macaque V1 during a spatial luminance change detection task. Firstly, iontophoretic application of ACh increased attentional rate modulation, showing that ACh affects attentional signals as early as V1. Next it was shown that ACh-mediated amplification of attention was dependent on muscarinic, but not nicotinic receptor subtypes. Whereas the nicotinic antagonist mecamylamine did not affect attentional coding, the muscarinic antagonist scopolamine decreased attentional signals (Herrero et al., 2008). In early visual areas, nicotinic receptors are mainly found either presynaptically on thalamic efferents to V1, or on interneurons within V1, and influence response gain and contrast detection specifically in the V1 input layer (Disney et al., 2007). As nicotinic receptors do not contribute to attentional signals in V1 (Herrero et al., 2008) but have behavioural effects during attentional tasks (Levin and Simon, 1998b), they have been suggested to contribute to cognitive processing in higher-order areas (Thiele and Bellgrove, 2018). Indeed, iontophoretic application of either mecamylamine or the specific nicotinic α7 antagonist methyllycaconitine in Macaque dlPFC decreased delay period firing during a spatial working memory task (Yang et al., 2013). Various selective α7 agonists, on the other hand, increased delay period firing activity, and their effects were found to follow an inverted-U shaped dose response curve. These cholinergic effects on working memory were moreover shown to depend on NMDA receptors, responsible for the maintenance of recurrent excitation of pyramidal cells during working memory (Wang et al., 2013), as the effects of both NMDA and NMDA blockers were reversed by α7 antagonists and agonists, respectively (Yang et al., 2013). Additional to a role for nicotinic receptors in working memory, systemic (Zhou et al., 2011) or local (Major et al., 2015) application of the muscarinic antagonist scopolamine decreased spatial or rule-based delay-period firing in Macaque dlPFC.

In addition to the effects of ACh on cognitive functions such as attention and working memory, similar to NA, ACh also influences specific neuronal signatures of cortical state. Electrical stimulation of the NB elicited desynchronisation of EEG over rat auditory cortex (Metherate et al., 1992). Additionally, both systemic as well as local application of

the muscarinic antagonist atropine prevented the desynchronisation due to NB stimulation, and increased Vm synchronisation. Interestingly, the effect of NB stimulation on auditory cortex was specific to a subset of stimulation locations, suggesting that the topographic nature of NB projections could produce localised desynchronisation. Furthermore, although local electrical stimulation in auditory cortex increased firing rates, it did not alter the pattern of Vm fluctuations (Metherate et al., 1992). This suggested that cortical desynchronisation does not solely rely on mere excitatory input, but that modulatory influences (such as ACh) are required for state changes. Similar results were described by Polack et al. (2013), who found that local perfusion of atropine or nACr antagonist mecamylamine specifically elicited cortical synchronisation, but did not prevent the locomotion-induced depolarisation of mouse V1 Vm (see above). Together these studies thus described dissociable effects of NA and ACh on cortical state, NA affected Vm depolarisation whereas ACh affected desynchronisation.

Simultaneous BF stimulation and V1 recording studies have allowed the characterisation of ACh-induced desynchronisation on sensory coding (Goard and Dan, 2009; Minces et al., 2017; Pinto et al., 2013). Electrical stimulation of NB in anaesthetised rats increased the trial-to-trial reliability of visual responses to natural movies, and decreased the between cell correlation of activity (Goard and Dan, 2009). Together, these effects improved stimulus classification, and decreased the redundancy between cells. The degree of decorrelation was reduced by local application of atropine, suggesting that desynchronisation is (partly) dependent on local ACh muscarinic receptor activation. It is, however, impossible to unequivocally ascribe these effects to cholinergic neurons of the BF, as electrical stimulation likely also engages non-cholinergic cells. Moreover, it is uncertain whether the effects in V1 rely (in part) on network effects, as other brain areas affected by BF stimulation could bring about the reported activity changes in V1. In a follow up study, Pinto et al. (2013) addressed these limitations by injecting a viral construct in the BF that selectively targeted cholinergic neurons, and optogenetically stimulating and recording in V1. Both BF and V1 stimulation elicited desynchronisation in V1, improved sensory coding, and increased behavioural performance in orientation discrimination. Additionally, inhibiting the BF had the opposite effect. In a re-analysis of this dataset Minces et al. (2017) suggested that ACh modulated sensory coding by influencing the signal-to-noise ratio of the population by affecting the relationship (slope) between signal and noise correlations, an effect found critical for population information coding (Averbeck et al., 2006; van Kempen et al., 2017). Cholinergic stimulation specifically increased the ability of neural responses to vary across different stimuli (signal), but left the trial-to-trial variability of responses to the same stimuli (noise) unchanged (Minces et al., 2017; van Kempen et al., 2017). Importantly, as mentioned above, selective attention has previously been described to have a similar effect on the population correlation structure in Macaque V4 (Ruff and Cohen, 2014). Altogether, these studies reveal a clear role for ACh in the modulation of attentional processes and cortical state fluctuations.

1.7 - **Pupil diameter**

Pupil diameter controls the amount of light that hits the retina through the pupillary light reflex (PLR), which constricts the pupil upon retinal luminance increases (Loewenfeld, 1993; McDougal and Gamlin, 2014). Pupillary dynamics are controlled through a small network that receives input from both the sympathetic ('fight-or-flight') and parasympathetic ('rest-and-digest') autonomic nervous system and drives the iris sphincter and dilator pupillae that constrict and dilate the pupil, respectively (Loewenfeld, 1993; McDougal and Gamlin, 2014). Retinal stimulation is relayed via bilateral efferents to the pretectal olivary nucleus of the midbrain, which projects bilaterally to the Edinger-Westphal (EW) nucleus. From here, projections via the ciliary ganglion stimulate the iris sphincter muscle (McDougal and Gamlin, 2014). Additional control of pupil size is provided by the dilator muscle, stimulated through sympathetic innervation via the superior cervical ganglion (McDougal and Gamlin, 2014). In addition to responding to increases and decreases in luminance, pupil diameter also reflects central arousal levels and the cognitive state of animals and humans (Aston-Jones and Cohen, 2005a; Gilzenrat et al., 2010; McDougal and Gamlin, 2014; McGinley et al., 2015b), potentially driven via direct or indirect projections from the superior colliculus (Wang and Munoz, 2015a).

Direct electrophysiological and imaging recordings in animals (Aston-Jones and Cohen, 2005a; Joshi et al., 2016; Reimer et al., 2016; Varazzani et al., 2015) as well as indirect fMRI recordings in humans (de Gee et al., 2017; Murphy et al., 2014a) suggest that under conditions of constant illumination, fluctuations in pupil diameter can index activity in multiple of the neuromodulatory nuclei discussed above. Although originally associated with activity in the LC (Aston-Jones and Cohen, 2005a), more recent research has highlighted that fluctuations in pupil diameter are also partly dependent on activity in other neuromodulatory centres. Indeed, pupil diameter not only tracks LC activity, but may also reflect cortical cholinergic activity (Reimer et al., 2016). Rapid changes in pupil dilation, the pupil derivative, were strongly related to cortical NA activity, whereas slower changes in pupil diameter correlated more strongly with the sustained activity in cholinergic axons (Reimer et al., 2016). Additionally, fMRI activity in other neuromodulatory nuclei, such as the dopaminergic substantia nigra and ventral tegmental area, as well as the cholinergic basal forebrain, were also found to correlate with pupil diameter (de Gee et al., 2017). In addition to its relationship to activity in these neuromodulatory nuclei, pupil diameter also correlates to activity in non-neuromodulatory brainstem nuclei, such as the superior colliculus (de Gee et al., 2017; Joshi et al., 2016; Wang et al., 2012; Wang and Munoz, 2015a). The activity in LC, however, displayed activity most strongly time-locked to pupillary dilations and might reflect LC mediated coordination of neuronal activity throughout distributed parts of the brain (Joshi et al., 2016).

Basic sensory and cognitive functioning varies strongly with neuromodulator availability (Harris and Thiele, 2011; Thiele and Bellgrove, 2018), and may thus be tracked by pupillary measures. It has been suggested that pupil diameter measured in a pre-target time window (baseline pupil diameter) is a reflection of the tonic mode of the LC, and

pupillary responses post stimulus-onset (task-evoked pupil diameter) reflect the complimentary phasic LC response (Einhäuser et al., 2010; Eldar et al., 2013; Gilzenrat et al., 2010). Because of its relationship with additional neuromodulators, this hypothesis may extend to the tonic and phasic responses of other neuromodulatory nuclei. Indeed, under conditions of constant illumination, both baseline pupil diameter (Gilzenrat et al., 2010; Kristjansson et al., 2009; McGinley et al., 2015a; Murphy et al., 2011) as well as the size of the pupillary response (Beatty, 1982a; Kristjansson et al., 2009) can be predictive of behavioural performance. Additionally, the pupil response has been shown to vary systematically with a variety of cognitive processes such as solving multiplication problems (Hess and Polt, 1964), attention (Hoeks and Levelt, 1993), visual target detection (Privitera et al., 2010, 2008), and has also been related to decision making (Cheadle et al., 2014; de Gee et al., 2017, 2014; Einhäuser et al., 2010; Murphy et al., 2014b; Simpson and Hale, 1969; Urai et al., 2017), generally scaling with the workload required to perform the task (Hess and Polt, 1964; Hoeks and Levelt, 1993).

In conjunction with the relationship between pupil diameter and activity in neuromodulatory nuclei, recent research has also revealed a close relationship to various (other) measures of cortical and behavioural state (McGinley et al., 2015b). Fluctuations in pupil diameter closely track fluctuations in the membrane potential of neurons in sensory cortex (McGinley et al., 2015a; Reimer et al., 2014). Specifically, the membrane potential variability of visual and somatosensory neurons was reduced during pupil dilation versus constriction (Reimer et al., 2014), and a subsequent study reported U-shaped relationships between baseline pupil diameter and the membrane potential variability as well as the evoked spike rate and neural gain of auditory neurons (McGinley et al., 2015a). In addition to the effects on neural activity, behavioural performance was optimal at intermediate baseline pupil diameter (McGinley et al., 2015a).

Additionally, there is some evidence that activity in higher-order association areas also varies with pupil diameter. During auditory target detection, human subjects displayed the least variable RT at intermediate baseline pupil diameter, as well as the highest amplitudes of the P3 event-related potential (ERP), an EEG component measured over parietal areas that is reliably elicited by task-relevant stimuli (Murphy et al., 2011). Furthermore, larger pupil diameter has been associated with lower spontaneous firing, higher signal-to-noise ratios and lower noise correlations in mouse V1 (Vinck et al., 2015) as well as increased durations of On episodes, i.e. periods of high firing activity, in Macaque V4 (Engel et al., 2016). Additionally, pupil diameter's strong relationship to network activity in mouse V1 (Lu et al., 2017) as well as fMRI measures of brain-wide neural gain (Eldar et al., 2013) indicate that these pupillometric measures reflect global changes in network state, likely driven by fluctuations in neuromodulatory drive.

1.8 - **Outstanding questions and current studies**

Although the (neuromodulatory) mechanisms driving (brain-wide) fluctuations in neural excitability, as well as their effect on sensory processing and behaviour, are

starting to be elucidated, the spatiotemporal scale on which these fluctuations occur, their effects on other stages of information processing, their interaction with cognitive functions, and their modulation by specific receptor agonists and antagonists during cognitive tasks are largely unknown.

In this thesis, I investigate these unknown characteristics by studying cortical state fluctuations across spatiotemporal scales and across species. To explore the effects of global excitability fluctuations, I investigated the effects of central arousal, as measured by pupil diameter, on activity throughout the brain during perceptual decision-making in human subjects. Here, I found that fluctuations in both tonic and phasic arousal affected behavioural performance as well as specific EEG signatures associated with successive neural processing stages of decision-making, revealing that pupil-linked arousal affects brain-wide task-related activity.

In the following two studies, In order to investigate these fluctuations on smaller spatiotemporal scales, I studied cortical state and selective attention in Macaque monkeys. First, I focused on how selective attention influences cortical state in and between Macaque V1 and V4. I describe how the local effects of top down attention modulate signatures of cortical state in each area individually, and how selective attention and the coordination of cortical state across areas interact to support behaviour.

Finally, in the third study, I examined the role of dopamine in the posterior parietal cortex during top-down attention. Specifically, I tested the effects of iontophoretic application of dopaminergic drugs on single and multi-unit activity in parietal cortex during top-down attention. Dopamine inhibited activity across the population of recorded cells, this modulation furthermore followed an inverted U-shaped dose-response curve for dopamine, and a monotonically increasing function for the D1-selective antagonist. In addition to general firing rate changes, for particular cell types, activity specific to top-down attention was affected. These results confirmed that dopamine plays an important role in shaping neural activity, including during selective attention, in parietal cortex.

Chapter 2 - Behavioural and neural signatures of perceptual decision-making are modulated by pupil-linked arousal

Jochem van Kempen[1,2*], Gerard M. Loughnane[3,4], Daniel P. Newman[2], Simon P. Kelly[6], Alexander Thiele[1], Redmond G O'Connell[2,4,5], Mark A. Bellgrove[2,5]

[1]Institute of Neuroscience, Newcastle University, Newcastle upon Tyne, NE1 7RU, United Kingdom, [2]Monash Institute for Cognitive and Clinical Neurosciences, School of Psychological Sciences, Monash University, Melbourne, Victoria 3800, Australia, [3]School of Engineering, [4]Trinity College Institute of Neuroscience, and [5]School of Psychology, Trinity College Dublin, Dublin 2, Ireland, and [6]School of Electrical and Electronic Engineering, University College Dublin, Dublin 4, Ireland

2.1 - Abstract

The timing and accuracy of perceptual decision making is exquisitely sensitive to fluctuations in arousal. Although extensive research has highlighted the role of various neural processing stages in forming decisions, our understanding of how arousal impacts these processes remains limited. Here we isolated electrophysiological signatures of decision making alongside signals reflecting target selection, attentional engagement and motor output and examined their modulation as a function of tonic and phasic arousal, indexed by baseline and task-evoked pupil diameter, respectively. Reaction times were shorter on trials with lower tonic, and higher phasic arousal. Additionally, these two pupil measures were predictive of a unique set of EEG signatures that together represent multiple information processing steps of decision making. Finally, behavioural variability associated with fluctuations in tonic and phasic arousal, indicative of neuromodulators acting on multiple timescales, was mediated by its effects on the EEG markers of attentional engagement, sensory processing and the variability in decision processing.

2.2 - Introduction

The speed and accuracy with which humans, as well as non-human animals, respond to a stimulus depends not only on the characteristics of the stimulus, but also on the cognitive state of the subject. When drowsy, a subject will respond more slowly to the same stimulus compared to when she is attentive and alert. Central arousal also fluctuates across a smaller range during quiet wakefulness, when the subject is neither drowsy nor inattentive, nor overly excited or distractible. Although these trial-to-trial fluctuations can impact on behavioural performance during decision making tasks (Aston-Jones and Cohen, 2005a), it is largely unknown how arousal modulates the underlying processes that support decision formation. Perceptual decision making depends on multiple neural processing stages that represent and select sensory

information, those that process and accumulate sensory evidence, and those that prepare and execute motor commands. Variability in central arousal could affect any one or potentially all of these processing stages, which in turn could influence behavioural performance.

The neuromodulatory systems that control central arousal state, such as the noradrenergic (NA) locus coeruleus (LC) and the cholinergic basal forebrain (BF), have also been suggested to drive fluctuations in endogenous activity linked to changes in cortical (de)synchronisation, i.e. cortical state (Harris and Thiele, 2011; Lee and Dan, 2012). They are furthermore linked to cognitive functions such as attention (Thiele and Bellgrove, 2018), both known to affect information processing and behavioural performance. These modulatory systems have both tonic and phasic firing patterns that are recruited on different timescales and support different functional roles (Aston-Jones and Cohen, 2005a; Peter Dayan and Yu, 2006; Parikh et al., 2007; Parikh and Sarter, 2008; Sarter et al., 2016). Tonic changes in neuromodulator activity occur over longer timescales that can span multiple trials, whereas fast (task-evoked) recruitment through phasic activation occurs on short enough timescales to influence neural activity and behavioural decisions within the same trial (Aston-Jones and Cohen, 2005a; Bouret and Sara, 2005; Peter Dayan and Yu, 2006; Parikh et al., 2007).

Pupil diameter correlates strongly with a variety of measurements of cortical state and behavioural arousal (Eldar et al., 2013; Engel et al., 2016; McGinley et al., 2015b, 2015a; Reimer et al., 2014; Vinck et al., 2015), and can thus be considered a reliable proxy of central arousal state. Indeed, there is a strong correlation between pupil size and activity in various neuromodulatory centres that control arousal (Aston-Jones and Cohen, 2005a; de Gee et al., 2017; Gilzenrat et al., 2010; Joshi et al., 2016; Murphy et al., 2014a; Reimer et al., 2016; Varazzani et al., 2015). Both pre-stimulus baseline pupil diameter, reflecting tonic activity levels in neuromodulatory centres (tonic arousal), and task-evoked pupil diameter changes (phasic arousal), have been related to specific neural processing stages of perceptual decision making. Baseline pupil diameter correlates with sensory sensitivity (McGinley et al., 2015a, 2015b) and is predictive of behavioural performance during elementary detection tasks (McGinley et al., 2015a; Murphy et al., 2011). Pupil diameter also changes phasically in the course of a single decision (Beatty, 1982b; de Gee et al., 2017, 2014; Lempert et al., 2015; Murphy et al., 2016; Urai et al., 2017), and has been related to specific elements of the decision making process, such as decision bias (de Gee et al., 2017, 2014), uncertainty (Urai et al., 2017), and urgency (Murphy et al., 2016). This suggests that these neuromodulatory systems do not only dictate network states (through tonic activity changes), but that they are recruited throughout the decision making process (Cheadle et al., 2014; de Gee et al., 2017, 2014). Although both baseline pupil diameter and the phasic pupil response have been associated with specific aspects of decision making, the relationship between pupil-linked arousal and the electrophysiological correlates of decision making are largely unknown.

Recently developed behavioural paradigms have made it possible to non-invasively study the individual electroencephalographic (EEG) signatures of perceptual decision making described above (Kelly and O'Connell, 2013; Loughnane et al., 2018, 2016;

Newman et al., 2017; O'Connell et al., 2012). In these paradigms, participants are required to continuously monitor (multiple) stimuli for subtle changes in a feature. Because stimuli are presented continuously, target onset times (and locations) are unpredictable, and sudden stimulus onsets are absent, eliminating sensory evoked deflections in the EEG traces. These characteristics allow for the investigation of the gradual development of build-to-threshold decision variables as well as signals that code for the selection of relevant information from multiple competing stimuli, a critical feature of visuospatial attentional orienting that impact evidence accumulation processes (Loughnane et al., 2016).

Here, we asked how arousal influences EEG signals that relate to each of the separate processing stages described above. Specifically, we tested the effects of pupil-linked arousal on pre-target preparatory parieto-occipital α-band activity, associated with fluctuations in the allocation of attentional resources (Kelly and O'Connell, 2013); early target selection signals measured over contra- and ipsilateral occipital cortex, the N2c and N2i (Loughnane et al., 2016); perceptual evidence accumulation signals measured as the centroparietal positivity (CPP), which is a build-to-threshold decision variable demonstrated to scale with the strength of sensory evidence and predictive of reaction time (RT) (Kelly and O'Connell, 2013; O'Connell et al., 2012); and motor-preparation signals measured via contralateral β-band activity (Donner et al., 2009; O'Connell et al., 2012). Of these signals, we extracted specific characteristics such as the latency, build-up rate and amplitude, and tested whether these were affected by pupil-linked arousal. Additionally, because the variance and response reliability of the membrane potential of sensory neurons varies with pupil diameter (McGinley et al., 2015a; Reimer et al., 2014), we also investigated whether arousal affected the inter-trial phase coherence (ITPC), a measure of across trial consistency in the EEG signal, of the N2 and the CPP.

We found that both baseline pupil diameter as well as the pupil response were predictive of behavioural performance, and that this relationship was best described by non-monotonic, but not U-shaped, second-order polynomial model fits. Furthermore, we found that both tonic and phasic arousal bore a predictive relationship with the neural signals coding for baseline attentional engagement, early target selection, decision processing as well as the preparatory motor response. Although neural activity representing all these stages varied with changes in arousal, unique variability in task performance due to tonic arousal (baseline pupil diameter) could only be explained by the amplitude of target selection signals and the consistency of the CPP, reflecting decision processing. In contrast, variability due to phasic arousal (pupil response) was explained by pre-target α-band activity as well as the consistency of the CPP.

2.3 - **Methods**

2.3.1 - Task procedures

Subjects (n=80, 42 female) and methods are largely overlapping with the details and procedures described elsewhere (Newman et al., 2017). Here we summarise details

necessary to understand this study, and we also describe procedures that differ from the previous study. Healthy right-handed participants, ages 18-37 (mean 23.2 years), with normal or corrected-to-normal vision were seated in a darkened room, 56 cm from the stimulus display (21 inch cathode ray tube (CRT) monitor, 85 Hz 1024 × 768 resolution), asked to perform a continuous bilateral variant (Kelly and O'Connell, 2013; O'Connell et al., 2012) of the random dot motion task (Britten et al., 1992; Newsome et al., 1989). Subjects fixated on a central dot while monitoring two peripheral patches of continuously presented randomly moving dots (Figure 2-5a). At pseudorandom times, an intermittent period of coherent downward motion (50%) occurred in either the left or the right hemifield. Upon detection of coherent motion, participants responded with a speeded right-handed button press. A total of 288 trials were presented over 16 blocks (18 trials per block). Data were collected under identical experimental procedures at either Monash University, Australia, or Trinity College Dublin, Ireland. The experimental protocol was approved by each University's human research ethics committee before testing (Project number Monash University: 3658, Trinity College: SPREC012014-1), and carried out in accordance with each University's approved guidelines. Informed consent was obtained from all participants before testing.

2.3.2 - Data acquisition and preprocessing

Electroencephalogram (EEG) was recorded from 64 electrodes using an ActiveTwo (Biosemi, 512Hz) system at Trinity College Dublin, Ireland or a BrainAmp DC (Brainproducts, 500Hz) at Monash University, Australia. Data were processed using both custom written scripts and EEGLAB functions (Delorme and Makeig, 2004) in Matlab (MathWorks). Noisy or broken channels (mean 1.9±0.18 channels, range: 0-7) were identified by investigation of the detrended average power spectrum (0.5 – 40 Hz) and interpolated. Hereafter, the data were notch filtered between 49-51 Hz, band-pass filtered (0.1-35Hz), and rereferenced to the average reference. Data recorded using the Biosemi system were resampled to 500Hz and combined with the data recorded with the Brainproducts system. Epochs were extracted from -800 to 2800 ms around target onset and baselined with respect to -100 to 0 ms before target onset. To minimize volume conduction and increase spatial specificity, for specific analyses the data were converted to current source density (Kayser and Tenke, 2006). We rejected trials from analyses if the reaction times were <150 or >1700 ms after coherent motion onset, or if either the EEG on any channel exceeded 100 mV, or if the subject broke fixation or blinked (Pupillometry) during the analysis period of the trial, the 500 ms preceding target onset (26.59 ± 2.94) for pre-target α power activity or the interval of 100 ms before target onset to 200 ms after the response (33.66 ± 3.95).

Pre-target α-band power (8-13 Hz), N2 amplitude and latency, CPP onset and build-up rate and response related β-power amplitude and build-up rate were computed largely in the same way as in Newman et al. (2017). Briefly, α-band power was computed over the 500 ms preceding target onset using temporal spectral evolution (TSE) methods (Thut, 2006), and pooled over two symmetrical parietal regions of interest, using

channels O1, O2, PO3, PO4, PO7 and PO8. The N2 components were measured at electrodes P7 and P8, ipsi- and contralateral to the target location (Loughnane et al., 2016; Newman et al., 2017), and the CPP was measured at central electrode Pz. These signals were aggregated to an average waveform for each pupil bin and each participant. We determined the latency of the N2c/N2i as the time point with the most negative amplitude value in the stimulus-locked waveform between 150-400/200-450 ms, while N2c/N2i amplitude was measured as the mean amplitude inside a 100 ms window centred on the stimulus-locked grand average peak (266/340 ms) (Loughnane et al., 2016; Newman et al., 2017).

Onset latency of the CPP was measured by performing running sample point by sample point t-tests against zero across each participant's stimulus-locked CPP waveforms. CPP onset was defined as the first point at which the amplitude reached significance at the 0.05 level for ≥15 consecutive points. Because we decreased our statistical power by binning the trials into 5 bins (see pupillometry), we did not find an onset for every bin for a subset of subjects (baseline pupil diameter: 13 bins over 11 subjects, pupil response: 16 bins over 12 subjects). Because of our use of linear mixed effect analyses, these subjects could still be included in the analysis, with only the missing values being omitted. Both CPP build-up rate and amplitude were computed using the response-locked waveform of the CSD transformed data to minimize influence from negative-going fronto-central scalp potentials (Kelly and O'Connell, 2013). Build-up rate was defined as the slope of a straight line fitted to this signal in the window from -250 ms to -50 ms before response. CPP amplitude was defined as the mean amplitude within the 100 ms around the response.

Response related left hemisphere β-power (LHB, 20-35 Hz) was measured over the left motor cortex at electrode C3 using short-time Fourier transform (STFT) with a 286 ms window size and 20 ms step size (Newman et al., 2017; O'Connell et al., 2012). We baselined LHB using an across-trial baseline for each subject. LHB amplitude was measured from the response-locked waveform in the window from -130 to -70 ms preceding the response, whereas the LHB build-up rate was defined as the slope of a straight line fitted to this same waveform in the 300 ms before the response.

Inter-trial phase coherence (ITPC) was estimated using single-taper spectral methods from the Chronux toolbox (Bokil et al., 2010) and adapted scripts. We used a 256 sample (512 ms) sliding short time window, with a step size of 25 samples (50 ms). This gave us a half bandwidth (W) of 1.95 Hz: $W = (K+1)/2T$, with K being the number of data tapers, K=1, and T (s) being the length of the time window. Frequencies were estimated from 0.1 to 35Hz.

2.3.3 - Pupillometry

Eye movements and pupil data were recorded using an SR Research EyeLink eye tracker (Eye-Link version 2.04, SR Research/SMI). Automatically identified blinks and saccades were linearly interpolated from 100 ms before to 100 ms after the event, the interpolated

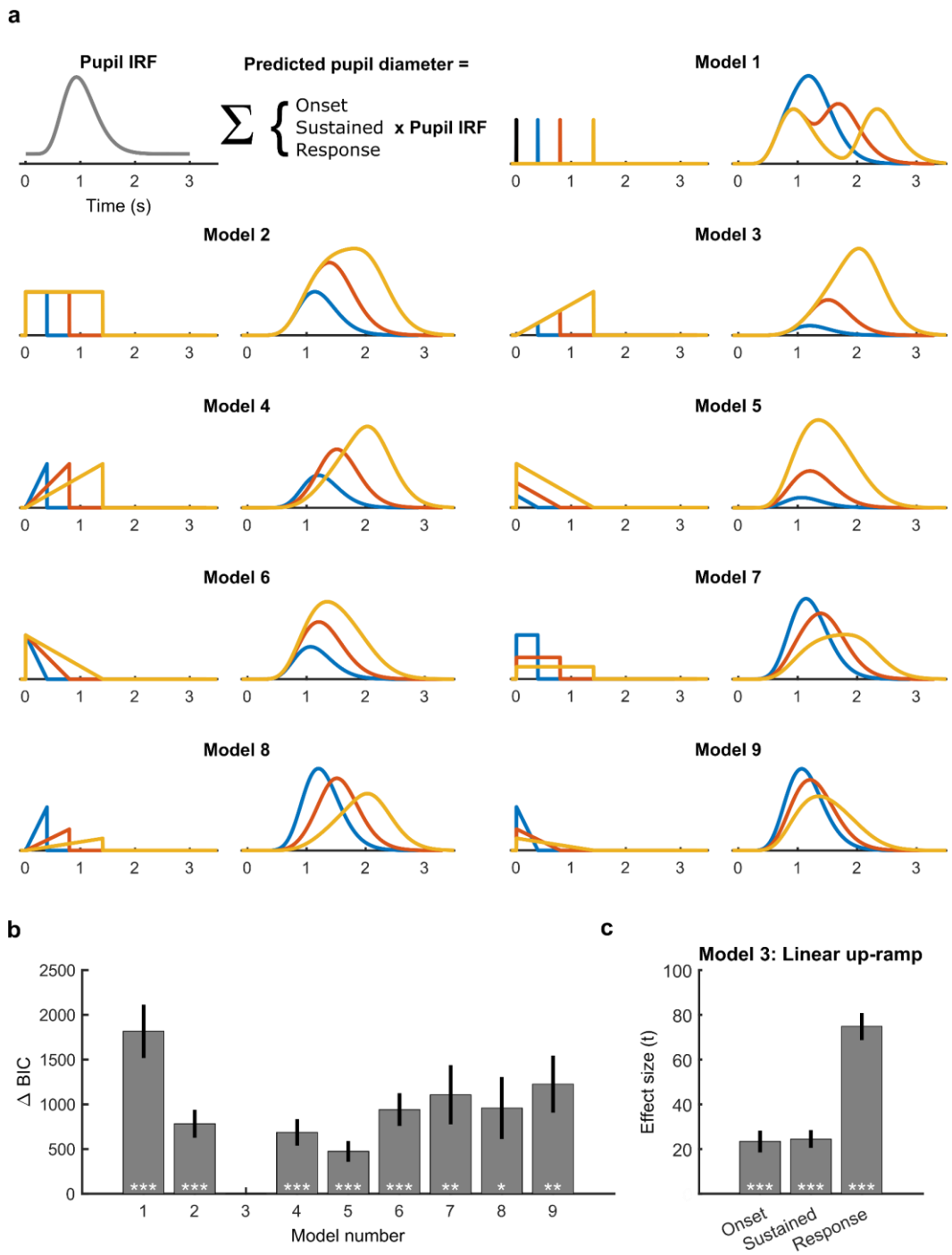

Figure 2-1. The neural input to the pupil diameter system is best described by a linear up-ramp.(**a**) The nine different general linear models (GLM) fit to the pupil diameter data of three example trials with short (blue), medium (red) and long (yellow) reaction times. Top, the canonical pupil input response function (IRF) convolved with target onset (black tick mark) and response (coloured tick marks) that were used for all models. In addition to target onset and response, models 2-9 also contain a sustained temporal component of varying shape. For each model, the left column illustrates the temporal components that described the neural input to the pupil diameter system, and the right column illustrates these components convolved with the pupil IRF. (**b**) Bayes Information Criterion (BIC) scores for the nine models fit to the pupil diameter time course, relative to the winning model (model 3, linear up-ramp). (**c**) Effect sizes (t-statistics) for each of the temporal components from the linear up-ramp model. Error bars denote ±1 standard error of the mean (SEM). Statistics: Wilcoxon signed rank test. This figure is based on Figure 5 in Murphy et al, (2016).

pupil data was then low-pass (< 6 Hz) or band-pass (0.01-6Hz) filtered (second order butterworth). The instantaneous phase of the pupil diameter was calculated by taking

the angle of the analytic signal acquired by using the Hilbert transform of the filtered data. Epochs were extracted from -800 to 4800 ms around coherent motion onset. Trials in which fixation errors or blinks occurred within the analysis period, from 100 ms before target onset to 200 ms after response, were excluded from analysis. Fixation errors were defined as gaze deviations of more than 3°. The pupil diameter was normalised by dividing by the maximum pupil diameter on any trial in the analysis window from 100 ms before target onset to 200 ms after the response for each subject, and baselined on a single trial basis. We computed the baseline pupil diameter by averaging the pupil diameter in the 100 ms before target onset, and the baseline phase was calculated as the average phase angle in the 100 ms preceding target onset.

We identified the shape of the neural input to the pupil system by applying various general linear models (GLM) to the pupil time course (de Gee et al., 2014; Hoeks and Levelt, 1993; Murphy et al., 2016) with two temporal components corresponding to target and response onset (all models), and a third sustained component (models 2-9) for which the shape varied across eight candidate models tested previously (Murphy et al., 2016). In model 1, only the stimulus and response onset were modelled. The sustained component in the remaining models took the shape of: (model 2) a boxcar component with a constant amplitude throughout the decision interval; (model 3) a linear up-ramp that grew in amplitude with increasing decision time; (model 4) a ramp-to-threshold; (model 5) a linear decay with a starting amplitude that was larger for slower RTs but whose amplitude always terminated at zero; (model 6) a linear decay-to-threshold which began at a fixed amplitude and terminated at zero; (model 7-9) versions of the boxcar, up-ramp and down-ramp models in which the sustained component was normalised by the number of the samples in that trial's decision interval (Figure 2-1a). We convolved these onset, response and/or sustained temporal components with a pupil impulse response function (IRF):

$$h(t) = t^{w} e^{-t \cdot w / t_{max}}$$

Equation 2-1

where w is the width (10.1) and t_{max} is the time-to-peak (930 ms) of the IRF (de Gee et al., 2014; Hoeks and Levelt, 1993; Murphy et al., 2016). Each model was regressed onto the concatenated band-pass filtered pupil diameter time series (from -800 ms before target onset to 2500 ms after the response). Bayes information criterion (BIC) was used to assess model fit:

$$\mathrm{BIC} = n + n\log(2\pi) + \log(SSR/n) + (k+1)\log(n)$$

Equation 2-2

where n is the number of samples, SSR is the residual sum of squares, and k is the number of free parameters. The goodness of fit between any two models was assessed non-parametrically by applying Wilcoxon signed rank tests to their difference score. We found that the linear up-ramp model (model 3) provided the best fit to the data. Figure

2-1b-c illustrates the relative goodness-of-fit of each model, compared to the best fitting linear up-ramp model, as well as the effect size of each of the components of the linear up-ramp model.

To investigate the relationship between pupil-linked arousal and behavioural performance during decision making, we binned our behavioural and EEG data according to either the baseline pupil diameter or the post target pupil response (see below) into 5 equally sized bins (mean 49.63 ± SEM 0.81 trials, minimum bin size = 20 trials). The division into 5 bins allowed us to investigate possible quadratic trends in the data. We used linear regression to remove the trial-by-trial fluctuations in single-trial pupil amplitudes that could be due to inter-trial interval, target side, as well as baseline pupil diameter amplitude or phase, all factors that are known to influence either the post target pupil response and/or behavioural response times (Kristjansson et al., 2009; de Gee et al., 2014; Kloosterman et al., 2015; Newman et al., 2017). To partial out the effect of phase, a circular variable, we used the sine and cosine of the phase as orthogonal, linear predictor variables (Fisher, 1993). To verify the (absence of) correlation between pupil baseline phase and response before and after the regression, we made use of the circstat toolbox (Berens, 2009).

We estimated the task-evoked phasic arousal response according to various single-trial scalar measurements of the amplitude of the pupil response, and investigated their relation to behaviour (Figure 2-2). The relationship between the average pupil diameter around RT and behavioural performance was best described by a non-monotonic, U-shaped, relationship (Figure 2-2a). Because of the temporal low-pass characteristics of the peripheral pupil system (Hoeks and Levelt, 1993), trial-to-trial variation in RT can affect the measurement of the size of the pupil response. To remove the trial-to-trial fluctuations in pupil responses due to variations in RT, we removed these components via linear regression (de Gee et al., 2017; Urai et al., 2017). After the elimination of the contribution of RT to the pupil response, we still observed a U-shaped relationship with behavioural performance (Figure 2-2b). This measure of the pupil response, however, likely reflects both the transient response to target onset as well as any activity that occurs thereafter (e.g. during decision formation). Therefore, we aimed to isolate activity specific to the phasic response to target onset. To this end, we computed the mean, slope

and linear projection (de Gee et al., 2014; Kloosterman et al., 2015) over a 400 ms time window around the peak of the derivative of the pupil IRF (636 ms using the canonical IRF illustrated in Figure 2-1a), a time-window in which activity occurring after the target onset transient is, presumably, not yet reflected. We found an inverse relationship between each of these measures and behavioural performance (Figure 2-2c-e), with better behavioural performance for larger pupil responses. Although these results suggest that measurements of the pupil response in this time-window reflect a different component of the neural input to the pupil system than the measurements of the amplitude around RT (Figure 2-2a-b), the use of any specific time window can be interpreted as arbitrary.

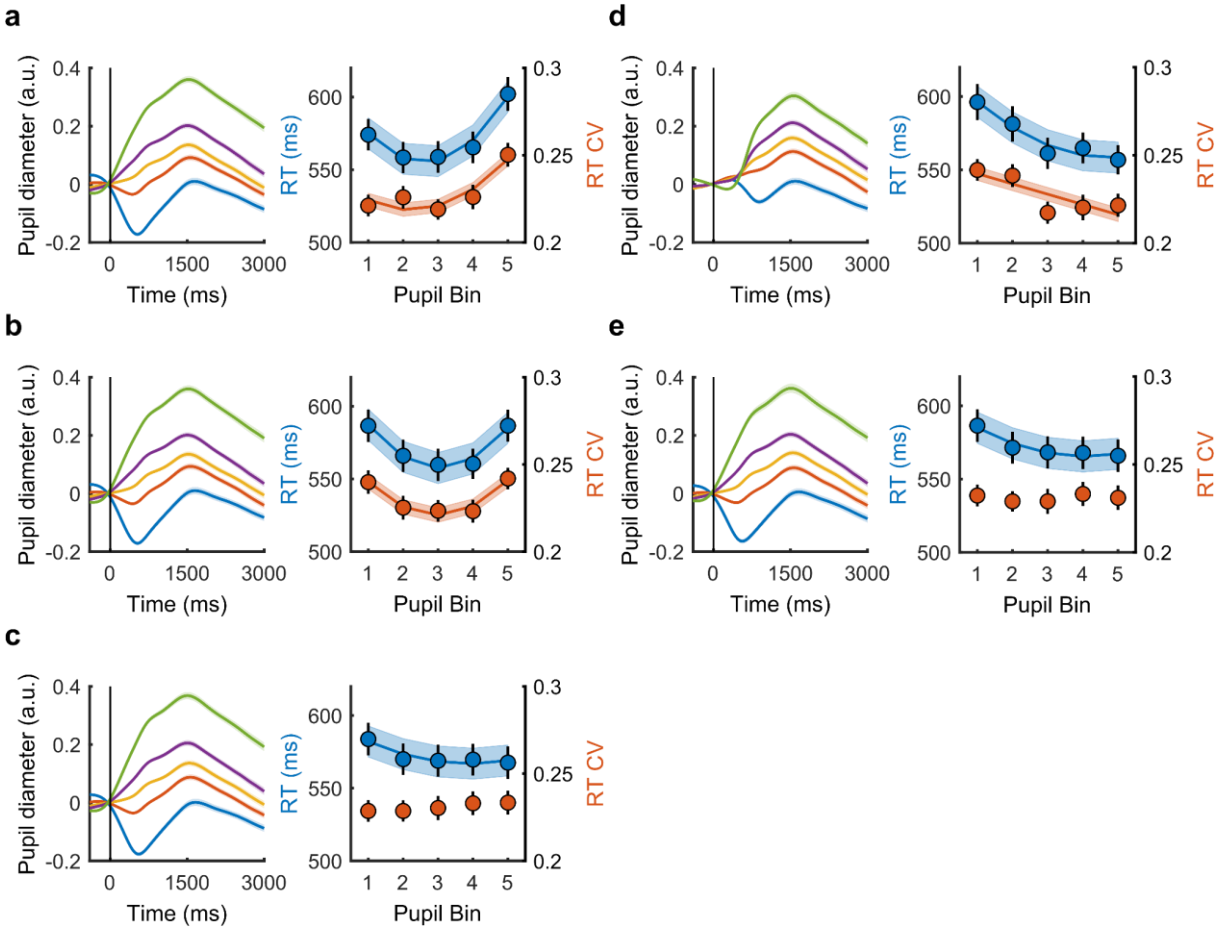

Figure 2-2. Relating various measures of the phasic pupil response to behavioural performance. The pupil time course (left) and behavioural performance (right) as measured by RT and RTcv binned by: (**a**) the mean pupil diameter in the 400 ms around RT; (**b**) the mean pupil diameter in the 400 ms around RT in which fluctuations in the measurement of pupil diameter due to fluctuations in RT were removed via linear regression; and (**c-e**) the mean pupil diameter (**c**) the slope as measured by fitting a straight line (least squares) (**d**) and linear projection (**e**) during the 400 ms around the maximum of the derivative of the pupil input response function (636 ms after target onset) used for the GLM analysis. Error bars and shaded regions denote ±1 standard error of the mean (SEM). Statistics: linear mixed effects model analyses.

To further disentangle the pupil response into separate temporal components, we applied the best-fitting GLM, the linear up-ramp model (Figure 2-1), to individual trials by considering each individual trial as a separate condition (Bach et al., 2018). Because we reduced the amount of data used for the regression analysis by applying it to single-trial data, we tested whether this led to collinearity amongst the temporal components by computing the variance inflation factor (VIF). Although large VIF values do not necessarily imply that no conclusions can be drawn from regression analysis (O'Brien, 2007), as a rule of thumb, VIF values larger than 5 or 10 indicate that predictors are collinear (James et al., 2017; Sheather, 2009). When applying the GLM across all trials, the average VIF values are within the range of collinearity (Figure 2-3a). When we apply the same model to single trial data, however, the average VIF values are substantially higher (Figure 2-3b). It seemed particularly problematic to reliably estimate the sustained and the response component as their average VIF scores are larger than 10. The target onset component, on the other hand, has an average VIF score of approximately 5. Single-trial VIF estimates larger than 5 for target onset (39.34 ± 2.84%

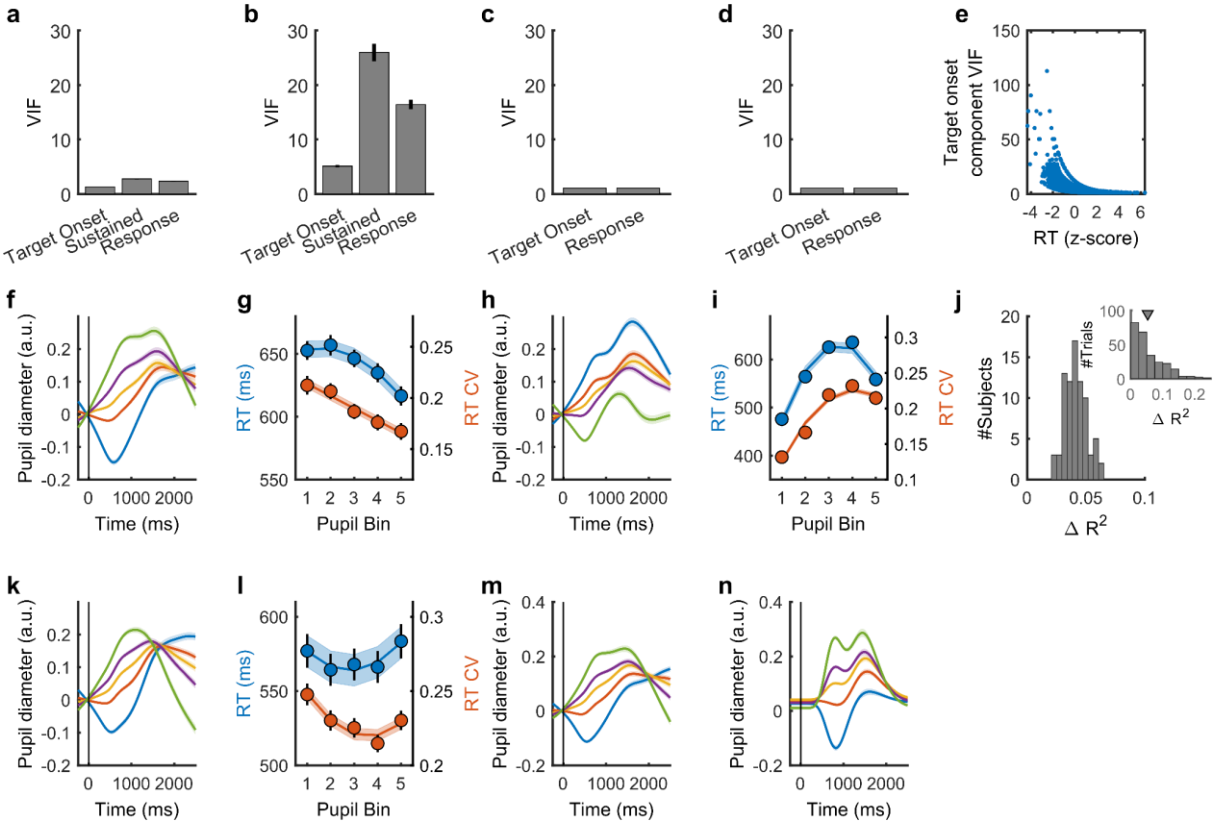

Figure 2-3. Application of the linear up-ramp model on a single-trial basis. (**a-d**) Variance inflation factor (VIF) values for each of the temporal components of the (**a**) linear up-ramp model applied across trials, (**b**) linear up-ramp model applied to individual trials, (**c**) target and response onset model applied across trials, and (**d**) target and response onset model applied to individual trials. (**e**) Single-trial VIF values for the target onset component of the linear up-ramp model, plotted against RT. (**f**) The pupil time course and (**g**) the relationship between the size of the pupil response to target onset and behavioural performance when trials with VIF values larger than five were excluded. (**h-i**) Same conventions as **f-g**, but binned by the estimated amplitude of the sustained component of the linear up-ramp model. (**j**) Average difference in R^2 between a single trial linear up-ramp model and the target-response onset model per subject, inset displays this same difference value for one example subject across trials. (**k-l**) Same conventions as **f-g**, but sorted by the estimated amplitude of the target onset component in the target-response onset model. (**m**) Pupil time course and (**n**) fitted pupil diameter time course binned by the estimated amplitude of the target onset component in the linear up-ramp model. Error bars and shaded regions denote ±1 standard error of the mean (SEM). Statistics: linear mixed effects model analyses.

of trials) were mainly found on trials with short RT (Figure 2-3e), revealing that it is difficult to distinguish between these temporal components on short trials. The overall results were, however, not affected by these trials. Repeating the analysis when excluding trials with VIF values larger than 5 revealed the same relationship pattern between pupil response amplitude and behavioural performance (Figure 2-3f-g). Sorting the pupil diameter according to the estimate of the amplitude of the sustained component, revealed that the largest sustained component occurred on trials with a small (or absent) response to target onset (Figure 2-3h). Rather than solely reflecting phasic arousal during decision formation, the presence of the sustained component could, for instance, indicate a compensatory mechanism for the absence of an early target onset transient. As the relationship with behavioural performance followed a downward trend when plotted against the target onset component (Figure 2-5c), and an upward trend when plotted against the sustained component (Figure 2-3i), together

these effects could explain the U-shaped relationship between behavioural performance and the pupil response when measured as the average pupil diameter around RT (Figure 2-2a-b).

Although a target-response onset only model was the worst fitting model across trials (Figure 2-1a), we tested whether a target-response only model could reliably estimate the single-trial target-onset response amplitude. The relationship between this component and behavioural performance (Figure 2-3k-l), however, strongly resembled the U-shaped relationship between behaviour and the pupil response amplitude when calculated as the mean amplitude around RT (Figure 2-2a), a measure likely to be confounded by both RT and the neural input that occurs after the target onset transient. This supports the notion that the inclusion of a sustained component can make the estimation of the target onset component (amongst others) more accurate, despite the potential collinearity of these predictors. Indeed, the difference in model fit (R^2) is significantly larger than 0 for each individual subject (one-sided Wilcoxon signed rank test, data not shown). Figure 2-3j illustrates the average difference in R^2 values between single-trial models with and without the sustained component. Lastly, Figure 2-3m-n illustrate the actual pupil diameter time course and the single trial fitted pupil diameter, revealing that this model is able to capture considerable variability in the pupil diameter trace.

Next, we applied the same linear up-ramp model to 5 subsets of trials, binned by RT (average bin size: 50.01 ± 0.82 trials). This analysis revealed that the relationship between RT bin and the estimated amplitude of the target component (Figure 2-4a) follows a pattern that is highly similar to the relationship between single-trial estimates of the phasic pupil response to target onset and RT (Figure 2-5c), further supporting the notion that the single-trial GLM approach can accurately estimate the target onset transient. We again investigated the VIF values for each of the temporal components of the model applied to the binned data. Although the sustained and response components displayed relatively large values, the target onset component was smaller than 5. Again, large VIF values by themselves are not necessarily cause for concern, if a regression coefficient is statistically significant, even when its VIF value is large, it is significant "in the face of that collinearity" (O'Brien, 2007). To further exclude the possibility that large VIF values brought about these results, we repeated this analysis using the data binned according to RT in 3 or 2 bins (Figure 2-4b-c). These analysis also revealed smaller target onset component coefficients for larger RT, with progressively lower VIF values. Finally, we investigated the relationship between RT and the target onset component after Gram-Schmidt orthogonalisation of the predictors (Figure 2-4d-e), which eliminated collinearity amongst the temporal components. After orthogonalisation, we also found that the estimates of the β weights of the target onset component were inversely related to RT, both when estimated across bins of trials (Figure 2-4d) as well as when estimating this component on a single trial basis (Figure 2-4e).

Altogether, these analyses reveal that although the estimation of different temporal components contributing to a single-trial pupil diameter time course has to be done

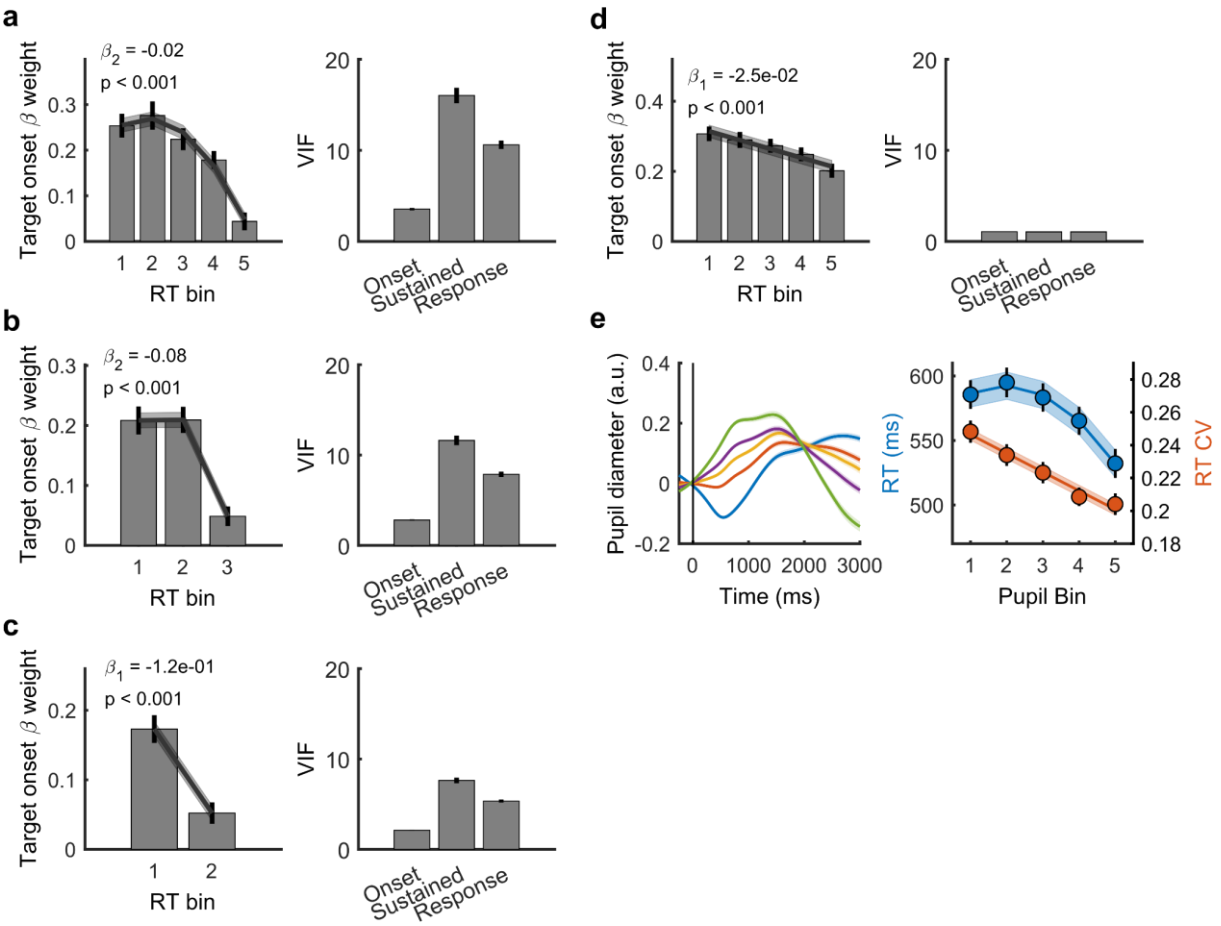

Figure 2-4. Application of the linear up-ramp model across bins of trials. Target onset component β weights for the linear up-ramp model applied to (**a**) five, (**b**) three or (**c**) two subsets of trials binned by RT (Left), and the average VIF values across bins and subjects for each of the temporal components in the linear up-ramp model (Right). (**d**) As in **a**, but after Gram-Schmidt orthogonalisation of the predictors. (**e**) The pupil time course (left), and task performance (right), binned by the estimated amplitude of the target onset component after orthogonalisation of the predictors. Error bars denote ±1 standard error of the mean (SEM). Statistics: linear mixed effects model analyses for trend across bins.

with caution, in the context of the various measures of the phasic pupil response (Figure 2-2) and the interpretation of VIF factors (Figure 2-3 & Figure 2-4), it is possible (in this dataset) to extract meaningful estimates of the target onset component.

2.3.4 - Statistical analyses

We used RStudio (RStudio Team (2016). RStudio: Integrated Development for R. RStudio, Inc., Boston, MA URL http://www.rstudio.com) with the package *lme4* (Bates et al., 2015) to perform a linear mixed effects analysis of the relationship between baseline pupil diameter or the pupil response and behavioural measures and EEG signatures of detection. As fixed effects, we entered pupil bin (see Pupillometry) into the model. As random effects, we had separate intercepts for subjects, accounting for the repeated measurements within each subject. We sequentially tested the fit of a monotonic relationship (first-order polynomial) against a baseline model (zero-order polynomial), and a non-monotonic (second-order polynomial) against the monotonic

fit by means of maximum likelihood ratio tests, using orthogonal polynomial contrast attributes. The behavioural or EEG measure y was modelled as a linear combination of polynomial basis functions of the pupil bins (X):

$$y \sim \beta_0 + \beta_1 X + \beta_2 X^2$$

with β as the polynomial coefficients. This multilevel approach was preferred over a standard repeated measures analysis of variance (ANOVA), because it allowed us to test for first and second-order polynomial relationships, as well as to account for missing values in the CPP onset estimation. We used a variant of the 'two-lines' approach (Simonsohn, 2017), to test for the presence of (inverted) U-shape relationships when a second-order polynomial best fit the data. Using the same multilevel model, we fit two straight lines to the first and last set of two/three bins. For a non-monotonic relationship to be classified as U-shaped, both components needed to have significant coefficients of opposite sign. We iteratively tested the first 3 against the last 2, the first 2 against the last 3 or the first 2 against the last 2 bins (omitting the middle bin), stopping if both criteria were met ($p < 0.05$, Bonferroni corrected).

To verify that the relationship between pupil diameter and task performance was not dependent on the binning procedure, we ran another regression analysis wherein we predicted single trial RT by sequentially adding the linear and quadratic coefficients for baseline pupil diameter (BPD) and pupil response (PR):

$$RT \sim \beta_0 + \beta_1 BPD + \beta_2 BPD^2 + \beta_3 PR + \beta_4 PR^2$$

with β as the polynomial coefficients. We compared the first model to a random-intercept-only model including subject ID, inter-trial interval, stimulus side, as well as the trial and block number (to control for potential time on task effects), and tested the fit of subsequent models to the previous model fit. This analysis revealed a significant improvement for each step of the sequential analysis, for which the results and parameters estimates are shown in Table 2-1. These analyses confirm that both the size of the baseline pupil diameter and the pupil response are predictive of task performance on a single trial basis. This relationship moreover follows a non-monotonic, quadratic, function.

After testing the relationship between behavioural and neural signatures of decision making and pupillometric measures individually, the neural signals were added sequentially into consecutive regression models predicting RT and RTcv. This model had both a random intercept for each subject, allowing for different baseline-levels of behavioural performance, as well as a random slope of pupil bin for each subject, which allowed for across-subject variation in the effect of pupil bin on behavioural performance. The hierarchical entry of the predictors allowed us to model the individual differences in behavioural performance, as a function of the EEG signals representing each temporal stage of neural processing. Starting with preparatory signals (α-power), to early target selection signals (N2), to evidence accumulation (CPP), to motor preparation (LHB). The hierarchical addition of the predictors informed us whether

each of the EEG signals reflecting successive stages of neural processing improved the fit of the model predicting behavioural data. The signals that explained unique variance were then simultaneously forced into a simplified model predicting RT or RTcv, which made it possible to obtain accurate parameter estimates not contaminated by signals that were shown not to improve model fits. Note that only subjects for which we could determine the CPP onset latency for all bins were included in this hierarchical model. For this final model, all behavioural and neural variables were scaled between 0 and 1 across subjects according to the formula: $y_i = (x_i - \min x_i)/(\max x_i - \min x_i)$, where y_i is the scaled variable, x_i is the variable to be scaled. This scaling procedure did not change the relationship of the variable within or across subjects, but scaled all predictor variables to the same range. Again, significance values were obtained by means of maximum likelihood ratio tests.

Data plotted in all figures are the mean and the standard error of the mean (SEM) across subjects. Linear fits are plotted when first-order fits were superior to the zero-order (constant) fit, quadratic fits are plotted when second-order fits were superior to the first-order fit.

2.4 - **Results**

80 subjects performed a continuous version of the random dot motion task in which they were asked to report temporally and spatially unpredictable periods of coherent motion within either of two streams of random motion (Figure 2-5a). We investigated whether the trial-to-trial fluctuations in behavioural performance and EEG signatures of perceptual decision making could, in part, be explained by trial-to-trial differences in the size of the baseline pupil diameter (reflecting tonic arousal) and the post-target pupil response (reflecting phasic arousal). We quantified this relationship by allocating data into 5 bins based on the size of either the baseline pupil diameter or the phasic pupil diameter response (Figure 2-5b-c). Baseline pupil diameter was computed as the average pupil diameter over the 100 ms preceding target onset. The phasic pupillary response was estimated using a single trial general linear model (GLM) approach. We first assessed the neural input to the peripheral pupil system by applying multiple models with onset and response components as well as various different shapes for the sustained component (Murphy et al., 2016) across all trials for each subject (Figure 2-1). Next we applied the grand average best-fitting model (linear up-ramp) on individual trials (Bach et al., 2018). This provided us with a trial-by-trial estimate of the amplitude of each temporal component. Comparison against several other measures of the pupil diameter response (Figure 2-2), controlling for variance inflation factors (Figure 2-3) and applying the same model across bins of trials, or orthogonalising the predictors (Figure 2-4) provided support for the reliability of the estimated amplitude of the pupillary response. Here we present the relationship of the amplitude of the target onset component to the behavioural and EEG signatures of perceptual decision making. We then used sequential multilevel model analyses and maximum likelihood ratio tests to test for fixed effects of pupil bin. We determined whether a linear fit was better than a constant fit and

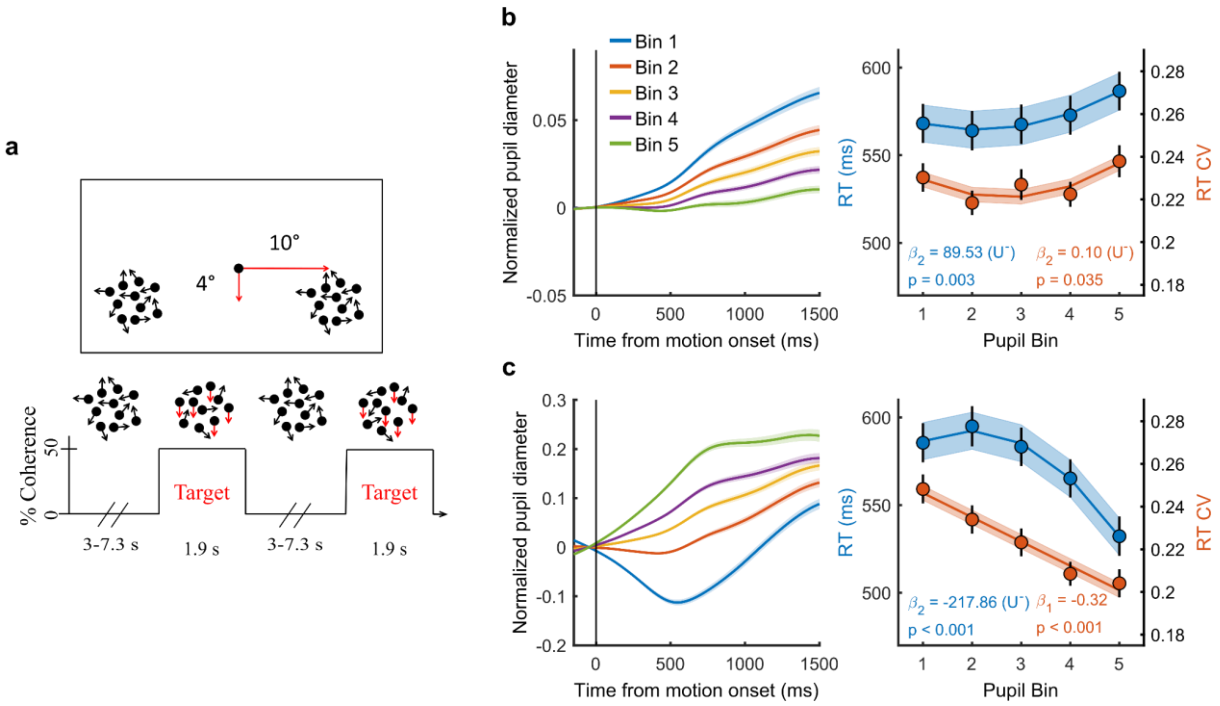

Figure 2-5. The effect of baseline pupil diameter on the relationship between the pupil response and behavioural performance. (**a**) Paradigm. Subjects fixated on a central dot while monitoring two peripheral patches of continuously presented randomly moving dots. At pseudorandom times an intermittent period of coherent downward motion (50%) occurred in either the left or the right hemifield. A speeded right handed button press was required upon detection of coherent motion. (**b**) Pupil diameter time course and task performance sorted by baseline pupil diameter. (Left) Pupil time-course for the five bins. (Right) Behavioural performance for the five bins. Markers indicate mean reaction times (RT, blue, left y-axis) and reaction time coefficient of variation (RTcv, red, right y-axis), lines and shading indicate significant model fits. (**c**) Same conventions as **b**, but sorted by the pupil diameter response. Error bars and shaded regions denote ±1 standard error of the mean (SEM). Statistics: β weights: linear mixed effects model analyses, U: indicates presence (+) or absence (-) of significant U-shaped relationship.

subsequently whether the fit of a second-order polynomial, indicating a non-monotonic relationship between pupil diameter and behaviour/EEG, was superior to a linear fit. We furthermore used a variant of the 'two-lines' approach (Simonsohn, 2017) to test whether any non-monotonic relationship was best described by an (inverted) U-shape.

2.4.1 - Both tonic and phasic arousal are predictive of task performance

We first investigated the relationship between trial-by-trial pupil dynamics and behavioural performance. As stimuli were presented well above perceptual threshold, our subjects performed at ceiling (mean, 98.7%; range: 92–100%, Newman et al., 2017). We therefore focused on RT and the RT coefficient of variation (RTcv), a measure of performance variability calculated by dividing the standard deviation in RT by the mean (Bellgrove et al., 2004), rather than accuracy. We found that baseline pupil diameter displayed a non-monotonic relationship with both measures of behavioural performance (RT $\chi^2_{(1)} = 8.84$, $p = 0.003$; RTcv $\chi^2_{(1)} = 4.43$, $p = 0.035$). Neither effects were,

Table 2-1. Parameter estimates for the single-trial mixed effect model analysis predicting RT using linear and polynomial basis functions of baseline pupil diameter (BPD) and the pupil response (PR).

	Model comparison		**Parameter estimates**			
	χ^2	*p*	β	β *SEM*	*t*	*p*
BPD	5.28	0.021	0.099	0.062	1.59	0.112
BPD²	57.47	3.43E-14	0.297	0.049	6.119	9.86E-10
PR	302.01	1.20E-67	-0.757	0.043	-17.55	1.85E-68
PR²	118.68	1.23E-27	-0.489	0.045	-10.91	1.22E-27

however, significantly U-shaped (Figure 2-5b). Rather, RT was slower on trials with higher baseline arousal levels. The pupil diameter response, on the other hand, displayed a non-monotonic (but not U-shaped) relationship with RT ($\chi^2_{(1)}$ = 51.89, p < 0.001) and an inverse linear relationship with RTcv ($\chi^2_{(1)}$ = 45.94, p < 0.001). For both RT and RTcv, best performance was found on trials with the largest pupil responses (Figure 2-5c). This relationship remained very similar when trial-by-trial fluctuations in the pupil response that are due to variability in the amplitude or phase of the baseline pupil diameter were not removed (Figure 2-6). We furthermore repeated the sequential regression analysis in single-trial, non-binned data, in which we additionally controlled for time-on-task effects, confirming that these effects were not dependent on the binning procedure (Table 2-1). Additionally, we noticed that when we band-pass filtered the pupil diameter, rather than low-pass filtered, the relationship between baseline pupil diameter and task performance was not significant (Figure 2-7). This suggests that slow fluctuations in baseline pupil diameter (<0.01Hz) are driving the effect on task performance.

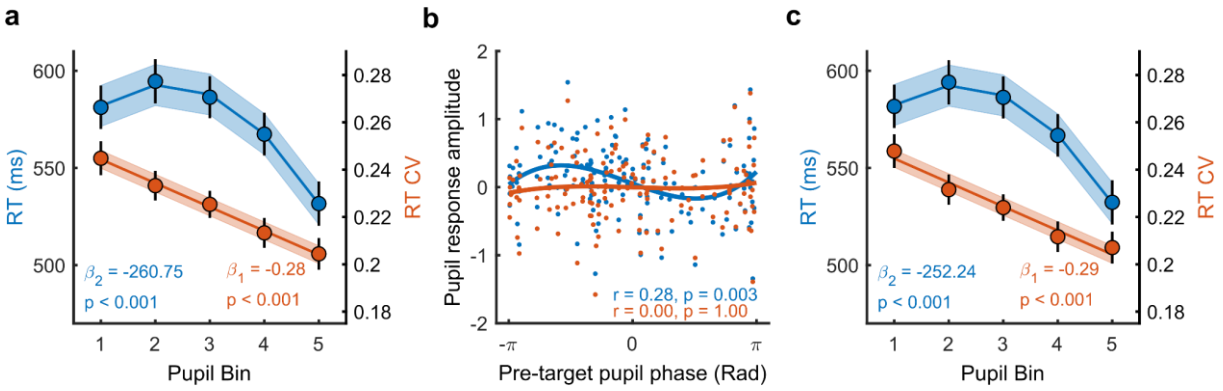

Figure 2-6. The effect of baseline pupil diameter on the relationship between the pupil response and behavioural performance.(**a**) Behavioural performance binned by the size of the phasic pupil response to target onset without removing the trial-to-trial fluctuations in baseline pupil diameter. (**b**) The relationship between the pre-target phase (radians) of the pupil diameter, and the amplitude of the post-target pupil response, before (blue) and after (red) the regression procedure for an example subject. Dots denote individual trials, lines indicate third order polynomial fits to the data. (**c**) As in **a**, but without the removal of the trial-to-trial fluctuations due to fluctuations in the phase of the baseline pupil diameter. Error bars and shaded regions denote ±1 standard error of the mean (SEM). Statistics: linear mixed effects model analyses and the circular correlation coefficient.

2.4.2 - Phasic arousal has an approximately linear relationship with decision processing

During decision making, perceptual evidence has to be accumulated over time. This accumulation process has long been related to build-to-threshold activity in single neurons in parietal cortex (Gold and Shadlen, 2007; but see Latimer et al., 2016, 2015; Shadlen et al., 2016). The centro-parietal positivity (CPP) measured from scalp EEG exhibits many of these same properties, including a representation of the accumulation of sensory evidence towards a decision bound (Kelly and O'Connell, 2013; O'Connell et al., 2018, 2012). Because in this study we used relatively strong sensory evidence (50% coherence), it is possible that subjects may not have relied upon any temporal integration of this motion signal to reach a decision. Rather, variability in RT could be brought about by variation in the onset transient of target selection due to the temporal and spatial uncertainty of the target stimulus. On single trials, decision formation could be a step-like signal that averaged across trials looks like an accumulate-to-bound signal (Latimer et al., 2015). Although we cannot discount this possibility, aligning the visual early target selection signals (N2c) to response reveals a much lower signal amplitude compared to aligning it to target onset (Figure 2-8). This indicates that there is no fixed delay between target selection and the response, and that there is variability in the duration of the sustained period of this task. This variation could indicate different trial-to-trial strategies (e.g. comparing motion in one stimulus against the stimulus on the other side of the screen), or in addition some variability in accumulation rate. Because of this uncertainty, we refer to the functional significance of the CPP as decision processing.

Here we tested the relationship between the pupil diameter response and the onset, build-up rate, amplitude and consistency (ITPC) of the CPP (Figure 2-9). We found that the onset latency of the CPP, defined as the first time point that showed a significant

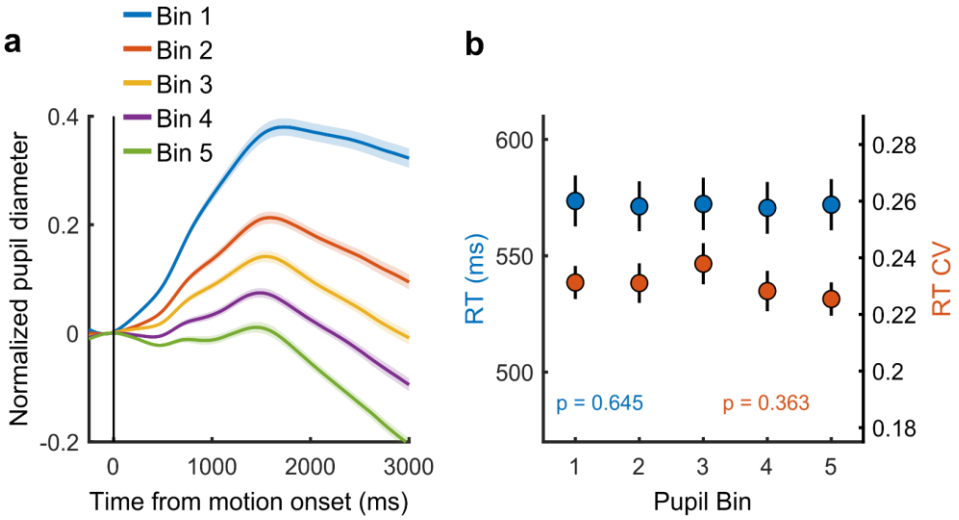

Figure 2-7. The relationship between baseline pupil diameter and task performance, for band-pass (0.1–6 Hz), rather than low-pass (<6 Hz) filtered pupil diameter data. (**a**) Pupil time-course for the five bins. (**b**) Behavioural performance for the five bins. Markers indicate mean reaction times (RT, blue, left y-axis) and reaction time coefficient of variation (RTcv, red, right y-axis). Error bars and shaded regions denote ±1 standard error of the mean (SEM). Statistics: linear mixed effects model analyses.

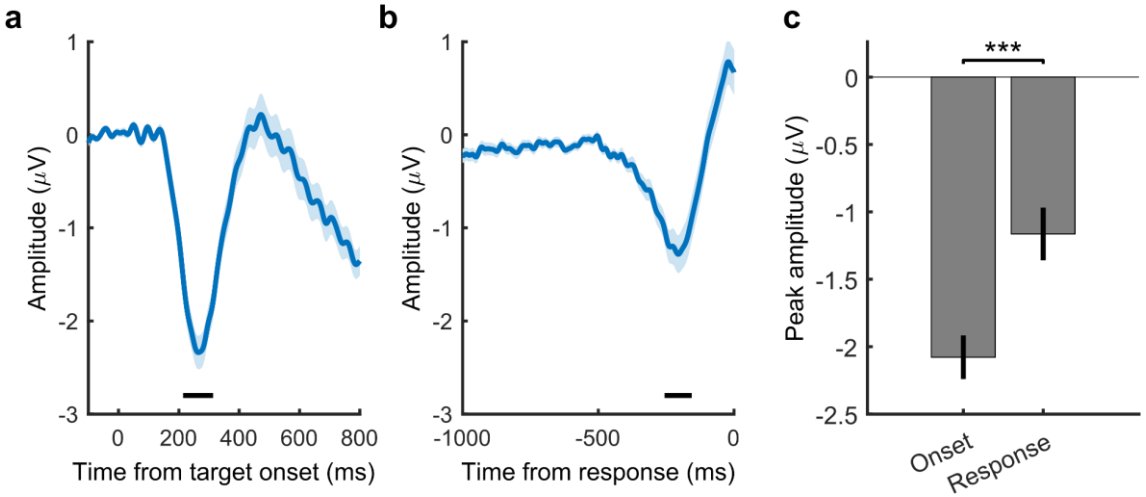

Figure 2-8. N2c amplitude is reduced when aligned to the response. (**a**) N2c signal aligned to target onset. (**b**) N2c signal aligned to response. (**c**) N2c amplitude over a 100 ms window (black bars in panels **a** and **b**) aligned to target onset and response. Error bars denote ±1 standard error of the mean (SEM). Statistics: Wilcoxon signed rank test.

difference from zero for 15 consecutive time points, displayed an inverse monotonic relationship with the size of the pupil response ($\chi^2_{(1)} = 5.60$, $p = 0.018$), such that the fastest onsets were found for the largest pupil response bins (Figure 2-9a). Likewise, the build-up rate ($\chi^2_{(1)} = 4.45$, $p = 0.035$), but not the amplitude ($p = 0.15$), of the CPP varied with the pupil response, displaying the steepest slope on trials with the largest pupil dilations (Figure 2-9b). Because the membrane potential of sensory neurons shows the least variance and highest response reliability at intermediate baseline pupil diameter (McGinley et al., 2015a), we additionally investigated the ITPC, a measure of across trial consistency, of the CPP. We computed ITPC with a single-taper spectral analysis in a 512 ms sliding window computed at 50 ms intervals, with a frequency resolution of 1.95 Hz. Based on the stimulus-locked grand average time-frequency spectrum, we selected a time (300-550 ms) and frequency window (<4 Hz) for further statistical analyses (Figure 2-9c). We found an approximately linear relationship between pupil diameter response and the consistency of the CPP signal ($\chi^2_{(1)} = 41.79$, $p < 0.001$), indicating that the CPP signal is less variable for larger pupil response bins (Figure 2-9d). This relationship was also present when we aligned the CPP to the response (Figure 2-10), indicating that this effect is unlikely to solely reflect variability in the onset of the CPP. Thus, we found that the size of the pupillary response was predictive of both the onset latency, build-up rate as well as the ITPC of the CPP. Moreover, the relationship with the neural parameters of the CPP resembled the relationship between the pupil response and behavioural performance (Figure 2-5c). Large pupil dilations were predictive of faster responses, earlier CPP onset latencies, as well as steeper build-up rates and more consistent CPP. Next, we asked whether other stages of information processing underpinning perceptual decision making also varied with the pupil response.

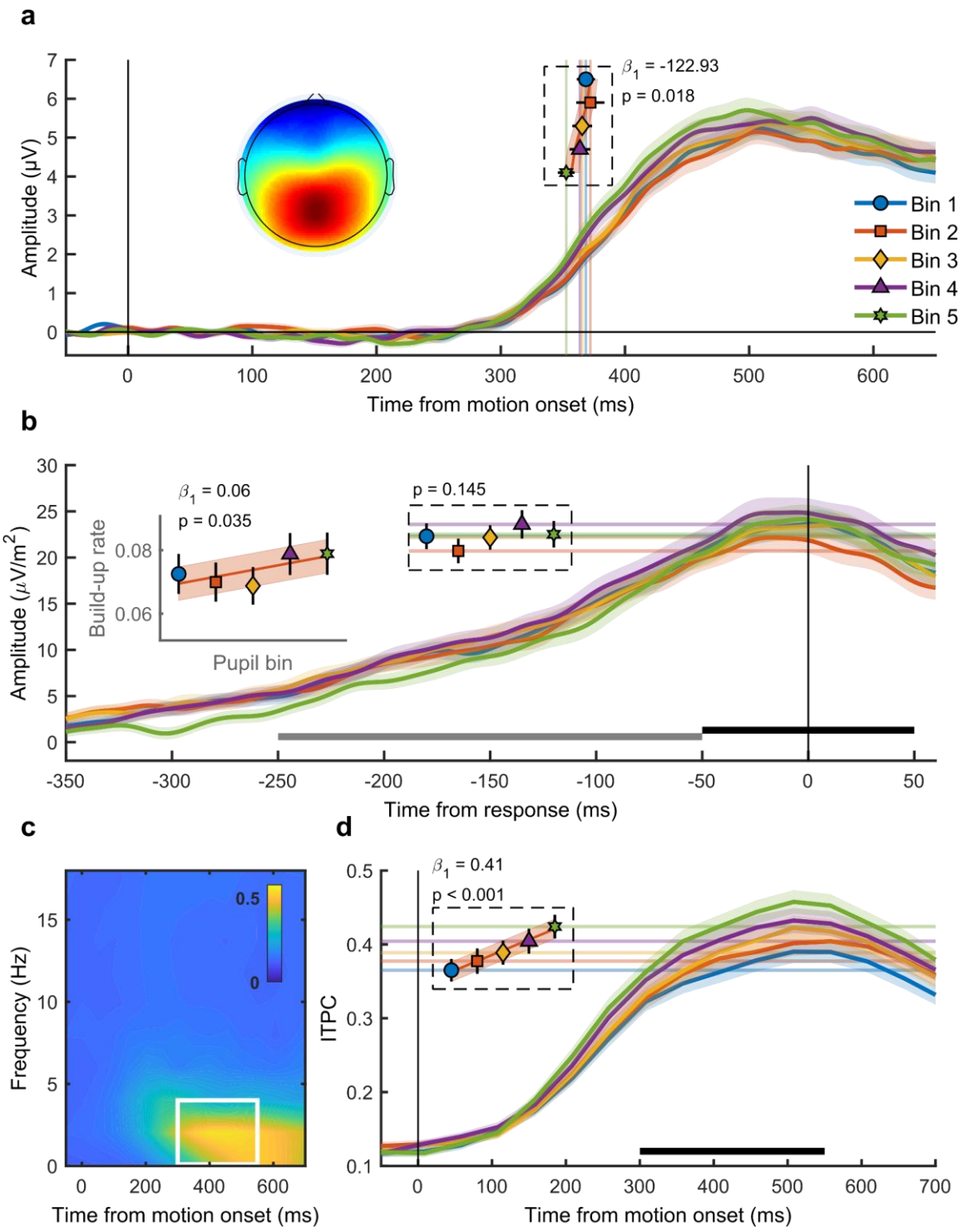

Figure 2-9. The centro-parietal positivity (CPP) in relation to phasic arousal. (**a**) The stimulus-locked CPP time-course showed faster onset times for larger pupil response bins. The inset shows the scalp topography of the CPP. Vertical lines and markers indicate the onset latencies per bin. (**b**) The response- locked CSD-transformed CPP time-course. Horizontal lines and markers indicate the CPP amplitude, and the inset displays the build-up rate of the CPP across pupil response bins. The black bar represents the time window used for the calculation of the CPP amplitude and the grey bar the time window used for the calculation of the build-up rate. (**c**) Grand average inter-trial phase coherence (ITPC) per time-frequency point for the CPP. The white box represents the time-frequency window selected for statistical analyses. (**d**) ITPC per pupil bin over time for frequencies below 4 Hz. The black bar indicates the time window used for further analysis. Horizontal lines and markers indicate the averaged ITPC in the time-frequency window indicated by the white box in panel **c**. Error bars and shaded regions denote ±1 SEM. Statistics: linear mixed effects model analyses. Lines and shading indicate significant fits to the data.

2.4.3 - The phasic pupil response relates monotonically to spectral measures of baseline attentional engagement, but not motor output

We next investigated pre-target preparatory α-band power (8-13 Hz), a sensitive index of attentional deployment that has been shown to vary with behavioural performance. Specifically, previous studies have found higher pre-target α-band power preceding trials with longer RT, and that fluctuations in α-power may reflect an attentional influence on variability in task performance (Ergenoglu et al., 2004; Kelly and O'Connell, 2013; O'Connell et al., 2009; van Dijk et al., 2008). We first verified the relationship between α-band power and behavioural performance by binning the data into 5 bins according to α-band power and performing the same sequential regression analysis as described above (Figure 2-11a). We replicated previous findings (Kelly and O'Connell, 2013) and found an approximately linear relationship between α-band power and RT ($\chi^2_{(1)} = 25.27$, $p < 0.001$) but not RTcv ($p = 0.48$). In line with previous research (Hong et al., 2014), pupil diameter response was inversely related to α-band power (Figure 2-11b), displaying an approximately linear relationship ($\chi^2_{(1)} = 28.24$, $p < 0.001$), suggesting that pre-target attentional engagement is related to phasic arousal.

We next focused on response-related motor activity in the form of left hemispheric β-power (LHB). LHB decreases before a button press and has been shown to reflect the motor-output stage of perceptual decision making, but also to trace decision formation, reflecting the build-up of choice selective activity (Donner et al., 2009). Here we investigated the LHB amplitude and build-up rate preceding response (Figure 2-11c). We found that neither LHB amplitude ($p = 0.63$) nor LHB slope ($p = 0.20$) varied with phasic arousal, suggesting that phasic arousal does not influence the build-up rate of choice-related activity over motor cortex.

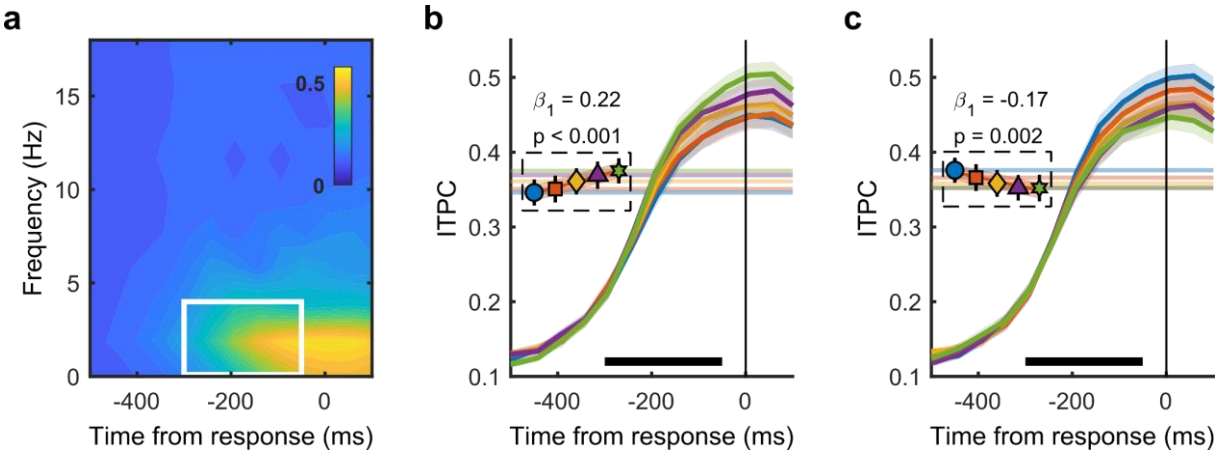

Figure 2-10. CPP ITPC aligned to response. (**a**) Grand average inter-trial phase coherence (ITPC) per time-frequency point for the CPP aligned to response. The white box represents the time-frequency window selected for statistical analyses. (**b**) ITPC per pupil response bin over time for frequencies below 4 Hz. The black bar indicates the time window used for further analysis. Horizontal lines and markers indicate the averaged ITPC in the time-frequency window indicated by the white box in panel **a**. (**c**) Same as **b**, but binned by baseline pupil diameter. Error bars and shaded regions denote ± 1 SEM. Statistics: linear mixed effects model analyses. Lines and shading indicate significant fits to the data.

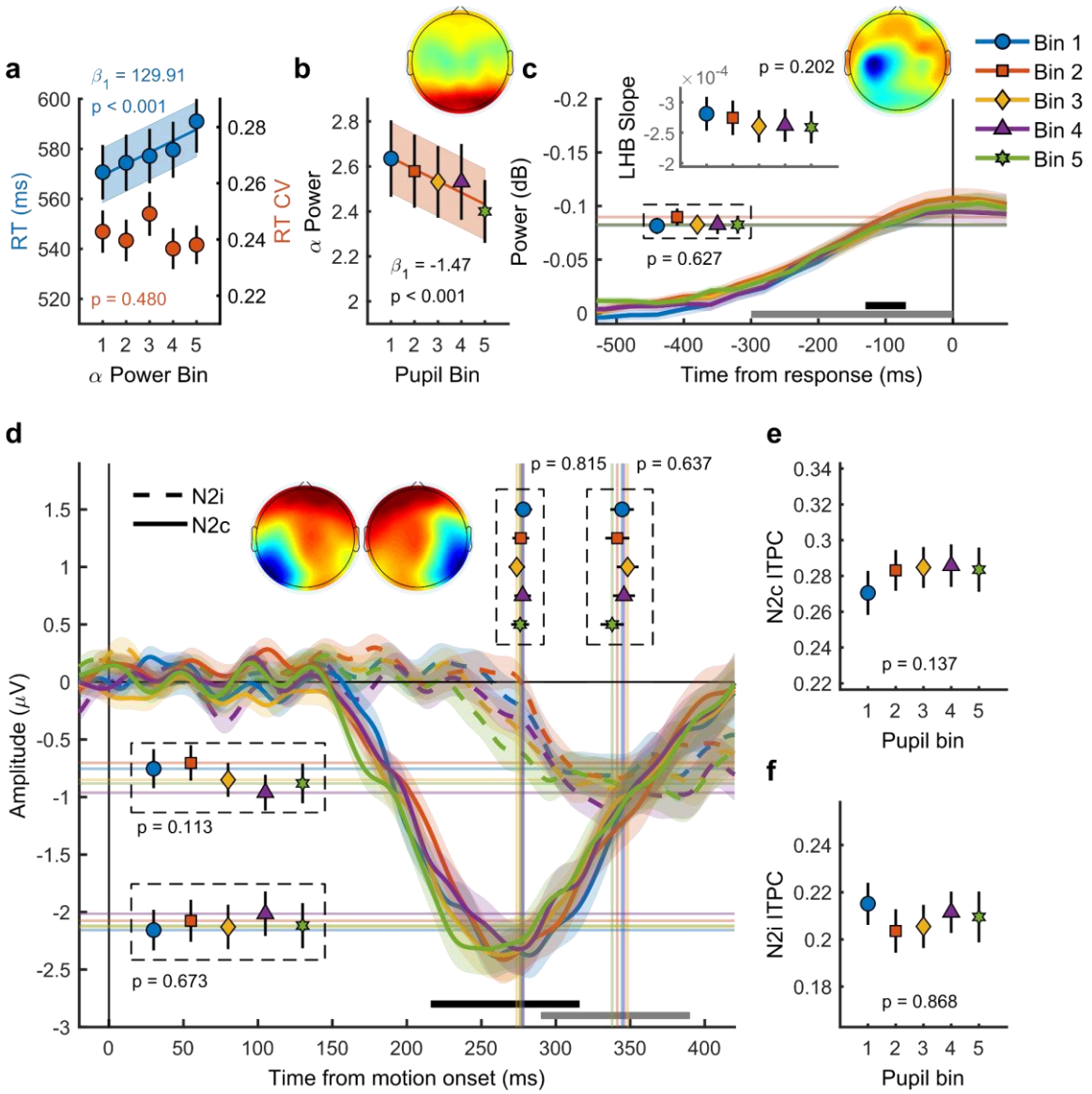

Figure 2-11. The phasic pupil response in relation to EEG signatures of attentional engagement, motor response and early target selection. (**a**) RT and RTcv in relation to pre-target α power. (**b**) Pre-target α power in relation to the pupil response. (**c**) Response-related left hemispheric β power (LHB) per pupil bin. Horizontal lines and markers indicate the average LHB in the time window indicated by the black bar. Inset shows LHB build-up rate, as determined by fitting a straight line through the LHB in the time window indicated by the grey bar. Note the reverse y-axis direction. (**d**) The stimulus- locked N2c (solid lines) and N2i (dashed lines) time-course binned by the pupil response. Vertical lines and markers show the peak latencies. Horizontal lines and markers show the average N2 amplitude during the time period indicated by the black (N2c) and grey (N2i) bars. (**e-f**) N2c (**e**) and N2i (**f**) ITPC per pupil bin over the time and frequency window determined based on the grand average ITPC (data not shown). Insets show the scalp topography of each neural signal. Error bars and shaded regions denote ±1 SEM. Statistics: linear mixed effects model analyses. Lines and shading indicate significant fits to the data.

2.4.4 - Target selection signals do not correlate with the phasic pupil response

Next we investigated the N2 (Figure 2-11d-f), a stimulus-locked early target selection signal that has been shown to predict behavioural performance and modulate the onset and build-up rate of the CPP (Loughnane et al., 2016). Because of the spatial nature of the task, we analysed the negative deflection over both the contra- (N2c) and ipsi-lateral

(N2i) hemisphere, relative to the target location. The pupil response was not predictive of any aspect of the N2. Specifically, phasic arousal was not predictive of N2c latency ($p = 0.82$) or amplitude ($p = 0.64$), nor did we find any relationship between the pupil response and the N2c ITPC ($p = 0.14$). Likewise, the pupil response was not predictive of N2i latency ($p = 0.64$), amplitude ($p = 0.11$) or ITPC ($p = 0.87$).

2.4.5 - The impact of phasic arousal on task performance is mainly mediated by the consistency in decision processing

We found that pupil-linked phasic arousal was predictive of specific neural signals at multiple information processing stages of perceptual decision making. To test which of these signals explained unique variability in behavioural performance across the 5 pupil response bins and subjects, the neural signals were added to a linear mixed effects model predicting either RT or RTcv with their order of entry determined hierarchically by their temporal order in the decision making process. This allowed us to test whether each successive stage of neural processing would improve the fit of the model to the behavioural data, over and above the fit of the previous stage.

Compared to the baseline model predicting RT with pupil bin, the addition of pre-target α-power significantly improved the model fit ($\chi^2_{(1)} = 10.30$, $p < 0.001$). None of the measures of early target selection improved the fit of the model; neither N2c latency ($\chi^2_{(1)} = 0.14$, $p = 0.70$) or amplitude ($\chi^2_{(1)} = 0.94$, $p = 0.33$), nor N2i latency ($\chi^2_{(1)} = 2.39$, $p = 0.12$) or amplitude ($\chi^2_{(1)} = 2.39$, $p = 0.12$). We found that both the addition of CPP onset ($\chi^2_{(1)} = 8.24$, $p = 0.004$) as well as the build-up rate ($\chi^2_{(1)} = 4.90$, $p = 0.027$) significantly improved the model fit. Whereas the addition of CPP amplitude did not ($\chi^2_{(1)} = 1.43$, $p = 0.23$), the addition of CPP ITPC substantially improved the fit of the model ($\chi^2_{(1)} = 19.25$, $p < 0.001$). Neither the LHB build-up rate nor amplitude improved the fit of the model (LHB build-up rate $\chi^2_{(1)} = 0.02$, $p = 0.88$; amplitude $\chi^2_{(1)} = 0.64$, $p = 0.42$). Overall, this model suggested that pre-target α-power, CPP onset, build-up rate and ITPC exert partially independent influences on RT. Because some variables were highly correlated (e.g. CPP onset and ITPC) we used an algorithm for forward/backward stepwise model selection (Venables and Ripley, 2002) to test whether each neural signal indeed explained independent variability that is not explained by any of the other signals. This procedure eliminated CPP onset ($F_{(1)} = 0.06$, $p = 0.80$) and build-up rate ($F_{(1)} = 1.86$, $p = 0.17$) from the final model. Thus, only pre-target α-power and CPP ITPC significantly improved the model fit for predicting RT. These two variables were forced into one linear mixed effects model predicting RT (Statistical analyses), and comparison to a baseline model revealed a good fit ($\chi^2_{(2)} = 38.61$, $p < 0.001$). The fixed effects of the model (the neural signals) explained 15.8% of the variability in RT (marginal r^2) across the 5 pupil response bins, and together with the random effects (across subject variability) it explained 92.6% of the variability (conditional r^2).

We performed the same hierarchical regression analysis to see which neural signals explained variability in RTcv. We summarised the results of this analysis in Table A. 1 and report the most important results here. The hierarchical regression analysis revealed

Table 2-2. Parameter estimates for the final linear mixed effect model of RT and RTcv binned by the pupil diameter response or baseline. The only parameters included are the neural signals that significantly improved the model fit.

	RT				**RTcv**			
	β	β SE	T	p	β	β SEM	t	P
Pupil response								
pre-target α-power	0.20	0.065	3.07	0.002				
CPP ITPC	-0.19	0.034	-5.51	<0.001	-0.21	0.049	-4.22	<0.001
Baseline pupil diameter								
N2c amplitude	0.06	0.027	2.33	0.021				
CPP ITPC	-0.17	0.033	-5.21	<0.001	-0.31	0.056	-5.48	<0.001

that both CPP onset and CPP ITPC improved the model fit, but eliminated CPP onset after the forward/backward model selection. Consequently, CPP ITPC was the only variable that exerted independent influence on RTcv. Comparison against a baseline model revealed a significant fit ($\chi^2_{(1)} = 15.36$, $p < 0.001$) that had a marginal r^2 of 16.0% and a conditional r^2 of 45.9%.

To test whether our assumptions about the temporal order of the neural signals influenced these results, we fitted a model in which all EEG signatures were added at the same time and investigated their coefficients. This analysis did not identify any additional neural components to those that were found using the hierarchical regression analysis (Table A. 2).

Table 2-2 shows the final parameter estimates for the neural signals that significantly predicted variability in RT or RTcv that is due to variability in phasic arousal. From this analysis we can conclude that CPP ITPC was the strongest predictor for RT and the only predictor for RTcv. These results provide novel insight into the mechanism by which the neuromodulators that control arousal can influence behaviour. The impact of these modulators on decision making, is thus mainly mediated by their effects on the consistency in decision formation. Next, we turn to tonic arousal and its relationship to these same EEG components of perceptual decision making.

2.4.6 - Baseline pupil diameter is inversely related to the consistency of decision processing

Figure 2-12 illustrates the relationship between baseline pupil diameter and the CPP. Unlike the pupil response, baseline pupil diameter was not predictive of the onset ($p = 0.20$) or build-up rate ($p = 0.12$), but it displayed an inverse relationship with both the amplitude ($\chi^2_{(1)} = 7.09$, $p = 0.01$) and the consistency of the CPP ($\chi^2_{(1)} = 9.34$, $p = 0.002$). In line with previous research that revealed increased variability in the rate of evidence accumulation during periods with larger baseline pupil diameter (Murphy et al., 2014b),

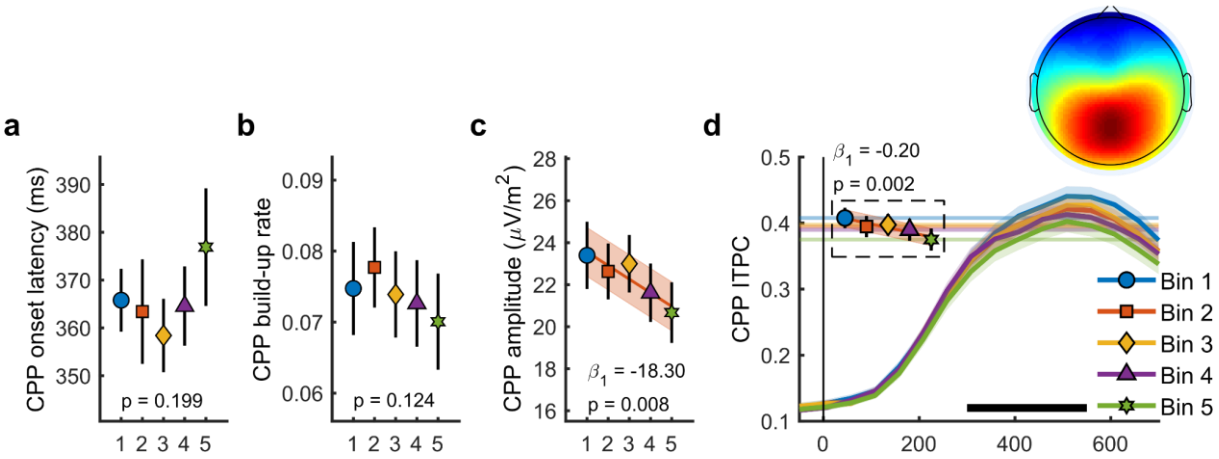

Figure 2-12. Relationship between baseline pupil diameter and the CPP. (**a**) CPP onset latency, (**b**) build-up rate, (**c**) amplitude and (**d**) ITPC per pupil bin over time for frequencies below 4 Hz. The black bar indicates the time window used for further analysis. Horizontal lines and markers indicate the averaged ITPC in the time-frequency window indicated by the white box in Figure 2-9c. Error bars and shaded regions denote ±1 SEM. Statistics: linear mixed effects model analyses. Lines and shading indicate significant fits to the data.

we found an inverse, approximately linear, relationship in which higher baseline pupil diameter displayed lower EEG signal consistency (Figure 2-12d). Thus, states of higher arousal are characterised by less consistency, i.e. more variability, in decision processing. Additionally, states of higher tonic arousal also display lower task performance (Figure 2-5b), indicating that higher variability in decision processing (due to higher tonic arousal) can affect behavioural performance.

2.4.7 - Baseline pupil diameter relates to spectral measures of baseline attentional engagement and motor output as well as early target selection

We found a relationship between baseline pupil diameter and specific characteristics of multiple neural processing stages of perceptual decision making. Specifically, as observed before (Hong et al., 2014), pre-target alpha power (Figure 2-13a) varied with baseline pupil diameter in a non-monotonic, but not inverted-U shaped, manner ($\chi^2_{(1)}$ = 4.49, p = 0.034). This suggests that with higher tonic arousal, alpha activity is higher (or less desynchronised). Next, we tested whether baseline pupil diameter was predictive of EEG characteristics representing motor output (Figure 2-13b). We found an inverse relationship with LHB build-up rate ($\chi^2_{(1)}$ = 10.99, p < 0.001), decreasing with larger baseline pupil diameter, but we did not find a relationship with LHB amplitude (p = 0.34).

Lastly, we investigated whether baseline pupil diameter affected early target selection signals, the N2 (Figure 2-13c-d). Previous studies have revealed that baseline pupil diameter affected the size and variability of neural responses to visual and auditory stimuli (McGinley et al., 2015a; Reimer et al., 2014). Here we found that baseline pupil diameter was not predictive of the peak latency of the N2c (p = 0.75), but that it did display a monotonic relationship with the N2c amplitude ($\chi^2_{(1)}$ = 13.72, p < 0.001). Trials

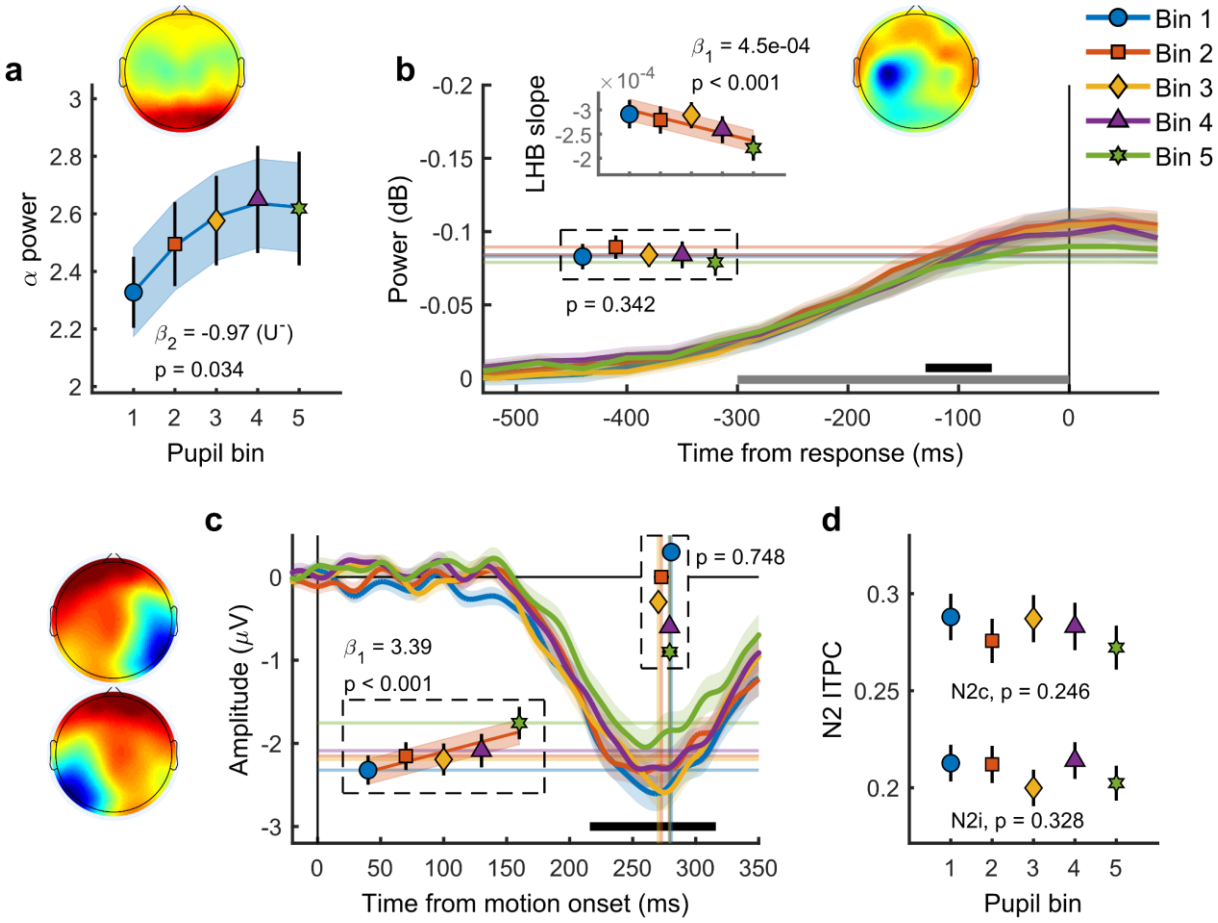

Figure 2-13. Baseline pupil diameter in relation to EEG signatures of attentional engagement, motor response and early target selection. (**a**) Pre-target α power by baseline pupil diameter. (**b**) Response-related left hemispheric β power (LHB) per pupil bin. Horizontal lines and markers indicate the average LHB in the time window indicated by the black bar. Inset shows the LHB build-up rate, as determined by fitting a straight line through the LHB in the time window indicated by the grey bar. Note the reverse y-axis direction. (**c**) The stimulus-locked N2c time-course binned by baseline pupil diameter. Vertical lines and markers show the peak latencies. Horizontal lines and markers show the average N2c amplitude during the time period indicated by the black bar. (**d**) N2c and N2i ITPC per pupil bin averaged in a time-frequency window based on the grand average. Insets show the scalp topography of each neural signal. Error bars and shaded regions denote ±1 SEM. Statistics: linear mixed effects model analyses. Lines and shading indicate significant fits to the data.

with larger baseline pupil diameter displayed smaller N2c amplitudes, suggesting that higher arousal has a negative impact on sensory encoding. N2c ITPC did not vary with baseline pupil diameter ($p = 0.25$), and nor did N2i ITPC ($p = 0.33$), N2i latency ($p = 0.78$) or amplitude ($p = 0.06$). We thus found that, similar to the phasic pupil diameter response, baseline pupil diameter is predictive of specific characteristics of each of the processing stages of perceptual decision making. Next, we investigated which of these components explained unique variance in task performance across pupil size bins.

2.4.8 - N2c amplitude and CPP ITPC are predictive of variability in task performance due to tonic arousal

We again performed the same hierarchical regression analysis as described above, to see which of the neural signals explained unique variability in task performance associated

with tonic arousal. The full results of this analysis are summarised in (Table A. 3). Here we discuss the main findings. After the application of a forward/backward model selection algorithm (Venables and Ripley, 2002), N2c amplitude and CPP ITPC were the only parameters that were predictive of RT. These variables were forced into one regression model predicting RT, and comparison against a baseline model with baseline pupil diameter as a factor revealed a significant fit ($\chi^2_{(2)} = 31.6$, $p < 0.001$) with a marginal (conditional) r^2 of 4.1% (94.4%). This same hierarchical regression procedure revealed that CPP ITPC was the only EEG component that explained unique variability in RTcv (Table A. 3). Comparison against a baseline model also led to a significant fit ($\chi^2_{(1)} = 26.83$, $p < 0.001$), with a marginal (conditional) r^2 of 11.9% (44.5%). None of the other EEG parameters that were excluded from the final model due to potential false assumptions about their temporal order revealed significant coefficients in a multilevel model analysis in which all components were added simultaneously (Table A. 4). Thus, additional to an effect of N2c amplitude on RT, the consistency of the CPP was the only stage of information processing that explained unique within and across-subject variability in task performance associated with changes in baseline pupil diameter.

2.5 - **Discussion**

Here we investigated whether behavioural and neural correlates of decision making varied as a function of baseline or task-evoked pupil diameter, indexing tonic and phasic arousal, respectively. The perceptual decision making paradigm employed (Figure 2-5a) allowed us to monitor the relationship between pupil diameter and independent measures of attentional engagement, early target selection, decision formation and motor output. We found that the trial-by-trial variability in both tonic and phasic arousal were predictive of behavioural performance (Figure 2-5b-c). For tonic arousal, this relationship was best described by a non-monotonic polynomial fit with slower RT for higher baseline pupil diameter. Higher phasic arousal, on the other hand, was predictive of better task performance.

We furthermore established that both tonic and phasic arousal were predictive of a subset of EEG signatures, together reflecting discrete aspects of information processing underpinning perceptual decision making. A hierarchical regression analysis allowed us to determine which of these processing stages exerted an independent influence on behavioural performance associated with central arousal. We found that pre-target α power, indexing baseline attentional engagement, and the consistency of the CPP, reflecting the decision formation, each explained unique variability in task performance that was due to variability in phasic arousal. Variability in task performance due to fluctuations in tonic arousal was explained by the amplitude of the target selection signal N2c and the consistency of the CPP. We thus revealed a direct relationship between both tonic and phasic measures of arousal, and a distinct but overlapping set of EEG signatures of perceptual decision making, and in particular the CPP.

2.5.1 - The functional significance of the CPP during perceptual decision making

Although the CPP has previously been found to reflect the accumulation of evidence (Kelly and O'Connell, 2013; Loughnane et al., 2018, 2016; Newman et al., 2017; O'Connell et al., 2012), as discussed in the results section, our task design does not allow us to unequivocally relate the CPP to a specific characteristic of the decision making process such as evidence accumulation. Because of the temporal and spatial uncertainty of the target stimulus, rather than accumulating evidence over an extended period of time on trials with slower RT, target onset transients could be delayed or subjects could be employing different strategies for motion detection on different trials (e.g. verifying the presence of coherent motion in one stimulus versus the other stimulus). Decision signals such as the CPP or LHB could on single trials behave analogously to a step-like signal that across trials seems to be accumulating to a threshold (Latimer et al., 2015; but see Shadlen et al., 2016), potentially supported by neural mechanisms in V4 that increase their activity transiently in response to changes in motion coherence (Costagli et al., 2014). Although we cannot discount that subjects use different strategies on different trials, previous studies in which subjects were required to monitor either one or multiple dot kinematograms revealed no differences in either RT or hit rate and both the early target selection signals and the CPP scaled with the percentage of coherently moving dots (Loughnane et al., 2016). We additionally showed here that there is no fixed delay between target selection and response (Figure 2-8) and that there is thus variability in the duration of the sustained period of the task. Any relationship between arousal and the CPP is therefore not solely the result of fluctuations in the latency of the target onset transient.

2.5.2 - Large phasic pupil responses are predictive of better task performance

We estimated the variability in phasic arousal using the amplitude of the task-evoked pupil diameter. Because of the sluggish nature of the pupil diameter response, pupil dilation after target onset likely reflects a combination of specific aspects of phasic arousal such as a response to target onset, decision formation as well as a motor response. Here we aimed to disentangle these different components by applying a general linear model on a single trial basis. First we determined the fit for various models for each subject across trials (Figure 2-1), after which we applied the best (across subject) fitting model to each individual trial. We addressed the reliability of the estimation of each of the temporal components by comparing their relationship to behavioural performance to those of other measures of the amplitude of the pupil diameter response (Figure 2-2), excluding trials with high VIF values (Figure 2-3), orthogonalising the predictors, and comparing the results from the single trial parameter estimation to those of groups of trials binned by RT (Figure 2-4). These results revealed that we can reliably estimate the target onset component, but that the estimation of the sustained component might not be as straightforward (Figure 2-3). Although the current measure

of the pupil response to target onset is unlikely to be completely independent of the estimation of the sustained component, inclusion of this predictor increased the fit of the model and captured variability in the pupil time course likely to reflect the influence of phasic arousal specific to decision formation. This reduced the influence of this sustained part of the arousal response on the estimation of the target onset component (Figure 2-3). To the extent that we could reliably estimate the amplitude of the target onset component, we investigated its relationship to the behavioural and neural signatures of perceptual decision making.

Larger target onset responses, presumably reflecting a phasic response in neuromodulatory brainstem centres, were predictive of faster and less variable RT (Figure 2-5c), faster onset, larger build-up rates and higher consistency of the CPP (Figure 2-9), as well as lower pre-target occipital α-power (Figure 2-11). These results can be interpreted in light of the relationship between pupil dilations and the activity in brain areas such as the LC or BF (Aston-Jones and Cohen, 2005a; de Gee et al., 2017; Gilzenrat et al., 2010; Joshi et al., 2016; Reimer et al., 2016; Varazzani et al., 2015). Direct electrophysiological recordings from the LC have revealed a positive correlation between LC phasic activity and behavioural performance on elementary target detection tasks (Aston-Jones et al., 1997, 1994; Rajkowski et al., 2004, 1994). Likewise, cue detection is enhanced on trials with a larger cholinergic response (Parikh et al., 2007), and previous studies have found that large pupil responses were predictive of higher behavioural performance (Beatty, 1982a; but see Kristjansson et al., 2009), and decreased decision bias (de Gee et al., 2017). Additionally, poor performance upon pupil constrictions is in line with studies showing that sensory target detection is suboptimal when a transient LC or BF response is absent (Aston-Jones et al., 1994; Gritton et al., 2016; Parikh et al., 2007; Rajkowski et al., 1994). Moreover, naturally occurring pupillary constrictions are preceded by transient activity decreases in the LC (Joshi et al., 2016), and are associated with increased synchronisation of cortical activity, a signature of cortical down states, as well as suboptimal processing of visual stimuli (Reimer et al., 2014). Our results suggest that event-related pupillary constrictions could be associated with similar neural mechanisms.

Trials with large pupil responses, and better task performance, were preceded by lower pre-target occipital α-power, i.e. more α desynchronisation (Figure 2-11). In line with these results and previous studies (Kelly and O'Connell, 2013), lower pre-target α-power itself was predictive of higher task performance. Fluctuations in α synchronisation have previously been related to variation in both arousal and attentional deployment (Ergenoglu et al., 2004; Kelly and O'Connell, 2013; Newman et al., 2016; O'Connell et al., 2009; van Dijk et al., 2008), often interpreted as a neurophysiological correlate of cortical excitability. Here, on trials with both higher phasic arousal and more α desynchronisation, behavioural performance was better. This could indicate that fluctuations in phasic arousal and attentional engagement rely on similar neuromodulatory mechanisms.

We additionally found that larger pupil responses were predictive of earlier onset latencies, faster build-up and higher consistency of the CPP signal (Figure 2-9). Thus,

the effects of the fluctuations in phasic arousal and attentional deployment on task performance are likely mediated by their effect on decision signals, and insofar as the CPP represents evidence accumulation (see above), these fluctuations could influence the build-to-threshold dynamics during perceptual decision making.

2.5.3 - Large baseline pupil diameter is predictive of relatively poorer task performance

We found a non-monotonic relationship between baseline pupil diameter and task performance (Figure 2-5b). This relationship was, however, not significantly U-shaped, but rather we found slower RT with higher baseline pupil diameter. This effect was moreover only observed when the pupil diameter data was not high-pass filtered (Figure 2-7), indicating that slow changes (<0.01 Hz) in pupil diameter are driving the effects on task performance.

In line with previous research (Hong et al., 2014), out of all the investigated EEG components, only pre-target α power displayed a small non-monotonic relationship with baseline pupil diameter. Approximately linear relationships were found with N2c amplitude, LHB build-up rate, as well as an inverse relationship with CPP amplitude and ITPC. Of these, only N2c amplitude and CPP ITPC explained within and across subject variability in task performance (Table 2-2). It thus seems that the effects of tonic arousal on task performance are mainly driven by an approximately linear relationship with target selection and consistency of decision formation.

These results appear at odds with a U-shaped relationship as predicted by the adaptive gain theory (Aston-Jones and Cohen, 2005a), and found during auditory target detection tasks (McGinley et al., 2015a; Murphy et al., 2011). One potential reason that we did not find a U-shaped relationship with task performance, is that we might not have observed the full range of possible baseline pupil diameter values, and thus not the full range of possible tonic arousal levels. Trials were presented in blocks of 18, after which subjects were allowed to take a short break, preventing them from becoming overly drowsy or too distracted. However, depending on the behavioural paradigm and task demands, the relationship between central arousal, performance and neural activity may take different forms (McGinley et al., 2015b; Shimaoka et al., 2018). Membrane potential recordings from sensory and association areas, as well as direct electrophysiological recordings from neuromodulatory brainstem centres during decision making tasks, are needed to gain further insight in the exact mechanisms that drive the relationship between cortical state, sensory encoding, decision formation and task performance.

2.5.4 - Variability in task performance due to pupil-linked arousal is best predicted by the consistency in decision formation

During epochs of quiet wakefulness, membrane potential fluctuations of neurons in visual, somatosensory and auditory cortex are closely tracked by baseline pupil diameter

(McGinley et al., 2015a; Reimer et al., 2014). These fluctuations in subthreshold membrane potential are characteristic of changing cortical state. Small pupil diameter is characterised by prominent low-frequency (2-10 Hz) and nearly absent high-frequency oscillations (30-80 Hz), whereas larger pupil diameter is characterised by reduced low-frequency, but increased high-frequency oscillations (McGinley et al., 2015a, 2015b). Thus, the average subthreshold membrane potential is most stable during intermediate pupil diameter, when neither low nor high-frequency components predominate. States of lower variability are furthermore characterised by more reliable sensory responses, higher spike rates, increased neural gain and better behavioural performance (McGinley et al., 2015a, 2015b; Reimer et al., 2014). In addition to activity in early sensory areas, there is some evidence that activity in higher-order association areas is also more reliable with intermediate arousal. During auditory target detection, human subjects displayed the least variable RT at intermediate baseline pupil diameter, as well as the highest amplitudes of the P3 component elicited by task-relevant stimuli (Murphy et al., 2011).

Here we found that the consistency of the CPP was the main EEG predictor of variability in task performance associated with both tonic and phasic arousal. For tonic arousal, our findings are largely in line with modelling studies which suggested that higher arousal is specifically predictive of more variability in evidence accumulation (Murphy et al., 2014b). For phasic arousal, higher consistency, and thus less variability, was found for larger pupil bins, which also displayed the best behavioural performance. These results suggest that similar neural mechanisms of cortical state described for sensory cortex (McGinley et al., 2015b, 2015a; Reimer et al., 2014; Vinck et al., 2015) might also affect neurons in higher-order association areas (e.g. parietal cortex) and thereby influence evidence accumulation and task performance. Simultaneous pupil diameter and membrane potential recordings in parietal cortex during decision making are needed to confirm this hypothesis.

2.5.5 - Target selection signal amplitude is modulated by pupil-linked arousal

In the present study, we used a paradigm in which two stimuli were continuously presented and target occurrence was both spatially and temporally unpredictable. Successful target detection thus relied on locating and selecting sensory evidence from multiple sources of information. Loughnane et al. (2016) have shown that early target selection signals, which occur contralateral to the target stimulus (N2c), modulate sensory evidence accumulation and behavioural performance. Although previous studies have characterised the dependence of the quality of sensory responses on fluctuations in cortical state, as measured by baseline pupil diameter (McGinley et al., 2015a; Reimer et al., 2014; Vinck et al., 2015), to the best of our knowledge, the influence of pupil-linked arousal on target selection signals has not been described before. Here, we showed that early target selection signals are modulated by tonic arousal such that larger baseline pupil diameter was predictive of smaller N2c amplitudes (Figure 2-13c).

Moreover, the amplitude of the N2c also explained unique variability in task performance across pupil bins and subjects (Table 2-2).

At first glance it seems counterintuitive that target selection signal amplitudes are decreased, whereas visual encoding in early visual cortex is enhanced on trials with larger baseline pupil diameter (Vinck et al., 2015), or during pupil dilation (Reimer et al., 2014). These differences could be due to differences in the nature of the recordings, as these previous studies used invasive electrophysiology and calcium imaging whereas we used scalp EEG, limiting especially the spatial resolution of our analyses that might be necessary to elucidate these effects (e.g. single neuron orientation tuning). Alternatively, they could constitute differential effects of arousal on visual encoding and target selection. More likely, however, they are due to specific task demands, in particular our use of multiple simultaneously presented competing stimuli. Indeed, there is some evidence that an increase in arousal, as measured by pupil diameter, can increase the ability of a distractor to disrupt performance on a Go/No-Go task in non-human primates (Ebitz et al., 2014). At high arousal levels, performance might thus be negatively affected when the task requires the successful suppression of distracting information, i.e. with higher arousal it is more difficult to focus on the task at hand (Aston-Jones and Cohen, 2005a; McGinley et al., 2015b). On the current task, it might thus be more difficult to select and process information from one of the two competing stimuli during states of high arousal, leading to reduced N2c amplitude as well as reduced performance.

2.5.6 - The overlap and dissociation between baseline pupil diameter and the pupil response

As in previous studies (de Gee et al., 2014; Gilzenrat et al., 2010; Murphy et al., 2011), we found a negative correlation between baseline pupil diameter and the size of the pupillary response. Both measures were predictive of task performance as well as a unique, but overlapping, set of EEG signatures of perceptual decision making. Because of the overlap in their effects on these EEG markers, in particular pre-target α power and CPP ITPC, it is possible that both (in part) reflect the same component of central arousal state. Although we removed (via linear regression) the variance in the pupil response that is due to fluctuations in the amplitude and the phase of the baseline pupil diameter, some variability in the baseline pupil diameter might not be fully dissociable from the pupil response, and both might thus reflect a noisy measure of tonic arousal. This interpretation is further supported by the finding that the relationship between the pupil response and task performance did not substantially change regardless of whether variability in the pupil response due to fluctuations in baseline amplitude and/or phase was removed or not (Figure 2-6). Importantly, however, the dissociation in the effect of baseline pupil diameter and the pupil response on these EEG markers, such as the effect on N2c amplitude, indicates that these measures also capture independent variability in central arousal (tonic and phasic) predictive of distinct information processing stages of decision making.

2.6 - **Concluding remarks**

In this study we investigated the relationship between measures of tonic and phasic pupil-linked arousal and behavioural and EEG measures of perceptual decision making. We found that trial-to-trial variability in both tonic and phasic arousal accounted for variability in task performance and were predictive of a unique, but overlapping, set of neural metrics of perceptual decision making. Specifically, tonic arousal exerted its influence on task performance through its effects on early target selection signals and the consistency of decision formation. Phasic arousal, on the other hand, affected behaviour through its relation with attentional engagement as well as the consistency of decision formation. These results indicate that during decision making both tonic and phasic activity in the (network of) neuromodulatory centres that control central arousal can affect behaviour during perceptual decision making. Thus, fluctuations in central arousal, mediated by neuromodulatory brainstem centres, act on multiple timescales to influence task performance through its effects on attentional engagement, sensory processing as well as decision formation.

2.7 - **Notes**

 Analysis scripts are freely available on github (https://github.com/jochemvankempen/2019_pupil_decisionMaking).

2.8 - **Acknowledgements**

We thank Peter R. Murphy for advice on data analysis. J.K. and A.T. are supported by research funding from the Henry Wellcome Trust (093104). M.A.B. is supported by fellowship and project grant support from the Australian Research Council (ARC; FT130101488; DP150100986; DP180102066). A.T. and M.A.B. are supported by research funding from a strategic research partnership between the Newcastle University and Monash University. M.A.B, R.O.C and A.T are supported by research funding from the Office of Naval Research Global (ONR Global).

Chapter 3 - Top-down retinotopic coordination of cortical states across Macaque V1 and V4 during selective attention

3.1 - Abstract

Spontaneous activity fluctuations are ubiquitous in cortex. The strength and coordination of these fluctuations between neuronal populations are affected by cortical state, reflecting changes to neural excitability that can influence sensory processing and behaviour. Although long assumed to reflect brain-wide activity changes, these dynamics were recently found to be modulated locally by spatially selective attention. in V4. Global cortical states can thus be coordinated by cognitive demands and operate on a local scale. Whether similar local attention-related state changes occur in primary sensory cortex, and whether (and how) cortical state changes are coordinated between cortical areas is currently unknown. We recorded simultaneously from V1 and V4 using 16-contact laminar electrodes in 3 Macaque monkeys performing a selective attention task. We used a Hidden Markov Model (HMM) to characterise On-Off dynamics in multi-unit activity, and investigated the effects of these dynamics on activity within and across areas. We found that cortical states are correlated between V1 and V4. State transitions in either area are preceded and followed by activity changes in the other area. Although coordination of state changes is not deterministic, on average, state transitions in V4 precede state transitions in V1 during selective attention. This suggests that V4 activity-changes drive cortical state changes in V1. Additionally, the strength of the coordination of cortical states across V1 and V4 was dependent on their receptive field (RF) separation, with higher correlations when RFs were closer together. Together, these results suggest that On-Off transitions traverse along retinotopically aligned cortical areas in a top-down manner. We tested the relationship between state transitions in V1 and V4 more directly by fitting a 4-state HMM simultaneously to activity from both areas. This model, in which either or both areas could be in an Off or On state, revealed that, when both areas were in an Off state, it was more likely for V4 than V1 to transition to an On state. Moreover, when both areas were in an On state, it was more likely for V4 than V1 to transition to an Off state. Critically, behavioural performance increased from when both areas were Off, through V1 On - V4 Off, through V1 Off - V4 On, to V1 and V4 On. Thus, our results show that ongoing cortical dynamics are shared across brain regions, modulated by cognitive demands and relevant for behaviour.

3.2 - Introduction

Cortical activity fluctuates across a continuum of highly synchronous activity and periods of desynchronised activity (Harris and Thiele, 2011; Kohn et al., 2009). These fluctuations are not solely determined by external inputs, but reflect spontaneous fluctuations in neural excitability referred to as cortical state. Endogenously produced variability in cortical state has been found to shape sensory responses and influence

behavioural performance (Arieli et al., 1996; Gutnisky et al., 2017; McGinley et al., 2015a; Renart and Machens, 2014; Scholvinck et al., 2015). Although these fluctuations were long thought to be a global phenomenon that influences activity throughout the cortex and relates to the behavioural state of the animal, recent evidence revealed that signatures of cortical state are modulated locally by spatially selective attention in V4 of the Macaque monkey (Engel et al., 2016). Global cortical state can thus be coordinated by cognitive demands and operate on a local scale. Whether such attention-related state changes occur in primary visual cortex, whether (and how) fluctuations in cortical state are coordinated across areas along the cortical hierarchy, and whether this coordination is relevant for behaviour is currently unknown.

In V4 of awake behaving macaques, fluctuations in cortical state bring about transitions between episodes of vigorous (On) and faint (Off) spiking activity that occur synchronously across cortical laminae (Engel et al., 2016). During On compared to Off episodes, the cortex was more desynchronised, as low-frequency power (<10 Hz) in the local field potential (LFP) was suppressed whereas high-frequency power (>40 Hz) was increased. Additionally, On-Off dynamics were modulated by central arousal, as larger pupil diameter was predictive of increased On episode durations. Fluctuations in pupil diameter reflect activity changes in neuromodulatory brainstem centres such as the noradrenergic (NA) locus coeruleus (LC) and the cholinergic basal forebrain (BF). On-Off dynamics are thus likely influenced by the global gain changes elicited by these neuromodulators. In addition to this influence of central arousal, spatially selective attention was also found to increase the duration of On episodes independently of arousal. Thus, On-Off dynamics in V4 relate to measures of global network state, but are also influenced by cognitive processes recruiting specific retinotopic locations.

To determine whether similar signatures of state changes can be found in area V1, and whether these are coordinated between areas, we simultaneously recorded in areas V1 and V4 with laminar electrodes while monkeys performed a feature based covert top-down spatial attention task. We investigated On-Off dynamics in Macaque V1 and V4 by applying a Hidden-Markov Model (HMM) to multi-unit activity (MUA) recorded from across all laminae. We replicated previous findings that revealed modulation of cortical state by spatially selective attention in V4, and additionally found a similar modulation in V1. Furthermore, On-Off dynamics were coordinated in a top-down manner between V1 and V4. This coordination was predictive of task performance, and the strength of the coordination depended on the distance between retinotopic locations of these two areas, suggesting that cortical state transitions, or the modulation of their dynamics, are driven in a top-down manner.

3.3 - **Methods**

3.3.1 - Animals and Procedures

The subjects in our study were 3 male rhesus macaque monkeys (*Macaca mulatta,* age 10-12 years, weight 8.5-12.5 kg). All animal procedures were performed in accordance

with the European Communities Council Directive RL 2010/63/EC, the National Institutes of Health's Guidelines for the Care and Use of Animals for Experimental Procedures, and the UK Animals Scientific Procedures Act.

3.3.2 - Surgical Preparation

The animals were implanted with a head post and recording chambers over area V1 and V4 under sterile conditions and general anaesthesia. Surgical procedures and postoperative care conditions have been described in detail previously (Thiele et al., 2006).

3.3.3 - Behavioural paradigm

Stimuli were presented on a cathode ray tube (CRT) monitor at 120 Hz, 1280 × 1024 pixels, at a distance of 54 cm. The location and size of the receptive field (RF) was measured as described in detail previously (Gieselmann and Thiele, 2008). Briefly, the location and size of RF was measured by a reverse correlation method. During fixation, a series of black squares (0.5-2° size, 100% contrast) were presented for 100 ms (with 100 ms interstimulus interval) at pseudorandom locations on a 9 × 12 grid (5-25 repetitions for each location) on a bright background. RF eccentricity ranged from 3.4 - 7.5° in V1, and from 2.5 to 8.9° in V4.

During the main task (Figure 3-1), the monkeys initiated a trial by holding on to a lever and fixating on a central white fixation spot (0.1°) displayed on a gray background (1.41 cd/m²). After a fixed delay (614, 424, 674 ms, for monkey 1, 2 and 3), three coloured (Table 4-1 for colour values) square wave gratings appeared equidistant from the fixation spot, one of which was centred on the RF of the V1 neurons under study. The colour locations of these gratings were fixed for each recording session, and were pseudorandomly assigned across sessions. Stimulus size varied between 2 and 4° diameter, depending on RF eccentricity and size. For most recordings we used drifting gratings, but presented one monkey with stationary gratings on 22 out of 34 recording

Table 3-1. Colour values used for the 3 coloured gratings across recording sessions and subjects, indicated as [RGB] – luminance (cd/m²). a = Undimmed values, b = Dimmed values. For monkey 1, we used a variety of dimmed values across recordings.

	Red	**Green**	**Blue**
Monkey 2 & 3, and monkey 1 (n=4)	a. [220 0 0] – 12.8 b. [140 0 0] – 4.2	a. [0 135 0] – 12.9 b. [0 90 0] – 4.6	a. [60 60 255] – 12.2 b. [30 30 180] – 4.6
Monkey 1 (n=1)	b. [170 0 0] –6.7	b. [0 105 0] – 6.4	b. [37 37 210] – 6.6
Monkey 1 (n=1)	b. [175 0 0] –7.2	b. [0 105 0] – 6.4	b. [40 40 220] – 7.7
Monkey 1 (n=8)	b. [180 0 0] –7.7	b. [0 110 0] – 7.3	b. [40 40 220] – 7.7

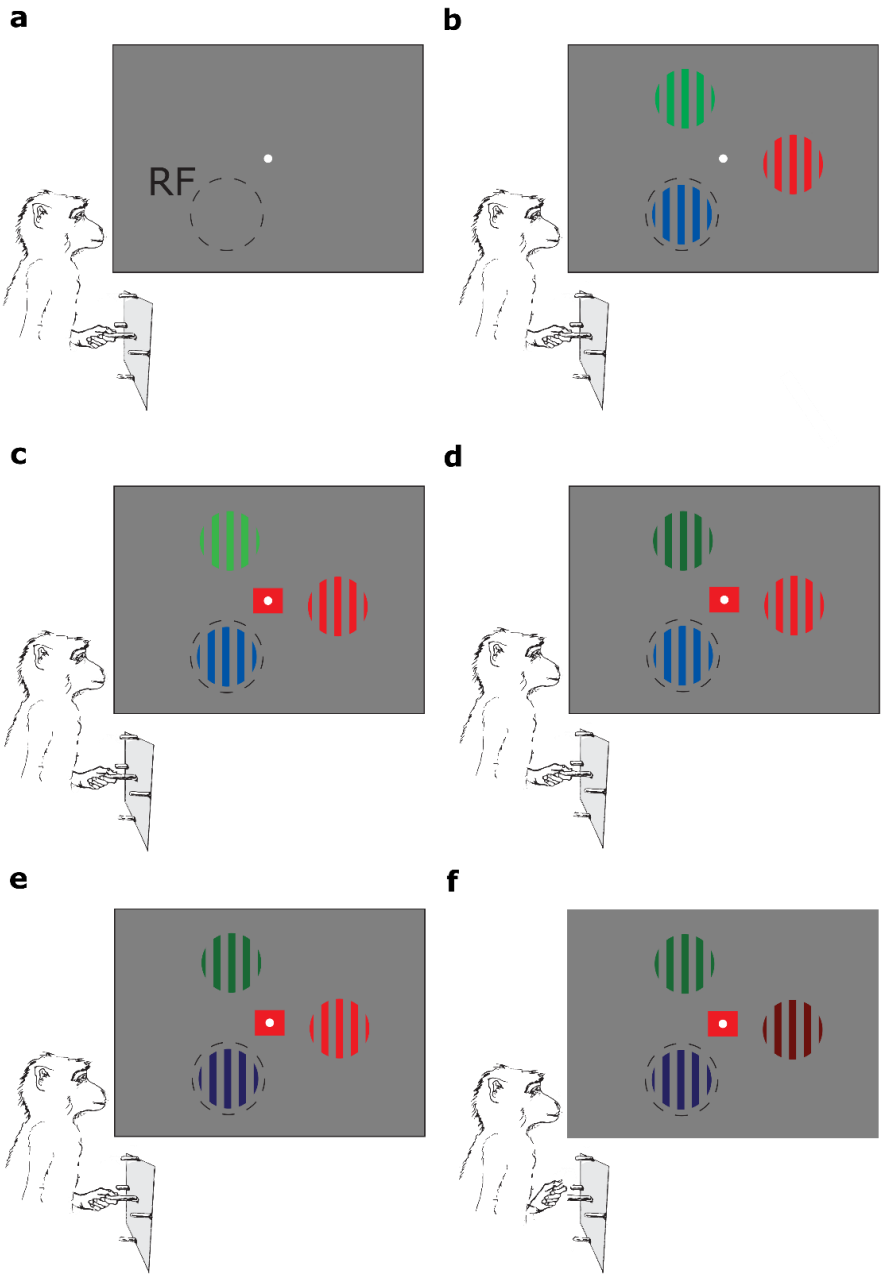

Figure 3-1. Behavioural paradigm. (**a**) The monkey holds on to a lever to initiate the trial, hereafter a central fixation spot turned on. (**b**) Upon fixation 3 coloured gratings appeared, one of which was presented inside the receptive field (RF) of the V1 neuron. (**c**) After a variable delay a cue matching one of the grating colours surrounded the fixation spot, indicating which grating was behaviourally relevant (target). (**d-f**) In pseudorandom order the stimuli decreased in luminance (dimmed). Upon dimming of the target, the monkey had to respond by releasing the lever.

days. The drifting gratings moved perpendicular to the grating orientation, with the motion direction pseudorandomly assigned on every trial. After a random delay (618-1131 ms for monkey 1, 618-948 ms for monkey 2 and 3; uniformly distributed), a central cue appeared that matched the colour of one of the gratings, indicating that this grating would be behaviourally relevant on the current trial. After a variable delay (1162-2133 ms for monkey 1, 1162-1822 ms for monkey 2 and 3; uniformly distributed), one of the pseudorandomly selected gratings changed luminance (Table 3-1 for colour values),

hereafter referred to as dimming. If the cued grating (target) dimmed, the monkey had to release the lever in order to obtain a reward. If, however, a non-cued grating (distractor) dimmed, the monkey had to ignore this and keep hold of the lever until the target dimmed on the second or third dimming event (each after another 792-1331 ms for monkey 1; 792-1164 ms for monkey 2 and 3; uniformly distributed).

3.3.4 - Animal training

All three animals had received training on fixation (e.g. RF mapping), simple luminance change detection (wherein target stimuli were presented without distractors) and visually guided saccade tasks prior to being trained on the main task (Figure 3-1). We began training on the main task by presenting a single grating with a circle surrounding this grating in the same colour, acting as a cue, presented after a random delay. During this stage, the monkeys were required to respond to the dimming of the only presented grating. As this stage did not differ too much from previously learned tasks, the monkeys did not require more than one week to become familiar with this version of the task.

Next, we introduced the distractor stimuli. During this training stage, we presented all three gratings simultaneously, with the cue presented around one of the gratings after a random delay. During the first days of this stage, the first grating that dimmed was always the cued stimulus. Afterwards, one or two of the distractors could change luminance before the target stimulus, which had to be ignored. Depending on how difficult the monkey found this training stage, the distracting gratings could initially be presented at lower contrast than the target grating.

Once the monkeys consistently performed well at this step (after approximately two months), we moved the cue incrementally closer to the fixation spot. Simultaneously, we gradually decreased the size (and shape) of a large circle that surrounded an entire grating, to smaller circles halfway between the fixation spot and the target grating, to a small square surrounding the fixation spot. This stage also took approximately two months for the monkeys to learn.

3.3.5 - Data acquisition

We recorded from all cortical layers of visual areas V1 and V4 using 16-contact laminar electrodes (Plexon V-probes & Atlas silicon probes). The electrodes were inserted perpendicular to the cortex on a daily basis. Neuronal data were acquired with Neuralynx preamplifiers and a Neuralynx Digital Lynx amplifier. Unfiltered data were sampled with 24 bit at 32.7 kHz and stored to disc. Data were replayed offline and band-pass filtered at 0.5-300 Hz, and down sampled to 1 kHz for local field potential (LFP) data, and filtered at 0.6-9 kHz for spike extraction. Eye position and pupil diameter was recorded at 220 Hz using a ViewPoint eyetracker (Arrington Research). Pupil diameter was recorded for 75 (90.4 %) recordings.

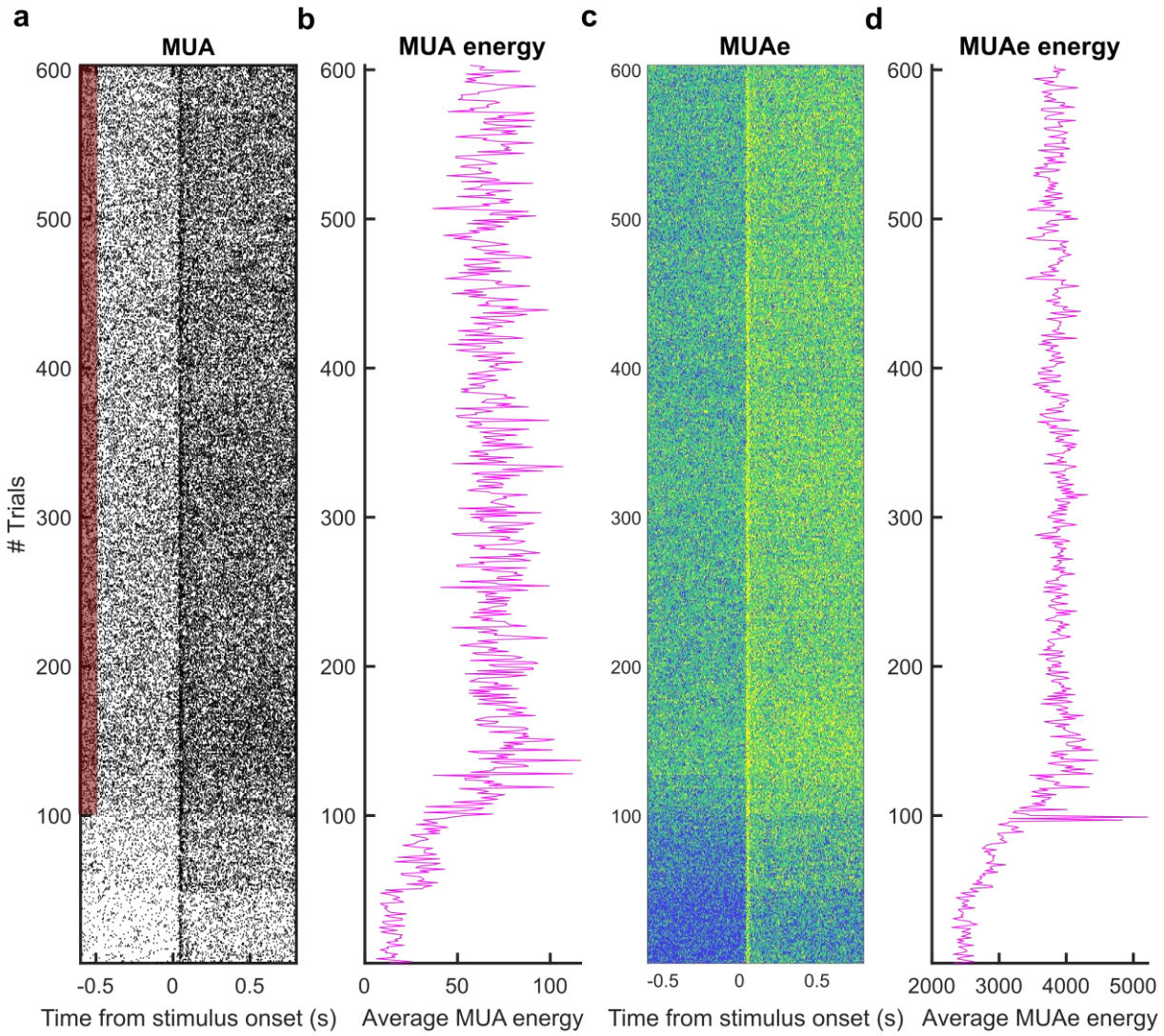

Figure 3-2. Trial selection based on recording stability. (**a**) Multi unit activity (MUA) aligned to stimulus onset across all trials of the attention task. Each vertical line indicates one spike. The red bar along the y-axis indicates the included trials. (**b**) Energy of the population activity during the baseline period (from 500 to 50 ms before stimulus onset), smoothed across 3 consecutive trials. (**c**) MUA envelope (MUAe) aligned to stimulus onset. (**d**) Energy of the MUAe during the baseline period smoothed across 3 consecutive trials.

3.3.6 - Data preprocessing

We corrected for any noise common to all channels via common average reference, in which the average of all included channels (based on criteria described below) is subtracted from each individual channel. We extracted population activity by progressively lowering spike extraction thresholds until approximately 100 Hz spiking activity was detected on each channel (Engel et al., 2016). Next, we computed the envelope of MUA (MUAe) by low-pass filtering (<300 Hz, fifth order butterworth) the rectified 0.6-9 kHz filtered signal. Because we noticed that during some recording sessions the electrode seemed to have moved (e.g. due to movement of the monkey), we visually inspected the stability of each recording by investigating the stimulus aligned firing rates, MUAe and their baseline (-500 to -50 ms) energy across all trials and channels (Figure 3-2). With energy (E) defined as:

$$E = \int_{i}^{t} V(i)^2$$

Equation 3-1

, where t is the number of time points in the vector (V) representing the single-trial histogram or MUAe. We selected the largest continuous time window that showed stable activity across all V1 & V4 channels.

In addition to selecting trials from stable periods, we selected channels for further processing that were determined to be in gray matter (Figure 3-3). Using current source density (CSD), we investigated on which channels currents were entering (sinks) and exiting (sources) cortical tissue, which allowed us to determine the relative recording depth compared to the known cortical anatomy (Schroeder, 1998; Schroeder et al., 1991). The CSD profile can be calculated according to the finite difference approximation, taking the inverse of the second spatial derivative of the stimulus-evoked voltage potential φ, defined by:

$$CSD(x) = \frac{\varphi(x+h) - 2\,\varphi(x) + \varphi(x-h)}{h^2}$$

Equation 3-2

, where x is the depth at which the CSD is calculated and h the electrode spacing (150 µm). We used the iCSD toolbox (Pettersen et al., 2006) to compute the CSD. With this toolbox we used a spline fitting method to interpolate φ smoothly between electrode contacts. We used a diameter of cortical columns of 500 µm (Mountcastle, 1957), and tissue conductance of 0.4 Sm^{-1} (Logothetis et al., 2007).

To aid determination of recording depth, we computed the signal-to-noise ratio (SNR), the RF estimation (see below) and the response latencies to stimulus onset (Figure 3-3d-f) for each channel. SNR was computed as:

$$SNR = \frac{Signal - Noise}{\sigma_{noise}}$$

Equation 3-3

, with $Signal$ defined as the average MUAe amplitude in one of eight 50 ms time windows, from 30 to 80 ms, with 10 ms steps, to 100 to 150 ms after stimulus onset, and $Noise$ as the average MUAe amplitude during the baseline period (-200 to 50 ms) before stimulus onset. SNR in at least one of these eight estimates was required to be higher than 3 for a channel to be included for further analyses.

We computed the response latency to stimulus onset for each channel (inset Figure 3-3f) according to the method described by Roelfsema et al. (2007). We fitted the visual response as a combination of an exponentially modified Gaussian and a cumulative Gaussian using a non-linear least-squares fitting procedure (function lsqcurvefit) to the average MUAe time course. There are two assumptions implicit in this method. First, the onset latency has a Gaussian distribution across trials and neurons that contribute

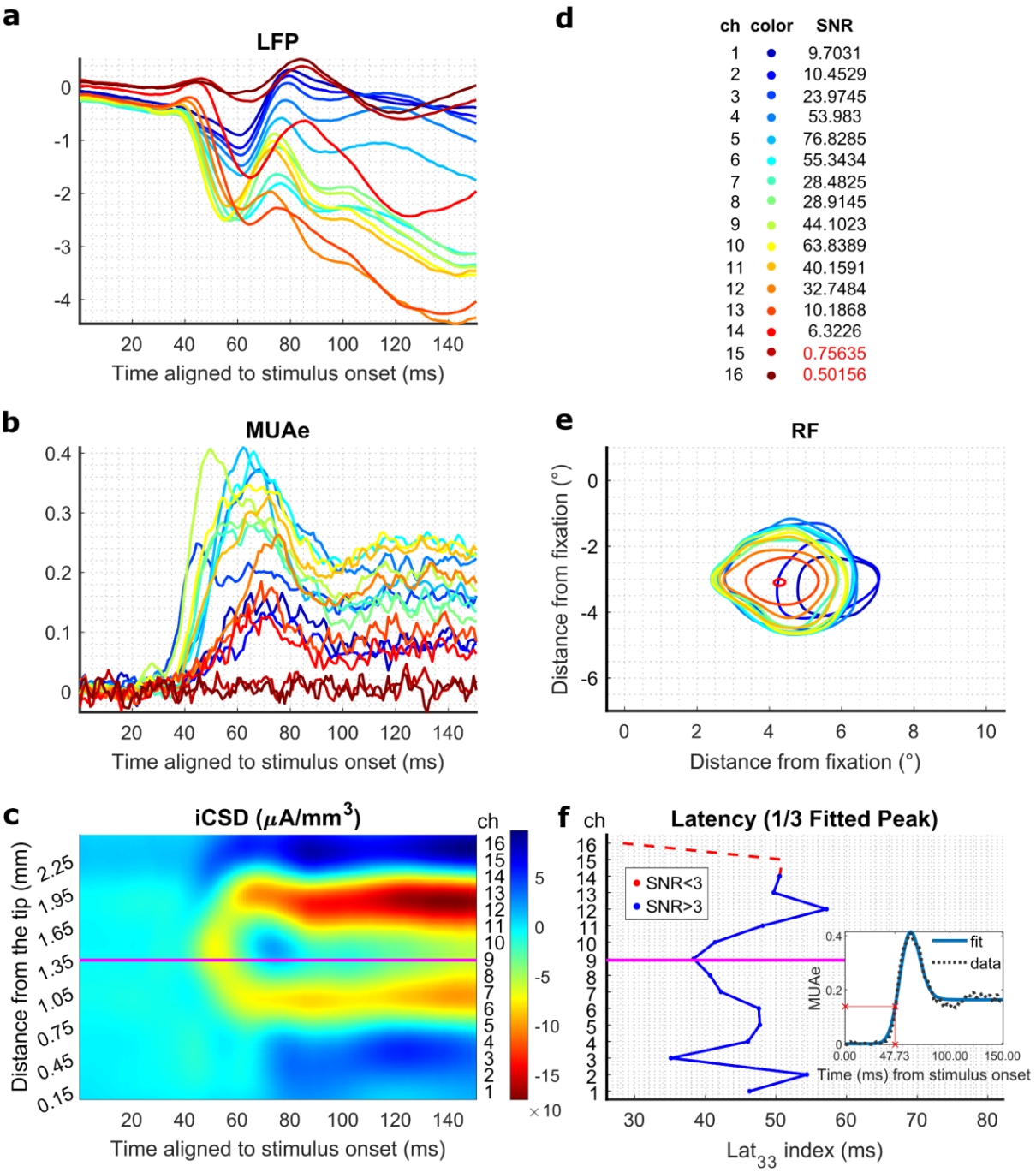

Figure 3-3. Determining the recording depth. (**a**) Baseline corrected, trial-averaged LFP signals aligned to stimulus onset for all recording channels (n=16) on one linear probe. (**b**) Baseline corrected MUAe signals. (**c**) Baseline corrected, CSD transformed LFP signals. Current sinks are displayed as red whereas sources are displayed as blue. The magenta line indicates the selected alignment channel. (**d**) Signal-to-noise (SNR) ratio for each channel. (**e**) Receptive field (RF) locations. (**f**) MUAe response latencies to stimulus onset. The inset illustrates the model fit used to determine the stimulus-response latency (channel 5), as described in Equation 3-4.

to the MUAe, and second, that (part of) the response dissipates exponentially. The visual response y across time t was modelled as:

$$y(t) = d \cdot Exp(\mu\alpha + 0.5\sigma^2\alpha^2 - \alpha t) \cdot G(t, u + \sigma^2\alpha, \sigma) + c \cdot G(t, \mu, \sigma)$$

, where μ is the mean, σ is the standard deviation, α^{-1} is the time constant of the dissipation, $G(t, \mu, \sigma)$ is a cumulative Gaussian, and c and d are the factors scaling the non-dissipating and dissipating modulation of the visual response. The response latency was defined as the time point where $y(t)$ reached 33% of the maximum of the earliest peak, the first Gaussian (Roelfsema et al., 2007; Self et al., 2013). Data was aligned to the earliest current sink, the presumed thalamic input layer (L4), channels were excluded if they were more than 1 mm more superficial or 0.75 mm deeper than this layer.

3.3.7 - Receptive field estimation

Offline RFs were determined for each channel via reverse correlation of the MUAe signal to stimuli (0.5 – 2 ° black squares) presented on a 9 × 12 grid (Gieselmann and Thiele,

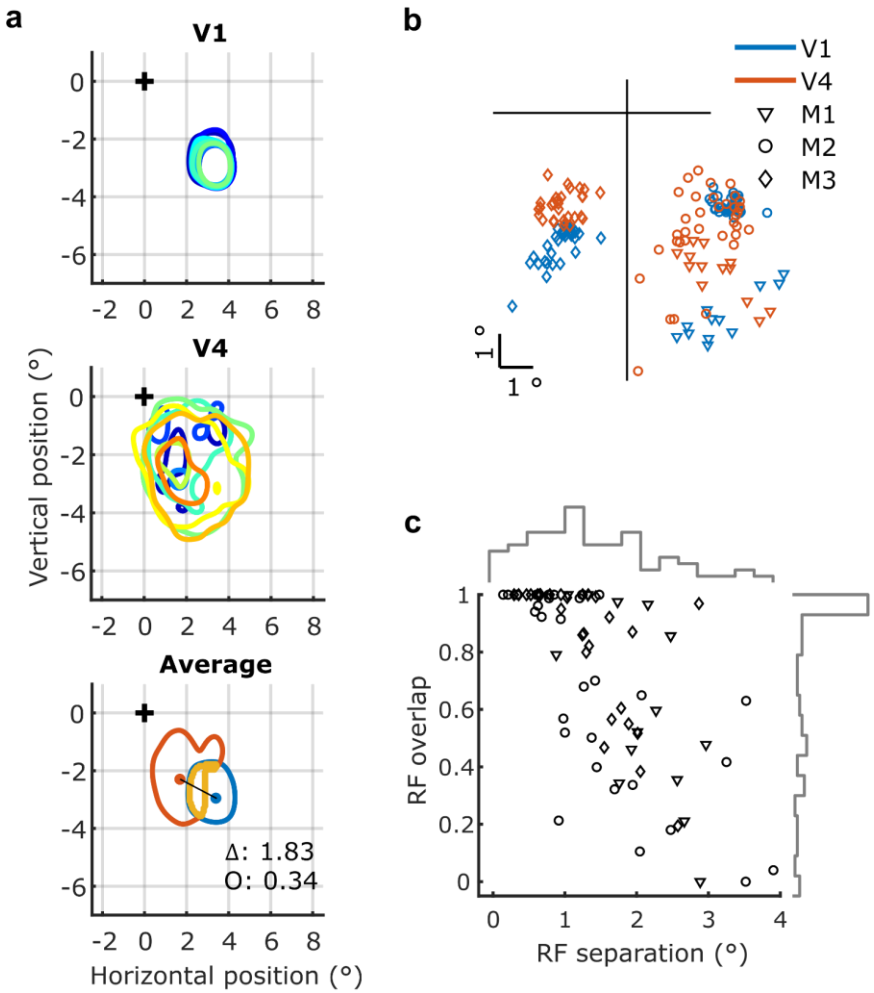

Figure 3-4. RF locations. (**a**) RF location for one example recording. Contour of RF location for included channels for V1 (top), V4 (middle) and their average (bottom). The bottom panel illustrates the overlap (yellow, O) between the V1 and V4 RF, expressed as the proportion of the V1 RF, and separation (Δ). (**b**) Average RF centre locations (across channels) for each recording, separately for each subject (M1-M3) and area. (**c**) RF separation between V1 and V4 plotted against their overlap, expressed as the proportion of the V1 RF. The histograms along the top (right) indicate the distribution of RF separation (overlap) across all recordings.

2008). The stimulus-response map was converted to z-scores, after which the RF for each channel was indicated by a contour (thresholded at a z-score of 3) surrounding the peak activity (Figure 3-3e, Figure 3-4a). These z-scored maps were averaged across all channels for each area (the population average z-score was computed according to stouffer's Z-score method according to $Z = \sum_{i=1}^{k} Z_i/\sqrt{k}$, with k as the number of channels), after which we determined the overlap and separation between the V1 and V4 RFs (Figure 3-4a, bottom panel). Figure 3-4b and Figure 3-4c illustrate the RF locations, separation and overlap for the population, for each individual monkey.

3.3.8 - Bipolar re-referencing

To ensure that global signals, common to multiple channels, did not affect our LFP and spectral analyses (see below), we re-referenced our LFP signals according to the bipolar derivation. Bipolar re-referenced LFP signals (LFPb) were computed by taking the difference between two neighbouring channels.

3.3.9 - Attentional modulation

The effect of selective attention on neural activity was computed via an attention modulation index ($attMI$), defined as:

$$attMI = \frac{A_{RF} - A_{out}}{A_{RF} + A_{out}}$$

Equation 3-5

, with A_{RF} as the neural activity when attention was directed towards the RF, and A_{out} the activity when attention was directed away from the RF. This index ranges from -1 to 1, with zero indicating no attentional modulation and with positive (negative) values indicating higher activity when attention was directed towards (away) from the RF.

3.3.10 - Hidden Markov Model (HMM)

To quantify On-Off dynamics in V1 and V4, we applied a Hidden Markov Model (HMM) to the population activity across all laminae. We fit the HMM both to activity from each individual area, following the procedures described by Engel et al. (2016), as well as to the activity from both areas simultaneously.

Our HMM assumes that spike counts on the recorded channels can be well characterised as a doubly-stochastic stochastic process, of which the parameters can be accurately estimated (Rabiner, 1989). In this study, spike counts on each channel are assumed to be produced by a Poisson process with different (constant) mean rates during On or Off phases of the underlying 'hidden' (latent) process s common to all channels that we need to infer (Engel et al., 2016). The mean firing rate on each channel j in phase s is defined by entry λ_j^s in the emission matrix Λ. The transition matrix P gives the probabilities of

transitioning between these latent phases. In the transition matrix P, each entry indicates the probability of transitioning between two specific phases. For instance, P_{11} indicates the probability of transitioning from $s = 0$ to $s = 0$ (remaining in the Off phase), whereas P_{12} indicates the probability of transitioning from $s = 0$ to $s = 1$, more formally: $P_{11} = P_{off} = P(s_{t+1} = 0|s_t = 0)$, $P_{12} = 1 - P_{off} = P(s_{t+1} = 1|s_t = 0)$. These probabilities do not depend on time, at any time step t, the probability of transitioning between phases depends only on the value of s at time t (s_t). The latent dynamics estimated by the HMM thus follows a discrete time series in which s_t summarises all information before time t. For each channel, MUA was discretised by determining spike counts in 10 ms bins following each time t, with the probability of observing spike count n on channel j during phase s defined as

$$P(n|s) = \frac{(\lambda_j^s)^n}{n!} e^{-\lambda_j^s}$$

Equation 3-6

The full description of an HMM is given by the emission matrix Λ, transition matrix P and the probabilities π^0 that indicate the initial values s_0, in which $\pi_i^0 \equiv P(s_0 = i)$. These parameters were estimated using the Expectation Maximisation (EM) algorithm (Bishop, 2006), maximising the probability of observing the data given the model according to the Baum-Welch algorithm (Rabiner, 1989). Because the EM procedure can converge to a local maximum, rather than the global maximum, we repeated the EM procedure ten times with random parameter initialisations, and chose the model with the highest likelihood. Random values were drawn from Dirichlet distributions for π^0 and P, and from a uniform distribution between zero and twice the channel's mean firing rate for Λ. The EM procedure was terminated if the relative change, computed as $|new - original|/|original|$, in the log-likelihood was smaller than 10^{-3} and the change in the transition and emission matrix was smaller than 10^{-5}, or if it reached the maximum number of iterations (n = 500).

Once the optimal parameters were estimated, we used the Viterbi algorithm to determine the most likely latent trajectory for each individual trial. We applied the HMM separately to each attention condition. For every trial, we applied the HMM during multiple time periods of the task, during fixation, around stimulus onset and during the time window from 400 ms after cue onset to 30 ms after the first dimming event. For the behavioural analysis (Figure 3-19), we additionally analysed the period up to 30 ms after the second dimming event for trials in which target dimming did not occur on the first dimming event, and for which the first distractor dimming was not inside the RFs.

To determine what number of latent phases best described the data, we fit HMMs with the number of phases ranging from 1 to 8, and used a four-fold cross-validation procedure to compute the cross-validation error for each HMM (Engel et al., 2016). We fit the HMM to a randomly selected subset of 3/4 of the trials, and computed the cross-validation error on the remaining 1/4 of trials. This procedure was repeated 4 times using a different 3/4 of trials for training and 1/4 of trials for testing the HMM. We computed

the cross-validation error CV_{var} for each channel j across all trials K and time bins T as the difference between the actual and expected spike count according to:

$$CV_{var}[n_j] = \sum_{k=1}^{K} \sum_{t=1}^{T} (n_t^j - \lambda_j^{s_t})^2$$

Equation 3-7

We normalised CV_{var} to the error in the 1-phase HMM, averaged across channels, cross-validations and conditions, and determined the difference in CV_{var} with each additional phase in the HMM. Figure 3-5 depicts the normalised mean cross-validation error across each of the eight HMM models for all recordings. For most recordings, and for both V1 and V4, CV_{var} decreased with the addition of a second phase, but did not decrease much further with additional phases. This allowed the identification of the elbow (kink) in this error plot as the model with two phases. We included areas/recordings for further analysis that revealed a reduction in cross-validation error of at least 10% with the addition of a second phase, but did not decrease by more than 10% with additional

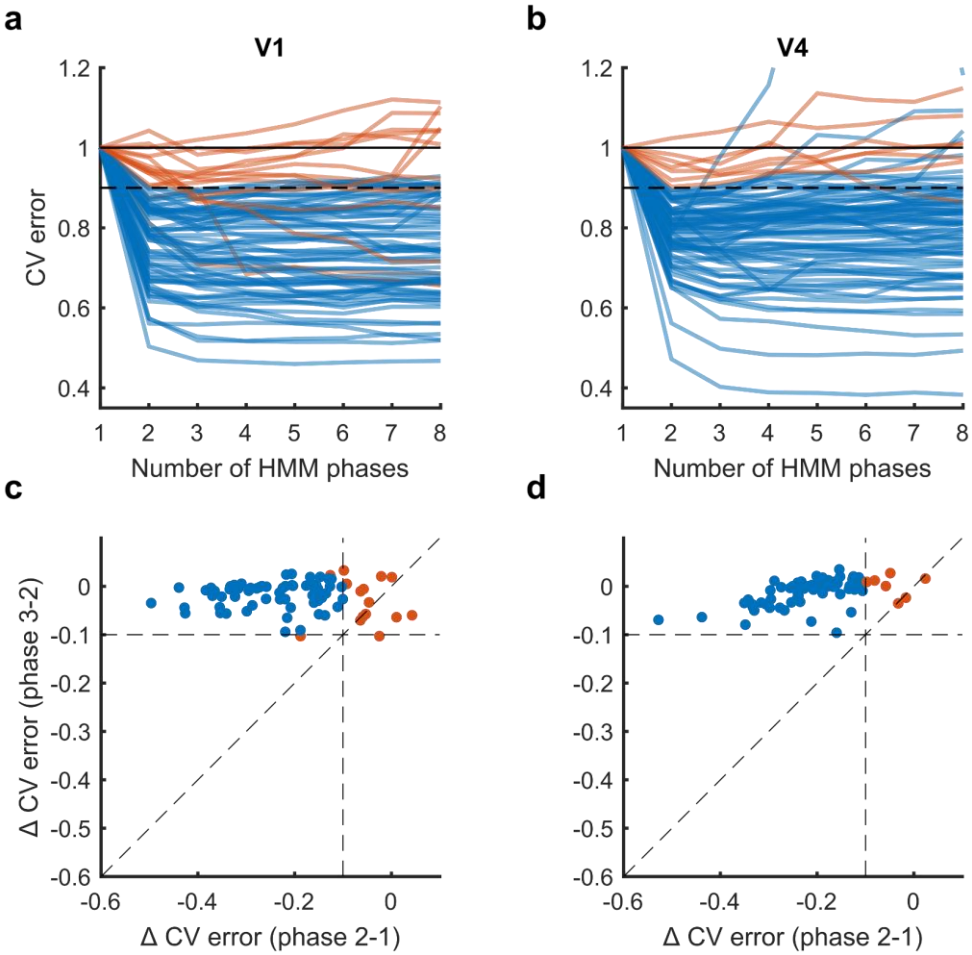

Figure 3-5. Determining the number of HMM phases in V1 and V4 MUA. (**a-b**) Cross validation (CV) error plotted against the number of phases in each HMM for V1 (**a**) and V4 (**b**). (**c-d**) The difference in cross validation error between the 1-phase and 2-phase model, plotted against the difference between 2-phase and 3-phase model, for V1 (**c**) and V4 (**d**). Most recordings show a large reduction in cross-validation error with the addition of a second phase, and only marginal changes with additional phases. Blue (red) lines and markers indicate the recordings included (excluded) for further analysis.

phases. For a small subset of recordings, a three or a four-phase model fit the data best, these recordings were excluded from further analysis.

To investigate the across-area coordination of On-Off dynamics, we fit a 4-state HMM to V1 and V4 data simultaneously. Across these four states, both V1 and V4 could be in either an Off or On phase, with the states defined as: $V1_{off} - V4_{off}$ (state 1), $V1_{on} - V4_{off}$ (state 2), $V1_{off} - V4_{on}$ (state 3) and $V1_{on} - V4_{on}$ (state 4). This model was fit according to the same steps as the HMM applied to individual areas, with one exception. For each channel j, the emission rate λ was constrained to be the same across states for which this channel (area) was in the same phase. For example, rates were constant for a V1 channel across state 1 and state 3 during which V1 was in an Off phase ($\lambda_j^{s=1} = \lambda_j^{s=3}$, $j \in V1$).

3.3.11 - Cross correlation

The temporal relationship between On-Off time series and transitions, microsaccade onset times and activity in V1 and V4 were investigated using cross-correlations. The cross-correlations based on HMM time series (CC_{HMM}) were calculated using the function xcorr in Matlab, according to:

$$CC_{HMM}(\tau) = \frac{1}{M}\sum_{m=1}^{M}\frac{\sum_{t=1}^{T} x(t)y(t+\tau)}{\sqrt{\sum_{t=1}^{T}|x(t)|^2 \cdot \sum_{t=1}^{T}|y(t)|^2}}$$

Equation 3-8

, where M is the number of trials, T is the number of discrete time bins, x and y the mean subtracted On-Off time series in V1 and V4 as determined by the HMM, and τ is the time lag. Here, the numerator indicates the cross-covariance, which is normalised (the denominator) such that the autocorrelation for each time series at zero lag is 1. This procedure normalised CC_{HMM} such that correlation coefficients were obtained. We furthermore subtracted the shift predictor CC_{shift} from CC_{HMM} to remove any task-related (stimulus-locked) correlations between x and y. CC_{shift} was computed by shifting y trials such that trial 1 becomes 2, 2 becomes 3, …, M becomes 1, ensuring that x and y were obtained from different trials.

Cross-correlations (CC) between state transitions and microsaccade onset times were computed in the same way as described in Equation 3-8, but for a different normalisation (denominator) factor. Here we normalised by the geometric mean rate (transition × saccade rate), resulting CC to be on the order of coincidences of state transitions per microsaccade.

For transition time cross correlations across areas, we used a jitter correction method that corrects for slow temporal and stimulus-locked correlations (Amarasingham et al., 2012; Engel et al., 2016; Smith and Kohn, 2008). Within a jitter time window (300 ms), each spike or transition (event) on each trial is randomly replaced by an event (with replacement) from the set of all events in the same time bin across all trials. This method

preserves the original event rate within each trial and time bin, but destroys the relationship on timescales greater than the jitter time window. We computed z-scores of the jitter-corrected cross-correlations by subtracting the mean and dividing by the standard deviation of the distribution of resampled cross-correlations (Engel et al., 2016).

To investigate the neural activity around the time of On-Off transitions, we computed the transition-triggered average (TTA). The TTA was estimated by computing the cross covariance, the numerator in Equation 3-8, divided by the number of transitions for each channel, and then averaged across channels and recordings.

3.3.12 - Power estimation

We estimated the power spectra of the LFPb, separately for On and Off states determined by the HMM, using a custom multitaper approach based on the Chronux toolbox (Bokil et al., 2010), only using epochs that lasted longer than 250 ms. Because epoch durations were variable, we zero-padded each segment to the next highest power of 2 of the longest epoch duration (2048 time points), ensuring we could extract the same frequencies for each segment. This approach gave us a half bandwidth (W) of approximately 1.95 Hz, according to $W = (K + 1)/2T$, with K being the number of data tapers (K = 7) and T the length of the time window in seconds. Frequencies were estimated from 4 to 200 Hz.

In order to analyse whether deflections in specific frequency bands in the LFPb were time-locked to HMM state transitions, we filtered the LFPb into the canonical frequency bands: δ (<4 Hz), θ (4-8 Hz), α (8-12 Hz), β (12-30 Hz), γ_{low} (30-60 Hz), γ_{high} (60-100 Hz), and γ_{high+} (100-200 Hz) using a fourth order butterworth filter. Next, we computed the instantaneous power by rectifying the Hilbert transformed band-passed LFPb.

3.3.13 - Microsaccade detection

We low-pass filtered the horizontal and vertical eye traces at 30 Hz (2nd order Butterworth filter) after which we detected microsaccades by using the algorithm developed by Engbert and Kliegl (2003). This algorithm converts eye position (Figure 3-6a-b) to velocity (Figure 3-6c), and classifies an eye movement as a microsaccade if the velocity is larger than a threshold for at least three consecutive time points. The threshold is set to 6 times the median estimator, given by: $\sqrt{median(x^2) - median(x)^2}$, where x is either eye position channel x or y. Thus the threshold is determined separately for the two eye position channels and for each single trial. The use of the median estimator and this threshold ensured that microsaccade detection is relatively robust to different levels of noise (Engbert and Kliegl, 2003). We stored microsaccade onset times, amplitudes and directions (Figure 3-6d).

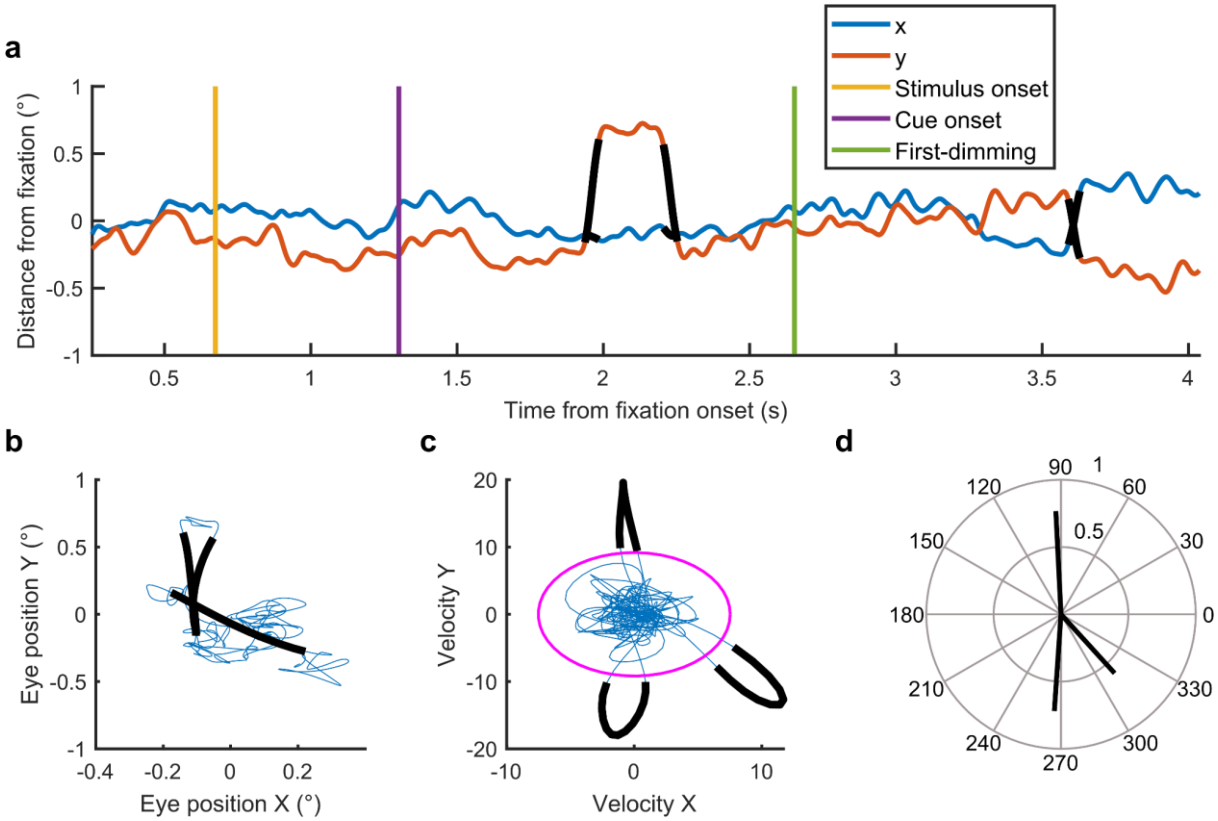

Figure 3-6. Microsaccade detection. (**a**) Eye position over time, separately for the x and y channel. Microsaccades are indicated by black lines. (**b**) Eye position channel x plotted against channel y. (**c**) Eye position velocity. Magenta line indicates the threshold. If the eye position velocity is outside of this threshold for at least 3 consecutive time points, it is classified as a microsaccade. (**d**) The direction and amplitude of the detected microsaccades.

3.3.14 - Statistical testing

To determine whether there were significant differences between attention conditions or HMM states (e.g. in firing rate or epoch duration) we made use of multiple statistical methods. We used (paired-sample) Wilcoxon signed rank tests whenever a comparison was made between two conditions (e.g. attend RF versus attend away), or to test whether a distribution was significantly different from zero. When a comparison involved multiple conditions, or multiple factors (e.g. attention and state), we used repeated measures analysis of variance (ANOVA) and linear mixed effect models to test for main effects of each condition/factor and interaction effects between factors. For the multi-level models, factors were defined as fixed effects, and we included random intercepts for each recording as random effects, accounting for the repeated measurements within each recording. We sequentially tested the fit of the relationship between the dependent variable (e.g. RT) and each of these factors by means of maximum-likelihood ratio tests. The addition of the first factor was tested against a baseline (intercept-only) model, and the addition of subsequent factors was tested against the previous model fit.

We used false discovery rate (FDR) to correct for multiple comparisons (Benjamini and Yekutieli, 2001). Error bars in all figures indicate the standard error of the mean (SEM).

3.4 - **Results**

We recorded simultaneously from V1 and V4 using 16-contact laminar electrodes in three awake behaving macaque monkeys performing the selective attention task illustrated in Figure 3-1 (Gregoriou et al., 2009). For all three monkeys, receptive fields (RFs) were close together (Figure 3-4b) and showed good overlap (Figure 3-4c). During task performance we placed one of three coloured gratings inside the RF of the recorded neurons. As V4 RF have been shown to remap towards target stimuli (Neupane et al., 2016) and V4 RFs are larger than those in V1, we centred this grating on the V1 RF. On each trial, the monkey attended to one of the coloured gratings, indicated by a centrally presented coloured square (cue) around the fixation spot. Attention was directed towards the grating inside the RF ('Attend RF') or to one of the gratings outside the RF ('Attend Away') to detect a change in luminance (dimming). After a variable delay, a sequence of one to three dimming events started, in which distractors and the target stimulus dimmed in pseudorandom order. Distractor dimmings were to be ignored, whereas the detection of the target dimming was indicated by the release of the lever. After the dimming of the target grating (plus the allocated maximal RT), which could occur on any of the dimming events, the trial was aborted.

We first examined, for each recording and independently for V1 and V4, whether population activity displayed spontaneous transitions between periods of high (On) and low (Off) spiking across the cortical layers, as has been described previously for V4 (Engel et al., 2016). To this end, we extracted population activity such that approximately 100 Hz of spiking activity was detected on each channel. Next, we binned spike count data in 10 ms time bins and fit a HMM to segment this across layer multi-unit activity into On and Off episodes, focusing on the time window from 400 ms after cue onset to 30 ms after the first grating dimmed. Out of a total of 77 V1 and 79 V4 recording sessions (of which 73 simultaneous V1-V4 recordings), we found a reduction of >10% in cross-validation error when fitting a 2-state versus 1-state model in 62 V1 (80.5 %), and 72 V4 (91.1 %) recordings; in 57 (78.1 %) recordings we found evidence for a 2-state model in both V1 and V4. Thus in addition to the previously described transitions in V4 (Engel et al., 2016), we found On-Off state transitions in V1 as well.

For a representative recording, Figure 3-7 illustrates the raw and colour coded (according to HMM state) V1 and V4 firing rates across cortical laminae aligned to stimulus and cue onset for 20 trials. On and Off transitions occurred irregularly and without ostensible periodicity (Figure 3-9) within and across trials during stimulus presentation. Critically, transitions occurred both independently as well as synchronously across V1 and V4.

3.4.1 - Selective attention modulates On-Off transition dynamics both in V1 and V4

Engel et al. (2016) revealed that selective attention modulates the On-Off dynamics found in V4. In particular, it was found that the duration of On episodes was increased

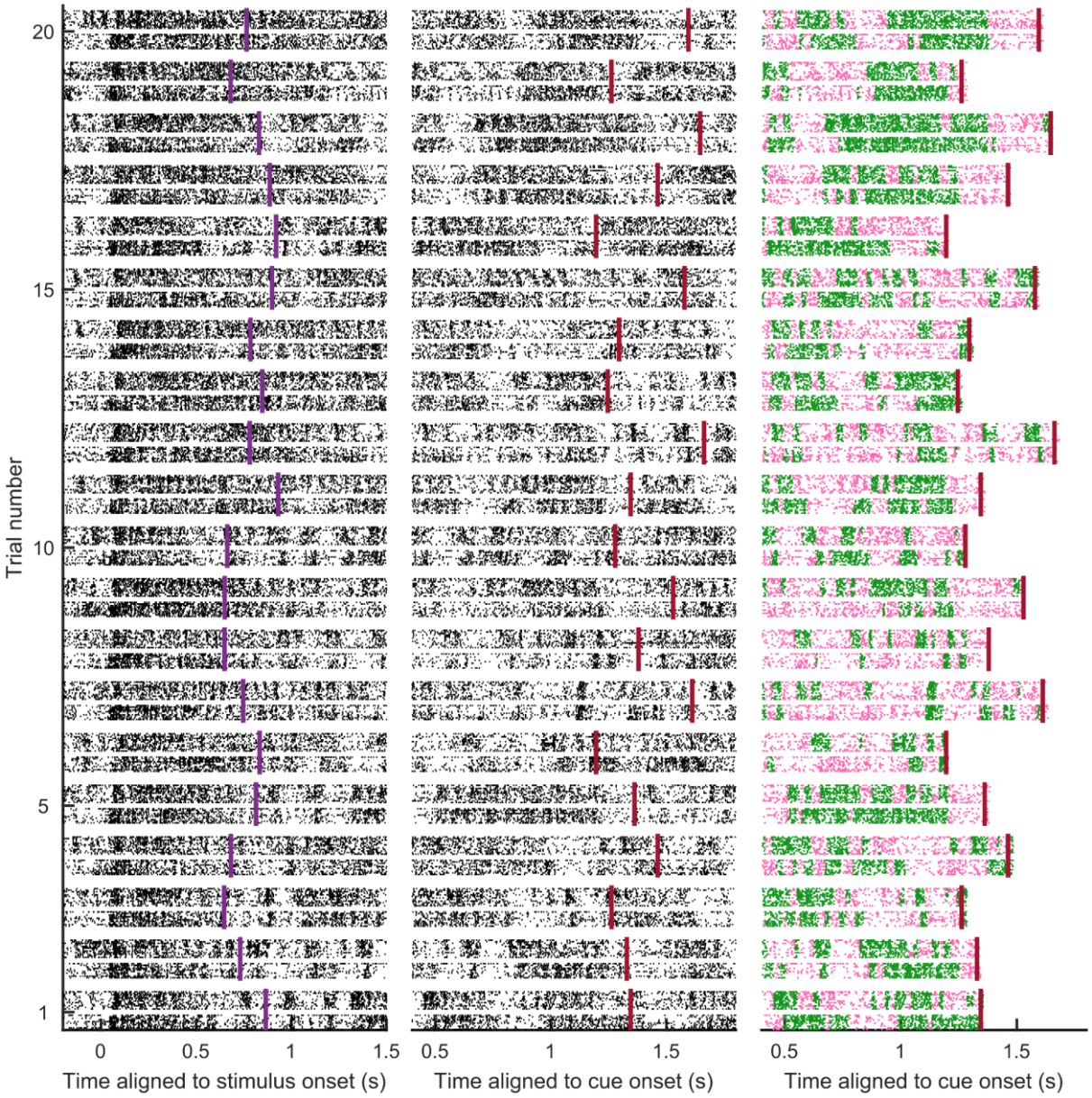

Figure 3-7. Raster plot of HMM fit to population activity in V1 and V4. Simultaneously recorded multi-unit spiking activity on 16-contact laminar electrodes in V1 and V4 for 20 example trials, aligned to stimulus (left) and cue onset (middle and right). Each trial shows across laminar activity in V1 (bottom) and V4 (top), as raw raster plots (left two columns) and colour coded according to HMM state estimation (right). Note that the middle and right column depict the same activity. The HMM was fit from 400 ms after cue onset to 30 ms after the first dimming event. Cue onset and first-dimming are indicated for each trial by purple and red vertical bars, respectively.

when attention was directed towards the RF compared to away from the RF. Additionally, firing rates were increased when attention was directed towards the RF during both Off and On phases. Together, this indicates that selective attention and the circuit mechanisms controlling cortical states interact on a local spatial scale. Here we replicated these findings: we found that when spatially selective attention was directed towards the RF, firing rates were higher during both On and Off phases (indicated by a rightward skew, Figure 3-8a) and the duration of On episodes was increased (Figure 3-8b). For V1, but not V4, the duration of Off episodes was also increased (Figure 3-8b). Additionally, we found that the total time spent in an On phase was increased in both

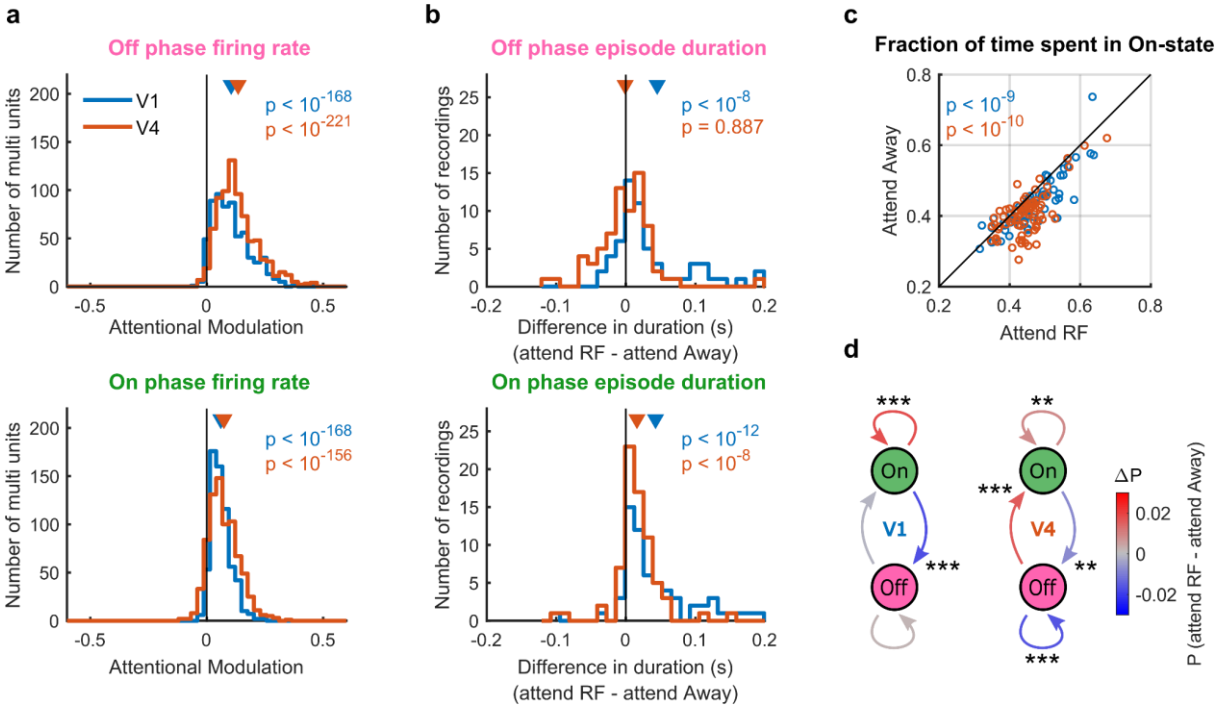

Figure 3-8. Attentional modulation of cortical state. (**a**) Attention increases firing rates during Off and On phases, both in V1 and V4. (**b**) Attention increases the duration of On episodes, both in V1 and V4, whereas it increases the duration of Off episodes only in V1. (**c**) The fraction of time spent in an On state is increased when attention is directed towards the RF. (**d**) Attentional influence on state-transition probabilities. Colour coding of arrows shows the change in state transition probabilities due to attention. Statistics: Wilcoxon signed rank tests; *, **, ***, indicate significance levels of $p < 0.05$, $p < 0.01$ and $p < 0.001$, respectively (FDR corrected).

areas when attention was directed towards the RF (Figure 3-8c). Furthermore, we found that selective attention increased the probability for V4 to switch from an Off to an On state, and it decreased the probability for both V1 and V4 to switch from an On to an Off state (Figure 3-8d). These results indicate that selective attention increases both the duration of On episodes as well as the probability of being in an On state, for both V1 and V4.

The increase in On-episode duration could be interpreted as activity overcoming inhibition, specific to an oscillatory frequency band, earlier when attention is directed towards the RF. This explanation is, however, unlikely, as the distribution of epoch durations follows an approximately exponentially decreasing function without obvious peaks at any particular duration (Figure 3-9), arguing against the premise that On-Off state transitions are brought about by any oscillatory influence on cortical state.

3.4.2 - State transitions coordinate activity across V1 and V4

To examine whether population spiking activity is coordinated between V1 and V4, we investigated spiking activity in one area time locked to transitions in the other area (Figure 3-10a). Around the time of a transition in V1, V4 activity changes in a specific way, so that when V1 transitions to an On-state, V4 activity increases, and when V1 transitions to an Off-state, V4 activity reduces. Likewise, state transitions in V4 elicit

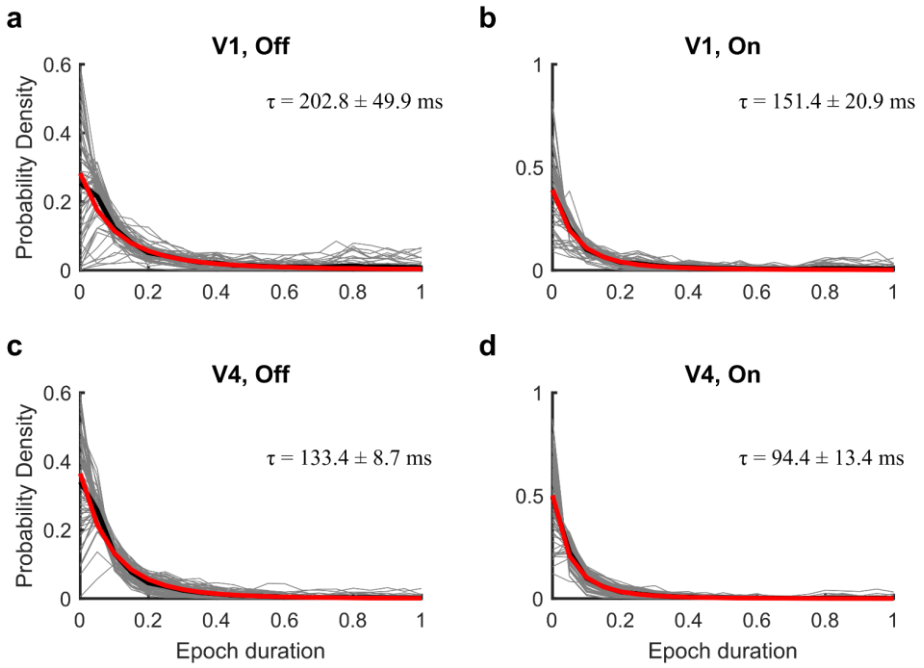

Figure 3-9. Distributions of On and Off episode durations. (**a**) Off episode durations in V1, (**b**) On episode durations in V1, (**c**) Off episode durations in V4, and (**d**) On episode durations in V4, overlaid by the average exponential model fits (red, $N(t) = N_0 e^{-\lambda t}$, where $N(t)$ is the quantity at time t, N_0 the initial quantity, and λ the exponential decay constant) and decay time-constants ($\tau = 1/\lambda$) computed for each recording and phase. Good match for these models indicates that On-Off dynamics were not driven by an oscillatory phenomenon. Individual recordings and their mean are indicated by grey and thick black lines, respectively.

similar firing rate changes in V1. Interestingly, this analysis also revealed that activity changes in V4 precede state transitions in V1, whereas activity changes in V1 shortly follow state transitions in V4. This suggests that V4 activity changes lead V1 state transitions.

To further investigate the coordination of cortical states, and the transition times between the two areas, we performed cross correlations between the V1 and V4 time courses as well as between V1 and V4 transition times. The cross correlation between the V1 and V4 state time courses revealed a correlation between V1 and V4 states that was skewed to negative values, again implying that V4 state transitions occur before transitions in V1 (Figure 3-10b). Indeed, the area under the cross correlation curve was larger for times < 0 compared to times > 0 (Figure 3-10b inset). Importantly, the strength of the cross-correlation between V1 and V4 states was inversely related to the distance between their RF locations (Figure 3-10c), showing that coordination of state transitions is stronger when V1 and V4 RFs were closer together. To get a more accurate estimate of the time delay between V1 and V4 state transitions, we performed a cross correlation between transition times using jitter-corrected cross-correlations (Amarasingham et al., 2012; Smith and Kohn, 2008). Figure 3-10d and Figure 3-10e illustrate that on average, V4 transitions precede V1 transitions, both for On-Off as well as Off-On transitions. Altogether, these results show that V1-V4 states are correlated, but that state transitions also occur independently within each area, i.e. the relationship between state transitions in V1 and V4 was not deterministic.

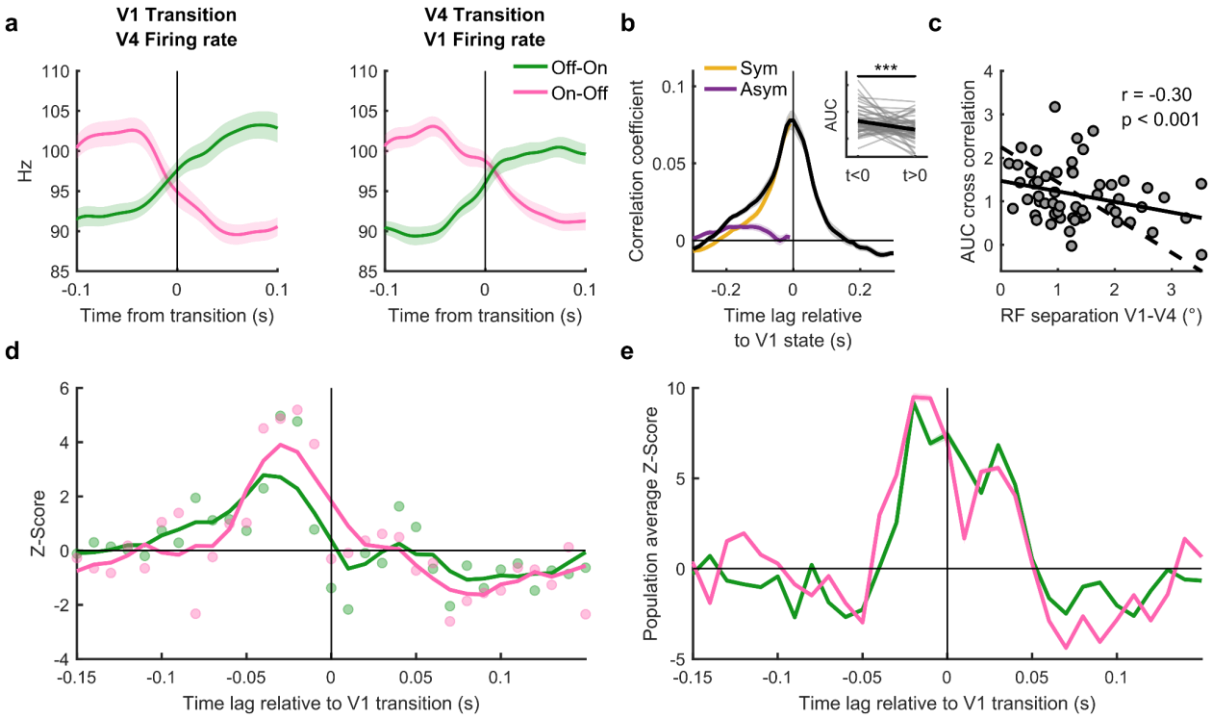

Figure 3-10. Across area coordination of cortical state. (**a**) Spiking activity in one area aligned to state transitions from the other area, averaged across all channels and recordings. Only epochs without transitions preceding or following the alignment transition within 100 ms were included. (**b**) Cross correlation coefficient between V1 and V4 state time series, relative to V1 state. The yellow and purple lines indicate the average and difference between the correlation coefficient for negative and positive times, respectively. The above-zero purple line indicates that the distribution is skewed to negative values. The inset shows the area under the cross correlation curve for times smaller and larger than zero. (**c**) RF separation plotted against the area under the cross-correlation curve from panel **b**. The least-squares regression and standardized major axis regression are indicated by the solid and broken line, respectively. (**d-e**) Cross correlation between V1 and V4 state transition times for an example subject (**d**) and across the population (**e**). Statistics: Wilcoxon signed rank tests; *, **, ***, indicate significance levels of $p < 0.05$, $p < 0.01$ and $p < 0.001$, respectively. Shaded regions denote ±1 SEM.

Next, we investigated whether the coordination of cortical state was specific to the attention period of the trial by additionally computing the cross-correlation between V1 and V4 HMM states during fixation and around stimulus onset. During fixation, as well as around stimulus onset, V1 and V4 states were correlated (Figure 3-11). Only during the period between cue onset and first-dimming, however, was the area under the cross-correlation curve larger for negative time lags (Figure 3-11c). This indicates that V4 state transitions preceded transitions in V1 more often when attention was engaged.

In addition to the firing rate changes described above, state transitions in either V1 or V4 were phase-locked to LFPb fluctuations across both areas (Figure 3-12). Both V1 and V4 LFPb displayed strong deflections when aligned to state transitions in either area. When LFPb and state transitions were from the same area, the pattern looked relatively similar for V1 and V4, with a slightly stronger oscillatory influence in V4 (Figure 3-12a & d). When LFPb and state transitions were from different areas, however, the activity patterns were more distinct. Around the time of a state transition in V4, the deflections in V1 LFPb resembled those after a transition in V1, albeit of smaller magnitude (Figure 3-12c). On the other hand, around the time of a transition in V1, V4 LFPb shows very

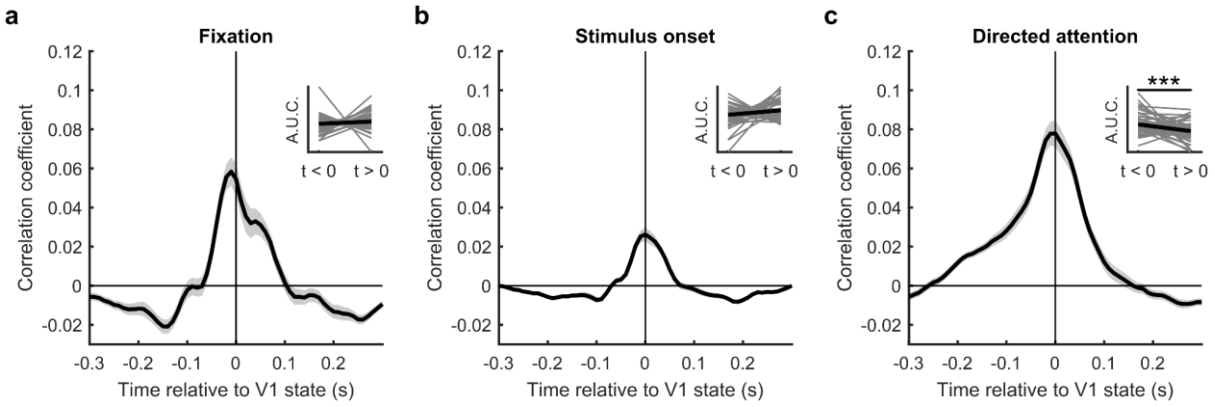

Figure 3-11. Cross correlation between V1 and V4 state time series during various time periods. Cross correlation during fixation (**a**), around stimulus onset (**b**) and between cue onset and the first dimming event (**c**). The insets show the area under the cross correlation curve for times smaller and larger than zero. Note that any event-locked components have been removed by the subtraction of the shift predictor. Statistics: Wilcoxon signed rank tests. Shaded regions denote ±1 SEM.

little modulation, with a small difference preceding V1 state transitions, and only moderate deflections afterwards. These results show that V4 transitions affect V1 LFPb to a larger degree than vice-versa.

A broadly similar pattern of activity is seen in the frequency specific (band-pass filtered) LFPb (Figure 3-13) and its power decomposition (Figure 3-14). We band-pass filtered the LFPb into multiple frequency bands, computed their spectral power using the Hilbert transform for the analysis depicted in Figure 3-14, and aligned them to state transitions. Specifically, we examined δ: <4 Hz, θ: 4-8 Hz, α: 8-12 Hz, β: 12-30 Hz, γ_{low}: 30-60 Hz, γ_{high}: 60-100 Hz, and γ_{high+}: 100-200 Hz. When LFPb and state transitions were from the same area (Figure 3-12 panel a and d), the transition aligned activity was comparable between V1 and V4, with clear phase-locked activity below 60 Hz (Figure 3-13), and clear power changes in frequency bands higher than 30 Hz (Figure 3-14). When V1 LFPb was aligned to V4 state transitions, the phase-locking looked qualitatively similar to the within-area phase-locking in either area (Figure 3-13b). With V4 LFPb aligned to V1 transitions, the phase-locking pattern seemed to have shifted compared to the oscillatory cycle (Figure 3-13c). Although it is not possible to say whether the V4 LFPb leads or lags the transition in V1 based on this analysis, in line with the firing rates aligned to state transitions (Figure 3-10a), high-frequency power changes in V4 occur before V1 transitions whereas V1 high-frequency power changes occur after V4 state transitions (Figure 3-14b-c). In addition to an increase in high-frequency power across areas around the time of a transition from an Off to an On state, power in the θ and α-band revealed an increase after a transition to the Off-state.

To test to what extent V4 activity influences state transitions in V1, and vice-versa, we fitted a 4-state HMM to V1 and V4 data simultaneously in which either or both areas could be in an On or Off state (Figure 3-15). We defined state 1 as V1 Off – V4 Off, state 2 as V1 On – V4 Off, state 3 as V1 Off – V4 On, and state 4 as V1 On – V4 On (Figure 3-15a). Figure 3-15a illustrates this 4-state HMM fit to the MUA for one example trial. We were interested in two specific scenarios, illustrated in Figure 3-15b. In the first (yellow)

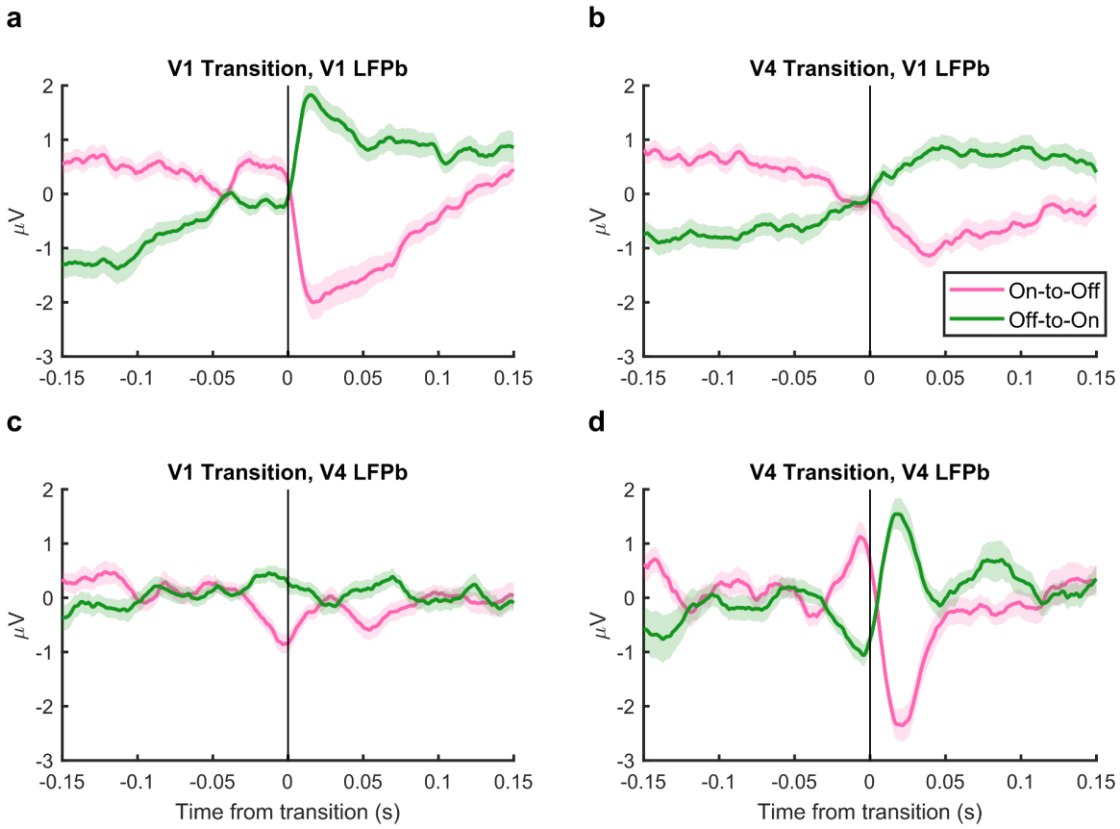

Figure 3-12. Transition triggered LFPb. (**a**) LFPb from area V1 aligned to HMM state transitions in V1. (**b-d**) Same conventions as in panel **a**, but for V1 LFPb and V4 HMM (**b**), V4 LFPb and V1 HMM (**c**) and V4 LFPb and V4 HMM. Only epochs without transitions preceding or following the alignment transition within 150 ms were included. Shaded regions denote ±1 SEM.

scenario, we asked the question: from a situation in which both areas are in an Off state (state 1), is it more likely for V1 (a, state 2) or V4 (b, state 3) to transition to an On state? The second scenario (purple) addresses a related question: from a situation in which both areas are in an On state (state 4), is it more likely for V1 (b, state 3) or V4 (a, state 2) to transition to an Off state? Investigation of the transition probabilities (Figure 3-15c & Figure 3-15d) revealed that when both areas were in an Off state, it was more likely for V4 to transition to an On state first ($p<0.001$). Likewise, if both areas were in an On state, it was more likely for V4 to transition to an Off state ($p<0.001$). Thus, when both areas are in the same state, it is more likely for V4 to transition away from this state first.

As indicated above, V1 and V4 states are correlated, but transitions are not deterministic. This suggests that some substantial amount of time is spent in state 2 and 3, the states where V1 and V4 are in opposite states. Indeed, the fraction of time spent in each of the 4 states illustrates that V1 and V4 are not always in the same state (Figure 3-15e). Although more time is spent in state 1 and 4, 30 to 40% of time was spent in state 2 and 3.

Next, we investigated how attention affected the time spent in each state and the estimated transition probabilities (Figure 3-15f). With attention directed towards the RF, the fraction of time spent in state 1 was reduced ($p < 0.001$) whereas the time spent in

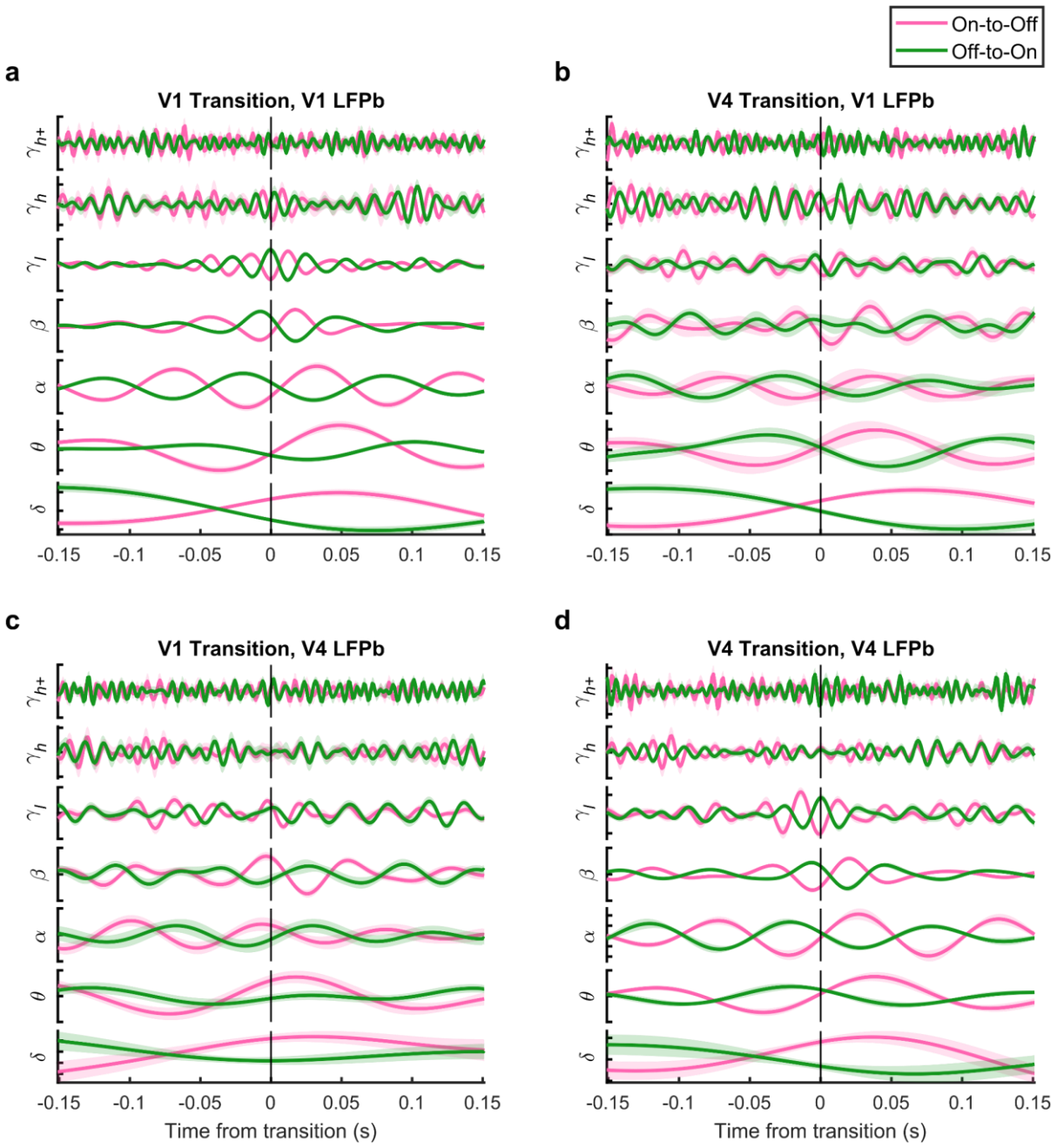

Figure 3-13. Transition triggered band-pass filtered LFPb. (**a**) Band-pass filtered LFPb from area V1 aligned to HMM state transitions in V1. (**b-d**) Same conventions as in panel **a**, but for V1 LFPb and V4 HMM (**b**), V4 LFPb and V1 HMM (**c**) and V4 LFPb and V4 HMM (**d**). δ: 0-4 Hz, θ: 4-8 Hz, α: 8-12 Hz, β: 12-30 Hz, γ_{low}: 30-60 Hz, γ_{high}: 60-100 Hz, and γ_{high+}: 100-200 Hz. Only epochs without transitions preceding or following the alignment transition within 150 ms were included. Shaded regions denote ±1 SEM.

state 3 ($p = 0.013$) and 4 was increased ($p < 0.001$). Attention thus decreased the time that both areas were in an Off state (state 1), while it increased the time either V4 was in an On state (state 3) or both areas were in an On state (state 4). As states 1 and 4 were most strongly affected, attention seemed to mainly influence the times that V1 and V4 states were aligned, perhaps driven top-down by state changes in V4. The effect of attention on the transition probabilities seemed to support this viewpoint (Figure 3-15g). With attention directed towards the RF, the probability of transitioning to state 1 from either state 2 ($p < 0.001$) or 3 ($p = 0.002$) was reduced. Additionally, the probability of

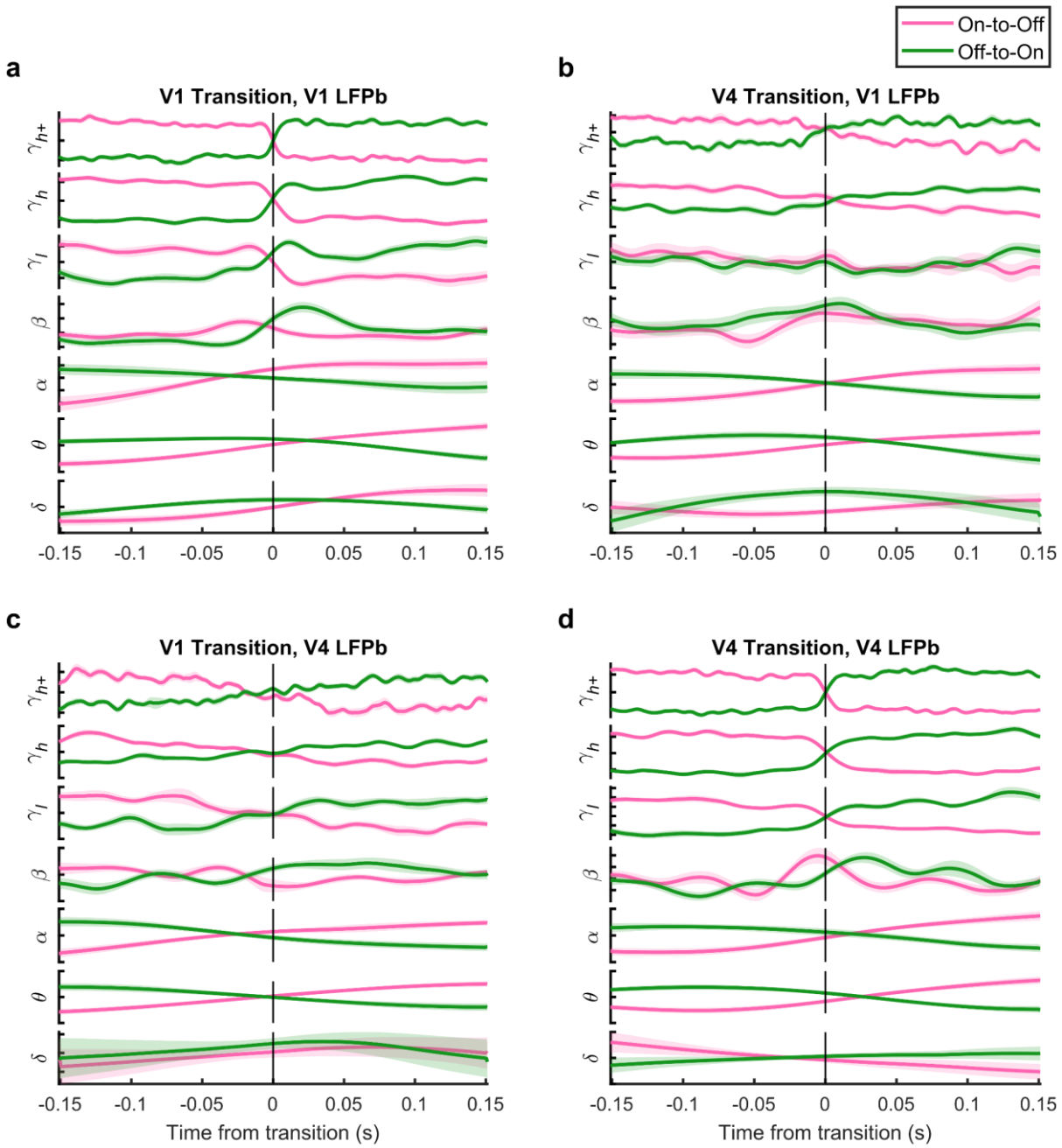

Figure 3-14. Transition triggered band-pass filtered LFPb power spectrum. (**a**) Band-pass filtered LFPb power spectrum from area V1 aligned to HMM state transitions in V1. (**b-d**) Same conventions as in panel **a**, but for V1 LFPb and V4 HMM (**b**), V4 LFPb and V1 HMM (**c**) and V4 LFPb and V4 HMM (**d**). δ: 0-4 Hz, θ: 4-8 Hz, α: 8-12 Hz, β: 12-30 Hz, γ_{low}: 30-60 Hz, γ_{high}: 60-100 Hz, and γ_{high+}: 100-200 Hz. Only epochs without transitions preceding or following the alignment transition within 150 ms were included. Shaded regions denote ±1 SEM.

transitioning to a state where V4 was in an On phase, either from state 1 ($p = 0.009$), state 2 ($p = 0.007$) or state 3 ($p = 0.001$) was increased. Together, these results again suggest that attention directed towards the RF increases the coordination of V1 and V4 cortical state, driven by recruitment of V4.

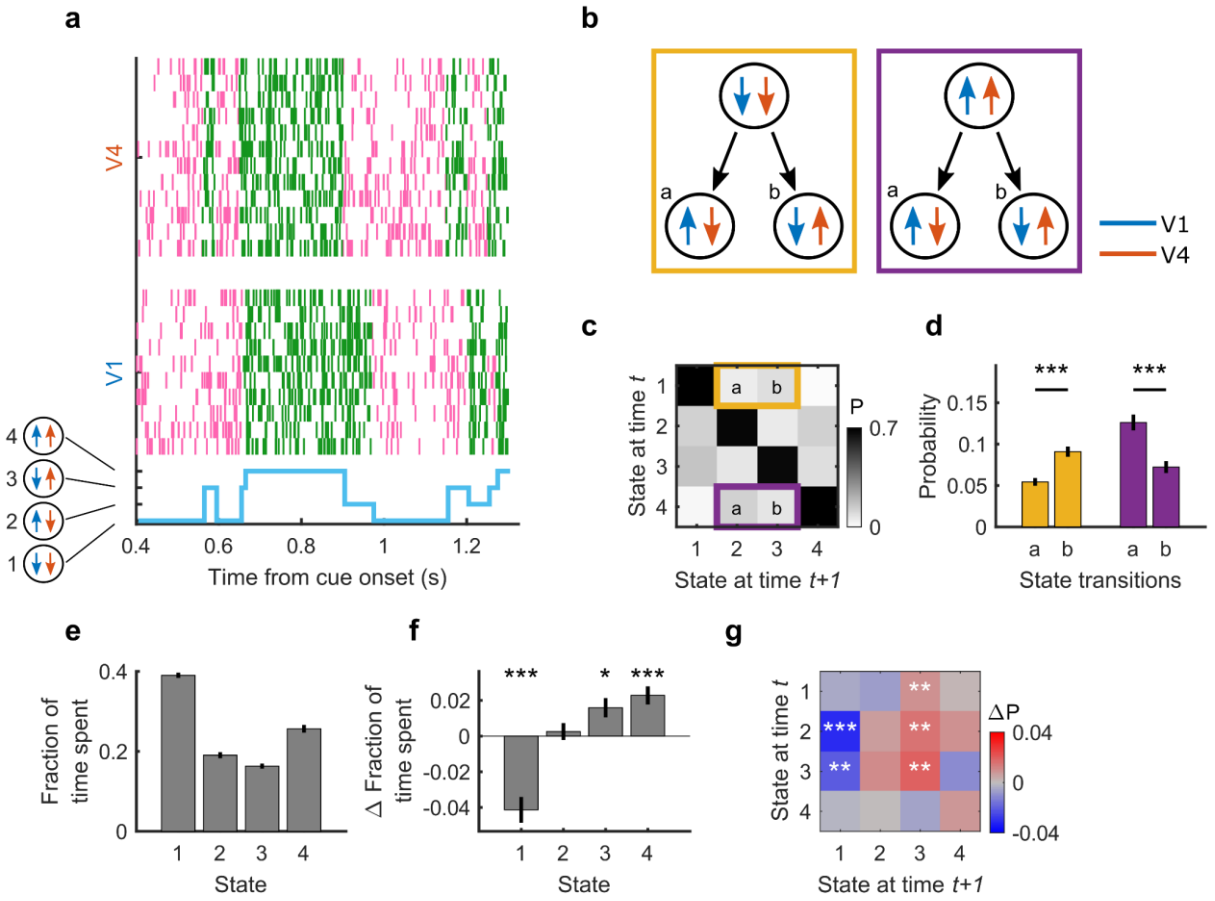

Figure 3-15. HMM with 4 states fit simultaneously to V1 and V4. (**a**) Example trial with the state trajectory (bottom) and across-laminar raster plot for V1 (middle) and V4 (top). (**b**) Schematic describing two scenarios accompanying the following questions; Left yellow box: from a state where both V1 and V4 are Off, is it more likely for V1 or V4 to transition to an On state first? Right purple box: from a state where both V1 and V4 are On, is it more likely for V1 or V4 to transition to an Off state first? (**c**) Transition probability matrix, indicating the probability of staying in a state (diagonal) or transitioning from one state to another. Highlighted are the scenarios set out in panel **b**. (**d**) Comparison of transition probabilities indicated in panel **b** and **c**. (**e**) The fraction of time spent in each of the 4 states. (**f**) The difference in time spent in each of the 4 states when attention is directed towards or away from the RF (attend RF – attend Away). (**g**) Attentional influence on state-transition probabilities, shown is the difference transition matrix (attend RF – attend Away). Statistics: Wilcoxon signed rank test (FDR corrected), error bars denote ±1 SEM across recordings and *, ** and *** indicate significance levels of $p < 0.05$, $p < 0.01$ and $p < 0.001$, respectively.

3.4.3 - Coordination of cortical states across V1 and V4 does not solely rely on microsaccades

Although Engel et al. (2016) showed that cortical state transitions can occur independently of microsaccades, it could be that V1 and V4 state coordination only occurs after a microsaccade. To test for this possibility, we first performed a cross correlation between microsaccade onset times and On-Off transition times (Figure 3-16a-b). Comparable to the previously described relationship between microsaccades and cortical state transitions (Engel et al., 2016), we found an increased probability of Off-On transitions following microsaccades. This relationship, however, did not influence the correlation between V1 and V4 states. After exclusion of trials in which microsaccades occurred, the cross-correlation between V1 and V4 (Figure 3-16c) closely resembled the relationship without trial exclusion (Figure 3-10b). This confirmed that

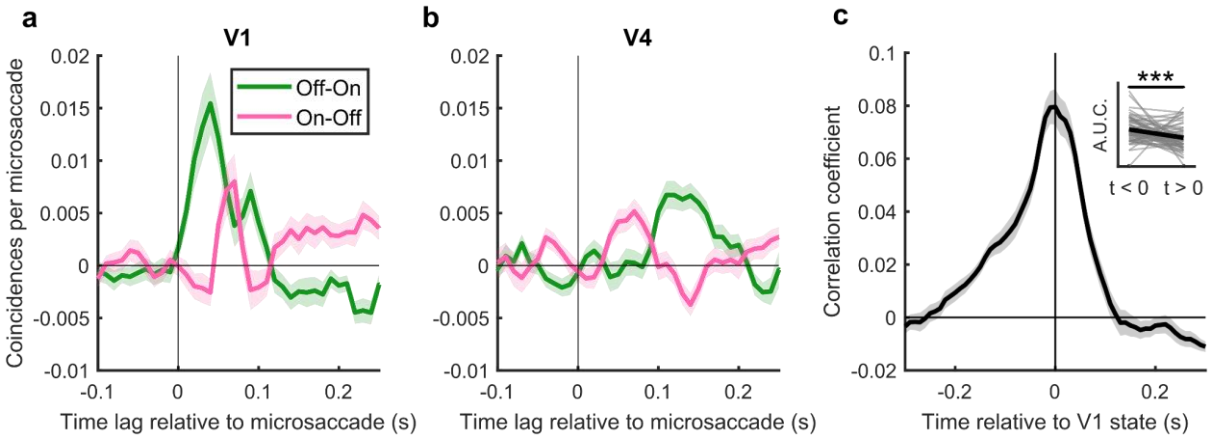

Figure 3-16. Relationship between microsaccades and cortical state transitions. (**a**) Cross-correlation of cortical state transitions in V1 triggered to microsaccade onset. (**b**) Same as panel **a**, but for cortical state transitions in V4. (**c**) Cross correlation between V1 and V4 cortical state time series after exclusion of trials in which microsaccades occurred. Statistics: Wilcoxon signed rank test. Shaded regions denote ±1 SEM across recordings, *, ** and *** indicate significance levels of $p < 0.05$, $p < 0.01$ and $p < 0.001$, respectively.

coordination of V1-V4 cortical state does not solely rely on the occurrence of microsaccades.

3.4.4 - Local On-Off dynamics relate to spectral power in LFPb

We compared the power spectrum in V1 and V4 between On and Off states in either area. When V1 was in an On compared to an Off state, the LFPb power spectrum showed decreased low-frequency and increased high frequency power across both areas (Figure 3-17a-b). Likewise, V4 On states elicited similar power changes across both V1 and V4 (Figure 3-17c-d), in line with the power changes described for V4 previously (Engel et al., 2016). Next, we investigated the power spectra across the four states of the HMM applied to both V1 and V4. Specifically, we tested whether power spectra within one area differed across the two states for which this area was in the same phase (i.e. the difference between these states is determined by the phase of the other area). For instance, there are two states in which V1 was found to be in an On phase across which V4 was in an On (state 4) or Off phase (state 2). The power spectra across these four states are depicted in Figure 3-17e (V1) and Figure 3-17f (V4), with the change in power in the panels beneath (Figure 3-17g-h). Across the two states where V1 was in an On phase (state 4 versus state 2), high frequency power (>50 Hz) was increased if V4 was also in an On phase, whereas low frequency power was reduced. Importantly, this change in high-frequency power occurred without corresponding increases in firing rate (Figure 3-17g-inset), showing that these changes are not driven by spike intrusion in the LFPb signal. Additionally, across the two states where V1 was in an Off phase (state 1 versus state 3), high frequency power was reduced when V4 was also in an Off phase. V4 phase thus modulated high frequency power in V1 regardless of what phase V1 was in. Interestingly, although high frequency power in V4 across Off phases (state 2 versus state 1) was decreased if V1 was also in an Off phase, high-frequency power between On phases (state 4 versus state 3)

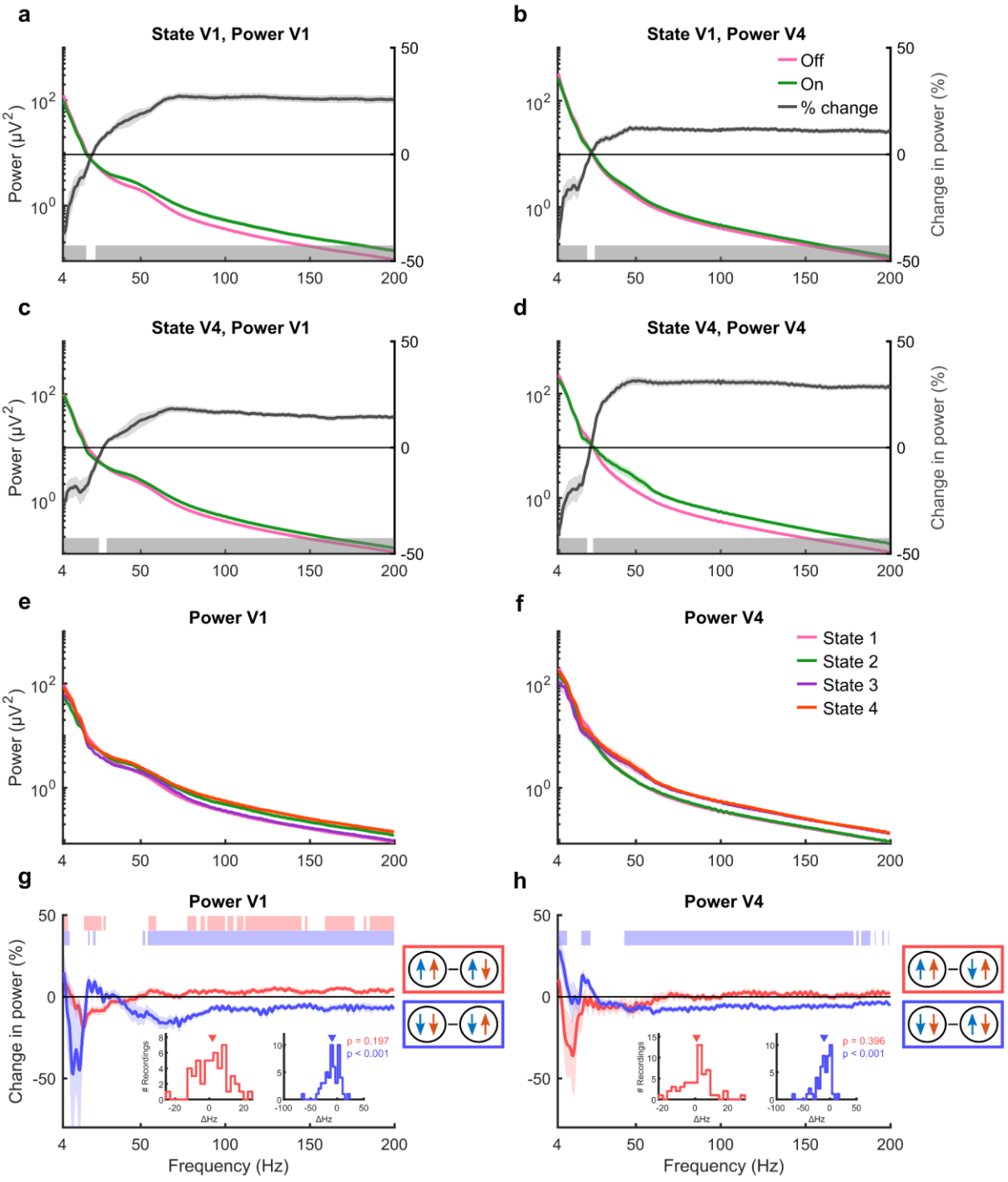

Figure 3-17. LFPb power spectrum for On and Off states. (**a**) Power in V1 during On and Off states in V1. (**b**) Power in V4 during On and Off states in V1. (**c**) Power in V1 during On and Off states in V4. (**d**) Power in V4 during On and Off states in V4. Right y-axis indicates the percentage change in power during On versus Off states (On-Off). (**e-f**) Power spectrum in V1 (**e**) and V4 (**f**) for the 4-state HMM fit across V1 and V4. (**g-h**) The within-area power difference between On phases (red, V1: state 4-2; V4: state 4-3), or off phases (blue, V1: state 1-3; V4: state 1-2). Insets show the firing rate differences during these same epochs. Only state epochs of at least 250 ms were included. Grey, red and blue bars indicate the significantly modulated frequencies ($p < 0.05$, Wilcoxon signed rank test, FDR corrected). Shaded regions denote ±1 SEM.

was not modulated by the state in V1 state. Together this suggests that during spatial attention, V4 state has a larger effect on high frequency activity in V1 than vice-versa.

3.4.5 - Local On-Off dynamics relate to global network state

In addition to finding changes in the LFPb power spectrum between On and Off phases, we found that baseline pupil diameter was predictive of the duration of On episodes in both V1 and V4 (Figure 3-18), as has been described for V4 before (Engel et al., 2016). Specifically, with higher baseline pupil diameter, indicative of higher central arousal state, the average duration of On episodes in both V1 and V4 was increased (Figure 3-18a-c). Furthermore, for the 4-state model (applied to both V1 and V4 simultaneously, see above) baseline pupil diameter was only predictive of the average epoch duration of state 1 and 4, the two states in which V1 and V4 are both in the same phase (Figure 3-18d). This is in line with pupil diameter being a proxy for central arousal, driving global network states that coordinate activity across distant brain areas. Note that the pupil diameter did not differ between attend RF and attend away conditions (Figure 3-18e), and that therefore differences in central arousal cannot explain the effect of selective attention on the duration of On episodes.

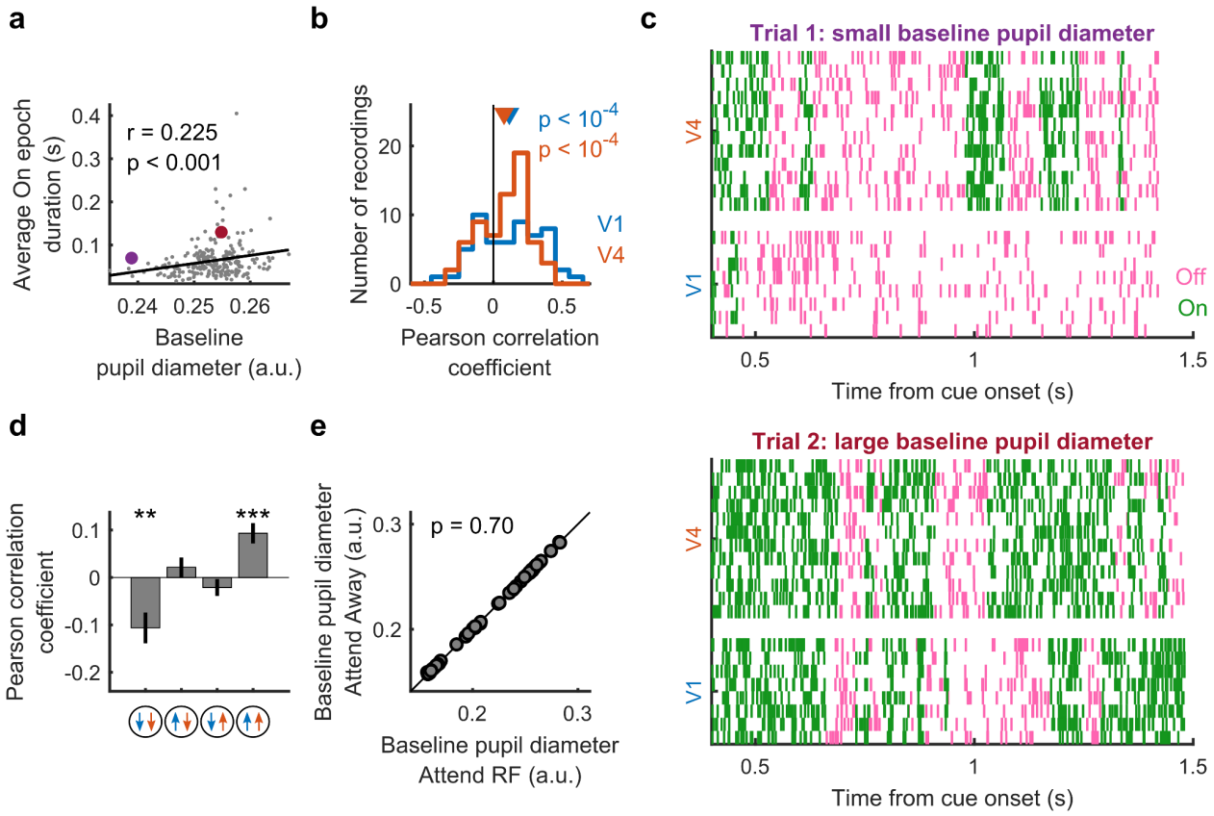

Figure 3-18. The relationship between baseline pupil diameter and state epoch duration. (**a**) Example recording showing that baseline pupil diameter is positively correlated to the average On episode duration in V4. Each dot represents one single trial, r is the Pearson correlation coefficient. The purple and red dot indicate the example trials used in panel **c**. (**b**) Across recordings, the average duration of On epochs in both V1 and V4 is positively correlated with the size of the baseline pupil diameter. (**c**) Two example trials in which the average On epoch duration is larger on the trial with larger (bottom) compared to the trial with smaller (top) baseline pupil diameter. (**d**) Across recordings, baseline pupil diameter is negatively (positively) correlated with the average epoch duration when both V1 and V4 or in an Off (On) state. (**e**) The average baseline pupil diameter does not differ between attention conditions. Each dot represents a recording session. Statistics: Wilcoxon signed rank test (FDR corrected) (**b, d, e**). Error bars and shaded regions denote ±1 SEM, and *, ** and *** indicate significance levels of $p < 0.05$, $p < 0.01$ and $p < 0.001$, respectively.

3.4.6 - State at target dimming is predictive of task performance

Finally, we tested whether cortical state influenced behaviour by investigating RT as a function of cortical state at the time of target dimming. In line with Engel et al., (2016), who found higher target detection probabilities if V4 was in an On-phase, we found faster RT on trials that ended in an On phase (Figure 3-19). Based on the 2-state HMM, we found that, individually for V1 and V4, cortical state was predictive of RT (Figure 3-19a). We found a significant interaction (2-factor repeated measures ANOVA) between attention and state for both V1 ($F = 23.8$, $p < 0.001$) and V4 ($F = 13.0$, $p < 0.001$), in neither area was there a main effect of attention ($p > 0.05$), but both showed a main effect of state (V1: $F = 6.7$, $p = 0.01$; V4: $F = 10.4$, $p = 0.002$). For both V1 and V4, task performance was better on trials where the target stimulus was inside the RF, and the population of neurons that coded for this stimulus was in an On phase around target dimming. Additionally, for V1, if the population of neurons inside the RF was in an On state, responses to targets away from the RF were slower.

Next, we tested how cortical state coordination across V1 and V4 influenced behavioural performance (Figure 3-19b). We used sequential multilevel model analyses and maximum likelihood ratio tests to test for fixed effects of attention and state on RT. From an intercept only model, the addition of the factor attention did not improve the fit of the model ($\chi_{(1)} = 1.34$, $p = 0.247$). However, both the addition of state ($\chi_{(1)} = 8.09$, $p = 0.004$) as well as the interaction between attention and state ($\chi_{(1)} = 12.60$, $p < 0.001$) significantly improved the model fit. As illustrated in Figure 3-19b, behavioural performance increased from when both areas were Off, through V1 On - V4 Off, through

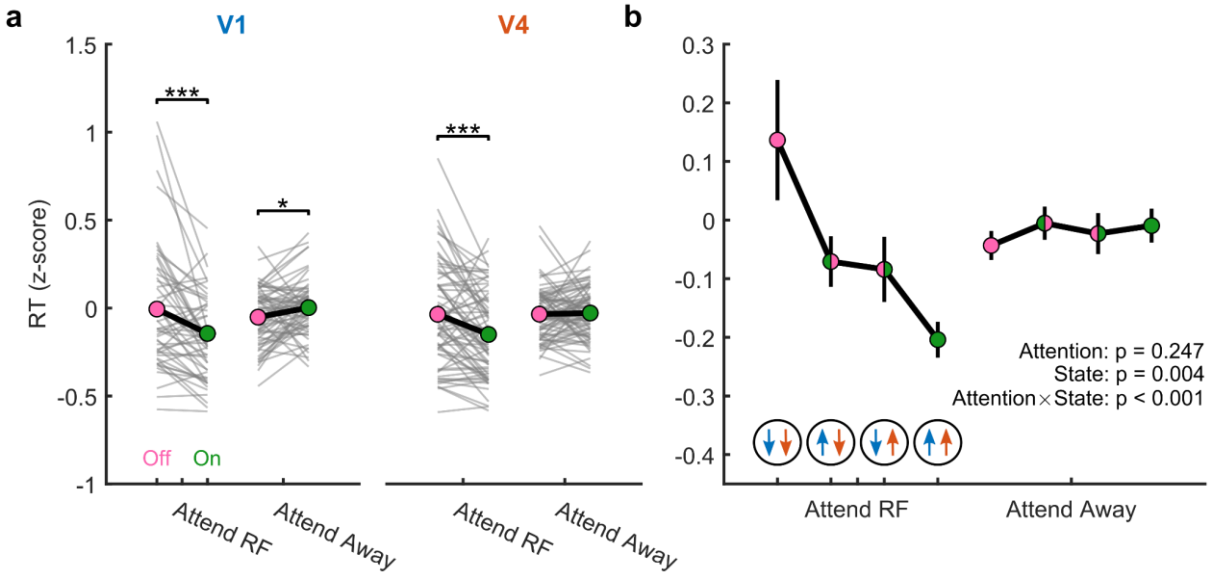

Figure 3-19. On-Off dynamics influence behavioural performance. (**a**) Cortical state at the time of target dimming, determined individually for V1 and V4, influences behavioural performance by decreasing RT when attention is directed towards the RF and either V1 or V4 is in an On state. Additionally, in V1 when neurons inside the RF are in an On state when attention is directed away from the RF, RT increases. (**b**) RT decreased from when both areas were Off, through V1 On - V4 Off, through V1 Off - V4 On, to V1 and V4 On when attention was directed towards the RF. Statistics: Wilcoxon signed rank test (**a**), and multilevel linear mixed effect model (**b**), FDR corrected. Error bars denote ±1 SEM, and *, ** and *** indicate significance levels of $p < 0.05$, $p < 0.01$ and $p < 0.001$, respectively.

V1 Off- V4 On, to V1 and V4 On, showing that there is an increased benefit for behavioural performance if cortical On phases are coordinated across visual cortex.

3.5 - **Discussion**

In this study we investigated the coordination of cortical state fluctuations across area V1 and V4 of the macaque monkey in the context of a selective spatial attention task. In both V1 and V4, periods of vigorous spiking alternated with periods of faint spiking activity. We classified these periods as On and Off periods using a 2-state HMM (Engel et al., 2016). We found that V1 and V4 states are correlated, and that On and Off periods in either area influenced activity in the other area such that transitions to an On state increased firing rates and high-frequency power and decreased low-frequency power, whereas transitions to an Off state had the opposite effect. We furthermore found that V4 activity changes, on average, preceded state transitions in V1, and concurrently that V1 activity changes followed state transitions in V4, suggesting that V4 generally takes the lead in driving cortical state transitions in V1 during spatial attention. This finding was further supported by a cross correlation analysis between V1 and V4 transition times and the application of a 4-state HMM simultaneously to V1 and V4 data. These analyses indicated that V4 transitions occurred before those in V1 and that it is more likely for V4 to transition away from a state in which V1 and V4 states correspond. Additionally, the correlation strength between V1 and V4 states was dependent on the distance between RF locations. Together, these results suggest that cortical state transitions and their coordination are driven in a retinotopically specific top-down manner.

We furthermore replicated previous findings which revealed that selective attention directed towards the RF increases the duration of On episodes in V4 (Engel et al., 2016), and found similar results for V1 (Figure 3-8). Testing the effect of selective attention on the fraction of time spent in each of the 4 states of the HMM applied to V1 and V4 moreover revealed that selective attention specifically increases the time spent in state 4 (Figure 3-15), suggesting that attention directed towards the RF increases the coordination of cortical state, through top down recruitment, between retinotopic locations in V1 and V4.

Finally, On-Off dynamics were predictive of behavioural performance. For V1 and V4, RT was faster on trials in which either area was in an On-state around the time of target dimming. Furthermore, we found an increased benefit on behavioural performance if both V1 and V4 were in an On-state at the time of target dimming, showing that the coordination of cortical state across these areas is relevant to behaviour.

Thus, On-Off transitions, which occur synchronously across the cortical layers, are found in V1 and V4. Coordination of these transitions is retinotopically organised, driven in a top-down manner, and beneficial for behavioural performance.

3.5.1 - Mechanisms of cortical state

What could be the neural mechanism that drives On-Off transitions across cortical areas during selective attention? Cortical state fluctuations, defined as activity varying along a continuum between periods of synchronisation and desynchronisation, have largely been ascribed to neuromodulatory influences that dynamically regulate network state (Buzsaki et al., 1988; Constantinople and Bruno, 2011; Lee and Dan, 2012). Direct stimulation (inhibition) of LC (Berridge and Foote, 1991; Berridge et al., 1993) or cholinergic nuclei (Metherate et al., 1992; Steriade et al., 1993a) can induce cortical depolarisation (hyperpolarisation) and desynchronisation (synchronisation). Additionally, both stimulation as well as locomotion-induced effects on cortical state are reversed by local application of noradrenergic or cholinergic antagonists (Goard and Dan, 2009; Metherate et al., 1992; Pinto et al., 2013; Polack et al., 2013), suggesting that the effects on cortical state depend (in part) on local neuromodulatory influences, rather than solely on large scale network effects.

In addition to neuromodulatory effects, cortical state can also be affected by feedback projections from downstream areas (Zagha et al., 2013), possibly through similar circuit mechanisms by which top-down attention influences sensory cortex (Harris, 2013; Harris and Thiele, 2011). In an elegant series of experiments Zagha et al., (2013) showed that feedback from primary motor cortex (vM1) influences cortical state in primary somatosensory cortex (S1). Inactivation of vM1 synchronised S1 by increasing low-frequency (1-5 Hz) and decreasing high-frequency (30-50 Hz) LFP power whereas stimulation had the opposite effect. In addition, vM1 stimulation increased firing rates in S1 but not V1, showing that vM1 stimulation produces pathway-specific, rather than general (brain-wide) cortical state changes. Furthermore, the influence of vM1 stimulation on S1 was rapid (~10 ms) and beneficial to sensory information coding in S1, reducing response variability both in MUA and LFP (Zagha et al., 2013). Together these results illustrate that feedback projections can selectively influence cortical state in sensory areas, and that these network dynamics can affect sensory stimulus processing.

Here we showed that On-Off dynamics relate to both these mechanisms. As the average On epoch duration was related to fluctuations in pupil diameter (Engel et al., 2016) (Figure 3-18), they are likely influenced by similar arousal-related neuromodulatory influences that drive cortical depolarisation and desynchronisation. Additionally, we found that activity changes and cortical state transitions in downstream areas preceded those in upstream areas, revealing that cortical state fluctuations can be influenced in a top-down manner.

Because projections from neuromodulatory nuclei to cortex are diffuse (Mesulam et al., 1992) and their effects of stimulation on cortical activity are relatively sluggish, the effects of neuromodulators are often assumed to lack the temporal and spatial specificity to support specific moment-to-moment (cognitive) demands (but see Sarter et al., 2009; Thiele and Bellgrove, 2018). Our findings provide support for the previously suggested neural mechanism (Deco and Thiele, 2011; Zagha et al., 2013), that feedback projections, together with thalamic feedforward drive (Poulet et al., 2012), operate in conjunction

with (global) neuromodulatory influences. Together, they provide both the required anatomical specificity and functional means to allow cortical state fluctuations to influence information-processing capacity and behaviour.

In addition to the well-established role of noradrenaline and acetylcholine in driving cortical state fluctuations (Harris and Thiele, 2011; Lee and Dan, 2012; Thiele and Bellgrove, 2018), dopaminergic effects might explain (part of) these results as well. VTA stimulation can increase the duration of UP-states in rat PFC, an effect prevented by systemic injection of a D1R-antagonist (Lewis and O'Donnell, 2000). Prefrontal dopamine has moreover been found to influence attentional signalling (Noudoost and Moore, 2011b; Thiele and Bellgrove, 2018), and within FEF, dopamine has been found to modulate activity in V4 neurons with overlapping RF in an "attention-like" manner (Noudoost and Moore, 2011a). Together, these results reveal that prefrontal dopamine can influence both the duration of cortical state epochs as well as modulate activity in extrastriate visual cortex through feedback projections, in line with a role for both feedback projections and neuromodulatory influences in the regulation of cortical state and attention.

3.5.2 - Relationship between On-Off dynamics and (global) signatures of cortical state

How do On-Off dynamics in visual cortex relate to the larger scale fluctuations in cortical state? As described above, cortical states do not only fluctuate between sleep and wake states, but also during wakefulness. During less active states, cortical activity displays highly synchronous activity characterised by low-frequency oscillations. During active states, on the other hand, the cortex is more desynchronised and displays suppressed low-frequency and increased high-frequency activity. Recent research has revealed that fluctuations in central arousal, as indicated by pupil diameter, closely tracks fluctuations in the subthreshold membrane potential (McGinley et al., 2015a; Reimer et al., 2014), as well as the LFP power spectrum (Vinck et al., 2015) of sensory neurons, characteristic of changing cortical state. Furthermore, the relationship between state fluctuations and pupil diameter provides additional support for a neuromodulatory influence on cortical state, as fluctuations in pupil diameter reliably reflect activity in various neuromodulatory centres that project to cortex (Aston-Jones and Cohen, 2005a; de Gee et al., 2017; Joshi et al., 2016; Murphy et al., 2014a; Reimer et al., 2016; Varazzani et al., 2015).

Here we found differences in the LFPb power spectrum between On and Off states, with decreased low-frequency and increased high-frequency power across both areas during On phases in either V1 or V4 (Figure 3-17a-d). Additionally, we found that V4 state modulated LFPb power in V1, even if V1 phase was constant. Specifically, On phases in V4 increased high-frequency power in V1, whereas Off phases in V4 decreased high-frequency power in V1. On the other hand, Off phases in V1 suppressed high-frequency power in V4, but On phases did not elicit any changes to the V4 power spectrum (Figure 3-17e-h). In addition to the important role of feedback projections in driving state

transitions, these results suggest that high-frequency power in V1 is also modulated in a top-down manner during spatial attention.

In addition to top-down attention, central arousal was also predictive of On-Off dynamics across V1 and V4. Higher arousal, characterised by larger baseline pupil diameter, was predictive of longer On epoch durations in both V1 and V4 (Figure 3-18b). In particular, higher arousal was predictive of epoch duration in the states where V1 and V4 were both in an Off (state 1) or On (state 4) phase (Figure 3-18d). Importantly, although central arousal was predictive of the time V1 and V4 were in the same state, pupil diameter did not differ across attention conditions (Figure 3-18e). This showed that arousal and attention interact, but that each had an independent contribution to cortical state dynamics.

3.5.3 - Across area interaction of cortical state and selective attention

As described above, the influence of selective attention and cortical state on local network dynamics might rely on similar circuit mechanisms (Harris, 2013; Harris and Thiele, 2011). Within visual cortical areas, spatial attention directed towards the RF generally increases mean firing rates (Desimone and Duncan, 1995), and decreases spike count correlations across neuronal pairs (Cohen and Maunsell, 2009; Mitchell et al., 2009; Ruff and Cohen, 2016a), depending on the signal correlation between these pairs (Rabinowitz et al., 2015; Ruff and Cohen, 2014).

It is currently unknown how information transfers across areas, and how this transfer is modulated by attention and cortical state on a trial-to-trial basis. Within visual areas, the attentional effects on the correlation structure of neural populations has been found to largely depend on feedback from higher order areas (Bondy et al., 2018), and can be modelled by a single modulator (per hemisphere, and weighted individually for each neuron) that affects each neuron's response gain (Rabinowitz et al., 2015). Although the attention-related modulation of correlated variability can improve coding within a sensory area, it is unclear how this modulation affects either activity on shorter timescales or transmission across areas. As neural codes are noisy, coordination of activity, and thus redundancy, might be a prerequisite for successful information transfer from one area to the next (Harris and Mrsic-Flogel, 2013). Indeed, retinotopically aligned visual areas reveal sharper peaks in their cross correlogram (Nowak et al., 1995), and V2 spikes are preceded by coordinated spiking bursts (activity packets) in V1 (Zandvakili and Kohn, 2015). Additionally, attention has been found to increase, rather than decrease, correlated variability in retinotopically aligned V1 and MT neurons (Ruff and Cohen, 2016a). This suggests that trial-by-trial coordination of activity across brain regions is beneficial for information transfer and can be selectively modulated according to task demands.

The periods of high firing activity observed here, occurring at seemingly random times during the trial, could constitute the transmission of "activity packets". During wakefulness, spontaneous fluctuations in population spiking activity have been

observed across sensory cortex in different modalities (Arieli et al., 1996; Engel et al., 2016; Luczak et al., 2013, 2009; Sakata and Harris, 2009; Shimaoka et al., 2018). These seemingly random periods of high firing rate can occur spontaneously, after stimulus onset, as well as during sustained stimulus presentation, and regardless of when they occur, their structure (partially) follows a stereotypical activity pattern (Luczak et al., 2013, 2009). Within activity packets, small variations in the temporal relationship and firing rates across the population code for distinct stimuli. Because of the structural similarity of activity packets across different conditions, it has been suggested that these packets might constitute a basic building block of information coding and a biologically plausible way for the cortex to transmit information between cortical areas (Luczak et al., 2015). Additionally, during sustained stimulus presentation, these packets have similar structure between synchronised and desynchronised states, but occur more frequently during cortical desynchronisation (Luczak et al., 2013).

Within this framework (Luczak et al., 2015), information is transmitted in discrete packets, occurring reliably at stimulus onset but irregularly otherwise. Even during sustained stimulus presentation, population activity is not constant or sustained. Rather, periods of high firing rates alternate with periods of relative network silence. Activity packets can also be initiated in higher-order areas, providing context to local processes in sensory areas by sending information through feedback projections. Top-down attention could hereby send information upstream that outlines which specific information about a stimulus should be processed preferentially. With a duration of 50-200 ms (Luczak et al., 2015, 2013), activity packet transmission might allow integration of feedforward and feedback activity. As activity packets are more likely to occur during the desynchronised state, in which desynchronised activity could be constituted of multiple overlapping packets, this could indicate an increase in packet transmission.

It is unclear, however, to what extent packet transmission propagates across brain areas. While the spread of sensory activity in rodents is well-characterised as travelling waves that extends to most of the cortex (Luczak et al., 2015; Mohajerani et al., 2013), the spatial extent of activity transmission in primate cortex is less-well described and might be much smaller. Indeed, in anaesthetised monkeys coordinated bursts of V1 activity only reach as far as the input layer of V2, without spreading further across other V2 layers, and depend strongly on retinotopic alignment (Zandvakili and Kohn, 2015). Similarly, our results also show that across-area coordination strongly depends on retinotopic alignment. Activity packet transmission might thus be much more constrained in primate cortex.

The increased duration of On episodes with attention directed towards the RF could reflect an increase in package transmission resulting in overlapping activity packets, which the HMM would not distinguish as distinct states and would therefore classify as a single longer state epoch. One reason why activity packets are unlikely to be the sole reason for the effects we have described here, is that activity packets usually last between 50 and 200 ms (Luczak et al., 2015, 2013). In our data, on the other hand, we find both much shorter epoch durations (10 ms), as well as much longer epochs (> 1 s), even in the attend away conditions. In fact, as the distribution of epoch durations seems to follow

an exponentially decaying function (Figure 3-9), these short epoch durations, in particular those of On phases, are the most common ones.

The mechanisms supporting cortico-cortical communication likely depend on some form of coordinated spiking activity, but the exact manner in which information is transmitted is still unclear. Cognitive processes such as attention have been found to selectively modulate across-area oscillatory coupling (Bosman et al., 2012; Gregoriou et al., 2009; Rohenkohl et al., 2018; Salazar et al., 2012) and correlated spiking variability (Oemisch et al., 2015; Ruff and Cohen, 2016a). Here we show that trial-by-trial across-area coordination of rapidly fluctuating On-Off dynamics was modulated by attention and improved behavioural performance, suggesting enhanced information transmission. It will be important to determine the specificity of these dynamics, in terms of their spatial extent (i.e. can spatial attention selectively modulate On-Off dynamics between two nearby cortical regions?), their functional extent (i.e. would coordination be higher for neurons with high signal correlation (e.g. similar orientation tuning curves)?), their relation to frequency-specific coherence, as well as the selectivity by which single neurons are recruited (Okun et al., 2015) to transmit stimulus-specific information (Semedo et al., 2019).

3.6 - **Conclusion**

Although the effects of attention and cortical state within cortical areas are relatively well characterised, little is known about how either affects the across-area coordination of activity deemed crucial for cognition. Our results show that cortical state can influence population activity on both short and long timescales, and that attention can modulate these network activity fluctuations both within and across brain regions in support of behaviour.

3.7 - **Acknowledgements**

We thank Tatiana Engel and Demetrio Ferro for advice on data analysis.

Chapter 4 - Dopamine influences attentional rate modulation in Macaque posterior parietal cortex

4.1 - Abstract

Selective attention facilitates the prioritisation of task-relevant sensory inputs over those which are irrelevant. Although cognitive neuroscience has made great strides in understanding the neural substrates of selective attention, our understanding of its neuropharmacology is incomplete. Cholinergic and glutamatergic contributions have recently been demonstrated, but emerging evidence also suggests an important influence of dopamine. Dopamine (DA) has historically been investigated in the context of frontal/prefrontal function arguing that dopaminergic receptor density in the posterior/parietal cortex is rather sparse. However, this notion was derived from rodent data, whereas in primates DA innervation is comparatively strong, matching that of many primate prefrontal areas. Using recently developed techniques, we recorded single- and multi-unit activity whilst iontophoretically administering dopaminergic agonists and antagonists to posterior parietal cortex of awake, behaving rhesus macaques engaged in a covert feature based spatial attention task. Across the population, drug application resulted in general modulations in firing rate as well as modulation of attentional signals. More specifically, we show that unselective DA receptor agonists as well as D1 receptor antagonists diminish spike rates across the population. In addition, unselective DA receptor agonists modulate attentional signals in broad, but not narrow-spiking cells. Out of 97 neurons, the majority of which showed a visual response and attention selectivity, we found 55 that show modulation of activity induced by drug administration, out of these 10 showed an interaction effect between drug administration and attention Additionally, the unselective DA receptor agonist decreased attentional rate modulation and revealed an inverted-U shaped dose-response curve, whereas the dose-response curve of the D1 antagonist followed a monotonic function. These data show that dopamine plays an important role in shaping neuronal responses in macaque parietal cortex, and contribute to attentional processing.

4.2 - Introduction

Selective attention refers to the prioritisation of behaviourally relevant, over irrelevant, sensory inputs. Convergent evidence from human neuropsychological, brain imaging and non-human primate studies shows that fronto-parietal brain networks are critical for selective attention (Corbetta and Shulman, 2011; Desimone and Duncan, 1995; Posner, 1990). Neuromodulation of attention-related activity in these fronto-parietal networks occurs at least in parts via glutamatergic (Herrero et al., 2013) and cholinergic inputs (Furey et al., 2008; Herrero et al., 2008; Levin and Simon, 1998b; Nelson et al., 2005; Parikh et al., 2007; Sarter et al., 2005; Warburton and Rusted, 1993). Multiple lines of evidence, however, also suggest catecholamine modulation (Bellgrove and Mattingley, 2008; Thiele and Bellgrove, 2018). Here we sought to understand how

dopamine applied to the posterior parietal cortex modulates attention-related activity in non-human primates.

The functional significance of dopamine for behaviour is well established for a number of brain areas, including the frontal cortex (executive control) and basal ganglia (motor control). For these brain areas, the substantial similarities between rodents, non-human primates and humans, have allowed the development of mechanistic models with clinical translational value for a number of disorders (e.g., Parkinson's disease, schizophrenia or attention deficit hyperactivity disorder (ADHD)) (Arnsten et al., 2012; Thiele and Bellgrove, 2018). Species differences with respect to patterns of dopamine innervation do however exist for a number of posterior cortical areas, including the posterior parietal cortex. Although dopaminergic innervation of posterior parietal cortex is sparse in the case of rodents, work in non-human primates demonstrated that dopaminergic innervation to parietal regions is largely comparable in strength to prefrontal areas (Berger et al., 1991). Moreover, high densities of dopamine transporter (DAT) immunoreactive axons have been reported in the posterior parietal cortex of macaques (Lewis et al., 2001). These observations align with data from human studies that revealed dense dopamine receptor expression in parietal cortex (Caspers et al., 2013), as well as brain imaging studies of clinical disorders such as ADHD and schizophrenia, where medications targeting dopamine receptors or transporters modulate activity in parietal cortex (Mehta et al., 2000). Given these data and the clinical significance of posterior parietal function for a number of clinical disorders, a greater understanding of the functional role of dopamine in this region is warranted.

One cognitive process, which relies heavily on the integrity of the posterior parietal cortex, is selective attention. A number of lines of evidence from both non-human primates and humans suggest that dopamine may modulate selective attention. First, dopamine agonists reduce the extent of spatial inattention in both neurological (Gorgoraptis et al., 2012) and psychiatric patients with disorders such as schizophrenia (Maruff et al., 1995) and ADHD (Bellgrove et al., 2008; Silk et al., 2014). Second, psychopharmacological studies in healthy volunteers suggest that dopamine antagonists modulate parameters of spatial cueing paradigms (e.g. validity effect) which are often associated with parietal function (Clark et al., 1989). Third, DNA variation in a polymorphism of the dopamine transporter gene (DAT1) has been associated with individual differences in measures of spatial selective attention (Bellgrove et al., 2009, 2007; Newman et al., 2014). Fourth, studies in non-human primates have shown that dopamine contributes to working memory signals in dorsolateral prefrontal cortex (dlPFC) (Williams and Goldman-Rakic, 1995), and in frontal eye fields (FEF) dopamine affects target selection and modulates V4 activity in an 'attention-like' manner by altering orientation selectivity and response variability (Noudoost and Moore, 2011a). Dopamine thus contributes to working memory, target selection and plausibly also spatial attention in dlPFC and FEF (Clark and Noudoost, 2014; Noudoost and Moore, 2011a, 2011b; Williams and Goldman-Rakic, 1995), critical nodes of the fronto-parietal attention networks. Nevertheless, a specific effect of dopamine on attention-related activity in posterior parietal cortex is yet to be established.

Here we sought to address this knowledge gap by directly infusing dopamine (including specific agonists and antagonist) into the posterior parietal cortex of two macaque monkeys while they performed a selective attention task. We show that single and multi-unit (SU, MU) activity is inhibited by iontophoresis of dopaminergic drugs into the gray matter of the intraparietal sulcus (IPS). The effects of the unselective agonist dopamine (DA) followed an inverted U-shaped dose-response curve, whereas the dose-response of the D1-selective antagonist SCH23390 followed a monotonic function. Additionally, we found cell-type specific effects on attentional modulation, whereby DA only affected attention-related activity in broad-spiking cells but not in narrow-spiking units.

4.3 - **Materials & Methods**

4.3.1 - Procedures and animals

All procedures were performed in accordance with the European Communities Council Directive RL 2010/63/EC, the National Institutes of Health's Guidelines for the Care and Use of Animals for Experimental Procedures, and the UK Animals Scientific Procedures Act. In the present investigation, two adult awake male macaques (Macaca mulatta, age 9-11 years, weight 8-12.9 kg) were used.

4.3.2 - Surgical preparation

The monkeys were implanted with a head post and recording chambers over the lateral intraparietal sulcus under sterile conditions and under general anaesthesia. Surgery and postoperative care were identical to those published in detail previously (Thiele et al., 2006).

4.3.3 - Saccade field (SF) and receptive field (RF) mapping

The location of SF was mapped using a visually guided saccade task. Here, monkeys fixated centrally for 400 ms after which a saccade target was presented in one of nine possible locations (8-10° from fixation, equally spaced between). After a random delay (800-1400 ms, uniformly distributed) the fixation point was extinguished, which indicated the monkey to perform a saccade towards the target. Online analysis of visual, sustained and saccade related activity determined an approximate SF location which guided our subsequent RF mapping. The location and size of RF was measured by a reverse correlation method. During fixation, a black square (1-3° size, 100% contrast) was presented at pseudorandom locations on a 9 × 12 grid (5-25 repetitions for each location, 100 ms stimulus presentation, 100 ms interstimulus interval) on a bright background. This RF mapping procedure followed published details (Gieselmann and Thiele, 2008). RF eccentricity ranged from 2.5° to 17° and were largely confined to the contralateral visual field.

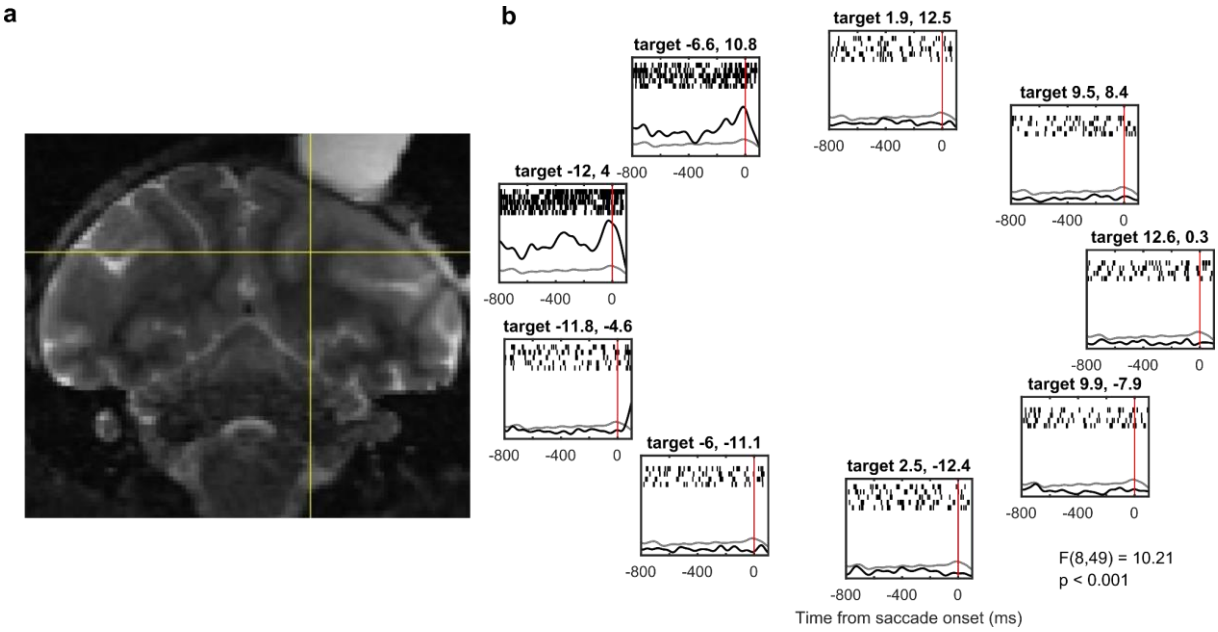

Figure 4-1. Identification of recording sites. (**a**) Targeting of recording site using structural magnetic resonance imaging (MRI). (**b**) Neural responses during saccade field mapping task aligned to saccade onset. Each panel shows the spiking activity as raster plots (each vertical line is a spike) across multiple trials and the average histogram (black line) to a visual stimulus presented in one of nine target locations around fixation (° from fixation, indicated in the title of each panel). The grey line indicates the average response across all stimulus locations for comparison. This example neuron showed selectivity for the targets presented in the upper left quadrant from fixation. Statistics: ANOVA across 50 trials distributed over 9 conditions (target locations).

4.3.4 - Identification of recording sites

The location of the intraparietal sulcus (IPS) was initially guided by means of postoperative structural magnetic resonance imaging (MRI), displaying the recording chamber (Figure 4-1a). During each recording, neuronal response properties where determined using SF and RF mapping tasks. During the SF mapping task, we targeted cells that showed spatially selective persistent activity and preparatory activity before the execution of a saccadic eye movement (Figure 4-1b).

4.3.5 - Behavioural task and stimuli

The task (Figure 3-1) and stimuli have been described previously (Thiele et al., 2016). In brief, stimuli were presented on a cathode ray tube (CRT) monitor (120 Hz, 1280 × 1024 pixels, 55 cm from the animal). The monkey initiated a trial by holding a touch bar and fixating a white fixation spot (0.1° diameter). After 425/674 ms (monkey 1/monkey 2) three coloured square wave gratings (2° - 6°, dependent on RF size and distance from fixation) appeared equidistant from the fixation spot, one of which was centred on the RF of the recorded neuron. Red, green and blue gratings (Table 4-1 for colour values) were presented on a gray background (0.8 cd/m²), with an orientation at a random angle to the vertical meridian (the same orientation for the three gratings in any given session). The locations of the colours, as well as the orientation, were pseudorandomly assigned between recording sessions and held constant for a given recording session.

Table 4-1. Colour values used for the 3 coloured gratings across recording sessions and subjects, indicated as [RGB] – luminance (cd/m²). a = Undimmed values, b = dimmed values.

	Red	Green	Blue
Monkey 1 **Early recordings (n=29)**	a. [255 0 0] - 14.5 b. [100 0 0] - 1.4	a. [0 128 0] – 9.1 b. [0 70 0] – 1.9	a. [60 60 255] - 11.5 b. [10 10 140] – 2.2
Monkey 2 **Early recordings (n=5)**	a. [220 0 0] – 12.8 b. [180 0 0] – 7.7	a. [0 135 0] – 12.9 b. [0 110 0] – 7.3	a. [60 60 255] – 12.2 b. [35 35 220] – 7.4
Monkey 1/2 (n=12/8) **Late recordings**	a. [220 0 0] – 12.8 b. [140 0 0] – 4.2	a. [0 135 0] – 12.9 b. [0 90 0] – 4.6	a. [60 60 255] – 12.2 b. [30 30 180] – 4.6

Gratings moved perpendicular to the orientation, whereby the direction of motion was pseudorandomly assigned for every trial. After a random delay (570-830/620-940 ms [monkey 1/monkey 2], uniformly distributed) a central cue appeared that matched the colour of the grating that would be relevant on the current trial. After 980-1780/1160-1780 ms [monkey 1/monkey 2] (uniformly distributed), one pseudorandomly selected grating changed luminance (dimmed). If the cued grating dimmed, the monkey had to release the touchbar within 600 ms. If a non-cued grating dimmed, the monkey had to ignore this and wait for the cued grating to dim. This could happen when the second or third (each after 750-1130/800-1130 ms [monkey 1/monkey 2], uniformly distributed) grating changed luminance. Drugs were administered in blocks of 36 trials.

4.3.6 - Electrode-pipette manufacturing

We recorded from the lateral (and in a few occasions medial) bank of the intraparietal sulcus (IPS) using custom-made electrode-pipettes (Figure 4-2) that allowed for simultaneous iontophoretic drug application and extracellular recording of spiking activity (Thiele et al., 2006). The manufacture of these electrodes was similar to the procedures described by Thiele et al., (2006), with minor changes to the design in order to reach areas deeper into the IPS, such as the laterial intraparietal area (LIP).

We sharpened tungsten wires (125 µm diameter, 75 mm length, Advent Research Materials Ltd., UK) by electrolytic etching off the tip (10-12 mm) in a solution of $NaNO_2$ (172.5 g), KOH (85 g) and distilled water (375 ml). We used borosilicate glass capillaries with three barrels (custom ordered, Hilgenberg GmBH, www.hilgenberg-gmbh.de), with the same dimensions as those described previously (Thiele et al., 2006). The sharpened tungsten wire was placed in the central capillary and secured in place by bending the non-sharpened end (approximately 10 mm) of the wire over the end of the barrel. After marking the location of the tip of the tungsten wire, shrink tubing was placed around the top and bottom of the glass. The glass was pulled around the tungsten wire using a PE-21 Narashige microelectrode puller with a heating coil made from Kanthal wire (1 mm diameter, 13 loops, inner loop diameter 3 mm) and the main (sub) magnet set to 30 (0) and the heater at 100. The electrode-pipette was placed such that the tip of the tungsten wire protruded 11 mm from the bottom of the heating coil. After pulling, we filled the central barrel (with the tungsten electrode inside) with superglue

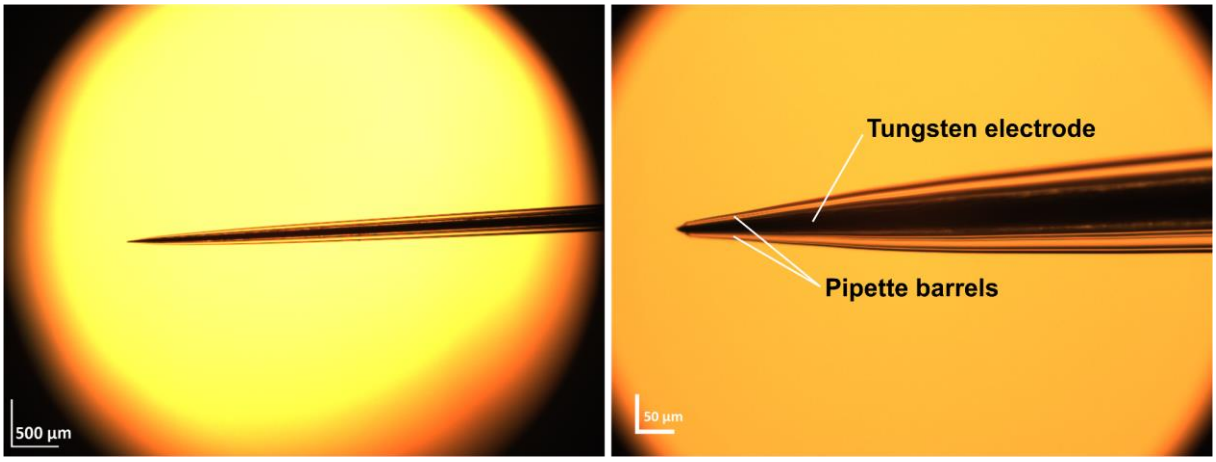

Figure 4-2. Micropipettes used for the simultaneous recording of neural activity and iontophoretical application of drugs in the near vicinity of the recording site. Two glass pipettes flank the etched tungsten wire. Electrode-pipette design based on that described by Thiele et al. (2006)

using a syringe and fine flexible injection canullae (MicroFil 28 AWG, MF28G67-5, World Precision Instruments, Ltd.). We found that if we did not fill (most of) the central barrel with superglue after pulling, the recorded signal was often very noisy, possibly due to small movements of the animal (such as drinking), which caused the free tungsten wire to resonate inside the glass. Using a micro grinder (Thomas Recording GmBH, tip grinding machine), we removed excess glass, sharpened the tip of the electrode and opened the flanking barrels of the pipette.

4.3.7 - Electrode-pipette filling and iontophoresis

Electrode-pipettes were back-filled with the same drug in both pipettes using a syringe, filter units (Millex® GV, 22 µm pore diameter, Millipore Corporation), and fine flexible injection canullae (MicroFil 34 AWG, MF34G-5, World Precision Instruments, Ltd.). The pipettes were connected to the iontophoresis unit (Neurophore-BH- 2, Medical systems USA) with tungsten wires (125 µm diameter) inserted inside the flanking barrels. Because of the exploratory nature of these recordings (it is unknown whether DA influences parietal neurons during spatial attention tasks and what modulation can be expected with different amounts of drug applied), we used a variety of iontophoretic ejection currents (20 - 90 nA). The details regarding concentration and pH of the drugs were: Dopamine (0.1M in water for injections, pH 4-5), SCH23390 (0.005-0.1M in water for injections, pH 4-5.5) and SKF81297 (0.01M in water for injections, pH ~5).

4.3.8 - Data acquisition

Stimulus presentation, behavioural control and drug administration was regulated by Remote Cortex 5.95 (Laboratory of Neuropsychology, National Institute for Mental Health, Bethesda, MD). Raw data were collected using Remote Cortex 5.95 (1-kHz sampling rate) and by Cheetah data acquisition (32.7-kHz sampling rate, 24 bit sampling resolution) interlinked with Remote Cortex 5.95. Data were replayed offline, band-pass

filtered (0.6-9 kHz) and spikes were sorted manually using SpikeSort3D (Neuralynx). Eye position and pupil diameter were recorded using a ViewPoint eyetracker (Arrington research) at 220 Hz. Pupil diameter was recorded in 40 out of 54 recording sessions.

4.3.9 - Pupillometry

Pupil diameter was low-pass filtered (10 Hz) using a second-order butterworth filter. Baseline activity was estimated as the average activity before stimulus onset (-300 to -50 ms), which was used to normalise the pupil diameter time course. Stimulus evoked constriction was baseline corrected (on a trial by trial basis) and averaged in a 250 ms time window centred on 500 ms after stimulus onset. Cue-evoked (250 ms window centred on 500 ms after cue onset) and pre-dimming (-300 to -50 ms) pupil diameter, was baseline subtracted with a pre-cue baseline (-300 to -50 ms). For visualisation, pupil diameter in each epoch was scaled to a range from zero to one, before averaging across trials.

4.3.10 - Analysis of cell type.

We distinguished between different cell types based on the duration of the extracellular spike waveform as described in Thiele et al. (2016). Specifically, we classified cells based on the peak-to-trough ratio, i.e. the duration between the peak and the trough of the interpolated (cubic spline) spike waveform (Figure 4-3a). To test whether the distribution of peak-to-trough distance of the spike waveforms was unimodal (null hypothesis) or bimodal, indicating that our distribution contained different cell types, a modified Hartigan's dip test was used (Ardid et al., 2015; Thiele et al., 2016). We used a cut-off of 250 µs to classify cells as narrow or broad spiking, as this was where our distribution revealed the main 'dip' (Figure 4-3). Note that during occasional recordings the iontophoresis unit introduced interference which, if spike waveforms were relatively small and multi rather than single-units were extracted, led to small oscillations on top of the spike waveforms.

4.3.11 - Fano factor

The variability of neural responses was quantified using Fano factors (FF), computed as the ratio between the variance (σ^2) and the mean (μ) spike counts within the time window of interest, defined as:

$$FF = \frac{\sigma^2}{\mu}$$

Equation 4-1

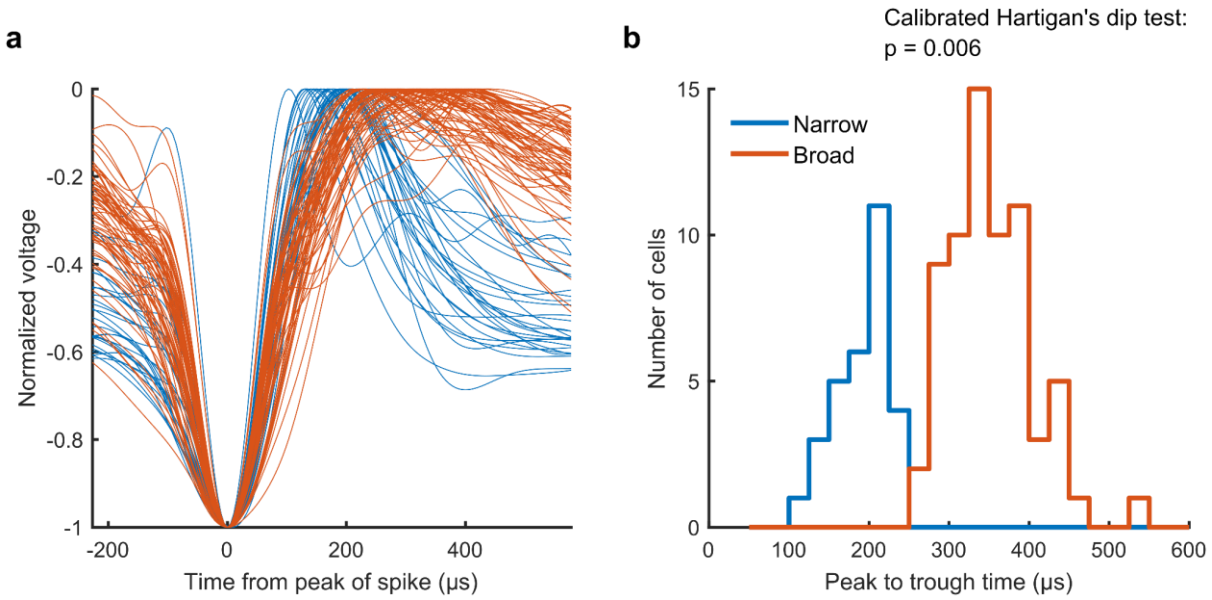

Figure 4-3. Distribution of broad and narrow-spiking cells. (**a**) Average spike waveforms for the population of cells. (**b**) Distribution of peak-to-trough ratios. Statistics: calibrated Hartigan's dip test (Ardid et al., 2015).

4.3.12 - Drug modulation

The strength of the effect of drug application on neural activity (firing rates) was determined via a drug modulation index ($drugMI$), defined as:

$$drugMI = \frac{drug_{on} - drug_{off}}{drug_{on} + drug_{off}}$$

Equation 4-2

with $drug_{on}$ as the neural activity when drug was applied, and $drug_{off}$ the activity when the drug was not applied. This index ranges from -1 to 1, with zero indicating no modulation due to drug application and with positive (negative) values indicating higher (lower) activity when the drug was applied.

4.3.13 - Quantification of attentional rate modulation.

To quantify the difference between neural responses when attention was directed towards the RF versus away from the RF, we computed the area under the receiver operating characteristic (AUROC) curve (Figure 4-4). Stemming from signal detection theory (Green and Swets, 1966), this measure represents the difference between two distributions as a single scalar value, taking into account both the average difference in magnitude as well as the variability of each distribution. This value indicates how well an ideal observer would be able to distinguish between two distributions, for example the neural response when attention is directed towards versus away from its RF. It is computed by iteratively increasing the threshold and computing the proportion (from the first sample to the threshold) of hits and false alarms (FA), i.e. the correct and false classification as samples belonging to one of the activity distributions (Figure 4-4a). The ROC curve is generated by plotting the proportions of hits against the proportion of FAs,

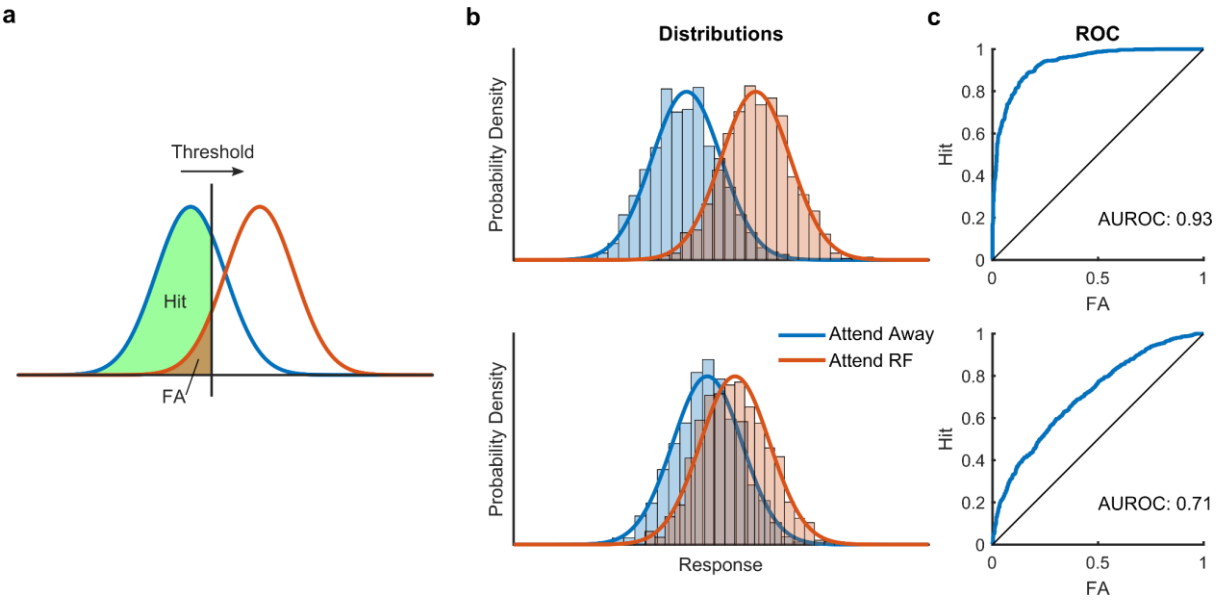

Figure 4-4. Graphic representation of receiver operating characteristic (ROC) computation. (**a**) Schematic illustrating the classification of samples belonging to the blue (hit) and red (false alarm, FA) distribution. The proportion of hits and FAs is computed for each iterative updating of the threshold. (**b-c**) Two sets of distributions, probability density functions (**b**) and their accompanying ROC curves (**c**) for which the blue and red distribution are relatively easy (top) or hard (easy) to classify. An AUROC value of 0.5 indicates that the two distributions are indistinguishable, in which case the ROC curve would fall along the unity line.

and AUROC is taken as the area under the ROC curve (Figure 4-4c). An AUROC of 0.5 indicates that the two distributions were indistinguishable, whereas an AUROC of 0 or 1 indicates that the two distributions were perfectly separable.

4.3.14 - Statistical testing and data selection

To determine whether DA significantly affected neural activity across the population of single and multi-units, we used paired-sample Wilcoxon signed rank tests. For comparisons within one recording, e.g. spike rates across trials for different conditions, we used analysis of variance (ANOVA) with three factors: attention (towards or away from the RF), drug (on or off) and stimulus direction. To test whether drug application affected behavioural performance, we used sequential linear mixed effects models with attention and drug as fixed effects and with the recording number as a random effect, to account for the repeated measurements in the data.

To test for significant linear or quadratic trends in the drug dose-response curve, we used sequential linear mixed effects models and likelihood ratio tests. Specifically, we tested whether a first-order (linear) polynomial fit was better than a constant (intercept-only) fit and subsequently whether a second-order (non-monotonic) polynomial fit was better than a linear fit. The modulation due to drug application of the neural response y was modelled as a linear combination of polynomial basis functions of the iontophoretic ejection current (X):

$$y \sim \beta_0 + \beta_1 X + \beta_2 X^2$$

, with β as the polynomial coefficients. When a significant quadratic relationship was found, we used the two-lines approach to determine whether this relationship was significantly U-shaped (Simonsohn, 2017). Error bars in all figures indicate the standard error of the mean (SEM), unless stated otherwise.

We selected which cells to include in each of the analyses based on the output of the 3-factor ANOVA described above. For example, if we wanted to investigate whether drug application affected attentional modulation of firing rates, we only included cells that revealed a main or interaction effect for both attention and drug application.

4.4 - **Results**

We recorded activity from 97 (73 from monkey 1, 24 from monkey 2) single (SU, n=46) and multi-units (MU, n=51) from intraparietal sulcus (IPS) in two awake, behaving Macaque monkeys performing a selective attention task (Figure 3-1). Of these cells, 95 (97.9%) showed a visual response to stimulus onset, and 81 (83.5%) were modulated by attention (Figure 4-5). During recording, we used an electrode-pipette combination (Figure 4-2) to iontophoretically administer dopaminergic (DA) drugs in the near vicinity of the recorded cells (Thiele et al., 2006). Across the two monkeys, we recorded from 59 units whilst administering the unselective agonist dopamine, from 29 units during which we administered the selective D1R antagonist SCH23390 and 9 units with the D1R agonist SKF81297. In line with previous studies (Jacob et al., 2016, 2013), firing rates in 36 (61%), 14 (48.3%), and 5 (55.6%) units were modulated by application of the unselective agonist dopamine, SCH23390 and SKF81297, respectively (Figure 4-5). Of these cells, 4 (11.1%), 5 (35.7%) and 1 (20%) units revealed an interaction effect between drug application (dopamine, SCH23390 and SKF81297) and attention. Although only a

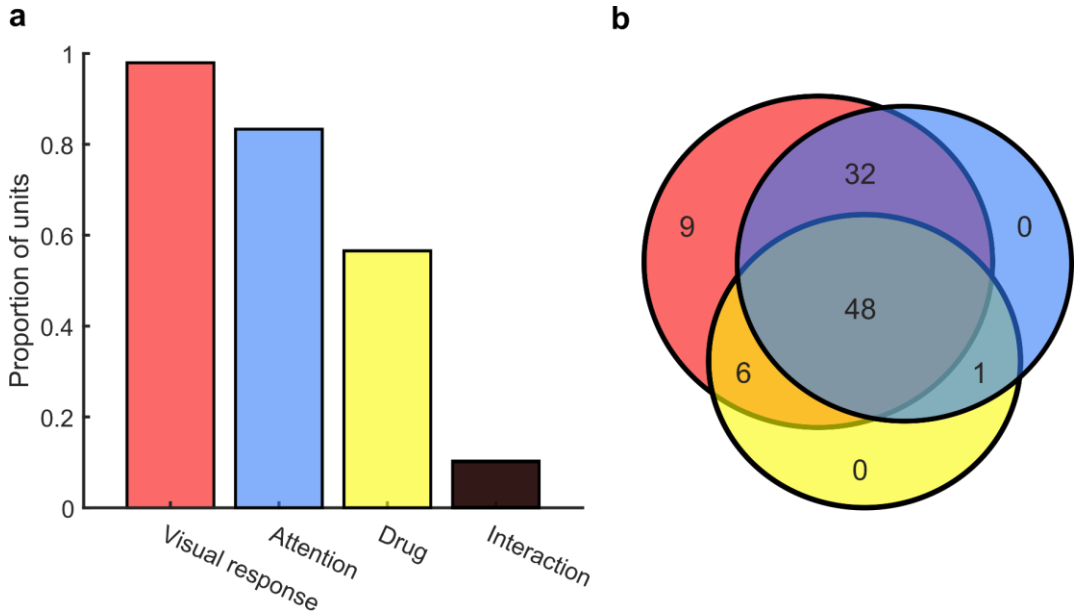

Figure 4-5. Selectivity of units. (**a**) Proportion of units that are visually responsive, that are modulated by attention, drug application, or that show an interaction between attention and drug application. (**b**) Venn diagram of unit selectivity. Note that 1 unit was not selective for any of the experimental factors.

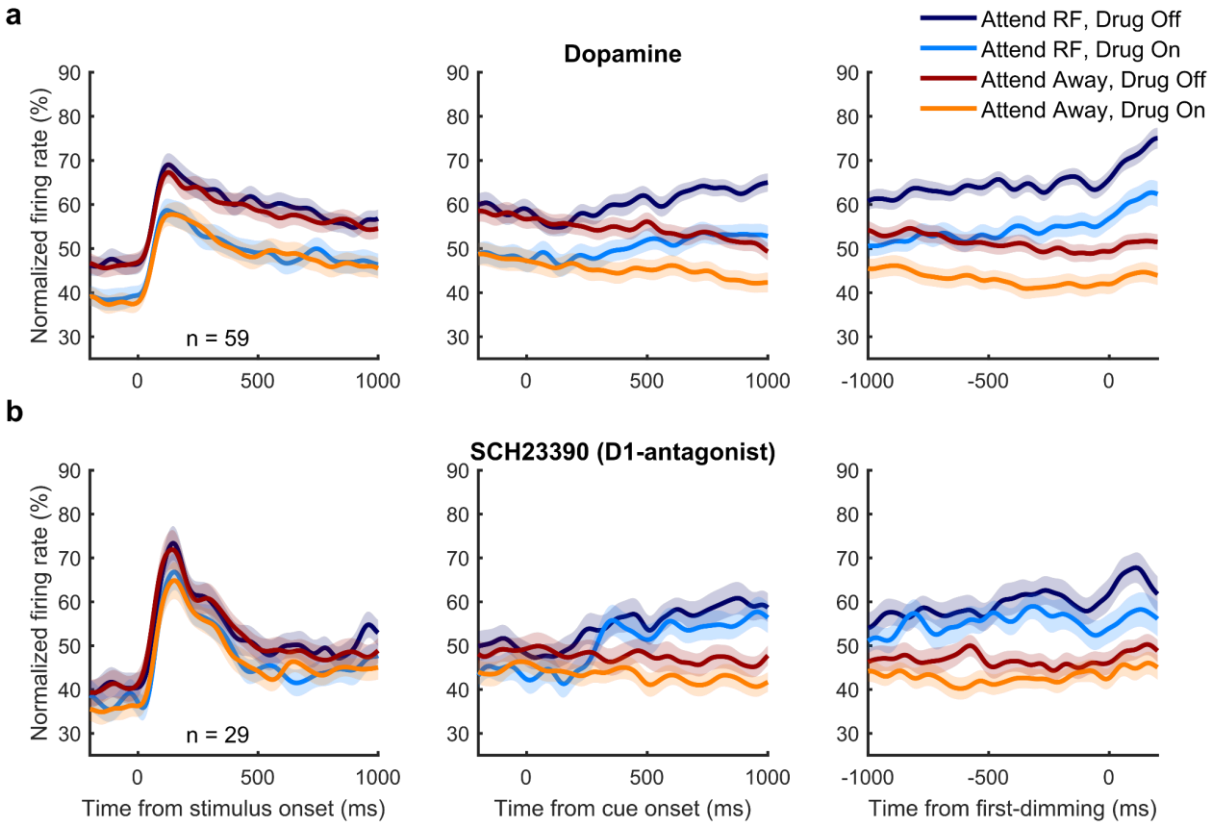

Figure 4-6. Population histograms for all cells recorded during dopaminergic drug application. Population activity aligned to stimulus onset (left), cue onset (middle) and the first dimming event (right), for the non-specific agonist dopamine (**a**) and the D1 antagonist SCH23390 (**b**). Error bars denote ±1 SEM.

small subset of units revealed an interaction effect, approximately half the units were modulated both by attention and drug application (Figure 4-5). Because of the low number of cells recorded during the application of SKF81297 (which were recorded from only one monkey), we focused our analyses on the recordings in which dopamine or SCH23390 was applied.

Figure 4-6 illustrates the population activity aligned to stimulus onset, cue onset and the first-dimming event, for both the no-drug and the drug conditions. For a given drug condition, neural activity between attention conditions did not differ when aligned to stimulus onset but started to diverge approximately 200 ms after cue onset, which indicated which of the three gratings was behaviourally relevant on that trial, and diverged further leading up to the first dimming event. Across the population, dopamine strongly reduced firing rates throughout the duration of the trial, including during baseline periods as well as stimulus and cue presentation (Figure 4-6a), whereas the effects of SCH23390 were of the same sign but weaker (Figure 4-6b). Although upon visual inspection, dopamine seemed to affect neural activity similarly when attention was directed towards or away from the RF of the neuron under study (compare the difference between the dark and light blue lines and the difference between the red and orange lines), a subset of neurons revealed an interaction between attention and drug application (Figure 4-5), as illustrated for an example neuron in Figure 4-7. Next, we specifically examined units for which the activity was modulated by attention and/or drug application, i.e. units that revealed a main effect or interaction effect for these

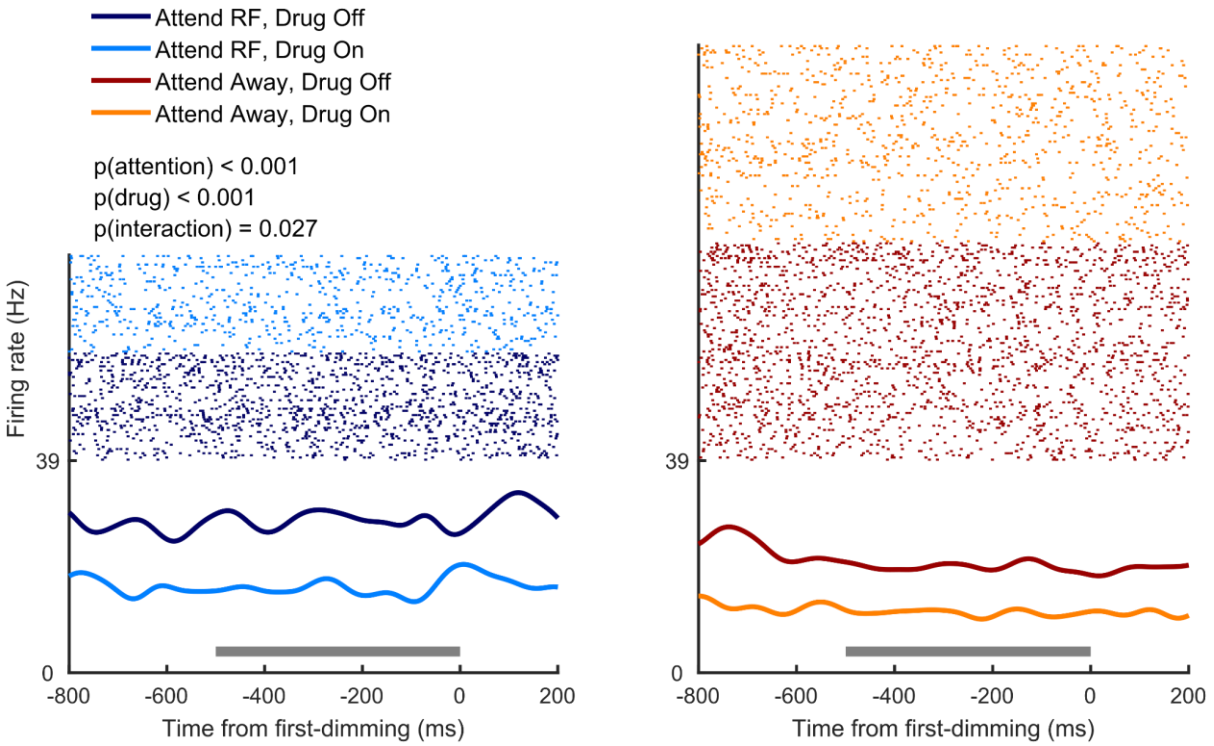

Figure 4-7. Activity from a representative cell recorded during application of the non-specific agonist dopamine. This cell's activity, aligned to the first dimming event, was significantly modulated by attention and drug application and showed a significant interaction between these factors. The grey bar indicates the time window used for statistical analyses. Statistics: two-factor ANOVA.

factors, and investigated whether activity modulation due to attention and drug application mapped onto different cell types.

Cells were classified as narrow or broad-spiking cells according to the median duration of the peak-to-trough time of the spike waveforms (Figure 4-3). These cell types have previously been found to respond differently to dopaminergic drug application (Jacob et al., 2016, 2013). Although narrow and broad-spiking cells have been argued to constitute inhibitory interneurons and excitatory pyramidal cells, respectively (Mitchell et al., 2007), a more recent study found that output cells in primary motor cortex (unequivocal pyramidal cells) had a narrow action potential waveform (Vigneswaran et al., 2011), and most pyramidal cell in macaque PFC express the Kv3.1b potassium channel, associated with the generation of narrow spikes (Soares et al., 2017). Therefore, the narrow-broad categorization thus solely allows us to distinguish between cell-types, without mapping this classification specifically onto interneurons or pyramidal cells.

The application of DA reduced firing rates across the population for both broad and narrow spiking cells, and for both attend towards or away from RF conditions (Figure 4-8a). Fano factors were unaffected by dopamine application (Figure 4-8b). The application of SCH23390 elicited a small but significant reduction of the average firing rates of broad-spiking cells during both attention conditions (Figure 4-8c) without affecting FFs (Figure 4-8d). Dopaminergic drug application thus mainly inhibited cellular activity, without affecting the variability.

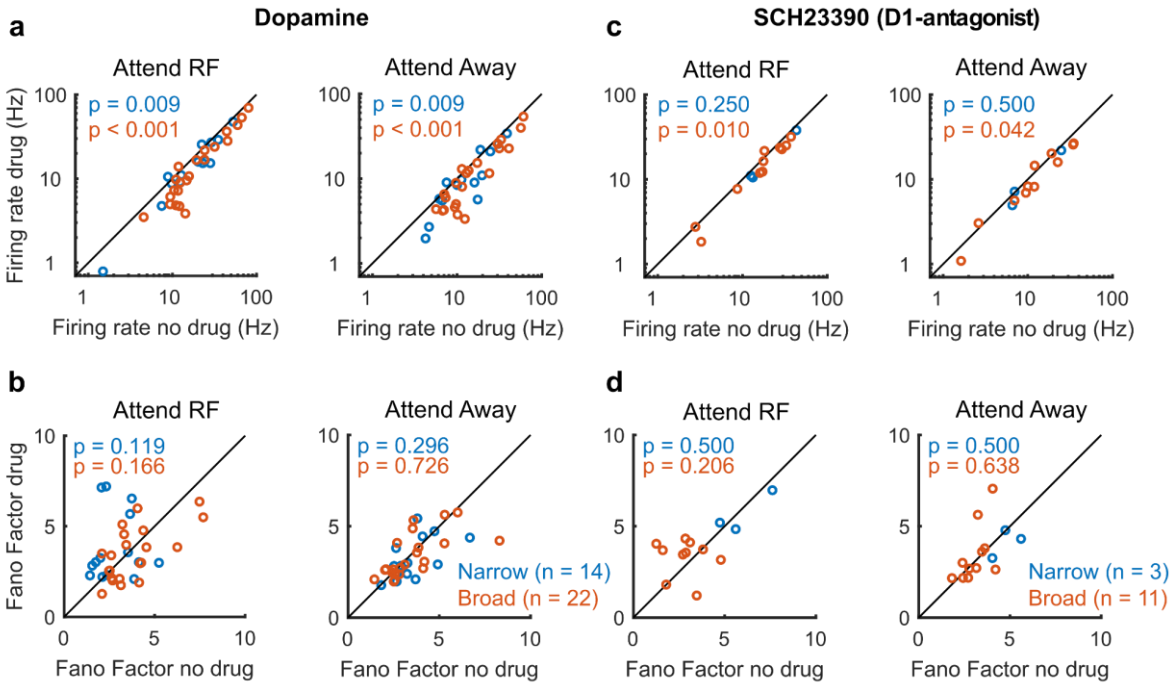

Figure 4-8. Dopaminergic modulation of population firing rates and Fano factors during the 500 ms before first-dimming. (**a**) Average firing rates between no drug and drug conditions for the non-specific agonist dopamine for attend RF (left) and attend away (right) conditions. (**b**) Fano factors between no drug and drug conditions for the non-specific agonist dopamine. (**c-d**) Same conventions as (**a-b**) but for the D1 antagonist SCH23390. Only cells that revealed a main or interaction effect for the factor drug were included in this analysis. Statistics: Wilcoxon signed rank tests.

To investigate whether dopamine affected attention-specific activity, we tested whether attention AUROC values were modulated by drug application. Attention AUROC values indicate how well an ideal observer can distinguish between neural activity during attend RF or attend away trials (Figure 4-4). A value of 0.5 indicates that the distributions are indistinguishable, whereas values of 0 or 1 indicate perfectly distinguishable distributions. The application of the non-specific agonist dopamine reduced AUROC values only for broad-spiking cells, whereas narrow-spiking cells were unaffected (Figure 4-9a). SCH23390 application did not modulate AUROC values for either cell type (Figure 4-9b). Dopamine thus had a cell-type specific effect on attentional rate modulation.

As drug application strongly inhibited firing rates across the population (Figure 4-8), and we found cell-type specific effects on attention-specific activity (Figure 4-9), we next investigated whether drug application affected behavioural performance (Figure 4-10). To this end, we used sequential multilevel model analyses to test for fixed effects of attention and drug application, as well as their interaction, on RT. Neither attention (Dopamine: β = -13.49±8.88, p = 0.132; SCH23390: β = 2.86±11.34, p = 0.802), nor drug application (Dopamine: β = -3.47±8.88, p = 0.697; SCH23390: β = 10.38±11.34, p = 0.363) nor their interaction (Dopamine: β = 2.87±5.62, p = 0.611; SCH23390: β = -4.33±7.17, p = 0.548) were predictive of RT for either drug. Given the focal nature of micro-iontophoretic drug application (Herz et al., 1969), the absence of an effect of drug application on behavioural performance is not surprising and in-line with comparable work on DA in PFC (Jacob et al., 2016, 2013; Vijayraghavan et al., 2007).

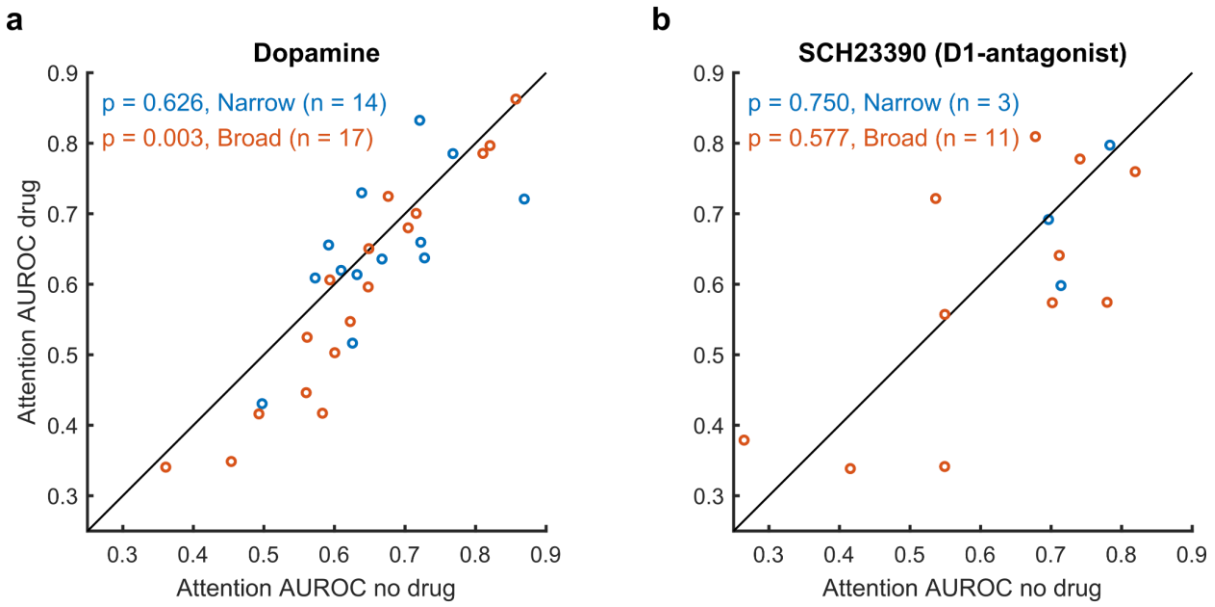

Figure 4-9. Dopaminergic modulation of attention AUROC values. Area under the receiver operating characteristic (AUROC) curve between no drug and drug conditions for the non-specific agonist dopamine (**a**) and the D1 antagonist SCH23390 (**b**). Only cells that revealed a main or interaction effect for the factors drug and attention were included in this analysis. Statistics: Wilcoxon signed rank tests.

Because of the exploratory nature of this study, we applied dopaminergic drugs with a variety of iontophoretic ejection currents (20-90 nA). Since dopamine has previously been shown to modulate neural activity according to an inverted U-shaped dose-response curve (Vijayraghavan et al., 2007), with maximal modulation at intermediate dopamine levels, we tested whether the ejection current was predictive of the firing rate modulation associated with drug application, estimated by a drug modulation index (drugMI). Specifically, we used sequential linear mixed effects model analyses and likelihood ratio tests to test for linear and quadratic trends. U-shaped trends were verified using the two-lines approach (Materials & Methods). Figure 4-11 illustrates the dopaminergic dose-response curves. The non-specific agonist dopamine displayed a non-monotonic relationship with drugMI ($\chi^2_{(1)} = 7.18$, $p = 0.007$) and revealed an inverted U-shaped curve ($p < 0.05$) in which intermediate ejection currents elicited the most negative drugMI, i.e. the largest inhibition of activity (Figure 4-11a). For SCH23390, on the other hand, we found a monotonic dose-response relationship ($\chi^2_{(1)} = 4.21$, $p = 0.040$), with more inhibition of firing rates with higher drug ejection currents (Figure 4-11b). To investigate whether drug dosage was also predictive of attentional rate modulation, we performed the same analysis on the difference score (drug – no drug) of attention AUROC values. Neither dopamine ($\chi^2_{(1)} = 0.95$, $p = 0.330$), nor SCH23390 ($\chi^2_{(1)} = 0.33$, $p = 0.568$) dosage were predictive of attention AUROC (Figure 4-11c-d). Because the effect of D1R stimulation can depend on the spatial tuning of the neuron (Vijayraghavan et al., 2007), we also tested whether drugMI was predictive of the drug induced modulation of attention AUROC values. DrugMI was neither predictive of attention AUROC for dopamine ($\chi^2_{(1)} = 0.27$, $p = 0.604$) nor SCH23390 ($\chi^2_{(1)} = 0.01$, $p = 0.929$) (Figure 4-11e-f). Comparable results were obtained when these analyses were limited to only broad spiking cells, or cells that showed both an attention and drug effect.

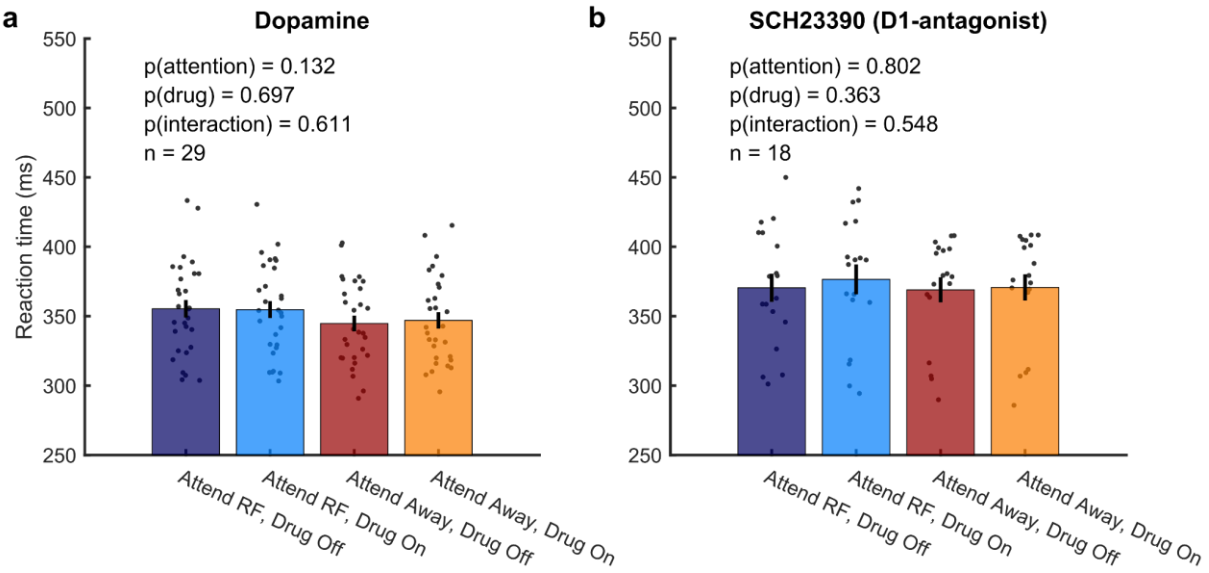

Figure 4-10. Behavioural performance is unaffected by iontophoretic application of dopaminergic drugs. Average RT on attend RF and attend away trials for the non-specific agonist dopamine (**a**) and the D1 antagonist SCH23390 (**b**). Dots represent average RT during a single recording session. Statistics: linear mixed-effects model analysis. Error bars denote ±1 SEM.

Interestingly, we additionally found that the application of both DA and SCH23390 influenced pupil diameter. We conducted a sliding-window Wilcoxon signed rank analysis for each 200 ms window, in 10 ms increments, comparing baseline normalised pupil diameter on drug compared to no-drug trials (Figure 4-12a). This analysis revealed a significant difference in pupil diameter that started after stimulus onset, and lasted until after cue onset. Specifically, we found a small, but significant, modulation of the pupillary light reflex (Figure 4-12). The magnitude of the constriction of the pupil upon stimulus onset was reduced during dopaminergic drug application compared to control trials, but neither drug influenced pupil diameter during any other time window (Figure 4-12b-e). Another sliding window analysis using a two factor (drug by attention) repeated measures ANOVA revealed no effect of attention (main or interaction) on pupil diameter (data not shown). Thus, locally applied dopaminergic drugs in parietal cortex modulated the pupillary light reflex.

4.5 - **Discussion**

We recorded from single and multi-units in intraparietal sulcus from two monkeys performing a selective attention task whilst iontophoretically applying dopaminergic drugs in the near vicinity of the recorded cells. The non-specific agonist dopamine, inhibited activity across the population of recorded cells, throughout the duration of the trial. This modulation furthermore followed an inverted U-shaped dose-response. The application of the D1-receptor specific antagonist SCH23390 also decreased firing rates, but much less than dopamine and only for broad-spiking cells, for which the modulation followed a monotonic dose-response curve. In addition to affecting overall firing rates, dopamine also reduced top-down attention-related firing rate modulations (attention

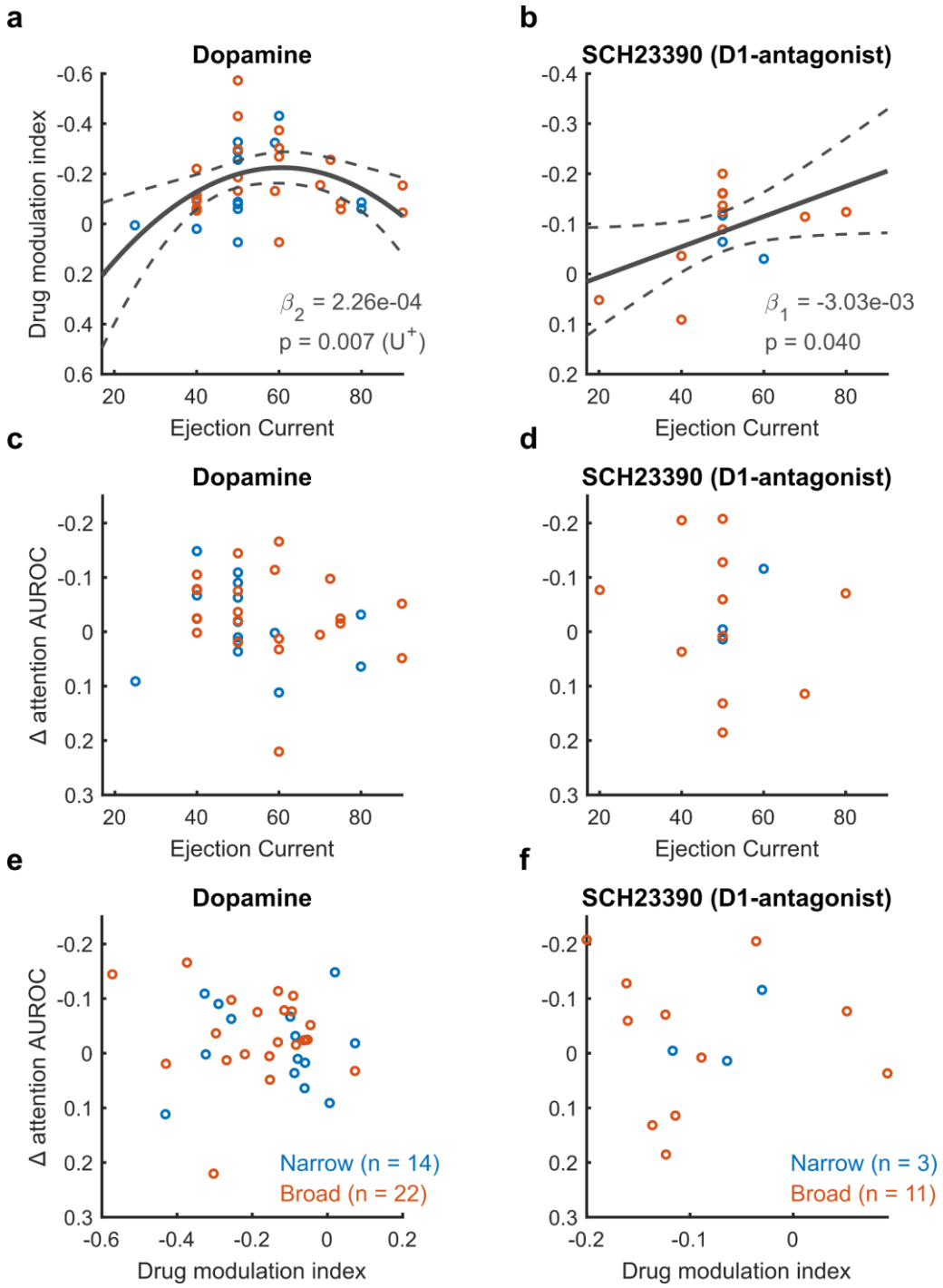

Figure 4-11. Dopaminergic dose-response curves in relation to attention AUROC. (**a-b**) Drug modulation index (before first-dimming, only for cells that were modulated by drug application) plotted against ejection current for the non-specific agonist dopamine (**a**) and the D1 antagonist SCH23390 (**b**). (**c-d**) Same conventions as (**a-b**) but for the difference score (drug – no drug) of attention AUROC values. (**e-f**) Attention AUROC values plotted against drug modulation index. Note the reversed y-axis in all panels. Solid and dotted lines represent significant model fits (applied to all cells simultaneously) and their 95% confidence intervals, respectively. A monotonic relationship is shown if a first-order fit was better than a constant fit, and a non-monotonic relationship is shown if a second-order fit was better than a linear fit. U^+ indicates a significant U-shaped relationship. Only cells that revealed a main or interaction effect for the factor drug were included in this analysis. Statistics: linear mixed-effects model analysis.

AUROC) in broad-spiking cells. Finally, local application of dopaminergic drugs in parietal cortex decreased the pupil light reflex to stimulus onset.

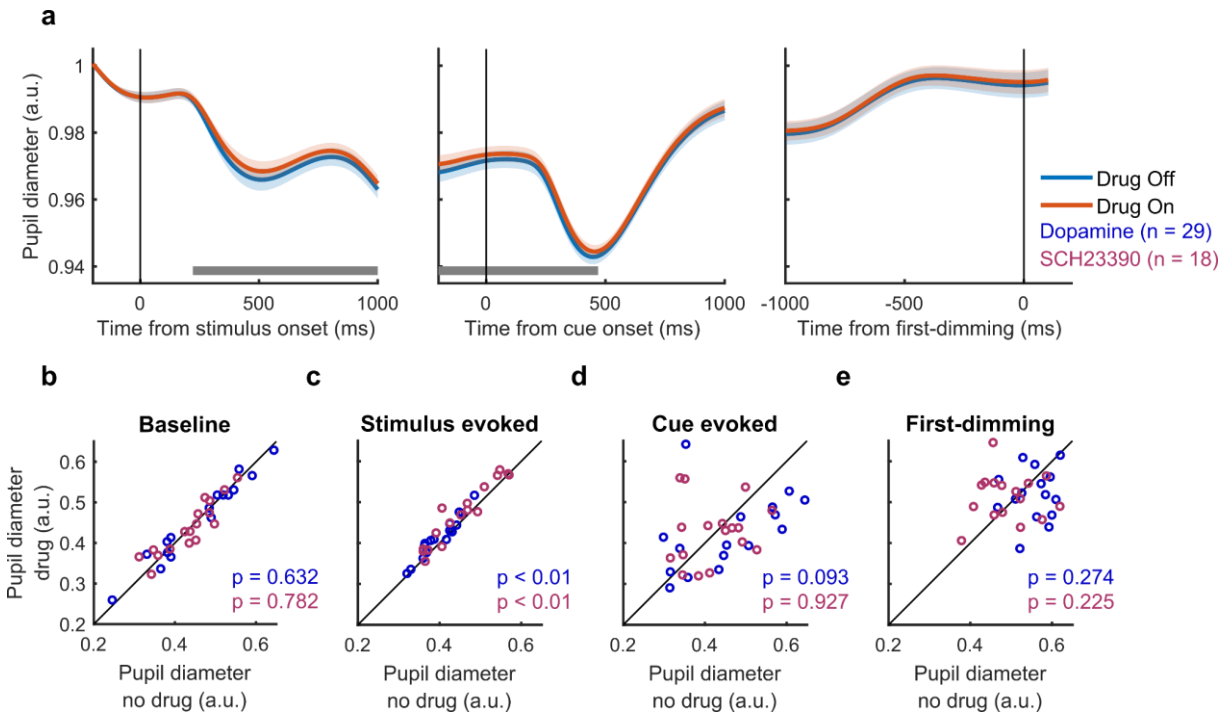

Figure 4-12. Modulation of pupil diameter by dopamine in Parietal cortex. (**a**) Baseline normalised pupil time course aligned to stimulus onset (left), cue onset (middle) and the first dimming event (right). The grey bar indicates the times where drug application brought about a significant difference in pupil diameter. (**b-e**) Average normalised pupil diameter during pre-stimulus baseline period (**b**), after stimulus onset (**c**), after cue onset (**d**), and before the first dimming event (**e**). Shaded regions denote ±1 SEM. Statistics: Wilcoxon signed rank test. FDR correction was applied for the analysis in panel **a**.

As the influence of dopamine on cognitive signals has largely been studied in the context of prefrontal cortex (Clark and Noudoost, 2014; Ott and Nieder, 2019), this is the first study to show that dopaminergic modulation plays an important role in 'tuning' top-down attention-related neuronal activity in parietal cortex.

4.5.1 - General and cell-type specific dopaminergic modulation in parietal cortex

We distinguished between cell classes based on the shape of the extracellularly recorded waveform. Specifically, we classified cells based on the median duration of the peak-to-trough time as narrow or broad-spiking cells, with a cutoff of 250 µs (Thiele et al., 2016). Even though, as discussed above, this classification does not reflect a one-to-one mapping onto inhibitory interneurons and excitatory pyramidal cells, this distinction does allow functional differentiation which may explain some of the results described in this study (Jacob et al., 2016, 2013).

Dopamine has a well-established role in modulating prefrontal signalling supporting cognitive functions such as working memory and attention (Noudoost and Moore, 2011b; Ott and Nieder, 2019; Thiele and Bellgrove, 2018; Vijayraghavan et al., 2007; Watanabe et al., 1997; Williams and Goldman-Rakic, 1995). Although D1R and D2R are expressed broadly throughout the cortex and fulfil complementary roles in the prefrontal cognitive control (Ott and Nieder, 2019), modulation of delay period activity during working

memory tasks has mostly been associated with stimulation or blockade of D1Rs (Sawaguchi et al., 1990; Sawaguchi and Goldman-Rakic, 1991, 1994; Williams and Goldman-Rakic, 1995), although D2Rs have also been implicated (Ott et al., 2014). Additionally, although manipulation of either receptor subtype in FEF can modulate behaviour by increasing saccadic choices towards the RF, only D1R blockade elicited activity that resembled the effects of attention in extrastriate visual areas (Noudoost and Moore, 2011a). Interestingly, D1-like receptors (D1 and D5) are expressed in higher proportions on excitatory pyramidal cells compared to inhibitory interneurons in FEF, and are expressed in particularly high numbers on neurons projecting towards extrastriate visual areas (Mueller et al., 2019, 2018).

Here, we found that both broad and narrow-spiking cells were inhibited by the application of dopamine, but only broad-spiking cells were significantly inhibited by SCH23390. Furthermore, dopamine modulated attention AUROC values only for broad-spiking cells. Although it is currently unknown whether the expression of D1 and D2-like receptors differs across pyramidal cells and interneurons in posterior parietal cortex, if it is similar to what has been found in FEF (Mueller et al., 2019, 2018), it could be that modulation of attentional signals in parietal cortex also relies on higher expression of D1-like, rather than D2-like, receptors in broad-spiking putative pyramidal cells.

It is remarkable that the majority of the recorded neurons were inhibited by dopamine and SCH23390 application, as previous studies (in prefrontal cortex) found mixed responses to unselective dopamine (Jacob et al., 2013) or D1R stimulation (Vijayraghavan et al., 2007; Williams and Goldman-Rakic, 1995). These effects could theoretically be due to our recording/iontophoresis setup. As both agonists and antagonists elicited responses of the same sign, unexpected effects unrelated to drug application could have been ruled out by control recordings using saline instead of (or in addition to) drugs, or compensating the ejection current from one pipette barrel by increasing the hold current in the other barrel. Similar control experiments from our lab have, however, never resulted in systematic (condition specific) effects on firing rates (Herrero et al., 2008). Further, the cell-type and attention specific effects, as well as the U-shaped dose-response curve argue against our results being an iontophoresis artefact.

Alternatively, these effects may be explained in part by the drug dosages, as increases in activity have been found for low dosages of D1-agonists and antagonists, and decreases with higher dosages (Vijayraghavan et al., 2007; Williams and Goldman-Rakic, 1995). Unfortunately, our sample size using lower dosages was rather small, but positive and less negative drugMI were found for lower ejection currents (Figure 4-11). However, Jacob et al. (2013) also used a variety of ejection currents (25-100 nA) and the proportion of cells that were inhibited or excited by dopamine application did not differ by dosage.

Another factor that could have influenced our low numbers of cells that are excited by dopaminergic drugs is the short duration of the blocks of trials used in our task. It has previously been reported that cells that were excited by dopamine application responded much slower to drug application compared to cells that were inhibited by dopamine (Jacob et al., 2013). This up-ramping modulation had an estimated average

time constant of 221.9 s. In our task, drug application was performed in blocks of 36 trials. With a median trial duration, including inter-trial interval, of approximately 8 s, a block of trials lasted approximately 288 s (depending on the number trials completed correctly). Therefore, it could be that neurons excited by dopamine only started to show modulation towards the end of the block, and therefore did not display significant modulation by drug application. This would result in a neural population of cells that are largely inhibited by dopamine. Alternatively, it could be that dopamine has mostly inhibitory effects in Macaque parietal cortex. Vijayraghavan et al. (2007) found that low doses (10-20 nA) of D1-agonists reduced firing rates, but increased spatial specificity of prefrontal neurons during a spatial working memory task mainly by reducing activity to non-preferred directions, and that high dosages (20-100 nA) further reduced activity, abolishing spatially selective information for single-units.

In sum, dopaminergic effects on (task-related) activity are complex (Seamans and Yang, 2004) and depend on various factors that have not been controlled for in this study, such as endogenous levels of dopamine. Within prefrontal cortex, coding can be enhanced by D1R agonists, and diminished by antagonists (Ott et al., 2014; Vijayraghavan et al., 2007), or vice-versa (Noudoost and Moore, 2011a; Williams and Goldman-Rakic, 1995). Indeed, dopaminergic effects show regional variability across different brain areas, even within PFC (Arnsten et al., 2012). Thus, the mechanisms discussed above might not apply to PPC. Future studies are needed to further elucidate the cell-type and receptor-subtype specific effects of dopamine in parietal cortex during task performance.

4.5.2 - Dopaminergic dose-response curve

Dopamine receptor stimulation has repeatedly been found to follow an inverted-U dose-response curve whereby too little or too much receptor stimulation leads to suboptimal behavioural performance (Arnsten et al., 1994; Zahrt et al., 1997) or neural coding (Vijayraghavan et al., 2007) during cognitive tasks. Indeed, low levels of D1R blockade (Williams and Goldman-Rakic, 1995), or stimulation (Vijayraghavan et al., 2007) can increase firing, whereas higher levels of either blockade or stimulation decreased cell firing in prefrontal cortex (Vijayraghavan et al., 2007; Williams and Goldman-Rakic, 1995). On a behavioural level, infusion of D1R-agonists in frontal cortex of rats (Zahrt et al., 1997) as well as monkeys (Arnsten et al., 1994; Cai and Arnsten, 1997) decreased performance on a spatial working memory task in a dose dependent manner, which was reversible by pre-treatment of D1R antagonists. In the latter studies the effect of the drug depended on the age of the monkey, presumably because of different levels of endogenous dopamine availability. In addition to the effects of D1R stimulation, D2R stimulation also reveals age and dose-dependent effects on working memory performance (Arnsten et al., 1995). The effects of dopaminergic drugs thus depend on endogenous levels of dopamine, as well as baseline levels of arousal, stress, and availability of other neuromodulators such as noradrenaline (Arnsten et al., 2012). In addition, the effects of dopamine on neural coding depends on the initial spatial tuning specificity; stronger increases in tuning were found for neurons with a wider tuning

profile, i.e. neurons that showed less spatially specific activity (Vijayraghavan et al., 2007). Whereas optimal levels of dopamine receptor stimulation can stabilize and tune neural activity, suboptimal levels decrease both neural coding and behavioural performance.

Here, we found an inverted-U shaped dose-response curve for the unselective agonist dopamine, and a monotonic function for the D1R antagonist SCH23390. Rather than predicting neural coding, however, ejection currents were merely predictive of drug modulation indices (Figure 4-11a), without any relationship to attention AUROC values (Figure 4-11b-c). For dopamine, maximal inhibition of firing rates was found at intermediate dosages, whereas inhibition was higher for higher dosages of SCH23390, although our sample size, especially for SCH23390, might have been too small to reliably determine the shape of the dose-response curve. Additionally, the observed effects for dopaminergic stimulation are likely partly driven by other receptor subtypes (e.g. D2R) that are not usually associated with modulation of delay period activity. This study therefore provides the initial early evidence of the effects of dopamine in parietal cortex during cognitive tasks, which requires further research to elucidate the underlying mechanism.

4.5.3 - Dopaminergic modulation of the pupil light reflex

The pupil light reflex (PLR) transiently constricts the pupil after exposure to increases in illumination or presentation of bright stimuli (Loewenfeld, 1993; McDougal and Gamlin, 2014). Although the PLR is found in most vertebrates, and is considered an elementary mechanism controlling the amount of light that hits the retina (McDougal and Gamlin, 2014), recent studies have shown that this behavioural reflex can be modified by covert attention (Binda and Murray, 2015a, 2015b; Naber et al., 2013). Specifically, when attention is directed towards a light or dark stimulus, the PLR is enhanced or decreased compared to when attention is directed away (Binda and Murray, 2015a; Naber et al., 2013). Additionally, subthreshold electrical microstimulation of the FEF enhanced the PLR when a light stimulus was presented inside the saccade field of the stimulated region, whereas it reduced the PLR when the light stimulus was presented away from the saccade field (Ebitz and Moore, 2017). Together these studies show that the PLR depends both on the change in luminance and the location of spatial attention, modulated by FEF stimulation. Top-down modulation of sensory processing can thus start as early as the PLR, although whether this also influences behavioural performance is currently unknown (Binda and Murray, 2015b).

To our surprise, we found that dopaminergic drug application in parietal cortex reduced the PLR (Figure 4-12). As we also found a reduction in attentional rate modulation with drug administration, these results are in agreement with the electrophysiological results. Our task design, however, did not allow differentiation between the effect of drug application and stimulus location, as all three gratings were presented simultaneously. Two (non-exclusive) mechanisms have been proposed by which FEF stimulation can modulate the PLR (Binda and Gamlin, 2017). Either by direct or indirect projections to

the olivary pretectal nucleus, or via indirect projections to the constrictor neurons in the Edinger-Westphal nucleus, for which the indirect projections were hypothesised to go through extrastriate visual cortex and/or the superior colliculus (SC).

Subthreshold microstimulation of the intermediate (SCi), but not superficial (SCs), layers of the superior colliculus elicits a short latency pupillary dilation (Joshi et al., 2016; Wang et al., 2012). Whereas the SCs receives input from early visual areas, including the retina, the SCi receives input from higher order association cortices. Along with preparing and executing eye movements, the SCi is involved in directing covert attention (Ignashchenkova et al., 2004; Kustov and Lee Robinson, 1996; Lovejoy and Krauzlis, 2010; Muller et al., 2005), and provides an essential contribution to the selection of stimuli amongst competing distractors (McPeek and Keller, 2004, 2002; reviewed in Mysore and Knudsen, 2011). Moreover, the SC receives dense projections from parietal cortex (Becker, 1989; Kuypers and Lawrence, 1967), and has been hypothesised to play an important role in pupil diameter modulation (Wang and Munoz, 2015b).

It is currently unclear whether dopaminergic modulation of frontal (or parietal) cortex modulates SC activity, as has been found for extrastriate cortex (Noudoost and Moore, 2011a), but this pathway seems a strong candidate for the modulation of the PLR (Wang and Munoz, 2015b). In addition to a role for dopamine, impairments in cholinergic signalling have been associated with an impaired PLR (Artoni et al., 2019), showing that the PLR is likely modulated by multiple neuromodulatory systems.

4.6 - **Conclusion**

Dopamine is an important modulator of high-level cognitive functions such as attention and working memory, both in the healthy and ageing brain as well as for a variety of clinical disorders (Arnsten et al., 2012; Robbins and Arnsten, 2009; Thiele and Bellgrove, 2018). Although the workings of dopamine within PFC are starting to be elucidated, the effects of dopamine in other brain areas such as parietal cortex, despite their well-established role in cognition and cognitive dysfunction, has largely been overlooked. This study is the first to show dopaminergic modulation of parietal activity in general, and activity specific to spatial attention in the non-human primate. Although valuable mechanistic insights have been gained from studies focused on neuromodulation of the prefrontal cortex, our work here encourages comparable studies in posterior areas, such as the parietal cortex, and across broader networks for cognition.

4.7 - **Acknowledgements**

We thank Michael Savage for providing the pictures of the micropipettes used for Figure 4-2.

Chapter 5 - General discussion

In this thesis I have shed light on the neural mechanisms by which cortical state fluctuations, neuromodulatory influences and selective attention modulate neural activity and behaviour. In the first chapter I revealed that global state fluctuations, assessed through pupillometry, influence perceptual decision making at various information processing stages. These fluctuations were moreover strongly predictive of task performance, underscoring the relevance of these global dynamics for behaviour. In the second chapter I investigated the effects of cortical state fluctuations on population activity within and across visual areas. Here, brain-wide cortical state fluctuations, as well as those localised to smaller networks, interacted with the more nuanced effects of attention on neural activity and behaviour. Finally, in chapter three, I showed through causal intervention that dopaminergic innervation in parietal cortex modulates attentional signals. Together, these results reveal the effects of cortical state fluctuations and attention across different neural scales, from global brain-wide activity fluctuations, to smaller scale network operations, to their effects on single cell activity. In this section, I will relate these findings to our current knowledge of neural and cognitive functioning and discuss areas for future research.

5.1 - Spatiotemporal scales of neuromodulation

Each modulatory system discussed in this thesis has both tonic and phasic firing modes that can affect neural activity and behaviour across different timescales (Aston-Jones and Cohen, 2005a; P Dayan and Yu, 2006; Parikh et al., 2007; Parikh and Sarter, 2008; Sarter et al., 2016, 2009). Comparatively slow changes in tonic firing support modulation of neural activity across timescales from seconds to hours (Totah et al., 2019), in support of functions such as the sleep-wake cycle and fluctuations in wakefulness (Aston-Jones and Cohen, 2005a; Harris and Thiele, 2011). The faster phasic activation can support behavioural task performance within the same trial, on a sub-second basis (Aston-Jones and Cohen, 2005a; Bouret and Sara, 2005; Peter Dayan and Yu, 2006; Ott and Nieder, 2019; Parikh et al., 2007; Totah et al., 2019). These different firing patterns have very different effects on their target structures (Devilbiss and Waterhouse, 2011). Compared to tonic activity, phasic activation of neuromodulatory systems leads to a larger instantaneous increase in neuromodulator availability within or nearby the synaptic cleft than tonic activity (Berridge and Waterhouse, 2003; Florin-Lechner et al., 1996; Schultz, 2007). Phasic arousal could therefore affect target structures and behaviour more strongly and selectively than tonic arousal. Because neuromodulator availability increases transiently upon phasic activation, and these modulators can rapidly be removed from the synaptic cleft (Sarter et al., 2009; Schultz, 2007), target structures could also be less affected by the effects of adaptation for instance, and would thus not display sensitivity decreases to neuromodulators that might be expected during tonic stimulation. Phasic, versus tonic, activity could thus lead to a more local modulator

release that supports attentional processes rather than global brain states per se (Thiele and Bellgrove, 2018).

In addition to a variety of temporal scales, neuromodulators can also affect their target structures in spatially specific manners. Although neuronal populations in neuromodulatory centres were long thought to fire synchronously, thereby eliciting changes throughout the brain, recent research has revealed more specificity in the spatial extent of their effects (Aston-Jones and Waterhouse, 2016; Chandler et al., 2014, 2013; Totah et al., 2018). For example, segregation between locus coeruleus (LC) neurons projecting to various regions of the cortex suggest that subsets of LC neurons could, for example through differences in excitability, asynchronously release noradrenaline (NA) and thereby differentially innervate cortical sub-regions (Aston-Jones and Waterhouse, 2016; Chandler et al., 2014). A similar segregation has been found for other neuromodulatory centres, such as the ventral tegmental area (VTA) (Chandler et al., 2013). Likewise, basal forebrain (BF) neurons have much more precise input and output projections than previously thought (Gielow and Zaborszky, 2017; Zaborszky et al., 2015). Furthermore, recent multi-electrode recordings revealed ensemble organisation in the LC, indicating that subsets of LC neurons, rather than large populations, fire synchronously (Totah et al., 2018). Thus, rather than the joint activity of entire neuromodulatory nuclei affecting global, brain-wide activity fluctuations, neuromodulators can likely exert their effects within relatively localised brain regions with specific functional roles. Finally, another neural mechanism that could contribute to both the temporal and spatial specificity of their effects is local neuromodulator release, controlled by glutamatergic inputs, through activation of presynaptic neuromodulatory projections terminals (Parikh et al., 2008; Schultz, 2007; Thiele and Bellgrove, 2018). These actions could locally control cellular and cortical state dynamics without altering activity of the neuromodulatory projection neurons themselves.

This spatial specificity of neuromodulatory projections, or the local stimulation of presynaptic terminals, described above, could bring about local excitability changes that allows segregation within and across brain areas in support of specific cognitive functions. Additionally, neuromodulators can functionally align activity through simultaneous modulation of neural populations along sensory pathways (Devilbiss et al., 2006; Devilbiss and Waterhouse, 2011; Noudoost and Moore, 2011a). For example, LC stimulation can modulate both the correlated activity within thalamus and cortex as well as between these areas (Devilbiss and Waterhouse, 2011). Together, these local and across-area effects could allow functionally specific activity to be processed within a brain area and effectively communicated across related brain areas. Selective attention, however, operates with very fine spatial resolution, between objects within a neuron's receptive field (Bosman et al., 2012; Luck et al., 1997), or even within a fraction of a visual degree within the foveola (Poletti et al., 2017). Although it is currently unknown whether neuromodulatory drive is precise enough to subserve these attentional mechanisms that operate on such a small scale, their modulatory influence likely has a finer resolution than has been assumed up to now.

In this thesis I found that, across spatial scales, both tonic changes in neuromodulatory drive (chapter 2, 3 and 4) as well as variability in the amplitude of phasic activity (chapter 2) can influence neural activity and behaviour. In addition to the modulatory effects on these timescales, we found modulation of the faster across-laminar activity fluctuations that occurred on timescales of the order of tens of milliseconds (chapter 3). Although we do not know whether these fluctuations were directly caused by neuromodulator release, neuromodulators likely affect the local network state, thereby affecting the durations and depths of these fluctuations. More insight into the mechanisms that drive neural variability during attention might be gained from modelling studies. For example, Rabinowitz and colleagues (2015) modelled the shared modulatory influence on population activity recorded from two arrays implanted bilaterally in left and right V4. It was shown that the trial-to-trial activity fluctuations during attention could largely be captured by a single model parameter per hemisphere. In this study, however, the fastest temporal scale considered was the activity fluctuation across trials. Additionally, although modulatory influences were considered to affect individual neurons differently, the two stimuli were presented in different hemifields, effectively limiting the spatial resolution of attentional effects to a single hemisphere. As a single model parameter captured much of this variability, it seems plausible that a limited number of (additional) parameters could capture neural variability on the timescales that we observed On-Off dynamics. Thus, more extensive models that consider modulatory actions across multiple (faster) timescales, as well as various spatial scales, could shed light on the neural mechanisms underlying the differential effects of tonic, phasic, and faster neuromodulation on its target structures and how they support cognitive behaviour.

Alongside modelling efforts, an experimental investigation of the neuromodulatory influences on faster timescales could be conducted through local optogenetic stimulation of the neuromodulatory axon terminals in sensory areas (Minces et al., 2017; Pinto et al., 2013). The effects of these fast modulations resembled those of cortical state changes and attention (van Kempen et al., 2017), which seemed to be induced on a sub-second scale. These techniques, applied on even faster timescales and during cognitive tasks, could provide important new insights into the local modulatory role of neuromodulators during cognition. Crucial to this endeavour will be to analyse large scale population activity on a single-trial basis, such as those described in chapter 3, in order to capture the trial-to-trial variability in these modulatory effects. Likewise, it will be important to control for fluctuations in global gain and behavioural state of the animal, for example through simultaneous measurement of pupil diameter.

Furthermore, investigations into the neuromodulatory mediation of across-area information transfer will determine their importance for the network interactions on which cognitive functions rely. As discussed above, attention benefits the across-area transfer of spikes, as spike-spike co-variability increases and microstimulation of V1 elicits more spikes in MT when attention is directed towards the receptive field (RF) (Ruff and Cohen, 2016a), likely mediated by divisive normalisation (Ruff et al., 2016; Ruff and Cohen, 2017, 2016b). During which step or at which level of information transfer do

neuromodulators exert their effects? Do they mediate temporally synchronous firing in a source area such that information is sent more reliably (Jia et al., 2013; Zandvakili and Kohn, 2015)? Can they influence the mutual inhibition seen during biased competition (Desimone, 1998; Desimone and Duncan, 1995)? Do they mediate divisive normalisation (Schmitz and Duncan, 2018)? And/or do they set the state of the target area such that postsynaptic activity is maximally modulated by its input? The latter could be achieved in various ways, such as by changing membrane potential dynamics from a synchronised to a desynchronised state (Constantinople and Bruno, 2011; Metherate et al., 1992; Minces et al., 2017; Pinto et al., 2013; Polack et al., 2013), or by regulating the balance between excitation and inhibition (e.g. by differently affecting pyramidal cells and interneurons) and thereby making a region more or less receptive to correlated input (Salinas and Sejnowski, 2001b). Alternatively, they could alter both feedforward and feedback activity, thereby allowing enhanced bidirectional communication, as suggested by previous studies (Noudoost and Moore, 2011a). Laminar recordings in multiple visual areas wherein either area is targeted by neuromodulators and/or microstimulation, or imaging widespread neuromodulator availability (Bonis-O'Donnell et al., 2017; Kruss et al., 2014; Reimer et al., 2016) combined with localised electrophysiology, ideally in task-performing animals, could shed light on these questions. Finally, speculatively following this line of reasoning even further, if indeed the spatiotemporal scale of neuromodulatory influence is smaller than assumed up to now, might neuromodulators even selectively modulate synaptic weights depending on task demands? If so, this could (de)couple neurons with (dis)similar tuning preferences by altering the correlation structure of the neural population, thereby supporting behaviour (Bondy et al., 2018; Nienborg et al., 2012). This could also allow the selective combination and weighting of neural activity that is sent to the next cortical area (Ruff and Cohen, 2017; Semedo et al., 2019).

In summary, given that it is likely that neuromodulators affect their target structures on much finer spatial and temporal scales than previously assumed, their effects could support more detailed (cognitive) functions that rely on activity modulations of smaller local neural populations, and inter-area communication of functionally related brain regions.

5.2 - Contribution of neuromodulators throughout the brain during cognition

The neuromodulators discussed in this thesis likely have varying but overlapping roles across different cognitive tasks. Many of these cognitive tasks are conceptually related to each other and to the degree they are different, they are likely intertwined and interdependent. During attention tasks the behaviourally relevant stimuli are distributed in (feature/object) space, whereas during working-memory tasks relevant stimuli and the corresponding response are distributed in time (Desimone, 1998). Decision making, in turn, relies on both the spatial and temporal distribution of stimulus-response associations, and additionally depends on successful accumulation of

stimulus information that is evaluated and translated into a (categorical) choice (Gold and Shadlen, 2007; Kelly and O'Connell, 2015; Smith and Ratcliff, 2004). During attention, working memory and perceptual decision making, the selection of a stimulus (or feature/object) has been argued to consist of attentional decisions that assign value to perceptual information, whereas motor decisions select the appropriate motor output given this information (Gottlieb and Balan, 2010). In this framework, attention encodes the selection of information through assigning weight (i.e. utility or value) to all alternatives. Selection is based on this utility, which allows focusing on stimuli or filtering distracting information. Here, attentional modulation of neural activity might thus reflect the decision between the relative utility of different sources of information. Top-down attention, in this definition, is much more dependent on (learned) stimulus-reward associations and might more directly address how higher-order neurons initiate attentional signals, how they determine where to direct attention before they elicit activity modulations upstream (Baluch and Itti, 2011; Gottlieb, 2012). Indeed, the effects of attention on neural activity are inherently difficult to dissociate from those of reward (expectation) (Maunsell, 2004).

Learning these associations, through reinforcement learning, is strongly associated with neuromodulatory systems, in particular DA and NA (Aston-Jones and Cohen, 2005a; Cohen et al., 2007; Mcclure et al., 2005; Montague et al., 2004). Stimulus-response associations are progressively strengthened by the DA-reward system (Montague et al., 2004), allowing exploitation of learned relationships (Cohen et al., 2007). This system, however, would prevent flexibly updating associations upon changing situations, when current stimulus-response associations need to be re-evaluated and the environment explored for alternatives. The NA system has been proposed to fulfil this role, thereby allowing flexible updating of learned associations in favour of exploring new situations (Aston-Jones and Cohen, 2005a; Cohen et al., 2007; Mcclure et al., 2005). Part of this exploitation-exploration trade-off is the coding of expected and unexpected uncertainty, proposed to be mediated by ACh (Yu and Dayan, 2005). During exploitation, reward variability that is within the expected range (coded by ACh) should not elicit a change in behaviour. Whereas variability that is larger than expected (unexpected uncertainty, coded by NA) should initiate an adjustment of the behavioural strategy (Cohen et al., 2007; Yu and Dayan, 2005). Neuromodulators, through signalling of prediction errors, are therefore thought to play a key role in predictive coding (Glimcher, 2011; Schultz, 2016, 2007).

In addition, neuromodulators have been implicated in a large variety of other functions spanning different spatiotemporal scales, such as long-term depression or potentiation (Bissière et al., 2003; Ge and Dani, 2005; Kirkwood et al., 1999; Pawlak and Kerr, 2008; Shen et al., 2008) and memory consolidation (Hasselmo, 1999; Packard and White, 1991). Further to these specific functions, they might also support flexible cognitive behaviour by determining the brain-wide balance between integrated and segregated information processing, thought to dynamically regulate network reconfiguration according to task demands (Shine, 2019). Central to all these functions is that neuromodulatory centres receive input from prefrontal areas thought to encode the value and cost of the options

presented (Jodo et al., 1998; Mesulam and Mufson, 1984; Nauta, 1971; Ongur, 2000; Sesack et al., 1989). These areas can thereby control (brain-wide) coding of utility, and regulate the trade-off between exploration and exploitation, reinforcement learning and selective attention amongst other cognitive functions. Because of the widespread effects of neuromodulators on cognitive functioning, their dysfunction has been associated with a large variety of cognitive disorders such as schizophrenia, attention deficit hyperactivity disorder (ADHD), Parkinson's disease, autism spectrum disorder and Alzheimer (Arnsten et al., 2012; Arnsten and Rubia, 2012; London, 2018; Mesulam, 1996; Nakamura et al., 2010; Nieoullon, 2002; Robbins and Arnsten, 2009; Rolls et al., 2008; Schultz, 2007; Winterer and Weinberger, 2004). Additionally, disruption of neuromodulatory functioning due to e.g. stress or aging can (temporarily) interfere with cognitive functioning (Arnsten, 2015; Arnsten et al., 2012).

The cognitive functions described above rely to varying degrees on the selection of the relevant sensory information, either through bottom-up salience or top-down selection, their evaluation (in the context of reward history) and selection and execution of the appropriate motor response. Neuromodulators have been implicated at every one of these stages of the information processing hierarchy and are thus central to cognitive functioning.

In the studies discussed in this thesis, attentional stimulus selection, i.e. the assignment of weight, utility or value (Gottlieb, 2012; Gottlieb and Balan, 2010), varied with global cortical state (chapter 2 and 3), On-Off dynamics (chapter 3) and dopamine levels in parietal cortex (chapter 4), and can thus vary with various modulatory sources and spatiotemporal scales at different levels in the cortical hierarchy. Additionally, neuromodulatory control of cortical state might have served the integration of disparate brain areas in support of task performance (chapters 2 and 3). The extent to which these functions are related and rely on similar underlying circuit mechanisms likely depends on similarities in both the time courses and spatial spread of their effects, but also on different neuromodulatory receptor subclass expression across laminae and cell types, as well as their sensitivity/affinity and response dynamics. More work is needed to elucidate their specific effects on neural activity and cognitive behaviour, but what is clear is that there is no one single role for each neuromodulator and interactions between them allow great behavioural flexibility.

Appendix A. Supplementary tables Chapter 2

Table A. 1: Results from model comparisons of the hierarchical regression analysis predicting variability in task performance due to phasic arousal. Boldface font indicates parameters that significantly improved the model fit compared to the addition of the neural signal associated with the previous neural processing stage. Red text indicates the parameters that were excluded from the final model during the forward/backward stepwise regression (main text). Final model fits revealed a marginal (conditional) r2 of 15.8% (92.6%) and 16.0% (45.9%) for RT and RTcv, respectively.

	RT				**RTcv**			
	Model comparison		Stepwise model selection		Model comparison		Stepwise model selection	
EEG component	χ^2	p	F	p	χ^2	p	F	p
Pre-target α Power	**10.30**	**< 0.001**	**9.41**	**0.002**	0.14	0.71		
N2c latency	0.14	0.70			2.07	0.15		
N2c amplitude	0.94	0.33			1.18	0.28		
N2i latency	2.39	0.12			0.04	0.84		
N2i amplitude	2.39	0.12			0.77	0.38		
CPP onset	**8.24**	**0.004**	0.06	0.80	0.87	0.35		
CPP build-up rate	**4.90**	**0.027**	1.86	0.17	0.32	0.57		
CPP amplitude	1.43	0.23			0.12	0.73		
CPP ITPC	**19.25**	**< 0.001**	**30.38**	**< 0.001**	**15.18**	**0.001**	**17.83**	**< 0.001**
LHB build-up rate	0.02	0.88			0.13	0.72		
LHB amplitude	0.64	0.42			0.19	0.66		

Table A. 2: Coefficients from the multilevel model analysis in which all EEG components were added simultaneously to predict variability in task performance due to variability in phasic arousal.

	RT				RTcv			
EEG component	β	se	t	p	β	se	t	p
Pre-target α Power	0.19	0.07	2.87	4.5E-03	-0.03	0.06	-0.42	0.68
N2c latency	7.5E-04	0.02	0.04	0.97	0.06	0.04	1.41	0.16
N2c amplitude	0.04	0.03	1.25	0.21	0.04	0.06	0.73	0.47
N2i latency	0.02	0.02	1.27	0.20	-0.01	0.03	-0.38	0.70
N2i amplitude	0.04	0.03	1.27	0.20	0.01	0.06	0.25	0.81
CPP onset	0.05	0.04	1.04	0.30	-0.09	0.08	-1.12	0.26
CPP build-up rate	-0.14	0.06	-2.25	0.03	1.0E-03	0.11	0.01	0.99
CPP amplitude	0.15	0.07	2.27	0.02	0.07	0.12	0.54	0.59
CPP ITPC	-0.18	0.04	-4.43	1.3E-05	-0.26	0.06	-4.13	5.4E-05
LHB build-up rate	-0.01	0.04	-0.29	0.77	-0.03	0.08	-0.33	0.74
LHB amplitude	0.05	0.06	0.86	0.39	0.03	0.09	0.27	0.78

Table A. 3: Results from model comparisons of the hierarchical regression analysis predicting variability in task performance due to tonic arousal. Boldface font indicates parameters that significantly improved the model fit compared to the addition of the neural signal associated with the previous neural processing stage. Red text indicates the parameters that were excluded from the final model during the forward/backward stepwise regression (main text). Final model fits revealed a marginal (conditional) r2 of 4.2% (94.4%) and 11.9% (44.5%) for RT and RTcv, respectively.

	RT				**RTcv**			
	Model comparison		Stepwise model selection		Model comparison		Stepwise model selection	
EEG component	χ^2	p	F	p	χ^2	p	F	p
Pre-target α Power	0.56	0.46			0.01	0.90		
N2c latency	0.83	0.36			0.06	0.80		
N2c amplitude	**6.18**	**0.013**	**6.38**	**0.012**	0.87	0.35		
N2i latency	0.10	0.75			0.01	0.93		
N2i amplitude	0.33	0.57			0.03	0.87		
CPP onset	**5.86**	**0.016**	0.01	0.92	2.50	0.11		
CPP build-up rate	**4.06**	**0.044**	2.02	0.16	0.47	0.49		
CPP amplitude	0.01	0.91			0.77	0.39		
CPP ITPC	**21.49**	**< 0.001**	**28.43**	**< 0.001**	**24.53**	**< 0.001**	**30.37**	**< 0.001**
LHB build-up rate	0.01	0.91			2.50	0.11		
LHB amplitude	0.07	0.80			0.27	0.60		

Table A. 4: Coefficients from the multilevel model analysis in which all EEG components were added simultaneously to predict variability in task performance due to variability in tonic arousal.

	RT				RTcv			
EEG component	β	se	t	p	β	se	t	p
Pre-target α Power	0.07	0.07	1.00	0.32	-0.06	0.08	-0.75	0.46
N2c latency	0.03	0.02	1.31	0.19	-0.01	0.04	-0.16	0.87
N2c amplitude	0.06	0.03	2.17	0.03	0.04	0.06	0.71	0.48
N2i latency	-2.2E-03	0.01	-0.16	0.87	0.00	0.03	0.14	0.89
N2i amplitude	0.02	0.03	0.46	0.65	-0.05	0.07	-0.64	0.52
CPP onset	0.01	0.04	0.22	0.83	-0.09	0.09	-0.97	0.33
CPP build-up rate	-0.12	0.06	-1.97	0.05	-0.04	0.13	-0.29	0.78
CPP amplitude	0.10	0.07	1.50	0.13	0.15	0.14	1.05	0.29
CPP ITPC	-0.19	0.04	-4.80	2.6E-06	-0.39	0.07	-5.40	1.71E-07
LHB build-up rate	-0.01	0.05	-0.18	0.86	-0.15	0.09	-1.63	0.10
LHB amplitude	0.01	0.05	0.26	0.79	0.05	0.09	0.53	0.60

Acknowledgements

I would like to thank everyone in the institute and the Thiele lab who I have worked with over the years, I had a lot of fun and learned a great deal! In particular I would like to thank my supervisor Alex for providing me with the opportunity to do my PhD in a friendly and open environment. Alex has given me a lot of freedom to pursue various interesting avenues, even if it was not directly beneficial to him or the lab, but he was available and has given me guidance whenever necessary. I also would like to specifically thank Alwin for being a great teacher and for being available whenever I ran into problems I had no idea how to solve. Similarly, I would like to thank everyone in the lab of Mark Bellgrove, my exchange was great fun and I hope to visit you many more times. Mark is a great supervisor that I had lots of fun with. He furthermore opened many doors for me, starting with the collaboration that led to my PhD position in Alex' lab.

Additionally, all the support staff at the Institute of Neuroscience deserve a special thanks, without you none of the research would be possible.

Also, last but not least, I thank my friends and family for their support. They have had to put up with me throughout almost 10 years of University education. I would like to especially thank my partner Catherine for remaining positive and trying to cheer me up during the last months leading up to the thesis deadline.

And thank you for reading my thesis!

References

Abbott LF, Dayan P. 1999. The effect of correlated variability on the accuracy of a population code. *Neural Comput*. doi:10.1162/089976699300016827

Albright TD. 1984. Direction and orientation selectivity of neurons in visual area MT of the macaque. *J Neurophysiol* **52**:1106–1130. doi:10.1152/jn.1984.52.6.1106

Amarasingham A, Harrison MT, Hatsopoulos NG, Geman S. 2012. Conditional modeling and the jitter method of spike resampling. *J Neurophysiol* **107**:517–531. doi:10.1152/jn.00633.2011

Andersen RA, Brotchie PR, Mazzoni P. 1992. Evidence for the lateral intraparietal area as the parietal eye field. *Curr Opin Neurobiol* **2**:840–846. doi:10.1016/0959-4388(92)90143-9

Ardid S, Vinck M, Kaping D, Marquez S, Everling S, Womelsdorf T. 2015. Mapping of functionally characterized cell classes onto canonical circuit operations in primate prefrontal cortex. *J Neurosci*. doi:10.1523/JNEUROSCI.2700-14.2015

Arieli A, Sterkin A, Grinvald A, Aertsen A. 1996. Dynamics of Ongoing Activity: Explanation of the Large Variability in Evoked Cortical Responses. *Science (80-)* **273**:1868–1871. doi:10.1126/science.273.5283.1868

Armstrong KM, Chang MH, Moore T. 2009. Selection and maintenance of spatial information by frontal eye field neurons. *J Neurosci* **29**:15621–9. doi:10.1523/JNEUROSCI.4465-09.2009

Arnsten A, Cai J, Goldman-Rakic P. 1988. The alpha-2 adrenergic agonist guanfacine improves memory in aged monkeys without sedative or hypotensive side effects: evidence for alpha-2 receptor subtypes. *J Neurosci* **8**:4287–4298. doi:10.1523/JNEUROSCI.08-11-04287.1988

Arnsten A, Cai J, Steere J, Goldman-Rakic P. 1995. Dopamine D2 receptor mechanisms contribute to age-related cognitive decline: the effects of quinpirole on memory and motor performance in monkeys. *J Neurosci*. doi:10.1523/jneurosci.15-05-03429.1995

Arnsten AFT. 2015. Stress weakens prefrontal networks: molecular insults to higher cognition. *Nat Neurosci* **18**:1376–1385. doi:10.1038/nn.4087

Arnsten AFT. 2011. Catecholamine influences on dorsolateral prefrontal cortical networks. *Biol Psychiatry*. doi:10.1016/j.biopsych.2011.01.027

Arnsten AFT. 1998. Catecholamine modulation of prefrontal cortical cognitive function. *Trends Cogn Sci* **2**:436–447. doi:10.1016/S1364-6613(98)01240-6

Arnsten AFT, Cai JX, Murphy BL, Goldman-Rakic PS. 1994. Dopamine D1 receptor mechanisms in the cognitive performance of young adult and aged monkeys. *Psychopharmacology (Berl)*. doi:10.1007/BF02245056

Arnsten AFT, Rubia K. 2012. Neurobiological Circuits Regulating Attention, Cognitive Control, Motivation, and Emotion: Disruptions in Neurodevelopmental Psychiatric Disorders. *J Am Acad Child Adolesc Psychiatry* **51**:356–367. doi:10.1016/j.jaac.2012.01.008

Arnsten AFT, Wang MJ, Paspalas CD. 2012. Neuromodulation of Thought: Flexibilities and Vulnerabilities in Prefrontal Cortical Network Synapses. *Neuron* **76**:223–239. doi:10.1016/j.neuron.2012.08.038

Artoni P, Piffer A, Vinci V, LeBlanc J, Nelson CA, Hensch TK, Fagiolini M. 2019. Deep learning of spontaneous arousal fluctuations detects early cholinergic defects across neurodevelopmental mouse models and patients. *Proc Natl Acad Sci* 201820847. doi:10.1073/pnas.1820847116

Aston-Jones G. 1985. Behavioral functions of locus coeruleus derived from cellular attributes. *Physiol Psychol* **13**:118–126. doi:10.3758/BF03326513

Aston-Jones G, Bloom F. 1981. Activity of norepinephrine-containing locus coeruleus neurons in behaving rats anticipates fluctuations in the sleep-waking cycle. *J Neurosci* **1**:876–886. doi:10.1523/JNEUROSCI.01-08-00876.1981

Aston-Jones G, Cohen JD. 2005a. An integrative theory of locus coeruleus-norepinephrine function: adaptive gain and optimal performance. *Annu Rev Neurosci* **28**:403–50. doi:10.1146/annurev.neuro.28.061604.135709

Aston-Jones G, Cohen JD. 2005b. Adaptive gain and the role of the locus coeruleus-norepinephrine system in optimal performanceJournal of Comparative Neurology. pp. 99–110. doi:10.1002/cne.20723

Aston-Jones G, Rajkowski J, Cohen J. 1999. Role of locus coeruleus in attention and behavioral flexibility. *Biol Psychiatry* **46**:1309–1320. doi:10.1016/S0006-3223(99)00140-7

Aston-Jones G, Rajkowski J, Kubiak P. 1997. Conditioned responses of monkey locus coeruleus neurons anticipate acquisition of discriminative behavior in a vigilance task. *Neuroscience* **80**:697–715. doi:10.1016/S0306-4522(97)00060-2

Aston-Jones G, Rajkowski J, Kubiak P, Alexinsky T. 1994. Locus coeruleus neurons in monkey are selectively activated by attended cues in a vigilance task. *J Neurosci* **14**:4467–4480. doi:10.1523/JNEUROSCI.14-07-04467.1994

Aston-Jones G, Waterhouse B. 2016. Locus coeruleus: From global projection system to adaptive regulation of behavior. *Brain Res* **1645**:75–78. doi:10.1016/j.brainres.2016.03.001

Averbeck BB, Latham PE, Pouget A. 2006. Neural correlations, population coding and computation. *Nat Rev Neurosci* **7**:358–366. doi:10.1038/nrn1888

Bach DR, Tzovara A, Vunder J. 2018. Blocking human fear memory with the matrix metalloproteinase inhibitor doxycycline. *Mol Psychiatry* **23**:1584–1589. doi:10.1038/mp.2017.65

Baluch F, Itti L. 2011. Mechanisms of top-down attention. *Trends Neurosci* **34**:210–224. doi:10.1016/j.tins.2011.02.003

Bashinski HS, Bacharach VR. 1980. Enhancement of perceptual sensitivity as the result of selectively attending to spatial locations. *Percept Psychophys* **28**:241–248. doi:10.3758/BF03204380

Bastos AM, Vezoli J, Bosman CA, Schoffelen J-M, Oostenveld R, Dowdall JR, De Weerd P, Kennedy H, Fries P. 2015. Visual Areas Exert Feedforward and Feedback Influences through Distinct Frequency Channels. *Neuron* **85**:390–401. doi:10.1016/j.neuron.2014.12.018

Bates D, Mächler M, Bolker B, Walker S. 2015. Fitting Linear Mixed-Effects Models Using lme4. *J Stat Softw* **67**. doi:10.18637/jss.v067.i01

Beaman CB, Eagleman SL, Dragoi V. 2017. Sensory coding accuracy and perceptual performance are improved during the desynchronized cortical state. *Nat Commun* **8**:1–14. doi:10.1038/s41467-017-01030-4

Beatty J. 1982a. Phasic Not Tonic Pupillary Responses Vary With Auditory Vigilance Performance. *Psychophysiology* **19**:167–172. doi:10.1111/j.1469-8986.1982.tb02540.x

Beatty J. 1982b. Task-evoked pupillary responses, processing load, and the structure of processing resources. *Psychol Bull* **91**:276–292. doi:10.1037/0033-2909.91.2.276

Becker W. 1989. The neurobiology of saccadic eye movements. Metrics. *Rev Oculomot Res* **3**:13–67. doi:044481017X

Bellgrove MA, Barry E, Johnson KA, Cox M, Dáibhis A, Daly M, Hawi Z, Lambert D, Fitzgerald M, McNicholas F, Robertson IH, Gill M, Kirley A. 2008. Spatial attentional bias as a marker of genetic risk, symptom severity, and stimulant response in ADHD. *Neuropsychopharmacology* **33**:2536–2545. doi:10.1038/sj.npp.1301637

Bellgrove MA, Chambers CD, Johnson KA, Daibhis A, Daly M, Hawi Z, Lambert D, Gill M, Robertson IH. 2007. Dopaminergic genotype biases spatial attention in healthy children. *Mol Psychiatry* **12**:786–792. doi:10.1038/sj.mp.4002022

Bellgrove MA, Johnson KA, Barry E, Mulligan A, Hawi Z, Gill M, Robertson I, Chambers CD. 2009. Dopaminergic Haplotype as a Predictor of Spatial Inattention in Children With Attention-Deficit/Hyperactivity Disorder. *Arch Gen Psychiatry* **66**:1135. doi:10.1001/archgenpsychiatry.2009.120

Bellgrove MA, Mattingley JB. 2008. Molecular genetics of attentionAnnals of the New York Academy of Sciences. pp. 200–212. doi:10.1196/annals.1417.013

Benjamini Y, Yekutieli D. 2001. The control of the false discovery rate in multiple testing under dependency. *Ann Stat* **29**:1165–1188. doi:10.1214/aos/1013699998

Berens P. 2009. CircStat : A MATLAB Toolbox for Circular Statistics. *J Stat Softw* **31**. doi:10.18637/jss.v031.i10

Berger B, Gaspar P, Verney C. 1991. Dopaminergic innervation of the cerebral cortex: Unexpected differences between rodents and primates. *Trends Neurosci* **14**:21–27. doi:10.1016/0166-2236(91)90179-X

Berridge C, Foote S. 1991. Effects of locus coeruleus activation on electroencephalographic activity in neocortex and hippocampus. *J Neurosci* **11**:3135–3145. doi:10.1523/JNEUROSCI.11-10-03135.1991

Berridge CW, Page ME, Valentino RJ, Foote SL. 1993. Effects of locus coeruleus

inactivation on electroencephalographic activity in neocortex and hippocampus. *Neuroscience* **55**:381–393. doi:10.1016/0306-4522(93)90507-C

Berridge CW, Waterhouse BD. 2003. The locus coeruleus–noradrenergic system: modulation of behavioral state and state-dependent cognitive processes. *Brain Res Rev* **42**:33–84. doi:10.1016/S0165-0173(03)00143-7

Bichot NP, Thompson KG, Chenchal Rao S, Schall JD. 2001. Reliability of macaque frontal eye field neurons signaling saccade targets during visual search. *J Neurosci* **21**:713–725. doi:21/2/713 [pii]

Binda P, Gamlin PD. 2017. Renewed Attention on the Pupil Light Reflex. *Trends Neurosci* **40**:455–457. doi:10.1016/j.tins.2017.06.007

Binda P, Murray SO. 2015a. Spatial attention increases the pupillary response to light changes. *J Vis* **15**:1–1. doi:10.1167/15.2.1

Binda P, Murray SO. 2015b. Keeping a large-pupilled eye on high-level visual processing. *Trends Cogn Sci* **19**:1–3. doi:10.1016/j.tics.2014.11.002

Bishop CM. 2006. Pattern Recognition and Machine Learning. Springer.

Bisley JW, Goldberg ME. 2010. Attention, intention, and priority in the parietal lobe. *Annu Rev Neurosci* **33**:1–21. doi:10.1146/annurev-neuro-060909-152823

Bissière S, Humeau Y, Lüthi A. 2003. Dopamine gates LTP induction in lateral amygdala by suppressing feedforward inhibition. *Nat Neurosci* **6**:587–592. doi:10.1038/nn1058

Blasdel G, Lund J, Fitzpatrick D. 1985. Intrinsic connections of macaque striate cortex: axonal projections of cells outside lamina 4C. *J Neurosci* **5**:3350–3369. doi:10.1523/JNEUROSCI.05-12-03350.1985

Blatt GJ, Andersen RA, Stoner GR. 1990. Visual receptive field organization and cortico-cortical connections of the lateral intraparietal area (area LIP) in the macaque. *J Comp Neurol* **299**:421–45. doi:10.1002/cne.902990404

Bokil H, Andrews P, Kulkarni JE, Mehta S, Mitra PP. 2010. Chronux: A platform for analyzing neural signals. *J Neurosci Methods* **192**:146–151. doi:10.1016/j.jneumeth.2010.06.020

Bondy AG, Haefner RM, Cumming BG. 2018. Feedback determines the structure of correlated variability in primary visual cortex. *Nat Neurosci* **21**:598–606. doi:10.1038/s41593-018-0089-1

Bonis-O'Donnell JT Del, Page RH, Beyene AG, Tindall EG, McFarlane IR, Landry MP. 2017. Dual Near-Infrared Two-Photon Microscopy for Deep-Tissue Dopamine Nanosensor Imaging. *Adv Funct Mater* **27**:1702112. doi:10.1002/adfm.201702112

Bosman CA, Schoffelen J-M, Brunet N, Oostenveld R, Bastos AM, Womelsdorf T, Rubehn B, Stieglitz T, De Weerd P, Fries P. 2012. Attentional Stimulus Selection through Selective Synchronization between Monkey Visual Areas. *Neuron* **75**:875–888. doi:10.1016/j.neuron.2012.06.037

Bouret S, Sara SJ. 2005. Network reset: a simplified overarching theory of locus coeruleus

noradrenaline function. *Trends Neurosci* **28**:574–582. doi:10.1016/j.tins.2005.09.002

Boyd JD, Mavity-Hudson JA, Casagrande VA. 2000. The connections of layer 4 subdivisions in the primary visual cortex (V1) of the owl monkey. *Cereb Cortex* **10**:644–662. doi:10.1093/cercor/10.7.644

Britten K, Shadlen M, Newsome W, Movshon J. 1992. The analysis of visual motion: a comparison of neuronal and psychophysical performance. *J Neurosci* **12**:4745–4765. doi:10.1523/JNEUROSCI.12-12-04745.1992

Britten KH, Newsome WT, Shadlen MN, Celebrini S, Movshon JA. 1996. A relationship between behavioral choice and the visual responses of neurons in macaque MT. *Vis Neurosci* **13**:87–100. doi:10.1017/S095252380000715X

Buschman TJ, Miller EK. 2007. Top-Down Versus Bottom-Up Control of Attention in the Prefrontal and Posterior Parietal Cortices. *Science (80-)* **315**:1860–1862. doi:10.1126/science.1138071

Bushnell MC, Goldberg ME, Robinson DL. 1981. Behavioral enhancement of visual responses in monkey cerebral cortex. I. Modulation in posterior parietal cortex related to selective visual attention. *J Neurophysiol* **46**:755–772. doi:10.1152/jn.1981.46.4.755

Buzsaki G, Bickford R, Ponomareff G, Thal L, Mandel R, Gage F. 1988. Nucleus basalis and thalamic control of neocortical activity in the freely moving rat. *J Neurosci* **8**:4007–4026. doi:10.1523/JNEUROSCI.08-11-04007.1988

Cai JX, Arnsten AF. 1997. Dose-dependent effects of the dopamine D1 receptor agonists A77636 or SKF81297 on spatial working memory in aged monkeys. *J Pharmacol Exp Ther* **283**:183–9.

Callaway EM, Wiser AK. 1996. Contributions of individual layer 2–5 spiny neurons to local circuits in macaque primary visual cortex. *Vis Neurosci* **13**:907–922. doi:10.1017/S0952523800009159

Carandini M. 2004. Amplification of trial-to-trial response variability by neurons in visual cortex. *PLoS Biol*. doi:10.1371/journal.pbio.0020264

Caspers S, Schleicher A, Bacha-Trams M, Palomero-Gallagher N, Amunts K, Zilles K. 2013. Organization of the human inferior parietal lobule based on receptor architectonics. *Cereb Cortex* **23**:615–628. doi:10.1093/cercor/bhs048

Chafee M V, Goldman-Rakic PS. 2000. Inactivation of Parietal and Prefrontal Cortex Reveals Interdependence of Neural Activity During Memory-Guided Saccades. *J Neurophysiol* **83**:1550–1566. doi:10.1152/jn.2000.83.3.1550

Chandler DJ, Gao W-J, Waterhouse BD. 2014. Heterogeneous organization of the locus coeruleus projections to prefrontal and motor cortices. *Proc Natl Acad Sci* **111**:6816–6821. doi:10.1073/pnas.1320827111

Chandler DJ, Lamperski CS, Waterhouse BD. 2013. Identification and distribution of projections from monoaminergic and cholinergic nuclei to functionally differentiated subregions of prefrontal cortex. *Brain Res* **1522**:38–58. doi:10.1016/j.brainres.2013.04.057

Cheadle S, Wyart V, Tsetsos K, Myers N, de Gardelle V, Herce Castañón S, Summerfield C. 2014. Adaptive Gain Control during Human Perceptual Choice. *Neuron* **81**:1429–1441. doi:10.1016/j.neuron.2014.01.020

Chen Y, Martinez-Conde S, Macknik SL, Bereshpolova Y, Swadlow HA, Alonso JM. 2008. Task difficulty modulates the activity of specific neuronal populations in primary visual cortex. *Nat Neurosci* **11**:974–982. doi:nn.2147 [pii]\r10.1038/nn.2147

Clark CR, Geffen GM, Geffen LB. 1989. Catecholamines and the covert orientation of attention in humans. *Neuropsychologia* **27**:131–139. doi:10.1016/0028-3932(89)90166-8

Clark KL, Noudoost B. 2014. The role of prefrontal catecholamines in attention and working memory. *Front Neural Circuits* **8**:33. doi:10.3389/fncir.2014.00033

Clayton EC. 2004. Phasic Activation of Monkey Locus Ceruleus Neurons by Simple Decisions in a Forced-Choice Task. *J Neurosci* **24**:9914–9920. doi:10.1523/JNEUROSCI.2446-04.2004

Cohen JD, McClure SM, Yu AJ. 2007. Should I stay or should I go? How the human brain manages the trade-off between exploitation and exploration. *Philos Trans R Soc B Biol Sci* **362**:933–942. doi:10.1098/rstb.2007.2098

Cohen MR, Maunsell JHR. 2009. Attention improves performance primarily by reducing interneuronal correlations. *Nat Neurosci* **12**:1594–1600. doi:10.1038/nn.2439

Colby CL, Duhamel JR, Goldberg ME. 1996. Visual, presaccadic, and cognitive activation of single neurons in monkey lateral intraparietal area. *J Neurophysiol* **76**:2841–2852. doi:10.1152/jn.1996.76.5.2841

Colby CL, Goldberg ME. 1999. Space and attention in parietal cortex. *Annu Rev Neurosci* **22**:319–49. doi:10.1146/annurev.neuro.22.1.319

Constantinople CM, Bruno RM. 2011. Effects and mechanisms of wakefulness on local cortical networks. *Neuron* **69**:1061–1068. doi:10.1016/j.neuron.2011.02.040

Contreras D, Steriade M. 1995. Cellular basis of EEG slow rhythms: a study of dynamic corticothalamic relationships. *J Neurosci* **15**:604–622. doi:10.1523/JNEUROSCI.15-01-00604.1995

Corbetta M, Shulman GL. 2011. Spatial Neglect and Attention Networks. *Annu Rev Neurosci* **34**:569–599. doi:10.1146/annurev-neuro-061010-113731

Corbetta M, Shulman GL. 2002. Control of goal-directed and stimulus-driven attention in the brain. *Nat Rev Neurosci* **3**:201–215. doi:10.1038/nrn755

Costagli M, Ueno K, Sun P, Gardner JL, Wan X, Ricciardi E, Pietrini P, Tanaka K, Cheng K. 2014. Functional signalers of changes in visual stimuli: Cortical responses to increments and decrements in motion coherence. *Cereb Cortex* **24**:110–118. doi:10.1093/cercor/bhs294

Coull JT, Nobre AC, Frith CD. 2001. The Noradrenergic α2 Agonist Clonidine Modulates Behavioural and Neuroanatomical Correlates of Human Attentional Orienting and Alerting. *Cereb Cortex* **11**:73–84. doi:10.1093/cercor/11.1.73

Cox J, Witten IB. 2019. Striatal circuits for reward learning and decision-making. *Nat Rev Neurosci*. doi:10.1038/s41583-019-0189-2

Croxson PL, Kyriazis DA, Baxter MG. 2011. Cholinergic modulation of a specific memory function of prefrontal cortex. *Nat Neurosci* **14**:1510–1512. doi:10.1038/nn.2971

Culham JC, Cavanagh P, Kanwisher NG. 2001. Attention response functions: Characterizing brain areas using fMRI activation during parametric variations of attentional load. *Neuron* **32**:737–745. doi:10.1016/S0896-6273(01)00499-8

Cutrell E, Marrocco R. 2002. Electrical microstimulation of primate posterior parietal cortex initiates orienting and alerting components of covert attention. *Exp Brain Res* **144**:103–113. doi:10.1007/s00221-002-1032-x

Dagnino B, Gariel-Mathis MA, Roelfsema PR. 2015. Microstimulation of area V4 has little effect on spatial attention and on perception of phosphenes evoked in area V1. *J Neurophysiol* **113**:730–739. doi:10.1152/jn.00645.2014

Dai J, Brooks DI, Sheinberg DL. 2014. Optogenetic and electrical microstimulation systematically bias visuospatial choice in primates. *Curr Biol* **24**:63–69. doi:10.1016/j.cub.2013.11.011

Dani JA, Bertrand D. 2007. Nicotinic Acetylcholine Receptors and Nicotinic Cholinergic Mechanisms of the Central Nervous System. *Annu Rev Pharmacol Toxicol* **47**:699–729. doi:10.1146/annurev.pharmtox.47.120505.105214

Davidson MC, Cutrell EB, Marrocco RT. 1999. Scopolamine slows the orienting of attention in primates to cued visual targets. *Psychopharmacology (Berl)*. doi:10.1007/s002130050855

Davidson MC, Marrocco RT. 2000. Local Infusion of Scopolamine Into Intraparietal Cortex Slows Covert Orienting in Rhesus Monkeys. *J Neurophysiol* **83**:1536–1549. doi:10.1152/jn.2000.83.3.1536

Dayan P, Yu A. 2006. Norepinephrine and neural interrupts. … *Neural Inf Process Syst*.

Dayan Peter, Yu AJ. 2006. Phasic norepinephrine: A neural interrupt signal for unexpected events. *Netw Comput Neural Syst* **17**:335–350. doi:10.1080/09548980601004024

de Gee JW, Colizoli O, Kloosterman NA, Knapen T, Nieuwenhuis S, Donner TH. 2017. Dynamic modulation of decision biases by brainstem arousal systems. *Elife* **6**:1–36. doi:10.7554/eLife.23232

de Gee JW, Knapen T, Donner TH. 2014. Decision-related pupil dilation reflects upcoming choice and individual bias. *Proc Natl Acad Sci* **111**:E618–E625. doi:10.1073/pnas.1317557111

Deco G, Thiele A. 2011. Cholinergic control of cortical network interactions enables feedback-mediated attentional modulation. *Eur J Neurosci* **34**:146–157. doi:10.1111/j.1460-9568.2011.07749.x

Delorme A, Makeig S. 2004. EEGLAB: an open source toolbox for analysis of single-trial EEG dynamics including independent component analysis. *J Neurosci Methods*

134:9–21. doi:10.1016/j.jneumeth.2003.10.009

Desimone R. 1998. Visual attention mediated by biased competition in extrastriate visual cortex. *Philos Trans R Soc B Biol Sci* **353**:1245–1255. doi:10.1098/rstb.1998.0280

Desimone R, Duncan J. 1995. Neural Mechanisms of Selective Visual Attention. *Annu Rev Neurosci* **18**:193–222. doi:10.1146/annurev.ne.18.030195.001205

Devilbiss DM, Page ME, Waterhouse BD. 2006. Locus Ceruleus Regulates Sensory Encoding by Neurons and Networks in Waking Animals. *J Neurosci* **26**:9860–9872. doi:10.1523/JNEUROSCI.1776-06.2006

Devilbiss DM, Waterhouse BD. 2011. Phasic and Tonic Patterns of Locus Coeruleus Output Differentially Modulate Sensory Network Function in the Awake Rat. *J Neurophysiol* **105**:69–87. doi:10.1152/jn.00445.2010

Devilbiss DM, Waterhouse BD. 2000. Norepinephrine exhibits two distinct profiles of action on sensory cortical neuron responses to excitatory synaptic stimuli. *Synapse* **37**:273–282. doi:10.1002/1098-2396(20000915)37:4<273::AID-SYN4>3.0.CO;2-#

Devoto P, Flore G. 2006. On the origin of cortical dopamine: is it a co-transmitter in noradrenergic neurons? *Curr Neuropharmacol* **4**:115–125. doi:10.2174/157340006775101463

Devoto P, Flore G, Saba P, Fà M, Gessa GL. 2005. Stimulation of the locus coeruleus elicits noradrenaline and dopamine release in the medial prefrontal and parietal cortex. *J Neurochem* **92**:368–374. doi:10.1111/j.1471-4159.2004.02866.x

Ding L, Gold JI. 2012. Neural correlates of perceptual decision making before, during, and after decision commitment in monkey frontal eye field. *Cereb Cortex* **22**:1052–1067. doi:10.1093/cercor/bhr178

Dinstein I, Heeger DJ, Behrmann M. 2015. Neural variability: Friend or foe? *Trends Cogn Sci* **19**:322–328. doi:10.1016/j.tics.2015.04.005

Disney AA, Aoki C, Hawken MJ. 2007. Gain Modulation by Nicotine in Macaque V1. *Neuron* **56**:701–713. doi:10.1016/j.neuron.2007.09.034

Donner TH, Siegel M, Fries P, Engel AK. 2009. Buildup of Choice-Predictive Activity in Human Motor Cortex during Perceptual Decision Making. *Curr Biol* **19**:1581–1585. doi:10.1016/j.cub.2009.07.066

Douglas RJ, Martin KAC. 2004. Neuronal Circuits of the Neocortex. *Annu Rev Neurosci* **27**:419–451. doi:10.1146/annurev.neuro.27.070203.144152

Doya K. 2008. Modulators of decision making. *Nat Neurosci* **11**:410–416. doi:10.1038/nn2077

Duncan J. 1984. Selective attention and the organization of visual information. *J Exp Psychol Gen* **113**:501–517. doi:10.1037/0096-3445.113.4.501

Durstewitz D, Seamans JK, Sejnowski TJ. 2000. Neurocomputational models of working memory. *Nat Neurosci* **3 Suppl**:1184–1191. doi:10.1038/81460

Ebitz RB, Moore T. 2017. Selective Modulation of the Pupil Light Reflex by

Microstimulation of Prefrontal Cortex. *J Neurosci* **37**:5008–5018. doi:10.1523/JNEUROSCI.2433-16.2017

Ebitz RB, Pearson JM, Platt ML. 2014. Pupil size and social vigilance in rhesus macaques. *Front Neurosci* **8**. doi:10.3389/fnins.2014.00100

Eckhorn R, Bauer R, Jordan W, Brosch M, Kruse W, Munk M, Reitboeck HJ. 1988. Coherent oscillations: A mechanism of feature linking in the visual cortex? *Biol Cybern* **60**:121–130. doi:10.1007/BF00202899

Einhäuser W, Koch C, Carter OL. 2010. Pupil dilation betrays the timing of decisions. *Front Hum Neurosci* **4**:18. doi:10.3389/fnhum.2010.00018

Eldar E, Cohen JD, Niv Y. 2013. The effects of neural gain on attention and learning. *Nat Neurosci* **16**:1146–1153. doi:10.1038/nn.3428

Engbert R, Kliegl R. 2003. Microsaccades uncover the orientation of covert attention. *Vision Res*. doi:10.1016/S0042-6989(03)00084-1

Engel AK, Konig P, Singer W. 1992. Synchronization of oscillatory neuronal responses in cat striate cortex: Temporal properties. *Vis Neurosci* **8**:337–347. doi:10.1017/S0952523800005071

Engel TA, Steinmetz NA, Gieselmann MA, Thiele A, Moore T, Boahen K. 2016. Selective modulation of cortical state during spatial attention. *Science (80-)* **354**:1140–1144. doi:10.1126/science.aag1420

Ergenoglu T, Demiralp T, Bayraktaroglu Z, Ergen M, Beydagi H, Uresin Y. 2004. Alpha rhythm of the EEG modulates visual detection performance in humans. *Cogn Brain Res* **20**:376–383. doi:10.1016/j.cogbrainres.2004.03.009

Everitt BJ, Robbins TW. 1997. Central Cholinergic Systems and Cognition. *Annu Rev Psychol* **48**:649–684. doi:10.1146/annurev.psych.48.1.649

Fisher NI. 1993. Statistical Analysis of Circular Data, Book. doi:10.1017/CBO9780511564345

Flores-Hernandez J. 2002. Dopamine Enhancement of NMDA Currents in Dissociated Medium-Sized Striatal Neurons: Role of D1 Receptors and DARPP-32. *J Neurophysiol* **88**:3010–3020. doi:10.1152/jn.00361.2002

Florin-Lechner SM, Druhan JP, Aston-Jones G, Valentino RJ. 1996. Enhanced norepinephrine release in prefrontal cortex with burst stimulation of the locus coeruleus. *Brain Res* **742**:89–97. doi:10.1016/S0006-8993(96)00967-5

Fontanini A, Katz DB. 2008. Behavioral states, network states, and sensory response variability. *J Neurophysiol* **100**:1160–1168. doi:10.1152/jn.90592.2008

Foote SL, Aston-Jones G, Bloom FE. 1980. Impulse activity of locus coeruleus neurons in awake rats and monkeys is a function of sensory stimulation and arousal. *Proc Natl Acad Sci* **77**:3033–3037. doi:10.1073/pnas.77.5.3033

Freedman DJ, Ibos G. 2018. An Integrative Framework for Sensory, Motor, and Cognitive Functions of the Posterior Parietal Cortex. *Neuron* **97**:1219–1234.

doi:10.1016/j.neuron.2018.01.044

Fries P. 2005. A mechanism for cognitive dynamics: Neuronal communication through neuronal coherence. *Trends Cogn Sci* **9**:474–480. doi:10.1016/j.tics.2005.08.011

Funahashi S, Bruce CJ, Goldman-Rakic PS. 1989. Mnemonic coding of visual space in the monkey's dorsolateral prefrontal cortex. *J Neurophysiol* **61**:331–349. doi:10.1152/jn.1989.61.2.331

Furey ML, Pietrini P, Haxby J V., Drevets WC. 2008. Selective effects of cholinergic modulation on task performance during selective attention. *Neuropsychopharmacology*. doi:10.1038/sj.npp.1301461

Ge S, Dani JA. 2005. Nicotinic acetylcholine receptors at glutamate synapses facilitate long-term depression or potentiation. *J Neurosci* **25**:6084–6091. doi:10.1523/JNEUROSCI.0542-05.2005

Gescheider GA. 1997. Psychophysics: The Fundamentals, Third. ed, Psychophysics: The Fundamentals. Mahwah. New Jersey: Lawrence Erlbaum Associates.

Gielow MR, Zaborszky L. 2017. The Input-Output Relationship of the Cholinergic Basal Forebrain. *Cell Rep* **18**:1817–1830. doi:10.1016/j.celrep.2017.01.060

Gieselmann MA, Thiele A. 2008. Comparison of spatial integration and surround suppression characteristics in spiking activity and the local field potential in macaque V1. *Eur J Neurosci* **28**:447–459. doi:10.1111/j.1460-9568.2008.06358.x

Gilzenrat MS, Nieuwenhuis S, Jepma M, Cohen JD. 2010. Pupil diameter tracks changes in control state predicted by the adaptive gain theory of locus coeruleus function. *Cogn Affect Behav Neurosci* **10**:252–269. doi:10.3758/CABN.10.2.252

Glimcher PW. 2011. Understanding dopamine and reinforcement learning: The dopamine reward prediction error hypothesis. *Proc Natl Acad Sci* **108**:15647–15654. doi:10.1073/pnas.1014269108

Gnadt JW, Andersen RA. 1988. Memory related motor planning activity in posterior parietal cortex of macaque. *Exp Brain Res* **70**:216–220. doi:10.1007/BF00271862

Goard M, Dan Y. 2009. Basal forebrain activation enhances cortical coding of natural scenes. *Nat Neurosci* **12**:1444–1449. doi:10.1038/nn.2402

Gold JI, Shadlen MN. 2007. The Neural Basis of Decision Making. *Annu Rev Neurosci* **30**:535–574. doi:10.1146/annurev.neuro.29.051605.113038

Gorgoraptis N, Mah YH, MacHner B, Singh-Curry V, Malhotra P, Hadji-Michael M, Cohen D, Simister R, Nair A, Kulinskaya E, Ward N, Greenwood R, Husain M. 2012. The effects of the dopamine agonist rotigotine on hemispatial neglect following stroke. *Brain* **135**:2478–2491. doi:10.1093/brain/aws154

Goris RLT, Movshon JA, Simoncelli EP. 2014. Partitioning neuronal variability. *Nat Neurosci* **17**:858–865. doi:10.1038/nn.3711

Gottlieb J. 2012. Attention, learning, and the value of information. *Neuron* **76**:281–95. doi:10.1016/j.neuron.2012.09.034

Gottlieb J, Balan P. 2010. Attention as a decision in information space. *Trends Cogn Sci* **14**:240–248. doi:10.1016/j.tics.2010.03.001

Gottlieb JP, Kusunoki M, Goldberg ME. 1998. The representation of visual salience in monkey parietal cortex. *Nature* **391**:481–4. doi:10.1038/35135

Green DM, Swets JA. 1966. Signal Detection Theory and Psychophysics. New York: Wiley. doi:10.1901/jeab.1969.12-475

Gregoriou GG, Gotts SJ, Desimone R. 2012. Cell-type-specific synchronization of neural activity in FEF with V4 during attention. *Neuron* **73**:581–94. doi:10.1016/j.neuron.2011.12.019

Gregoriou GG, Gotts SJ, Zhou H, Desimone R. 2009. High-frequency, long-range coupling between prefrontal and visual cortex during attention. *Science* **324**:1207–1210. doi:10.1126/science.1171402

Gregoriou GG, Rossi AF, Ungerleider LG, Desimone R. 2014. Lesions of prefrontal cortex reduce attentional modulation of neuronal responses and synchrony in V4. *Nat Neurosci* **17**:1003–1011. doi:10.1038/nn.3742

Gritton HJ, Howe WM, Mallory CS, Hetrick VL, Berke JD, Sarter M. 2016. Cortical cholinergic signaling controls the detection of cues. *Proc Natl Acad Sci* **113**:E1089–E1097. doi:10.1073/pnas.1516134113

Gutnisky DA, Beaman CB, Lew SE, Dragoi V. 2017. Spontaneous Fluctuations in Visual Cortical Responses Influence Population Coding Accuracy. *Cereb Cortex* **27**:1409–1427. doi:10.1093/cercor/bhv312

Hanks TD, Ditterich J, Shadlen MN. 2006. Microstimulation of macaque area LIP affects decision-making in a motion discrimination task. *Nat Neurosci* **9**:682–9. doi:10.1038/nn1683

Harris KD. 2013. Top-Down control of cortical state. *Neuron* **79**:408–410. doi:10.1016/j.neuron.2013.07.034

Harris KD, Mrsic-Flogel TD. 2013. Cortical connectivity and sensory coding. *Nature* **503**:51–8. doi:10.1038/nature12654

Harris KD, Thiele A. 2011. Cortical state and attention. *Nat Rev Neurosci* **12**:509–523. doi:10.1038/nrn3084

Hasselmo ME. 1999. Neuromodulation: acetylcholine and memory consolidation. *Trends Cogn Sci* **3**:351–359. doi:10.1016/S1364-6613(99)01365-0

Henze DA, González-Burgos GR, Urban NN, Lewis DA, Barrionuevo G. 2000. Dopamine Increases Excitability of Pyramidal Neurons in Primate Prefrontal Cortex. *J Neurophysiol* **84**:2799–2809. doi:10.1152/jn.2000.84.6.2799

Herrero JL, Gieselmann M a, Sanayei M, Thiele A. 2013. Attention-induced variance and noise correlation reduction in macaque v1 is mediated by NMDA receptors. *Neuron* **78**:729–739. doi:10.1016/j.neuron.2013.03.029

Herrero JL, Roberts MJ, Delicato LS, Gieselmann MA, Dayan P, Thiele A. 2008.

Acetylcholine contributes through muscarinic receptors to attentional modulation in V1. *Nature* **454**:1110–1114. doi:10.1038/nature07141

Herz A, Zieglgänsberger W, Färber G. 1969. Microelectrophoretic studies concerning the spread of glutamic acid and GABA in brain tissue. *Exp Brain Res* **9**. doi:10.1007/BF00234456

Hess EH, Polt JM. 1964. Pupil Size in Relation to Mental Activity during Simple Problem-Solving. *Science (80-)* **143**:1190–1192. doi:10.1126/science.143.3611.1190

Hoeks B, Levelt WJM. 1993. Pupillary dilation as a measure of attention: a quantitative system analysis. *Behav Res Methods, Instruments, Comput*. doi:10.3758/BF03204445

Hof PR, Morrison JH. 1995. Neurofilament protein defines regional patterns of cortical organization in the macaque monkey visual system: A quantitative immunohistochemical analysis. *J Comp Neurol* **352**:161–186. doi:10.1002/cne.903520202

Hong L, Walz JM, Sajda P. 2014. Your Eyes Give You Away: Prestimulus Changes in Pupil Diameter Correlate with Poststimulus Task-Related EEG Dynamics. *PLoS One* **9**:e91321. doi:10.1371/journal.pone.0091321

Horwitz GD, Batista AP, Newsome WT. 2004. Representation of an Abstract Perceptual Decision in Macaque Superior Colliculus. *J Neurophysiol* **91**:2281–2296. doi:10.1152/jn.00872.2003

Hubel DH, Wiesel TN. 1968. Receptive fields and functional architecture of monkey striate cortex. *J Physiol*. doi:10.1113/jphysiol.1968.sp008455

Ignashchenkova A, Dicke PW, Haarmeier T, Thier P. 2004. Neuron-specific contribution of the superior colliculus to overt and covert shifts of attention. *Nat Neurosci* **7**:56–64. doi:10.1038/nn1169

Jacob SN, Ott T, Nieder A. 2013. Dopamine regulates two classes of primate prefrontal neurons that represent sensory signals. *J Neurosci* **33**:13724–34. doi:10.1523/JNEUROSCI.0210-13.2013

Jacob SN, Stalter M, Nieder A. 2016. Cell-type-specific modulation of targets and distractors by dopamine D1 receptors in primate prefrontal cortex. *Nat Commun*. doi:10.1038/ncomms13218

James G, Witten D, Hastie T, Tibshirani R. 2017. An Introduction to Statistical Learning, 8th ed. New York: Springer Science+Business Media New York.

Jia X, Tanabe S, Kohn A. 2013. Gamma and the Coordination of Spiking Activity in Early Visual Cortex. *Neuron* **77**:762–774. doi:10.1016/j.neuron.2012.12.036

Jodo E, Chiang C, Aston-Jones G. 1998. Potent excitatory influence of prefrontal cortex activity on noradrenergic locus coeruleus neurons. *Neuroscience* **83**:63–79. doi:10.1016/S0306-4522(97)00372-2

Joshi S, Li Y, Kalwani RM, Gold JI. 2016. Relationships between Pupil Diameter and Neuronal Activity in the Locus Coeruleus, Colliculi, and Cingulate Cortex. *Neuron* **89**:221–234. doi:10.1016/j.neuron.2015.11.028

Kajikawa Y, Schroeder CE. 2011. How local is the local field potential? *Neuron*. doi:10.1016/j.neuron.2011.09.029

Kandel ER, Schwartz JH, Jessell TM. 2000. Principles of Neural Science, 4th ed.

Kaplan E, Shapley RM. 1986. The primate retina contains two types of ganglion cells, with high and low contrast sensitivity. *Proc Natl Acad Sci* **83**:2755–2757. doi:10.1073/pnas.83.8.2755

Kaplan E, Shapley RM. 1982. X and Y cells in the lateral geniculate nucleus of macaque monkeys. *J Physiol* **330**:125–143. doi:10.1113/jphysiol.1982.sp014333

Kayser J, Tenke CE. 2006. Principal components analysis of Laplacian waveforms as a generic method for identifying ERP generator patterns: I. Evaluation with auditory oddball tasks. *Clin Neurophysiol* **117**:348–368. doi:10.1016/j.clinph.2005.08.034

Kelly SP, O'Connell RG. 2015. The neural processes underlying perceptual decision making in humans: Recent progress and future directions. *J Physiol Paris* **109**:27–37. doi:10.1016/j.jphysparis.2014.08.003

Kelly SP, O'Connell RG. 2013. Internal and External Influences on the Rate of Sensory Evidence Accumulation in the Human Brain. *J Neurosci* **33**:19434–19441. doi:10.1523/JNEUROSCI.3355-13.2013

Kim J-N, Shadlen MN. 1999. Neural correlates of a decision in the dorsolateral prefrontal cortex of the macaque. *Nat Neurosci* **2**:176–185. doi:10.1038/5739

Kira S, Yang T, Shadlen MN. 2015. A Neural Implementation of Wald's Sequential Probability Ratio Test. *Neuron* **85**:861–873. doi:10.1016/j.neuron.2015.01.007

Kirkwood A, Rozas C, Kirkwood J, Perez F, Bear MF. 1999. Modulation of Long-Term Synaptic Depression in Visual Cortex by Acetylcholine and Norepinephrine. *J Neurosci* **19**:1599–1609. doi:10.1523/JNEUROSCI.19-05-01599.1999

Kloosterman NA, Meindertsma T, van Loon AM, Lamme VAF, Bonneh YS, Donner TH. 2015. Pupil size tracks perceptual content and surprise. *Eur J Neurosci* **41**:1068–1078. doi:10.1111/ejn.12859

Kohn A, Zandvakili A, Smith MA. 2009. Correlations and brain states: from electrophysiology to functional imaging. *Curr Opin Neurobiol* **19**:434–438. doi:10.1016/j.conb.2009.06.007

Krauzlis RJ, Lovejoy LP, Zénon A. 2013. Superior Colliculus and Visual Spatial Attention. *Annu Rev Neurosci* **36**:165–182. doi:10.1146/annurev-neuro-062012-170249

Kristjansson SD, Stern JA, Brown TB, Rohrbaugh JW. 2009. Detecting phasic lapses in alertness using pupillometric measures. *Appl Ergon* **40**:978–986. doi:10.1016/j.apergo.2009.04.007

Kruss S, Landry MP, Vander Ende E, Lima BMA, Reuel NF, Zhang J, Nelson J, Mu B, Hilmer A, Strano M. 2014. Neurotransmitter detection using corona phase molecular recognition on fluorescent single-walled carbon nanotube sensors. *J Am Chem Soc* **136**:713–724. doi:10.1021/ja410433b

Kustov AA, Lee Robinson D. 1996. Shared neural control of attentional shifts and eye movements. *Nature* **384**:74–77. doi:10.1038/384074a0

Kuypers HGJM, Lawrence DG. 1967. Cortical projections to the red nucleus and the brain stem in the rhesus monkey. *Brain Res* **4**:151–188. doi:10.1016/0006-8993(67)90004-2

Latimer KW, Yates JL, Meister MLR, Huk AC, Pillow JW. 2016. Response to Comment on "Single-trial spike trains in parietal cortex reveal discrete steps during decision-making." *Science (80-)* **351**:1406–1406. doi:10.1126/science.aad3596

Latimer KW, Yates JL, Meister MLR, Huk AC, Pillow JW. 2015. Single-trial spike trains in parietal cortex reveal discrete steps during decision-making. *Science (80-)* **349**:184–187. doi:10.1126/science.aaa4056

Lee J, Maunsell JHR. 2009. A normalization model of attentional modulation of single unit responses. *PLoS One* **4**. doi:10.1371/journal.pone.0004651

Lee S-H, Dan Y. 2012. Neuromodulation of Brain States. *Neuron* **76**:209–222. doi:10.1016/j.neuron.2012.09.012

Lempert KM, Chen YL, Fleming SM. 2015. Relating Pupil Dilation and Metacognitive Confidence during Auditory Decision-Making. *PLoS One* **10**:e0126588. doi:10.1371/journal.pone.0126588

Levin ED, Simon BB. 1998a. Nicotinic acetylcholine involvement in cogitive function in animals. *Psychopharmacology (Berl)*. doi:10.1007/s002130050667

Levin ED, Simon BB. 1998b. Nicotinic acetylcholine involvement in cognitive function in animals. *Psychopharmacology (Berl)* **138**:217–230. doi:10.1007/s002130050667

Levitt P, Rakic P, Goldman-Rakic P. 1984. Region-specific distribution of catecholamine afferents in primate cerebral cortex: a fluorescence histochemical analysis. *J Comp Neurol* **227**:23–36. doi:10.1002/cne.902270105

Lewis BL, O'Donnell P. 2000. Ventral tegmental area afferents to the prefrontal cortex maintain membrane potential "up" states in pyramidal neurons via D(1) dopamine receptors. *Cereb Cortex* **10**:1168–1175. doi:10.1093/cercor/10.12.1168

Lewis DA, Melchitzky DS, Sesack SR, Whitehead RE, Auh S, Sampson A. 2001. Dopamine transporter immunoreactivity in monkey cerebral cortex: Regional, laminar, and ultrastructural localization. *J Comp Neurol* **432**:119–136. doi:10.1002/cne.1092

Lewis DA, Morrison JH, Goldstein M. 1988. Brainstem dopaminergic neurons project to monkey parietal cortex. *Neurosci Lett* **86**:11–16. doi:10.1016/0304-3940(88)90174-7

Lewis JW, Van Essen DC. 2000. Corticocortical connections of visual, sensorimotor, and multimodal processing areas in the parietal lobe of the macaque monkey. *J Comp Neurol* **428**:112–137. doi:10.1002/1096-9861(20001204)428:1<112::AID-CNE8>3.0.CO;2-9

Li BM, Mao ZM, B.m., Wang M, Mei ZT. 1999. Alpha-2 adrenergic modulation of prefrontal cortical neuronal activity related to spatial working memory in monkeys. *Neuropsychopharmacology* **21**:601–610. doi:10.1016/S0893-133X(99)00070-6

Livingstone M, Hubel D. 1988. Segregation of form, color, movement, and depth: anatomy, physiology, and perception. *Science (80-)* **240**:740–749. doi:10.1126/science.3283936

Loewenfeld IE. 1993. The pupil: anatomy, physiology, and clinical applications. Detroit: Wayne State University.

Logothetis NK, Kayser C, Oeltermann A. 2007. In Vivo Measurement of Cortical Impedance Spectrum in Monkeys: Implications for Signal Propagation. *Neuron* **55**:809–823. doi:10.1016/j.neuron.2007.07.027

Loizou LA. 1969. Projections of the nucleus locus coeruleus in the albino rat. *Brain Res* **15**:563–566. doi:10.1016/0006-8993(69)90185-1

London EB. 2018. Neuromodulation and a Reconceptualization of Autism Spectrum Disorders: Using the Locus Coeruleus Functioning as an Exemplar. *Front Neurol*. doi:10.3389/fneur.2018.01120

Loughnane GM, Brosnan MB, Barnes JJM, Dean A, Nandam SL, O'Connell RG, Bellgrove MA. 2019. Catecholamine Modulation of Evidence Accumulation during Perceptual Decision Formation: A Randomized Trial. *J Cogn Neurosci* **31**:1044–1053. doi:10.1162/jocn_a_01393

Loughnane GM, Newman DP, Bellgrove MA, Lalor EC, Kelly SP, O'Connell RG. 2016. Target Selection Signals Influence Perceptual Decisions by Modulating the Onset and Rate of Evidence Accumulation. *Curr Biol* **26**:496–502. doi:10.1016/j.cub.2015.12.049

Loughnane GM, Newman DP, Tamang S, Kelly SP, O'Connell RG. 2018. Antagonistic interactions between microsaccades and evidence accumulation processes during decision formation. *J Neurosci* **38**:2163–2176. doi:10.1523/JNEUROSCI.2340-17.2018

Lovejoy LP, Krauzlis RJ. 2010. Inactivation of primate superior colliculus impairs covert selection of signals for perceptual judgments. *Nat Neurosci* **13**:261–266. doi:10.1038/nn.2470

Lu R, Sun W, Liang Y, Kerlin A, Bierfeld J, Seelig JD, Wilson DE, Scholl B, Mohar B, Tanimoto M, Koyama M, Fitzpatrick D, Orger MB, Ji N. 2017. Video-rate volumetric functional imaging of the brain at synaptic resolution. *Nat Neurosci* **20**:620–628. doi:10.1038/nn.4516

Luck SJ, Chelazzi L, Hillyard SA, Desimone R. 1997. Neural Mechanisms of Spatial Selective Attention in Areas V1, V2, and V4 of Macaque Visual Cortex. *J Neurophysiol* **77**:24–42. doi:10.1152/jn.1997.77.1.24

Luczak A, Bartho P, Harris KD. 2013. Gating of Sensory Input by Spontaneous Cortical Activity. *J Neurosci* **33**:1684–1695. doi:10.1523/jneurosci.2928-12.2013

Luczak A, Barthó P, Harris KD. 2009. Spontaneous Events Outline the Realm of Possible Sensory Responses in Neocortical Populations. *Neuron* **62**:413–425. doi:10.1016/j.neuron.2009.03.014

Luczak A, McNaughton BL, Harris KD. 2015. Packet-based communication in the cortex. *Nat Rev Neurosci* **16**:745–755. doi:10.1038/nrn4026

Lund JS, Yoshioka T. 1991. Local circuit neurons of macaque monkey striate cortex: III. Neurons of laminae 4B, 4A, and 3B. *J Comp Neurol*. doi:10.1002/cne.903110206

Major AJ, Vijayraghavan S, Everling S. 2015. Muscarinic attenuation of mnemonic rule representation in macaque dorsolateral prefrontal cortex during a pro-and anti-saccade task. *J Neurosci*. doi:10.1523/JNEUROSCI.2454-15.2015

Mark Williams S, Goldman-Rakic PS. 1998. Widespread origin of the primate mesofrontal dopamine system. *Cereb Cortex* **8**:321–345. doi:10.1093/cercor/8.4.321

Markov NT, Vezoli J, Chameau P, Falchier A, Quilodran R, Huissoud C, Lamy C, Misery P, Giroud P, Ullman S, Barone P, Dehay C, Knoblauch K, Kennedy H. 2014. Anatomy of hierarchy: Feedforward and feedback pathways in macaque visual cortex. *J Comp Neurol* **522**:225–259. doi:10.1002/cne.23458

Martinez-Trujillo JC, Treue S. 2004. Feature-Based Attention Increases the Selectivity of Population Responses in Primate Visual Cortex. *Curr Biol* **14**:744–751. doi:10.1016/j.cub.2004.04.028

Maruff P, Hay D, Malone V, Currie J. 1995. Asymmetries in the covert orienting of visual spatial attention in schizophrenia. *Neuropsychologia* **33**:1205–1223. doi:10.1016/0028-3932(95)00037-4

Maunsell JHR. 2004. Neuronal representations of cognitive state: reward or attention? *Trends Cogn Sci* **8**:261–265. doi:10.1016/j.tics.2004.04.003

McAdams CJ, Maunsell JHR. 1999. Effects of Attention on Orientation-Tuning Functions of Single Neurons in Macaque Cortical Area V4. *J Neurosci* **19**:431–441. doi:10.1523/JNEUROSCI.19-01-00431.1999

Mcclure SM, Gilzenrat MS, Cohen JD. 2005. An exploration-exploitation model based on norepinepherine and dopamine activity. *Adv Neural Inf Process Syst*.

McDougal DH, Gamlin PD. 2014. Autonomic Control of the EyeComprehensive Physiology. Hoboken, NJ, USA: John Wiley & Sons, Inc. pp. 439–473. doi:10.1002/cphy.c140014

McGinley MJ, David S V., McCormick DA. 2015a. Cortical Membrane Potential Signature of Optimal States for Sensory Signal Detection. *Neuron* **87**:179–192. doi:10.1016/j.neuron.2015.05.038

McGinley MJ, Vinck M, Reimer J, Batista-Brito R, Zagha E, Cadwell CR, Tolias AS, Cardin JA, McCormick DA. 2015b. Waking State: Rapid Variations Modulate Neural and Behavioral Responses. *Neuron* **87**:1143–1161. doi:10.1016/j.neuron.2015.09.012

McPeek RM, Keller EL. 2004. Deficits in saccade target selection after inactivation of superior colliculus. *Nat Neurosci* **7**:757–763. doi:10.1038/nn1269

McPeek RM, Keller EL. 2002. Saccade target selection in the superior colliculus during a visual search task. *J Neurophysiol* **88**:2019–34. doi:10.1152/jn.2002.88.4.2019

Mehta MA, Owen AM, Sahakian BJ, Mavaddat N, Pickard JD, Robbins TW. 2000. Methylphenidate Enhances Working Memory by Modulating Discrete Frontal and Parietal Lobe Regions in the Human Brain. *J Neurosci* **20**:RC65–RC65.

doi:10.1523/JNEUROSCI.20-06-j0004.2000

Merbs SL, Nathans J. 1992. Absorption spectra of human cone pigments. *Nature* **356**:433–435. doi:10.1038/356433a0

Merigan WH, Maunsell JHR. 1993. How Parallel are the Primate Visual Pathways? *Annu Rev Neurosci* **16**:369–402. doi:10.1146/annurev.ne.16.030193.002101

Merrikhi Y, Clark K, Albarran E, Parsa M, Zirnsak M, Moore T, Noudoost B. 2017. Spatial working memory alters the efficacy of input to visual cortex. *Nat Commun* **8**:15041. doi:10.1038/ncomms15041

Mesulam M-M. 1996. Chapter 28 The systems-level organization of cholinergic innervation in the human cerebral cortex and its alterations in Alzheimer's diseaseProgress in Brain Research. pp. 285–297. doi:10.1016/S0079-6123(08)62112-3

Mesulam M -Marsel, Hersh LB, Mash DC, Geula C. 1992. Differential cholinergic innervation within functional subdivisions of the human cerebral cortex: A choline acetyltransferase study. *J Comp Neurol*. doi:10.1002/cne.903180308

Mesulam MM, Mufson EJ. 1984. Neural inputs into the nucleus basalis of the substantia innominata (ch4) in the rhesus monkey. *Brain*. doi:10.1093/brain/107.1.253

Metherate R, Cox C, Ashe J. 1992. Cellular bases of neocortical activation: modulation of neural oscillations by the nucleus basalis and endogenous acetylcholine. *J Neurosci* **12**:4701–4711. doi:10.1523/JNEUROSCI.12-12-04701.1992

Minces V, Pinto L, Dan Y, Chiba AA. 2017. Cholinergic shaping of neural correlations. *Proc Natl Acad Sci U S A* 201621493. doi:10.1073/pnas.1621493114

Mishkin M, Ungerleider LG, Macko KA. 1983. Object vision and spatial vision: two cortical pathways. *Trends Neurosci* **6**:414–417. doi:10.1016/0166-2236(83)90190-X

Missale C, Nash SR, Robinson SW, Jaber M, Caron MG. 1998. Dopamine receptors: from structure to function. *Physiol Rev* **78**:189–225. doi:10.1186/1471-2296-12-32

Mitchell JF, Sundberg K a, Reynolds JH. 2009. Spatial attention decorrelates intrinsic activity fluctuations in macaque area V4. *Neuron* **63**:879–88. doi:10.1016/j.neuron.2009.09.013

Mitchell JF, Sundberg K a, Reynolds JH. 2007. Differential Attention-Dependent Response Modulation across Cell Classes in Macaque Visual Area V4. *Neuron* **55**:131–141. doi:10.1016/j.neuron.2007.06.018

Mohajerani MH, Chan AW, Mohsenvand M, Ledue J, Liu R, McVea DA, Boyd JD, Wang YT, Reimers M, Murphy TH. 2013. Spontaneous cortical activity alternates between motifs defined by regional axonal projections. *Nat Neurosci*. doi:10.1038/nn.3499

Montague PR, Hyman SE, Cohen JD. 2004. Computational roles for dopamine in behavioural control. *Nature* **431**:760–767. doi:10.1038/nature03015

Moore T, Armstrong KM. 2003. Selective gating of visual signals by microstimulation of frontal cortex. *Nature* **421**:370–373. doi:10.1038/nature01341

Moore T, Fallah M. 2001. Control of eye movements and spatial attention. *Proc Natl Acad*

Sci **98**:1273–1276. doi:10.1073/pnas.98.3.1273

Moran J, Desimone R. 1985. Selective attention gates visual processing in the extrastriate cortex. *Science (80-)* **229**:782–784. doi:10.1126/science.4023713

Motter BC. 1993. Focal attention produces spatially selective processing in visual cortical areas V1, V2, and V4 in the presence of competing stimuli. *J Neurophysiol* **70**:909–919. doi:10.1152/jn.1993.70.3.909

Mountcastle VB. 1957. Modality and topographic properties of single neurons of cat's somatic sensory cortex. *J Neurophysiol* **20**:408–34. doi:10.1152/jn.1957.20.4.408

Mueller A, Krock RM, Shepard S, Moore T. 2019. Dopamine Receptor Expression Among Local and Visual Cortex-Projecting Frontal Eye Field Neurons. *Cereb Cortex* 1–17. doi:10.1093/cercor/bhz078

Mueller A, Shepard SB, Moore T. 2018. Differential Expression of Dopamine D5 Receptors across Neuronal Subtypes in Macaque Frontal Eye Field. *Front Neural Circuits*. doi:10.3389/fncir.2018.00012

Muller JR, Philiastides MG, Newsome WT. 2005. Microstimulation of the superior colliculus focuses attention without moving the eyes. *Proc Natl Acad Sci* **102**:524–529. doi:10.1073/pnas.0408311101

Müller U, von Cramon DY, Pollmann S. 1998. D1- Versus D2-Receptor Modulation of Visuospatial Working Memory in Humans. *J Neurosci* **18**:2720–2728. doi:10.1523/JNEUROSCI.18-07-02720.1998

Munk MHJ, Salin PA, Arzi M, Bullier J. 1992. Spatial and temporal coherence in cortico-cortical connections: A cross-correlation study in areas 17 and 18 in the cat. *Vis Neurosci* **9**:21–37. doi:10.1017/S0952523800006349

Murphy PR, Boonstra E, Nieuwenhuis S. 2016. Global gain modulation generates time-dependent urgency during perceptual choice in humans. *Nat Commun* **7**:13526. doi:10.1038/ncomms13526

Murphy PR, O'Connell RG, O'Sullivan M, Robertson IH, Balsters JH. 2014a. Pupil diameter covaries with BOLD activity in human locus coeruleus. *Hum Brain Mapp* **35**:4140–4154. doi:10.1002/hbm.22466

Murphy PR, Robertson IH, Balsters JH, O'connell RG. 2011. Pupillometry and P3 index the locus coeruleus-noradrenergic arousal function in humans. *Psychophysiology* **48**:1532–1543. doi:10.1111/j.1469-8986.2011.01226.x

Murphy PR, Vandekerckhove J, Nieuwenhuis S. 2014b. Pupil-Linked Arousal Determines Variability in Perceptual Decision Making. *PLoS Comput Biol* **10**:e1003854. doi:10.1371/journal.pcbi.1003854

Mysore SP, Knudsen EI. 2011. The role of a midbrain network in competitive stimulus selection. *Curr Opin Neurobiol* **21**:653–660. doi:10.1016/j.conb.2011.05.024

Naber M, Alvarez GA, Nakayama K. 2013. Tracking the allocation of attention using human pupillary oscillations. *Front Psychol*. doi:10.3389/fpsyg.2013.00919

Nakamura K, Sekine Y, Ouchi Y, Tsujii M, Yoshikawa E, Futatsubashi M, Tsuchiya KJ, Sugihara G, Iwata Y, Suzuki K, Matsuzaki H, Suda S, Sugiyama T, Takei N, Mori N. 2010. Brain serotonin and dopamine transporter bindings in adults with high-functioning autism. *Arch Gen Psychiatry*. doi:10.1001/archgenpsychiatry.2009.137

Nandy A, Nassi JJ, Jadi MP, Reynolds J. 2019. Optogenetically induced low-frequency correlations impair perception. *Elife* **8**:252841. doi:10.7554/eLife.35123

Nauta WJH. 1971. The problem of the frontal lobe: A reinterpretation. *J Psychiatr Res* **8**:167–187. doi:10.1016/0022-3956(71)90017-3

Nelson CL, Sarter M, Bruno JP. 2005. Prefrontal cortical modulation of acetylcholine release in posterior parietal cortex. *Neuroscience* **132**:347–359. doi:10.1016/j.neuroscience.2004.12.007

Neupane S, Guitton D, Pack CC. 2016. Two distinct types of remapping in primate cortical area V4. *Nat Commun* **7**:10402. doi:10.1038/ncomms10402

Newman DP, Cummins TDR, Tong JHS, Johnson BP, Pickering H, Fanning P, Wagner J, Goodrich JTT, Hawi Z, Chambers CD, Bellgrove M a. 2014. Dopamine Transporter Genotype Is Associated with a Lateralized Resistance to Distraction during Attention Selection. *J Neurosci* **34**:15743–15750. doi:10.1523/JNEUROSCI.2327-14.2014

Newman DP, Lockley SW, Loughnane GM, Martins ACP, Abe R, Zoratti MTR, Kelly SP, O'Neill MH, Rajaratnam SMW, O'Connell RG, Bellgrove MA. 2016. Ocular exposure to blue-enriched light has an asymmetric influence on neural activity and spatial attention. *Sci Rep* **6**:27754. doi:10.1038/srep27754

Newman DP, Loughnane GM, Kelly SP, O'Connell RG, Bellgrove MA. 2017. Visuospatial Asymmetries Arise from Differences in the Onset Time of Perceptual Evidence Accumulation. *J Neurosci* **37**:3378–3385. doi:10.1523/JNEUROSCI.3512-16.2017

Newsome WT, Britten KH, Movshon JA. 1989. Neuronal correlates of a perceptual decision. *Nature* **341**:52–54. doi:10.1038/341052a0

Ni AM, Ray S, Maunsell JHR. 2012. Tuned Normalization Explains the Size of Attention Modulations. *Neuron* **73**:803–813. doi:10.1016/j.neuron.2012.01.006

Nienborg H, R. Cohen M, Cumming BG. 2012. Decision-Related Activity in Sensory Neurons: Correlations Among Neurons and with Behavior. *Annu Rev Neurosci* **35**:463–483. doi:10.1146/annurev-neuro-062111-150403

Nieoullon A. 2002. Dopamine and the regulation of cognition and attention. *Prog Neurobiol*. doi:10.1016/S0301-0082(02)00011-4

Nieuwenhuis S, Aston-Jones G, Cohen JD. 2005. Decision making, the P3, and the locus coeruleus--norepinephrine system. *Psychol Bull* **131**:510–532. doi:10.1037/0033-2909.131.4.510

Noudoost B, Moore T. 2011a. Control of visual cortical signals by prefrontal dopamine. *Nature* **474**:372–375. doi:10.1038/nature09995

Noudoost B, Moore T. 2011b. The role of neuromodulators in selective attention. *Trends Cogn Sci*. doi:10.1016/j.tics.2011.10.006

Nowak LG, Munk MH, Nelson JI, James a C, Bullier J. 1995. Structural basis of cortical synchronization. I. Three types of interhemispheric coupling. *J Neurophysiol* **74**:2379–400. doi:10.1152/jn.1995.74.6.2379

Nowak LG, Munk MHJ, James AC, Girard P, Bullier J. 1999. Cross-correlation study of the temporal interactions between areas V1 and V2 of the macaque monkey. *J Neurophysiol* **81**:1057–1074. doi:10.1152/jn.1999.81.3.1057

O'Brien RM. 2007. A Caution Regarding Rules of Thumb for Variance Inflation Factors. *Qual Quant* **41**:673–690. doi:10.1007/s11135-006-9018-6

O'Connell RG, Dockree PM, Kelly SP. 2012. A supramodal accumulation-to-bound signal that determines perceptual decisions in humans. *Nat Neurosci* **15**:1729–1735. doi:10.1038/nn.3248

O'Connell RG, Dockree PM, Robertson IH, Bellgrove MA, Foxe JJ, Kelly SP. 2009. Uncovering the Neural Signature of Lapsing Attention: Electrophysiological Signals Predict Errors up to 20 s before They Occur. *J Neurosci* **29**:8604–8611. doi:10.1523/JNEUROSCI.5967-08.2009

O'Connell RG, Shadlen MN, Wong-Lin K, Kelly SP. 2018. Bridging Neural and Computational Viewpoints on Perceptual Decision-Making. *Trends Neurosci* **xx**:1–15. doi:10.1016/j.tins.2018.06.005

O'Connor DH, Fukui MM, Pinsk MA, Kastner S. 2002. Attention modulates responses in the human lateral geniculate nucleus. *Nat Neurosci* **5**:1203–1209. doi:10.1038/nn957

Oades RD. 1985. The role of noradrenaline in tuning and dopamine in switching between signals in the CNS. *Neurosci Biobehav Rev* **9**:261–282. doi:10.1016/0149-7634(85)90050-8

Oemisch M, Westendorff S, Everling S, Womelsdorf T. 2015. Interareal Spike-Train Correlations of Anterior Cingulate and Dorsal Prefrontal Cortex during Attention Shifts. *J Neurosci* **35**:13076–13089. doi:10.1523/jneurosci.1262-15.2015

Okun M, Steinmetz N a., Cossell L, Iacaruso MF, Ko H, Barthó P, Moore T, Hofer SB, Mrsic-Flogel TD, Carandini M, Harris KD. 2015. Diverse coupling of neurons to populations in sensory cortex. *Nature* **521**:511–515. doi:10.1038/nature14273

Ongur D. 2000. The Organization of Networks within the Orbital and Medial Prefrontal Cortex of Rats, Monkeys and Humans. *Cereb Cortex* **10**:206–219. doi:10.1093/cercor/10.3.206

Opris I, Barborica A, Ferrera VP. 2005. Microstimulation of the dorsolateral prefrontal cortex biases saccade target selection. *J Cogn Neurosci*. doi:10.1162/0898929054021120

Ott T, Jacob SN, Nieder A. 2014. Dopamine Receptors Differentially Enhance Rule Coding in Primate Prefrontal Cortex Neurons. *Neuron* **84**:1317–1328. doi:10.1016/j.neuron.2014.11.012

Ott T, Nieder A. 2019. Dopamine and Cognitive Control in Prefrontal Cortex. *Trends Cogn Sci* **23**:213–234. doi:10.1016/j.tics.2018.12.006

Packard MG, White NM. 1991. Dissociation of Hippocampus and Caudate Nucleus Memory Systems by Posttraining Intracerebral Injection of Dopamine Agonists. *Behav Neurosci* **105**:295–306. doi:10.1037/0735-7044.105.2.295

Panzeri S, Schultz SR, Treves A, Rolls ET. 1999. Correlations and the encoding of information in the nervous system. *Proc R Soc London Ser B Biol Sci* **266**:1001–1012. doi:10.1098/rspb.1999.0736

Parikh V, Kozak R, Martinez V, Sarter M. 2007. Prefrontal Acetylcholine Release Controls Cue Detection on Multiple Timescales. *Neuron* **56**:141–154. doi:10.1016/j.neuron.2007.08.025

Parikh V, Man K, Decker MW, Sarter M. 2008. Glutamatergic Contributions to Nicotinic Acetylcholine Receptor Agonist-Evoked Cholinergic Transients in the Prefrontal Cortex. *J Neurosci* **28**:3769–3780. doi:10.1523/JNEUROSCI.5251-07.2008

Parikh V, Sarter M. 2008. Cholinergic Mediation of Attention. *Ann N Y Acad Sci* **1129**:225–235. doi:10.1196/annals.1417.021

Patrick Hardy SG, Lynch JC. 1992. The spatial distribution of pulvinar neurons that project to two subregions of the inferior parietal lobule in the macaque. *Cereb Cortex* **2**:217–230. doi:10.1093/cercor/2.3.217

Pawlak V, Kerr JND. 2008. Dopamine receptor activation is required for corticostriatal spike-timing-dependent plasticity. *J Neurosci*. doi:10.1523/JNEUROSCI.4402-07.2008

Petersen SE, Robinson DL, Morris JD. 1987. Contributions of the pulvinar to visual spatial attention. *Neuropsychologia* **25**:97–105. doi:10.1016/0028-3932(87)90046-7

Pettersen KH, Devor A, Ulbert I, Dale AM, Einevoll GT. 2006. Current-source density estimation based on inversion of electrostatic forward solution: Effects of finite extent of neuronal activity and conductivity discontinuities. *J Neurosci Methods* **154**:116–133. doi:10.1016/j.jneumeth.2005.12.005

Pinto L, Goard MJ, Estandian D, Xu M, Kwan AC, Lee S-H, Harrison TC, Feng G, Dan Y. 2013. Fast modulation of visual perception by basal forebrain cholinergic neurons. *Nat Neurosci* **16**:1857–1863. doi:10.1038/nn.3552

Platt ML, Glimcher PW. 1999. Neural correlates of decision variables in parietal cortex. *Nature* **400**:233–238. doi:10.1038/22268

Polack PO, Friedman J, Golshani P. 2013. Cellular mechanisms of brain state-dependent gain modulation in visual cortex. *Nat Neurosci* **16**:1331–1339. doi:10.1038/nn.3464

Poletti M, Rucci M, Carrasco M. 2017. Selective attention within the foveola. *Nat Neurosci*. doi:10.1038/nn.4622

Porrino LJ, Goldman-Rakic PS. 1982. Brainstem innervation of prefrontal and anterior cingulate cortex in the rhesus monkey revealed by retrograde transport of HRP. *J Comp Neurol*. doi:10.1002/cne.902050107

Posner M. 1990. The Attention System Of The Human Brain. *Annu Rev Neurosci* **13**:25–42. doi:10.1146/annurev.neuro.13.1.25

Posner MI. 1980. Orienting of attention. *Q J Exp Psychol* **32**:3–25. doi:10.1080/00335558008248231

Posner MI, Cohen Y, Rafal RD. 1982. Neural systems control of spatial orienting. *Philos Trans R Soc Lond B Biol Sci* **298**:187–198. doi:10.1098/rstb.1982.0081

Posner MI, Walker J a, Friedrich FJ, Rafal RD. 1984. Effects of parietal injury on covert orienting of attention. *J Neurosci* **4**:1863–1874. doi:10.1136/jnnp.72.1.73

Poulet JFA, Fernandez LMJ, Crochet S, Petersen CCH. 2012. Thalamic control of cortical states. *Nat Neurosci* **15**:370–372. doi:10.1038/nn.3035

Privitera CM, Renninger LW, Carney T, Klein S, Aguilar M. 2010. Pupil dilation during visual target detection. *J Vis* **10**:3. doi:10.1167/10.10.3

Privitera CM, Renninger LW, Carney T, Klein S, Aguilar M. 2008. The pupil dilation response to visual detection. *Hum Vis Electron Imaging XIII* **6806**:68060T-1-68060T–11. doi:10.1117/12.772844

Rabiner LR. 1989. A tutorial on hidden Markov models and selected applications in speech recognition. *Proc IEEE* **77**:257–286. doi:10.1109/5.18626

Rabinowitz NC, Goris RL, Cohen M, Simoncelli EP. 2015. Attention stabilizes the shared gain of V4 populations. *Elife* **4**:1–24. doi:10.7554/eLife.08998

Rajkowski J, Kubiak P, Aston-Jones G. 1994. Locus coeruleus activity in monkey: Phasic and tonic changes are associated with altered vigilanceBrain Research Bulletin. pp. 607–616. doi:10.1016/0361-9230(94)90175-9

Rajkowski J, Majczynski H, Clayton E, Aston-Jones G. 2004. Activation of Monkey Locus Coeruleus Neurons Varies With Difficulty and Performance in a Target Detection Task. *J Neurophysiol* **92**:361–371. doi:10.1152/jn.00673.2003

Reimer J, Froudarakis E, Cadwell CR, Yatsenko D, Denfield GH, Tolias AS. 2014. Pupil Fluctuations Track Fast Switching of Cortical States during Quiet Wakefulness. *Neuron* **84**:355–362. doi:10.1016/j.neuron.2014.09.033

Reimer J, McGinley MJ, Liu Y, Rodenkirch C, Wang Q, McCormick DA, Tolias AS. 2016. Pupil fluctuations track rapid changes in adrenergic and cholinergic activity in cortex. *Nat Commun* **7**:13289. doi:10.1038/ncomms13289

Renart A, Machens CK. 2014. Variability in neural activity and behavior. *Curr Opin Neurobiol* **25**:211–220. doi:10.1016/j.conb.2014.02.013

Reynolds JH, Heeger DJ. 2009. The Normalization Model of Attention. *Neuron* **61**:168–185. doi:10.1016/j.neuron.2009.01.002

Reynolds JH, Pasternak T, Desimone R. 2000. Attention Increases Sensitivity of V4 Neurons. *Neuron* **26**:703–714. doi:10.1016/S0896-6273(00)81206-4

Ribrault C, Sekimoto K, Triller A. 2011. From the stochasticity of molecular processes to the variability of synaptic transmission. *Nat Rev Neurosci* **12**:375–387. doi:10.1038/nrn3025

Ringach DL. 2009. Spontaneous and driven cortical activity: implications for

computation. *Curr Opin Neurobiol* **19**:439–444. doi:10.1016/j.conb.2009.07.005

Robbins TW, Arnsten AFT. 2009. The neuropsychopharmacology of fronto-executive function: monoaminergic modulation. *Annu Rev Neurosci* **32**:267–87. doi:10.1146/annurev.neuro.051508.135535

Rockland KS, Lund JS. 1983. Intrinsic laminar lattice connections in primate visual cortex. *J Comp Neurol* **216**:303–318. doi:10.1002/cne.902160307

Roelfsema PR, Tolboom M, Khayat PS. 2007. Different Processing Phases for Features, Figures, and Selective Attention in the Primary Visual Cortex. *Neuron* **56**:785–792. doi:10.1016/j.neuron.2007.10.006

Rohenkohl G, Bosman CA, Fries P. 2018. Gamma Synchronization between V1 and V4 Improves Behavioral Performance. *Neuron* **100**:953-963.e3. doi:10.1016/j.neuron.2018.09.019

Roitman JD, Shadlen MN. 2002. Response of Neurons in the Lateral Intraparietal Area during a Combined Visual Discrimination Reaction Time Task. *J Neurosci* **22**:9475–9489. doi:10.1523/JNEUROSCI.22-21-09475.2002

Rolls ET, Loh M, Deco G, Winterer G. 2008. Computational models of schizophrenia and dopamine modulation in the prefrontal cortex. *Nat Rev Neurosci*. doi:10.1038/nrn2462

Rossi AF, Paradiso MA. 1995. Feature-specific effects of selective visual attention. *Vision Res* **35**:621–634. doi:10.1016/0042-6989(94)00156-G

Ruff DA, Alberts JJ, Cohen MR. 2016. Relating normalization to neuronal populations across cortical areas. *J Neurophysiol* **116**:1375–1386. doi:10.1152/jn.00017.2016

Ruff DA, Cohen MR. 2017. A normalization model suggests that attention changes the weighting of inputs between visual areas. *Proc Natl Acad Sci* **114**:E4085–E4094. doi:10.1073/pnas.1619857114

Ruff DA, Cohen MR. 2016a. Attention Increases Spike Count Correlations between Visual Cortical Areas. *J Neurosci* **36**:7523–7534. doi:10.1523/JNEUROSCI.0610-16.2016

Ruff DA, Cohen MR. 2016b. Stimulus Dependence of Correlated Variability across Cortical Areas. *J Neurosci* **36**:7546–7556. doi:10.1523/JNEUROSCI.0504-16.2016

Ruff DA, Cohen MR. 2014. Attention can either increase or decrease spike count correlations in visual cortex. *Nat Neurosci* **17**:1591–1597. doi:10.1038/nn.3835

Sakata S, Harris KD. 2009. Laminar Structure of Spontaneous and Sensory-Evoked Population Activity in Auditory Cortex. *Neuron* **64**:404–418. doi:10.1016/j.neuron.2009.09.020

Salazar RF, Dotson NM, Bressler SL, Gray CM. 2012. Content-specific fronto-parietal synchronization during visual working memory. *Science* **338**:1097–100. doi:10.1126/science.1224000

Salinas E, Sejnowski TJ. 2001a. Gain modulation in the central nervous system: where behavior, neurophysiology, and computation meet. *Neuroscientist* **7**:430–40.

doi:10.1177/107385840100700512

Salinas E, Sejnowski TJ. 2001b. Correlated neuronal activity and the flow of neural information. *Nat Rev Neurosci* **2**:539–550. doi:10.1038/35086012

Salzman CD, Britten KH, Newsome WT. 1990. Cortical microstimulation influences perceptual judgements of motion direction. *Nature* **346**:174–177. doi:10.1038/346174a0

Sanayei M, Herrero JL, Distler C, Thiele A. 2015. Attention and normalization circuits in macaque V1. *Eur J Neurosci* **41**:947–962. doi:10.1111/ejn.12857

Sarter M, Hasselmo ME, Bruno JP, Givens B. 2005. Unraveling the attentional functions of cortical cholinergic inputs: Interactions between signal-driven and cognitive modulation of signal detection. *Brain Res Rev* **48**:98–111. doi:10.1016/j.brainresrev.2004.08.006

Sarter M, Lustig C, Berry AS, Gritton H, Howe WM, Parikh V. 2016. What do phasic cholinergic signals do? *Neurobiol Learn Mem* **130**:135–141. doi:10.1016/j.nlm.2016.02.008

Sarter M, Parikh V, Howe WM. 2009. Phasic acetylcholine release and the volume transmission hypothesis: time to move on. *Nat Rev Neurosci* **10**:383–390. doi:10.1038/nrn2635

Sawaguchi T, Goldman-Rakic P. 1991. D1 dopamine receptors in prefrontal cortex: involvement in working memory. *Science (80-)* **251**:947–950. doi:10.1126/science.1825731

Sawaguchi T, Goldman-Rakic PS. 1994. The role of D1-dopamine receptor in working memory: local injections of dopamine antagonists into the prefrontal cortex of rhesus monkeys performing an oculomotor delayed-response task. *J Neurophysiol* **71**:515–528. doi:10.1152/jn.1994.71.2.515

Sawaguchi T, Iba M. 2001. Prefrontal Cortical Representation of Visuospatial Working Memory in Monkeys Examined by Local Inactivation With Muscimol. *J Neurophysiol* **86**:2041–2053. doi:10.1152/jn.2001.86.4.2041

Sawaguchi T, Matsumura M, Kubota K. 1990. Effects of dopamine antagonists on neuronal activity related to a delayed response task in monkey prefrontal cortex. *J Neurophysiol* **63**:1401–1412. doi:10.1152/jn.1990.63.6.1401

Schmitz TW, Duncan J. 2018. Normalization and the Cholinergic Microcircuit: A Unified Basis for Attention. *Trends Cogn Sci* **22**:422–437. doi:10.1016/j.tics.2018.02.011

Schmolesky MT, Wang Y, Hanes DP, Thompson KG, Leutgeb S, Schall JD, Leventhal AG. 1998. Signal timing access the macaque visual system. *J Neurophysiol* **79**:3272–3278. doi:10.1152/jn.1998.79.6.3272

Scholvinck ML, Saleem AB, Benucci A, Harris KD, Carandini M. 2015. Cortical State Determines Global Variability and Correlations in Visual Cortex. *J Neurosci* **35**:170–178. doi:10.1523/JNEUROSCI.4994-13.2015

Schroeder C. 1998. A spatiotemporal profile of visual system activation revealed by

current source density analysis in the awake macaque. *Cereb Cortex* **8**:575–592. doi:10.1093/cercor/8.7.575

Schroeder CE, Tenke CE, Givre SJ, Arezzo JC, Vaughan HG. 1991. Striate cortical contribution to the surface-recorded pattern-reversal vep in the alert monkey. *Vision Res* **31**:1143–1157. doi:10.1016/0042-6989(91)90040-C

Schultz W. 2016. Dopamine reward prediction- error signalling: a two-component response. *Nat Publ Gr* **17**:183–195. doi:10.1038/nrn.2015.26

Schultz W. 2007. Multiple Dopamine Functions at Different Time Courses. *Annu Rev Neurosci* **30**:259–288. doi:10.1146/annurev.neuro.28.061604.135722

Schultz W. 1998. Predictive reward signal of dopamine neurons. *J Neurophysiol* **80**:1–27. doi:10.1007/s00429-010-0262-0

Seamans JK, Yang CR. 2004. The principal features and mechanisms of dopamine modulation in the prefrontal cortex. *Prog Neurobiol* **74**:1–58. doi:10.1016/j.pneurobio.2004.05.006

Séguéla P, Watkins KC, Geffard M, Descarries L. 1990. Noradrenaline axon terminals in adult rat neocortex: an immunocytochemical analysis in serial thin sections. *Neuroscience* **35**:249–64. doi:10.1016/0306-4522(90)90079-J

Selemon L, Goldman-Rakic P. 1988. Common cortical and subcortical targets of the dorsolateral prefrontal and posterior parietal cortices in the rhesus monkey: evidence for a distributed neural network subserving spatially guided behavior. *J Neurosci* **8**:4049–4068. doi:10.1523/JNEUROSCI.08-11-04049.1988

Self MW, van Kerkoerle T, Supèr H, Roelfsema PR. 2013. Distinct Roles of the Cortical Layers of Area V1 in Figure-Ground Segregation. *Curr Biol* **23**:2121–2129. doi:10.1016/j.cub.2013.09.013

Semedo JD, Zandvakili A, Machens CK, Yu BM, Kohn A. 2019. Cortical Areas Interact through a Communication Subspace. *Neuron* 249–259. doi:10.1016/j.neuron.2019.01.026

Servan-Schreiber D, Printz H, Cohen JD. 1990. A network model of catecholamine effects: gain, signal-to-noise ratio, and behavior. *Science* **249**:892–895. doi:10.1126/science.2392679

Sesack SR, Deutch AY, Roth RH, Bunney BS. 1989. Topographical organization of the efferent projections of the medial prefrontal cortex in the rat: An anterograde tract-tracing study with Phaseolus vulgaris leucoagglutinin. *J Comp Neurol* **290**:213–242. doi:10.1002/cne.902900205

Shadlen M, Britten K, Newsome W, Movshon J. 1996. A computational analysis of the relationship between neuronal and behavioral responses to visual motion. *J Neurosci* **16**:1486–1510. doi:10.1523/JNEUROSCI.16-04-01486.1996

Shadlen MN, Kiani R, Newsome WT, Gold JI, Wolpert DM, Zylberberg A, Ditterich J, de Lafuente V, Yang T, Roitman J. 2016. Comment on "Single-trial spike trains in parietal cortex reveal discrete steps during decision-making." *Science (80-)* **351**:1406–1406. doi:10.1126/science.aad3242

Shadlen MN, Newsome WT. 2001. Neural Basis of a Perceptual Decision in the Parietal Cortex (Area LIP) of the Rhesus Monkey. *J Neurophysiol* **86**:1916–1936. doi:10.1152/jn.2001.86.4.1916

Sheather SJ. 2009. A Modern Approach to Regression with R, 1st ed. New York: Springer. doi:10.1016/j.peva.2007.06.006

Shen W, Flajolet M, Greengard P, Surmeier DJ. 2008. Dichotomous dopaminergic control of striatal synaptic plasticity. *Science (80-)*. doi:10.1126/science.1160575

Shimaoka D, Harris KD, Carandini M. 2018. Effects of Arousal on Mouse Sensory Cortex Depend on Modality. *Cell Rep* **22**:3160–3167. doi:10.1016/j.celrep.2018.02.092

Shine JM. 2019. Neuromodulatory Influences on Integration and Segregation in the Brain. *Trends Cogn Sci* **xx**:1–30. doi:10.1016/j.tics.2019.04.002

Silk TJ, Newman DP, Eramudugolla R, Vance A, Bellgrove MA. 2014. Influence of methylphenidate on spatial attention asymmetry in adolescents with attention deficit hyperactivity disorder (ADHD): Preliminary findings. *Neuropsychologia* **56**:178–183. doi:10.1016/j.neuropsychologia.2014.01.015

Silver RA. 2010. Neuronal arithmetic. *Nat Rev Neurosci* **11**:474–489. doi:10.1038/nrn2864

Simonsohn U. 2017. Two-Lines: A Valid Alternative to the Invalid Testing of U-Shaped Relationships with Quadratic Regressions. *Ssrn*. doi:10.2139/ssrn.3021690

Simpson HM, Hale SM. 1969. Pupillary Changes during a Decision-Making Task. *Percept Mot Skills* **29**:495–498. doi:10.2466/pms.1969.29.2.495

Singer W. 1999. Neuronal Synchrony: A Versatile Code for the Definition of Relations? *Neuron* **24**:49–65. doi:10.1016/S0896-6273(00)80821-1

Smith MA, Kohn A. 2008. Spatial and Temporal Scales of Neuronal Correlation in Primary Visual Cortex. *J Neurosci* **28**:12591–12603. doi:10.1523/JNEUROSCI.2929-08.2008

Smith PL, Ratcliff R. 2004. Psychology and neurobiology of simple decisions. *Trends Neurosci* **27**:161–168. doi:10.1016/j.tins.2004.01.006

Snyder LH, Batista AP, Andersen RA. 2000. Intention-related activity in the posterior parietal cortex: A review. *Vision Res* **40**:1433–1441. doi:10.1016/S0042-6989(00)00052-3

Soares D, Goldrick I, Lemon RN, Kraskov A, Greensmith L, Kalmar B. 2017. Expression of Kv3.1b potassium channel is widespread in macaque motor cortex pyramidal cells: A histological comparison between rat and macaque. *J Comp Neurol* **525**:2164–2174. doi:10.1002/cne.24192

Soltani A, Noudoost B, Moore T. 2013. Dissociable dopaminergic control of saccadic target selection and its implications for reward modulation. *Proc Natl Acad Sci U S A* **110**:3579–84. doi:10.1073/pnas.1221236110

Spitzer H, Desimone R, Moran J. 1988. Increased attention enhances both behavioral and neuronal performance. *Science (80-)* **240**:338–340. doi:10.1126/science.3353728

Spitzer H, Richmond BJ. 1991. Task difficulty: ignoring, attending to, and discriminating a visual stimulus yield progressively more activity in inferior temporal neurons. *Exp Brain Res* **83**:340–348. doi:10.1007/BF00231157

St. Peters M, Demeter E, Lustig C, Bruno JP, Sarter M. 2011. Enhanced control of attention by stimulating mesolimbic-corticopetal cholinergic circuitry. *J Neurosci* **31**:9760–9771. doi:10.1523/JNEUROSCI.1902-11.2011

Steriade, Amzica, Nunez. 1993a. Cholinergic and noradrenergic modulation of the slow (approximately 0.3 Hz) oscillation in neocortical cells. *J Neurophysiol* **70**:1385–1400. doi:10.1152/jn.1993.70.4.1385

Steriade M, Timofeev I, Grenier F. 2001. Natural Waking and Sleep States: A View From Inside Neocortical Neurons. *J Neurophysiol* **85**:1969–1985. doi:10.1152/jn.2001.85.5.1969

Steriade, McCormick, Sejnowski. 1993b. Thalamocortical oscillations in the sleeping and aroused brain. *Science (80-)* **262**:679–685. doi:10.1126/science.8235588

Steriade, Nunez, Amzica. 1993c. Intracellular analysis of relations between the slow (< 1 Hz) neocortical oscillation and other sleep rhythms of the electroencephalogram. *J Neurosci* **13**:3266–3283. doi:10.1523/JNEUROSCI.13-08-03266.1993

Thiele A. 2013. Muscarinic Signaling in the Brain. *Annu Rev Neurosci* **36**:271–294. doi:10.1146/annurev-neuro-062012-170433

Thiele A, Bellgrove MA. 2018. Neuromodulation of Attention. *Neuron* **97**:769–785. doi:10.1016/j.neuron.2018.01.008

Thiele A, Brandt C, Dasilva M, Gotthardt S, Chicharro D, Panzeri S, Distler C. 2016. Attention Induced Gain Stabilization in Broad and Narrow-Spiking Cells in the Frontal Eye-Field of Macaque Monkeys. *J Neurosci* **36**:7601–12. doi:10.1523/JNEUROSCI.0872-16.2016

Thiele A, Delicato LS, Roberts MJ, Gieselmann MA. 2006. A novel electrode-pipette design for simultaneous recording of extracellular spikes and iontophoretic drug application in awake behaving monkeys. *J Neurosci Methods* **158**:207–211. doi:10.1016/j.jneumeth.2006.05.032

Thiele A, Herrero JL, Distler C, Hoffmann K-P. 2012. Contribution of cholinergic and GABAergic mechanisms to direction tuning, discriminability, response reliability, and neuronal rate correlations in macaque middle temporal area. *J Neurosci* **32**:16602–15. doi:10.1523/JNEUROSCI.0554-12.2012

Thiele A, Stoner G. 2003. Neuronal synchrony does not correlate with motion coherence in cortical area MT. *Nature* **421**:366–70. doi:10.1038/nature01285

Thompson KG, Biscoe KL, Sato TR. 2005. Neuronal basis of covert spatial attention in the frontal eye field. *J Neurosci* **25**:9479–87. doi:10.1523/JNEUROSCI.0741-05.2005

Thut G. 2006. -Band Electroencephalographic Activity over Occipital Cortex Indexes Visuospatial Attention Bias and Predicts Visual Target Detection. *J Neurosci* **26**:9494–9502. doi:10.1523/JNEUROSCI.0875-06.2006

Tomko GJ, Crapper DR. 1974. Neuronal variability: non-stationary responses to identical visual stimuli. *Brain Res* **79**:405–418. doi:10.1016/0006-8993(74)90438-7

Totah NK, Neves RM, Panzeri S, Logothetis NK, Eschenko O. 2018. The Locus Coeruleus Is a Complex and Differentiated Neuromodulatory System. *Neuron* **99**:1055-1068.e6. doi:10.1016/j.neuron.2018.07.037

Totah NKB, Logothetis NK, Eschenko O. 2019. Noradrenergic ensemble-based modulation of cognition over multiple timescales. *Brain Res* **1709**:50–66. doi:10.1016/j.brainres.2018.12.031

Treue S, Maunsell JHR. 1996. Attentional modulation of visual motion processing in cortical areas MT and MST. *Nature* **382**:539–541. doi:10.1038/382539a0

Treue S, Trujillo JCM. 1999. Feature-based attention influences motion processing gain in macaque visual cortex. *Nature* **399**:575–579. doi:10.1038/21176

Twomey DM, Murphy PR, Kelly SP, O'Connell RG. 2015. The classic P300 encodes a build-to-threshold decision variable. *Eur J Neurosci* **42**:1636–1643. doi:10.1111/ejn.12936

Urai AE, Braun A, Donner TH. 2017. Pupil-linked arousal is driven by decision uncertainty and alters serial choice bias. *Nat Commun* **8**:14637. doi:10.1038/ncomms14637

Usher M, Cohen JD, Servan-Schreiber D, Rajkowski J, Aston-Jones G. 1999. The Role of Locus Coeruleus in the Regulation of Cognitive Performance. *Science (80-)* **283**:549–554. doi:10.1126/science.283.5401.549

van Dijk H, Schoffelen J-M, Oostenveld R, Jensen O. 2008. Prestimulus Oscillatory Activity in the Alpha Band Predicts Visual Discrimination Ability. *J Neurosci* **28**:1816–1823. doi:10.1523/JNEUROSCI.1853-07.2008

van Kempen J, Loughnane GM, Newman DP, Kelly SP, Thiele A, O'Connell RG, Bellgrove MA. 2019. Behavioural and neural signatures of perceptual decision-making are modulated by pupil-linked arousal. *Elife* **8**:1–27. doi:10.7554/eLife.42541

van Kempen J, Panzeri S, Thiele A. 2017. Cholinergic Control of Information Coding. *Trends Neurosci* **xx**:1–3. doi:10.1016/j.tins.2017.06.006

van Kerkoerle T, Self MW, Dagnino B, Gariel-Mathis M-A, Poort J, van der Togt C, Roelfsema PR. 2014. Alpha and gamma oscillations characterize feedback and feedforward processing in monkey visual cortex. *Proc Natl Acad Sci* **111**:14332–14341. doi:10.1073/pnas.1402773111

Varazzani C, San-Galli A, Gilardeau S, Bouret S. 2015. Noradrenaline and Dopamine Neurons in the Reward/Effort Trade-Off: A Direct Electrophysiological Comparison in Behaving Monkeys. *J Neurosci* **35**:7866–7877. doi:10.1523/JNEUROSCI.0454-15.2015

Venables WN, Ripley BD. 2002. Modern Applied Statistics with S, 4th ed. New York: Springer. doi:10.1016/j.electacta.2013.08.022.

Vigneswaran G, Kraskov A, Lemon RN. 2011. Large Identified Pyramidal Cells in Macaque

Motor and Premotor Cortex Exhibit “Thin Spikes”: Implications for Cell Type Classification. *J Neurosci* **31**:14235–14242. doi:10.1523/jneurosci.3142-11.2011

Vijayraghavan S, Wang M, Birnbaum SG, Williams G V, Arnsten AFT. 2007. Inverted-U dopamine D1 receptor actions on prefrontal neurons engaged in working memory. *Nat Neurosci* **10**:376–384. doi:10.1038/nn1846

Vinck M, Batista-Brito R, Knoblich U, Cardin JA. 2015. Arousal and Locomotion Make Distinct Contributions to Cortical Activity Patterns and Visual Encoding. *Neuron* **86**:740–754. doi:10.1016/j.neuron.2015.03.028

Voytko M, Olton D, Richardson R, Gorman L, Tobin J, Price D. 1994. Basal forebrain lesions in monkeys disrupt attention but not learning and memory [published erratum appears in J Neurosci 1995 Mar;15(3): following table of contents]. *J Neurosci* **14**:167–186. doi:10.1523/JNEUROSCI.14-01-00167.1994

Wang C-A, Boehnke SE, White BJ, Munoz DP. 2012. Microstimulation of the Monkey Superior Colliculus Induces Pupil Dilation Without Evoking Saccades. *J Neurosci* **32**:3629–3636. doi:10.1523/JNEUROSCI.5512-11.2012

Wang C-A, Munoz DP. 2015a. A circuit for pupil orienting responses: implications for cognitive modulation of pupil size. *Curr Opin Neurobiol* **33**:134–140. doi:10.1016/j.conb.2015.03.018

Wang C-A, Munoz DP. 2015b. A circuit for pupil orienting responses: implications for cognitive modulation of pupil size. *Curr Opin Neurobiol* **33**:134–140. doi:10.1016/j.conb.2015.03.018

Wang M, Ramos BP, Paspalas CD, Shu Y, Simen A, Duque A, Vijayraghavan S, Brennan A, Dudley A, Nou E, Mazer JA, McCormick DA, Arnsten AFT. 2007. Alpha2A-Adrenoceptors Strengthen Working Memory Networks by Inhibiting cAMP-HCN Channel Signaling in Prefrontal Cortex. *Cell* **129**:397–410. doi:10.1016/j.cell.2007.03.015

Wang M, Yang Y, Wang CJ, Gamo NJ, Jin LE, Mazer JA, Morrison JH, Wang XJ, Arnsten AFT. 2013. NMDA Receptors Subserve Persistent Neuronal Firing during Working Memory in Dorsolateral Prefrontal Cortex. *Neuron*. doi:10.1016/j.neuron.2012.12.032

Warburton DM, Rusted JM. 1993. Cholinergic control of cognitive resources. *Neuropsychobiology* **28**:43–6. doi:10.1159/000118998

Wardak C, Ibos G, Duhamel J-R, Olivier E. 2006. Contribution of the monkey frontal eye field to covert visual attention. *J Neurosci* **26**:4228–4235. doi:10.1523/JNEUROSCI.3336-05.2006

Wardak C, Olivier E, Duhamel JR. 2004. A Deficit in covert attention after parietal cortex inactivation in the monkey. *Neuron* **42**:501–508. doi:10.1016/S0896-6273(04)00185-0

Watanabe M, Kodama T, Hikosaka K. 1997. Increase of Extracellular Dopamine in Primate Prefrontal Cortex During a Working Memory Task. *J Neurophysiol* **78**:2795–2798. doi:10.1152/jn.1997.78.5.2795

Williams-Gray CH, Hampshire A, Robbins TW, Owen AM, Barker RA. 2007. Catechol O-methyltransferase Val158Met genotype influences frontoparietal activity during

planning in patients with Parkinson's disease. *J Neurosci* **27**:4832–4838. doi:10.1523/JNEUROSCI.0774-07.2007

Williams SM, Goldman-Rakic PS. 1993. Characterization of the dopaminergic innervation of the primate frontal cortex using a dopamine-specific antibody. *Cereb Cortex*. doi:10.1093/cercor/3.3.199

Williams G V, Goldman-Rakic PS. 1995. Modulation of memory fields by dopamine D1 receptors in prefrontal cortex. *Nature* **376**:572–575. doi:10.1038/376572a0

Winterer G, Weinberger DR. 2004. Genes, dopamine and cortical signal-to-noise ratio in schizophrenia. *Trends Neurosci* **27**:683–690. doi:10.1016/j.tins.2004.08.002

Witte E a., Davidson MC, Marrocco RT. 1997. Effects of altering brain cholinergic activity on covert orienting of attention: Comparison of monkey and human performance. *Psychopharmacology (Berl)* **132**:324–334. doi:10.1007/s002130050352

Womelsdorf T, Lima B, Vinck M, Oostenveld R, Singer W, Neuenschwander S, Fries P. 2012. Orientation selectivity and noise correlation in awake monkey area V1 are modulated by the gamma cycle. *Proc Natl Acad Sci U S A* **109**:4302–7. doi:10.1073/pnas.1114223109

Yang C, Seamans J. 1996. Dopamine D1 receptor actions in layers V-VI rat prefrontal cortex neurons in vitro: modulation of dendritic-somatic signal integration. *J Neurosci* **16**:1922–1935. doi:10.1523/JNEUROSCI.16-05-01922.1996

Yang T, Shadlen MN. 2007. Probabilistic reasoning by neurons. *Nature* **447**:1075–1080. doi:10.1038/nature05852

Yang Y, Paspalas CD, Jin LE, Picciotto MR, Arnsten AFT, Wang M. 2013. Nicotinic 7 receptors enhance NMDA cognitive circuits in dorsolateral prefrontal cortex. *Proc Natl Acad Sci* **110**:12078–12083. doi:10.1073/pnas.1307849110

Yates JL, Park IM, Katz LN, Pillow JW, Huk AC. 2017. Functional dissection of signal and noise in MT and LIP during decision-making. *Nat Neurosci* **20**:1285–1292. doi:10.1038/nn.4611

Yerkes RM, Dodson JD. 1908. The relation of strength of stimulus to rapidity of habit-formation. *J Comp Neurol Psychol* **18**:459–482. doi:10.1002/cne.920180503

Yu AJ, Dayan P. 2005. Uncertainty, Neuromodulation, and Attention. *Neuron* **46**:681–692. doi:10.1016/j.neuron.2005.04.026

Zaborszky L, Csordas A, Mosca K, Kim J, Gielow MR, Vadasz C, Nadasdy Z. 2015. Neurons in the basal forebrain project to the cortex in a complex topographic organization that reflects corticocortical connectivity patterns: An experimental study based on retrograde tracing and 3D reconstruction. *Cereb Cortex*. doi:10.1093/cercor/bht210

Zagha E, Casale AE, Sachdev RNS, McGinley MJ, McCormick DA. 2013. Motor cortex feedback influences sensory processing by modulating network state. *Neuron* **79**:567–578. doi:10.1016/j.neuron.2013.06.008

Zahrt J, Taylor JR, Mathew RG, Arnsten AFT. 1997. Supranormal Stimulation of D 1 Dopamine Receptors in the Rodent Prefrontal Cortex Impairs Spatial Working

Memory Performance. *J Neurosci* **17**:8528–8535. doi:10.1523/JNEUROSCI.17-21-08528.1997

Zandvakili A, Kohn A. 2015. Coordinated Neuronal Activity Enhances Corticocortical Communication. *Neuron* **87**:827–839. doi:10.1016/j.neuron.2015.07.026

Zhou X, Qi X-L, Douglas K, Palaninathan K, Kang HS, Buccafusco JJ, Blake DT, Constantinidis C. 2011. Cholinergic modulation of working memory activity in primate prefrontal cortex. *J Neurophysiol* **106**:2180–2188. doi:10.1152/jn.00148.2011

Zhou Y, Freedman DJ. 2019. Posterior parietal cortex plays a causal role in perceptual and categorical decisions. *Science* **365**:180–185. doi:10.1126/science.aaw8347

Zohary E, Shadlen MN, Newsome WT. 1994. Correlated neuronal discharge rate and its implications for psychophysical performance. *Nature* **370**:140–3. doi:10.1038/370140a0